Higher Order QCD Corrections to Timelike Processes

P.J. Rijken

Higher Order QCD Corrections to Timelike Processes

Higher Order QCD Corrections to Timelike Processes

PROEFSCHRIFT

ter verkrijging van de graad van Doctor
aan de Rijksuniversiteit te Leiden, op gezag
van de Rector Magnificus Dr. W.A. Wagenaar,
hoogleraar in de faculteit der Sociale Wetenschappen,
volgens besluit van het College van Dekanen
te verdedigen op woensdag 12 maart 1997
te klokke 16.15 uur

door

Pieter Johannes Rijken

geboren te Nijmegen op 23 oktober 1969

Promotiecommissie:

Promotor:	Prof.dr. F.A. Berends
Co-promotor:	Dr. W.L.G.A.M. van Neerven
Overige leden:	Prof.dr. P.J. van Baal
	Prof.dr. L.J. de Jongh
	Prof.dr. R.H.P. Kleiss
	Prof.dr. J. Smith

Aan Annette,
mijn broer
en mijn ouders

Contents

1 Introduction **3**
1.1 QCD as the theory of the strong interactions . . . 3
1.2 The Feynman parton model . . . 4
1.3 Timelike processes . . . 6
1.4 Outline . . . 9
References . . . 9

2 Order $\mathcal{O}(\alpha_s^2)$ contributions to the Drell-Yan cross section at fixed target energies **13**
2.1 Introduction . . . 13
2.2 Higher order QCD corrections to $d^2\sigma/dmdx_F$ ($d^2\sigma/dmdy$) and $d\sigma/dm$ 15
2.3 Results . . . 19
2.3.1 The validity of the soft plus virtual gluon approximation . . . 19
2.3.2 The order $\mathcal{O}(\alpha_s^2)$ contributions at fixed target energies . . . 28
2.4 Summary . . . 38
Appendix A . . . 38
Appendix B . . . 43
References . . . 48

3 Heavy flavour contributions to the Drell-Yan cross section **51**
3.1 Introduction . . . 51
3.2 The order α_s^2 corrections to the DY cross section due to heavy flavour production . . . 52
3.3 Hadronic cross sections . . . 63
3.3.1 Heavy flavour contributions to $d\sigma/dQ^2$ for Z-production . . . 65
3.3.2 Heavy flavour contributions to $d\sigma/dQ^2$ for W-production . . . 66
3.3.3 Heavy flavour contributions to $d\sigma/dQ^2$ for $\sqrt{Q^2} < 60\,\mathrm{GeV}$ . . . 68
3.3.4 Contributions of the heavy flavours to the total cross section for Z- and W-production . . . 69
3.3.5 The asymptotic region where $m^2 << Q^2$ . . . 70
3.4 Conclusions . . . 72
Appendix A . . . 72
References . . . 73

4 Order $\mathcal{O}(\alpha_s^2)$ contributions to hadron production in electron positron annihilation **75**
4.1 Introduction . . . 75
4.2 Single particle inclusive cross sections . . . 77
4.3 Fragmentation coefficient functions in e^+e^--annihilation up to order α_s^2 . . . 81
4.3.1 The first order results . . . 84
4.3.2 Diagrams contributing at second order . . . 86
4.3.3 Prescription of the γ_5-matrix and the Levi-Civita tensor in n-dimensions . . . 92
4.3.4 Soft contributions to the parton fragmentation functions . . . 94
4.4 Determination of the coefficient functions in the $\overline{\rm MS}$- and the annihilation scheme (A-scheme) . . . 95
4.5 Results for the longitudinal and transverse fragmentation functions . 109
4.5.1 Conclusions . . . 119
4.6 Results for the asymmetric fragmentation function . . . 120
4.6.1 Conclusions . . . 127
Appendix A . . . 128
A.1 The coefficient functions in the $\overline{\rm MS}$-scheme . . . 129
A.2 The coefficient functions in the annihilation scheme . . . 145
References . . . 154

Samenvatting **159**

Curriculum vitae **167**

List of publications **169**

1 Introduction

1.1 QCD as the theory of the strong interactions

In the two decades after the second world war an enormous amount of particles was discovered, in particular hadrons. Cosmic ray experiments found the mesons π, K, and the hyperons Λ, Σ and Ξ. In particular, when the particle accelerators came into operation in the fifties, many new hadrons were discovered. During this period their decay rates and masses were experimentally well measured but one was unable to make any quantitative or qualitative predictions about these quantities. This unlike in Quantum Electrodynamics (QED), where for example the anomalous magnetic moment of the electron was calculated with high precision (for a review see [1]). In 1961 Gell-Mann [2] and independently Ne'eman [3] shed new light on the mass spectrum of the hadrons by classifying them according to the higher irreducible representations, like the octet **8** and decuplet **10**, of the flavour symmetry group $SU(3)_F$. In view of the mass differences between the hadrons within a multiplet the flavour symmetry is a, medium strong, broken symmetry. The Gell-Mann–Okubo mass formula [4] provided a very good description of this symmetry breaking. In 1961 the decuplet had one vacancy. The mass of this missing particle, called Ω^-, could be predicted rather accurately using the Gell-Mann–Okubo mass formula. The discovery [5] of this particle in 1964 with the correct predicted mass was a great success putting the $SU(3)_F$ symmetry of Gell-Mann and Ne'eman on a firm footing. Since the higher $SU(3)$ representations can be obtained from the fundamental representation **3**, it lead to a model in which all hadrons can be described in terms of only two (mesons) or three (baryons) constituents. This so-called quark model, proposed by Gell-Mann [6] and independently by Zweig [7] needed three quarks ("up", "down", and "strange") as the constituents to build all known hadrons. However, in spite of this success, there still remained many unsolved technical difficulties. One of them was that e.g. the delta resonance $\Delta(1236)$ (consisting of three S-wave up quarks) which has a spin equal to 3/2 was described by a symmetric wave function in spite of the fact that it is a fermion. According to the Pauli-principle its wave function should be totally anti-symmetric in contrast to what follows from the quark model. This led to the introduction [8] of an additional symmetry group given by $SU(3)_C$ where the quarks are put in the fundamental representation of the group. This implies that the quarks are coming out in three species distinguished by a new quantum number called colours. These colours predicted the correct decay rate of the neutral pion to two photons and the correct ratio of the cross sections of the

processes $e^+ + e^- \rightarrow$ "hadrons" and $e^+ + e^- \rightarrow \mu^+ + \mu^-$. In the standard model of the electroweak and strong interactions colour was also needed in order to cancel anomalies which occur when fermions appear in closed triangular loops characteristic of a quantum field theory. Besides theoretical considerations crucial experimental evidence that all existing hadrons consist of quarks was found at SLAC in 1969 [9] where one studied deep inelastic scattering of electrons and protons. In this experiment the phenomenon of scaling (see the next section) was observed indicating that the constituents of the proton behave as free point-like particles at very large momentum transfers. This led to a cross section which was much larger than originally was expected. Unfortunately at that time there was no quantum field theory which was able to describe the interaction between the electron and the constituents of the proton. This last obstacle was overcome with the introduction of non-abelian Yang-Mills theories [10] together with the discovery that these field theories have two interesting properties, i.e. asymptotic freedom [11] and confinement [12]. The first property implies the vanishing of the coupling constant (interaction strength) at an increasing energy scale explaining the behaviour of quarks inside the proton at large momentum transfers. The second property predicts an ever increasing coupling constant at low energy scales, i.e. large distances, possibly explaining why quarks are confined within hadrons. Theoretical considerations as well as overwhelming experimental evidence have shown that the only candidate to explain the phenomena of the strong interactions is Quantum Chromo Dynamics (QCD). Technically, QCD is an $SU(3)_C$ locally gauge invariant Yang-Mills field theory describing the interactions between six flavours of quarks and anti-quarks ("up", "down", "strange", "charm", "bottom", and "top" of which the last one was discovered only recently [13]). The force between the quarks is mediated by the gluons (massless vector bosons). This description is analogous to the one given for the successful standard model of the electroweak interactions where the electromagnetic and weak forces are mediated by the massless photon and massive Z-, $W^{\pm}$-bosons respectively. In the case of QCD the quarks and the gluons are put in the fundamental and adjoint representation of the symmetry group $SU(3)$ respectively. This means that for each type of quark there are three colours and there exist eight coloured combinations for the gluons. Another interesting property of QCD is that the gluons interact among each other which is a consequence of the non-abelian nature of $SU(3)_C$. The same phenomena is observed for the vector bosons Z and $W^{\pm}$ which appear in the standard electroweak model mentioned above. This is in contrast to the behaviour of the photon which does not have a self-interaction because here the underlying gauge group is given by $U(1)$ which is abelian.

1.2 The Feynman parton model

Using current algebra [14] Bjorken [15] predicted the scaling behaviour of the deep inelastic structure functions measured at SLAC [9]. These structure functions are relativistic invariant dimensionless quantities containing all information about the structure of the proton and they appear in the cross section of the afore mentioned

process. Unfortunately one could only predict results for the integrated structure functions rather than for the structure functions themselves. Another limitation of current algebra is that one cannot make predictions for other deep inelastic processes like massive lepton pair production in hadron–hadron collisions (Drell-Yan process, see section 1.3). These shortcomings were amended by the parton model originally introduced by Feynman [16].

The main results of the parton model can be summarized as follows. In deep inelastic scattering an electron is scattered inelastically off a proton via the exchange of a spacelike photon. The aforementioned experiments at SLAC revealed that the structure functions do not depend both on ν (energy loss of the electron in the laboratory frame) and q^2 (the four-momentum squared of the virtual photon), but instead only depend on the scaling variable $x = -q^2/(2M\nu)$, where M is the mass of the proton and the variable x lies between 0 and 1. Applying Feynman's parton model to deep inelastic electron–proton scattering Bjorken and Paschos [17] assumed that at large $-q^2$ and x kept fixed the electron views the "partons", of which the proton is made up, as frozen free point-like particles. The scattering of the electron and proton then can de viewed as an incoherent sum of electron–parton scatterings weighted by a probability function (parton density). The above mentioned scaling variable x is interpreted as the fraction of the proton's momentum carried by the parton participating in the scattering. The parton density, denoted by $f_i^p(x)$, is defined as the probability of finding a parton of type "i" inside the proton. One of the most important predictions of the parton model is that the deep inelastic structure function can be written as a sum of over all parton densities weighted by the charge squared of each parton. Since the parton densities only depend on the dimensionless variable x above it explains the scale independence of the deep inelastic structure functions meaning that they are independent of the momentum squared of the virtual photon given by q^2. Another important prediction of Feynman's parton model is that other deep inelastic processes can be described by the same parton densities as those observed in deep inelastic electron–proton scattering. This implies that different processes are related to each other.

Since the experiments at SLAC in 1969 many experiments have been performed. Because of higher statistics the latter [18] provided us with a higher accuracy of the deep inelastic structure functions than those measured at SLAC. In [18] one could show a small violation of scale invariance of the deep inelastic structure functions. This breaking of scaling could be explained by QCD because in this theory the partons, which are represented by the quarks and gluons, no longer behave as free particles but interact with each other. Because QCD possesses the property of asymptotic freedom the strong coupling constant α_s vanishes as the energy scale increases. This implies that at large momentum transfer the partons are almost free particles, explaining why just a small breaking of scaling is observed. Due to the smallness of α_s at large scales it is possible to make a series expansion in α_s for the structure functions. In such an expansion the results of the scaling parton model of Feynman just represents the lowest order term. If the higher order corrections are included one can then speak about the QCD improved parton model.

To understand the breaking of scaling quantitatively it is necessary to calculate at least the next-to-leading order term in the perturbation series mentioned above. Such an expansion only makes sense if its convergence is ensured. For this to be true it is necessary that the strong coupling constant α_s is small, or equivalently, that the scale at which the scattering takes place is large. Compared to this scale the masses of the light quarks, represented by u, d and s, are negligible and are usually put equal to zero. The masses of the heavy quarks take their experimental values and they are unequal to zero. Since the light quarks are taken to be massless one encounters collinear divergences in a next-to-leading order calculation. These collinear divergences, sometimes called mass singularities, occur when the momenta of two massless partons emerging from another massless parton become parallel. In a renormalization procedure named "mass factorization" these divergences are absorbed by the parton densities. For the parton densities to be uniquely defined the mass singularities that appear in the calculation should be independent of the process under consideration. In this procedure the removal of the mass singularities introduces an arbitrary scale μ^2 (factorization scale) in the parton densities. Another consequence of mass factorization is that the deep inelastic structure function can be written as a convolution of the parton densities and the so-called coefficient functions. The latter depend on μ^2 as well as on the virtual photon momentum squared q^2. In this way the structure functions become dependent on q^2 which explains the scaling violation of these quantities mentioned before. Since the latter are physical they should be independent of μ^2. This however only happens when one includes all terms in the perturbation series which can be proven using the renormalization group equations. However, in practice one can only compute the structure functions up to finite order of perturbation theory introducing an artificial dependence on μ^2. This dependence is one of the main obstacles in making accurate predictions of physical quantities in perturbative QCD.

1.3 Timelike processes

Besides deep inelastic lepton–hadron scattering there exist other processes to which the QCD improved parton model can be applied. Examples are massive lepton pair production in hadron–hadron scattering and electron–positron annihilation into hadrons. In contrast to deep inelastic scattering which is spacelike the other two processes are timelike. Here spacelike and timelike refer to the momentum of the virtual vector boson (γ, Z or $W^{\pm}$) in the standard model of electroweak interactions through which the process proceeds. In this thesis we will limit ourselves to the two timelike processes mentioned above.

In the early seventies Drell and Yan [19] applied the parton model to massive lepton pair production in hadron–hadron scattering. They assumed that the massive lepton pair was produced in parton–anti-parton annihilation where the parton and anti-parton emerged from each of the two incoming hadrons. Secondly, they made the assumption that the probability to find a (anti) parton inside the hadron, is the same as the one found in deep inelastic electron–proton scattering, discussed

in the previous section. Using the parton densities obtained from the latter reaction one can now make a firm prediction of the cross section of the Drell-Yan process. Furthermore this process enables us to determine the parton densities of unstable particles like $\pi^{\pm}$, $K^{\pm}$ which cannot be measured in deep inelastic lepton–hadron scattering.
Early fixed target experiments [20] revealed that when the Drell-Yan cross section was calculated in the scaling parton model (leading order QCD) the measured cross section exceeds the theoretical one by a factor of two (so-called Drell-Yan K-factor). Higher order corrections should explain this factor providing us with another test of QCD. Besides these higher order corrections the theory also predicts scaling violation of the Drell-Yan cross section. However due to low statistics of the data this phenomenon has never been observed for this process contrary to deep inelastic electron–proton scattering where the number of events is much larger than for the Drell-Yan process.

The calculation of the next-to-leading order corrections [21] could partially explain the large K-factor. However, the corrections turned out to be big at small as well as at large energies raising some questions about the convergence of the perturbation series. Moreover the corrected cross section depends on an arbitrary mass factorization scale μ^2 which also shows up in the calculation of the deep inelastic structure functions. In order to reduce this dependence and to obtain more information about the convergence of the expansion one has calculated higher order corrections to a variety of observables. In particular one has completed the second order corrections [22] to the differential cross section $d\sigma/dQ$ where Q denotes the mass of the di-lepton pair. In the case of the double differential cross section $d^2\sigma/dQdp_T$, where p_T equals the transverse momentum of the electroweak vector boson, one has only calculated the virtual and soft contributions to the next-to-next-to-leading order [23] because the remaining contributions are very hard to obtain. These contributions are determined by infrared (soft) gluons which appear in virtual as well as radiative corrections. Keeping only these contributions one gets the so-called virtual plus soft gluon approximation. The calculation of the first order corrections revealed that the cross section is dominated by the virtual and soft contributions thereby indicating that this might also hold in next-to-next-to-leading order. An analysis of these corrections at collider energies (630 GeV at $Sp\bar{p}S$ and 1.8 TeV at TEVATRON) has been already done in [22] but such an analysis at fixed target energies which are much smaller is still lacking and will be presented in this thesis.

In the calculation of the higher order QCD corrections to the Drell-Yan cross sections above (see [21, 22, 23]) one has taken all quark masses equal to zero. This approximation is correct for the light quarks but is in general wrong for the heavy quarks like charm, bottom or top. For instance in the case of vector boson (γ, Z, $W^{\pm}$) production via the Drell-Yan process one cannot neglect the masses of the bottom and top quark anymore except for the charm which can be treated as massless. Therefore in this thesis we study the effect of the heavy quark mass for the computation of $d\sigma/dQ$ where Q denotes the di-lepton pair mass and compare it with

the case where all quark masses are equal to zero. To that purpose we extend the calculation carried out for Z-production in [24]. In the latter reference only one- and two-loop vertex corrections containing the heavy quark loop have been computed. However there are other two-loop corrections to vector boson production which were not computed in the reference above. Therefore we will calculate these missing parts in this thesis. Besides the virtual corrections the authors in [24] also omitted many parton subprocesses where in addition to the vector boson a heavy quark pair is produced. These subprocesses will be presented in this thesis too so that now, at least up to second order in perturbation theory, all heavy flavour contributions to the Drell-Yan process are complete.

Another important timelike process where the QCD improved parton model can be applied is hadron production in electron–positron annihilation. This process is called semi-inclusive if only one hadron in the final state is detected. Analogous to deep inelastic electron–proton scattering one can express the cross section in relativistic invariant dimensionless quantities which in this case are called fragmentation functions. These describe how the virtual photon or virtual Z-boson, which is produced by the annihilation of the electron and positron, couple to the detected hadron. The angular distribution of the differential cross section consists of three parts. The longitudinal and transverse cross section correspond to the polarization states of the virtual photon and Z-boson with respect to the beam direction. The asymmetrical cross section is related to parity violating terms present in the coupling of the Z-boson to the incoming electron and positron and is absent in purely electromagnetic interactions. From these cross sections one can derive the longitudinal, transverse and asymmetrical fragmentation functions. In the parton model the photon or Z-boson decays into a quark–anti-quark pair. One of these quarks then fragments into the hadron which is detected. In this model only two fragmentation functions appear, namely the transverse and the asymmetrical one which show the behaviour of scaling. They only depend on the scaling variable z which is equal to the fraction of the beam energy carried away by the detected hadron. In order to describe the fragmentation of a parton into hadrons one introduces the concept of a parton fragmentation density. This density, denoted by $D_i^H(z)$, is defined as the probability that a parton of type "i" fragments into a hadron "H" with a fraction "z" of the parton's momentum. The parton model then predicts that the fragmentation functions can be written as the sum over all parton fragmentation densities weighted by the charge squared of each parton. Notice that the "charge" can also stand for the weak coupling constant. As in the case of deep inelastic electron–proton scattering the breaking of scaling is achieved by including higher order QCD corrections. Therefore the fragmentation functions depend in addition to the variable z also on the beam energy. Furthermore QCD predicts the existence of the longitudinal fragmentation function and the gluon fragmentation density, which are both absent in the parton model.
The order α_s corrections to the longitudinal and transverse fragmentations have been calculated in [25] and those to the asymmetrical one are presented in [26]. The analysis of these corrections in [26, 27] showed that the longitudinal fragmentation

function, is far below the data presented in [28]. A large part of this discrepancy between theory and experiment is expected to be due to the omission of higher order corrections and therefore we will present the next-to-next-to-leading order contributions to the fragmentation functions.

1.4 Outline

This thesis will be organized as follows. In chapter 2 the analysis of the next-to-next-to-leading order corrections to the Drell-Yan process at fixed target energies will be presented. In particular since the corrections to the double differential cross section are not complete the validity of the virtual plus soft approximation and the dependence of the results on the mass factorization scale will be discussed.

Chapter 3 deals with the contributions of the heavy flavours (charm, bottom and top quark) to the Drell-Yan cross section at large energies. The relevance of these contributions and the validity and consequences of the zero mass approximation will be investigated.

The remaining chapters will be devoted to the calculation of the order α_s^2 corrections to the longitudinal, transverse and asymmetry fragmentation functions in electron–positron annihilation in the case of the production of hadrons.

References

[1] B.E. Lautrup, A. Peterman and E. de Rafael, Phys. Rep. 3^C (1972) 193. 3

[2] M. Gell-Mann, "The Eightfold Way", Caltech Report CTSL-20 (1961). 3

[3] Y. Ne'eman, Nucl. Phys. **26** (1961) 222. 3

[4] M. Gell-Mann, Proc. 1962 Int. Conf. on High Energy Physics at CERN, editor J. Prentki, page 805;
S. Okubo, Prog. Theor. Phys. **27** (1962) 949. 3

[5] V.E. Barnes *et al.*, Phys. Rev. Lett. **12** (1964) 134, *ibid.* Phys. Rev. Lett. **12** (1964) 204;
G.S. Abrams *et al.*, Phys. Rev. Lett. **13** (1964) 670. 3

[6] M. Gell-Mann, Phys. Lett. **8** (1964) 214. 3

[7] G. Zweig, Unpublished. CERN Preprints, Th. 401, 412 (1964). 3

[8] O.W. Greenberg, Phys. Rev. Lett. **13** (1964) 598. 4

[9] E.D. Bloom, Phys. Rev. Lett. **23** (1969) 931;
M. Breidenbach, J.I. Friedman, H.W. Kendall, E.D. Bloom, D.H. Coward, H. DeStaebler, J. Drees, L.W. Mo and R.E. Taylor, Phys. Rev. Lett. **23** (1969) 935. 4

[10] C.N. Yang and R.L. Mills, Phys. Rev. **96** (1954) 191. 4

[11] I.B. Khriplovich, Yad. Fiz. **10** (1969) 409, *ibid.* Sov. J. Nucl. Phys. **10** (1970) 235;
D.J. Gross and F. Wilczek, Phys. Rev. Lett. **30** (1973) 1343;
H.D. Politzer, Phys. Rev. Lett. **30** (1973) 1346. 4

[12] K.G. Wilson, Phys. Rev. **D10** (1974) 2445. 4, 51, 57, 62

[13] F. Abe *et al.* (CDF Collaboration), Phys. Rev. **D50** (1994) 2966. 4

[14] M. Gell-Mann, Phys. Rev. **125** (1962) 1067. 4

[15] J.D. Bjorken, Phys. Rev. **179** (1969) 1547. 5

[16] R.P. Feynman, Phys. Rev. Lett. **23** (1969) 1415. 5

[17] J.D. Bjorken and E.A. Paschos, Phys. Rev. **185** (1969) 1975. 5

[18] R.E. Taylor, Proceedings of the International Symposium on Lepton and Photon Interactions at High Energies, Stanford 1975. 6, 13, 14, 15, 51

[19] S.D. Drell and T.M. Yan, Phys. Rev. Lett. **25** (1970) 316, *ibid.* Ann. Phys. **66** (1971) 578. 7, 14

[20] J.H. Christenson *et al.*, Phys. Rev. Lett. **25** (1970) 1523, *ibid.* Phys. Rev. **D8** (1973) 2016;
J. Badier *et al.* (NA3 Collaboration), Phys. Lett. **89B** (1979) 145;
R. Barate *et al.*, Phys. Rev. Lett. **43** (1979) 1541. 7, 14, 17

[21] J. Kubar-Andre and F.E. Paige, Phys. Rev. **D19** (1979) 221;
G. Altarelli, R.K. Ellis, and G. Martinelli, Nucl. Phys. **B157** (1979) 461;
B. Humpert, and W.L. van Neerven, Nucl. Phys. **B184** (1981) 225;
G. Parisi, Phys. Lett. **90B** (1980) 295. 7, 14, 18, 19, 20, 42, 51, 52, 53, 61, 63, 64, 66

[22] R. Hamberg, W.L. van Neerven, and T. Matsuura, Nucl. Phys. **B359** (1991) 343;
W.L. van Neerven, and E.B. Zijlstra, Nucl. Phys. **B382** (1992) 11. 7, 14, 17, 19, 43, 51, 86

[23] T. Matsuura, and W.L. van Neerven, Z. Phys. **C38** (1988) 623;
T. Matsuura, S.C. van der Marck and W.L. van Neerven, Phys. Lett. **B211** (1988) 171. 8, 52, 53, 55, 72

[24] D.A. Dicus and S.S.D. Willenbrock, Phys. Rev. **D34** (1986) 148;
R.J. Gonsalves, C.M. Hung and J. Pawłowski, Phys. Rev. **D46** (1992) 4930. 8, 84, 85, 128

[25] G. Altarelli, R.K. Ellis, G. Martinelli, and S.-Y. Pi, Nucl. Phys. **B160** (1979) 301;
R. Baier, and K. Fey, Z. Phys. **C2** (1979) 339. 8, 76, 77, 82, 84, 85, 107, 109, 112, 116, 118, 119, 120, 121, 128

[26] P. Nason, and B.R. Webber, Nucl. Phys. **B421** (1994) 473. 8, 112, 113, 114, 115, 118, 119, 120, 121, 124, 125, 126, 127, 128

[27] J. Binnewies, B.A. Kniehl, and G. Kramer, Z. Phys. **C65** (1995) 471, *ibid.* Phys. Rev. **D52** (1995) 4947. 8, 76, 111, 112, 113, 114, 115, 120, 123, 126, 127, 128

[28] R. Akers *et al.* (OPAL Collaboration), Z. Phys. **C68** (1995) 203;
D. Buskulic *et al.* (ALEPH Collaboration), Phys. Lett. **B357** (1995) 487.

2 Order $\mathcal{O}(\alpha_s^2)$ contributions to the Drell-Yan cross section at fixed target energies

2.1 Introduction

Massive lepton pair production in hadronic interactions is besides deep inelastic lepton–hadron scattering one of the most important probes of the structure of hadrons. It is well established that one of the dominant production mechanisms is the Drell-Yan (DY) process [1]. Here the lepton pair is the decay product of one of the electroweak vector bosons of the standard model (γ^*, W and Z) which in the Born approximation are produced by the annihilation of quarks and anti-quarks coming from the colliding hadrons. This process is of experimental interest because it provides us with an alternative way to measure the parton densities of the proton and neutron which have been very accurately determined by the deep inelastic lepton–hadron experiments. Moreover it enables us to measure the parton densities of unstable hadrons like pions and kaons which is impossible in deep inelastic lepton–hadron scattering. Besides the measurement of the parton densities there are other important tests of perturbative quantum chromo dynamics (QCD) which can be carried out by studying the DY process. Here we want to mention the scale evolution of the parton densities, although not observed in this process because of the low statistics, and the measurement of the running coupling constant $\alpha_s(\mu^2)$ which includes the QCD scale Λ. Finally this process constitutes an important background for other production mechanisms of lepton pairs. Examples are J/Ψ and Υ decays or thermal emission of lepton pairs in heavy-ion collisions [2].
The DY process is also of theoretical interest. Since it is one of the few reactions which can be calculated up to second order in perturbation theory it enables us to study the origin of large QCD corrections which are mostly due to soft gluon bremsstrahlung and virtual gluon contributions. In order to control these corrections in the perturbation series one has constructed various kinds of resummation techniques mostly leading to the exponentiation of the dominant terms [3]-[7]. Another issue is the dependence of the physical quantities on the chosen scheme and the choice of scales. Since the perturbation series is truncated the theoretical cross section will depend on the scheme and the renormalization/factorization scale μ. These dependences can be reduced by including higher order terms in the perturba-

tion series. An alternative way is to determine μ itself (optimum scale) by using so called improved perturbation theory like the principle of minimal sensitivity (PMS) [8], fastest apparent convergence (FAC) [9] or the Brodsky-Lepage-Mackenzie (BLM) procedure [10].
The first fixed target experiment on massive lepton pair production was carried out by the Columbia-BNL group [11]. Later on this process was studied in many other experiments which were carried out at increasing energies (for reviews see [12]). When the statistics of the data was improving one discovered that the cross section could not be described by the simple parton model given by Drell and Yan in [1]. This was revealed for the first time by the NA3 experiment [13] (see also [14]) where the data show a discrepancy in the normalization between the experimental and theoretical cross section. This discrepancy is expressed by a so called K-factor which is defined by the ratio between the experimentally observed cross section and its theoretical prediction. The above group and the experiments carried out later on [15] show that this K-factor ranges between 1.5 and 2.5 and is roughly independent of the type of incoming hadrons. The most generally accepted explanation of this K-factor was provided by perturbative QCD. The calculation of the order α_s corrections [16]-[19] to the DY cross section in [1] show that a considerable part of the K-factor can be attributed to next-to-leading order effects. However the order α_s corrections do not account for the whole K-factor. More recent experiments [20]-[23] still indicate that the ratio between the experimental cross section and the order α_s corrected theoretical prediction is about 1.4, a number which might be explained by including QCD corrections beyond order α_s as we will show in this chapter.
As has been mentioned at the beginning the DY process is one of the few processes where the order α_s^2 corrections to the coefficient function are completely known. The latter refers to the cross section $d\sigma/dm$ only where m denotes the lepton pair invariant mass. This coefficient function has been calculated in the $\overline{\rm MS}$ [24] as well as in the DIS [25] scheme. However in the case of the double differential cross section $d^2\sigma/dmdx_F$ ($d^2\sigma/dmdy$) one has only calculated the order α_s^2 part of the coefficient function which is due to soft and virtual gluon contributions [26] because the remaining part is very complicated to compute. Fortunately as is shown in the literature [16]-[19] the soft plus virtual gluon corrections dominate the total and differential DY cross sections in particular at fixed target energies so that we can restrict to them to make reliable predictions.
An analysis of the higher order corrections to the total DY cross section for W- and Z-production at large hadron collider energies has been performed in [24, 25]. Such an analysis is still missing for the DY process at fixed target energies and therefore we present it here. In particular we want to show that the discrepancy in the normalization between the order α_s corrected DY cross section and the one measured at the fixed target experiments can be partially explained by including the order α_s^2 contributions due to soft plus virtual gluon effects.
This chapter is organized as follows. In section 2 we present the expressions for the various DY cross sections and give a review of the partonic subprocesses included in our analysis. In section 3 the validity of the soft plus virtual gluon approximation

will be discussed and we make a comparison between the order α_s^2 corrected cross section and the most recent fixed target DY data. In appendices A and B we give the coefficient functions for $d^2\sigma/dmdx_F$ ($d^2\sigma/dmdy$) corrected up to order α_s and order α_s^2 respectively. They are presented for arbitrary renormalization and mass factorization scale in the $\overline{\rm MS}$- as well as in the DIS-scheme.

2.2 Higher order QCD corrections to $d^2\sigma/dmdx_F$ ($d^2\sigma/dmdy$) and $d\sigma/dm$

Massive lepton pair production in hadron-hadron collisions proceeds through the following reaction

$$\begin{aligned} H_1 + H_2 \;\rightarrow\; & V \;+\; \text{“}X\text{”} \\ & \hookrightarrow\; \ell_1 + \ell_2, \end{aligned} \tag{2.2.1}$$

Here H_1 and H_2 denote the incoming hadrons and V is one of the vector bosons of the standard model (γ^*, Z or W) which subsequently decays into a lepton pair (ℓ_1, ℓ_2). The symbol “X” denotes any inclusive hadronic final state which is allowed by conservation of quantum numbers. Following the QCD improved parton model as originally developed in [1] the double differential DY cross section can be written as

$$\frac{d^2\sigma}{dQ^2dx_F} = \sum_{i,j} \sigma_V(Q^2, M_V^2) \int_{x_1}^1 dt_1 \int_{x_2}^1 dt_2\, H_{ij}(t_1, t_2, \mu^2)\Delta_{ij}(t_1, t_2, x_1, x_2, Q^2, \mu^2). \tag{2.2.2}$$

Here $Q^2 = m^2$ where m denotes the lepton pair invariant mass. The longitudinal momentum fraction x_F of the lepton pair and the Bjorken scaling variable are defined by

$$x_F = x_1 - x_2 = \frac{2p_L}{\sqrt{S}}, \qquad\qquad \tau = \frac{Q^2}{S} = x_1 x_2, \tag{2.2.3}$$

where $\sqrt{S}$ stands for the center of mass energy of the incoming hadrons H_1 and H_2. The quantity σ_V is the pointlike DY cross section which describes the process

$$q_1 + \bar{q}_2 \rightarrow V \rightarrow \ell_1 + \ell_2, \tag{2.2.4}$$

where q_1 and $\bar{q}_2$ denote the incoming quark and anti-quark respectively. If we limit ourselves to $V = \gamma^*$,Z then σ_V gets the form

$$\begin{aligned} \sigma_V(Q^2, M_Z^2) \;=\; & \tau\, \frac{4\pi\alpha^2}{9Q^4} \left[e_\ell^2 e_q^2 + \frac{2Q^2(Q^2 - M_Z^2)}{|Z(Q^2)|^2} e_\ell e_q C_{V,\ell} C_{V,q} \right. \\ & \left. + \frac{(Q^2)^2}{|Z(Q^2)|^2} (C_{V,\ell}^2 + C_{A,\ell}^2)(C_{V,q}^2 + C_{A,q}^2) \right], \end{aligned} \tag{2.2.5}$$

with

$$Z(Q^2) = Q^2 - M_Z^2 + iM_Z\Gamma_Z. \tag{2.2.6}$$

Here the width of the Z-boson is taken to be energy independent and all fermion masses are neglected since they are much smaller than $\sqrt{Q^2}$. The charges of the leptons and quarks are given by

$$e_\ell = -1, \quad e_u = \frac{2}{3}, \quad e_d = -\frac{1}{3}. \tag{2.2.7}$$

The vector- and axial-vector coupling constants of the Z-boson to the leptons and quarks are equal to

$$\begin{aligned} &C_{A,\ell} = \frac{1}{2\sin 2\theta_W} && C_{V,\ell} = -C_{A,\ell}(1 - 4\sin^2\theta_W) \\ &C_{A,u} = -C_{A,d} = -C_{A,\ell} \\ &C_{V,u} = C_{A,\ell}\left(1 - \tfrac{8}{3}\sin^2\theta_W\right) && C_{V,d} = -C_{A,\ell}\left(1 - \tfrac{4}{3}\sin^2\theta_W\right). \end{aligned} \tag{2.2.8}$$

The function H_{ij} in (2.2.2) stands for the combination of parton densities corresponding to the incoming partons i and j $(i, j = q, \bar{q}, g)$. Finally Δ_{ij} denotes the DY coefficient function which is determined by the partonic subprocess

$$i + j \to V + \text{“}X\text{”}, \tag{2.2.9}$$

where “X” now represents any multi partonic final state. Both functions H_{ij} and Δ_{ij} depend in addition to the scaling variables t_i and x_i also on the renormalization and mass factorization scales which are usually put to be equal to μ. Besides the cross section in (2.2.2) one is sometimes also interested in the rapidity distribution of the lepton pair. In this case the left hand side in (2.2.2) is replaced by $d^2\sigma/dQ^2dy$ where y denotes the rapidity defined by (see (2.2.3))

$$y = \frac{1}{2}\ln\frac{x_1}{x_2}, \quad x_1 = \sqrt{\tau}\, e^y, \quad x_2 = \sqrt{\tau}\, e^{-y}, \tag{2.2.10}$$

or

$$y = \frac{1}{2}\ln\frac{x_F + \sqrt{x_F^2 + 4\tau}}{-x_F + \sqrt{x_F^2 + 4\tau}}. \tag{2.2.11}$$

Furthermore on the right hand side the coefficient function Δ_{ij} is replaced by its analogue corresponding to the cross section $d^2\sigma/dQ^2dy$.
The coefficient function Δ_{ij} (2.2.2) can be expanded as a power series in the running coupling constant $\alpha_s(\mu^2)$ as follows

$$\Delta_{ij} = \sum_{n=0}^{\infty}\left(\frac{\alpha_s(\mu^2)}{4\pi}\right)^n \Delta_{ij}^{(n)}. \tag{2.2.12}$$

In lowest order the coefficient function of the differential cross section (2.2.2) is determined by the subprocess

$$q + \bar{q} \to V. \tag{2.2.13}$$

Here V either stands for the virtual photon γ^* or the Z-boson and the coefficient function is given by

$$\Delta_{q\bar{q}}^{(0)} = \frac{1}{x_1 + x_2}\delta(t_1 - x_1)\,\delta(t_2 - x_2). \tag{2.2.14}$$

The order α_s corrections to the Born process (2.2.13) denoted by $\Delta_{q\bar{q}}^{(1)}$ are given by the one-loop contributions to (2.2.13) and the gluon bremsstrahlung process

$$q + \bar{q} \to V + g. \tag{2.2.15}$$

In addition to the process above we have another reaction which instead of a quark or anti-quark has a gluon in the initial state

$$g + q(\bar{q}) \to V + q(\bar{q}). \tag{2.2.16}$$

This reaction contributes to $\Delta_{gq}^{(1)}$. Both contributions $\Delta_{q\bar{q}}^{(1)}$ and $\Delta_{gq}^{(1)}$ have been calculated in [17, 18, 27] (DIS-scheme) and in [28] ($\overline{\rm MS}$-scheme) and are presented in (A.1) and (A.7), (A.8) respectively. A part of the order α_s^2 corrections to the coefficient function corresponding to $d^2\sigma/dQ^2dx_F$ has also been calculated in [26]. These corrections originate from the soft plus virtual gluon contributions. They consist of the two-loop corrections to process (2.2.13) and the one-loop correction to process (2.2.15) where the gluon is taken to be soft. Furthermore one has also included the bremsstrahlungs process

$$q + \bar{q} \to V + g + g, \tag{2.2.17}$$

and fermion pair production

$$q + \bar{q} \to V + q + \bar{q}, \tag{2.2.18}$$

where the gluons were taken to be soft and the quark–anti-quark pair in the final state of (2.2.18) has a low invariant mass.
All above corrections contribute to $\Delta_{q\bar{q}}^{(2)}$ and can be found in appendix B for arbitrary factorization and renormalization scale μ where they are presented in the $\overline{\rm MS}$- as well as in the DIS-scheme. The hard gluon corrections (2.2.17) and the other two-to-three body processes (see below) are very hard to compute at least for the double differential cross sections. Fortunately as has been shown in [16]-[19] the bulk of the order α_s radiative corrections to the cross sections $d\sigma/dQ^2$ and $d^2\sigma/dQ^2dx_F$ is constituted by the soft plus virtual gluon contributions to $\Delta_{q\bar{q}}^{(1)}$. Therefore within the experimental and theoretical uncertainties one can assume that the order α_s^2 part of the coefficient function $\Delta_{q\bar{q}}$ which is only due to soft plus virtual gluon contributions

is sufficient to describe the next-to-next-to-leading order DY cross section at fixed target energies. This can be tested for the quantity $d\sigma/dQ^2$ which is defined by

$$\frac{d\sigma}{dQ^2} = \int_{\tau-1}^{1-\tau} dx_F \frac{d^2\sigma}{dQ^2 dx_F} \quad \text{or} \quad \frac{d\sigma}{dQ^2} = \int_{\frac{1}{2}\ln\tau}^{-\frac{1}{2}\ln\tau} dy \frac{d^2\sigma}{dQ^2 dy}, \tag{2.2.19}$$

which can also be written as

$$\frac{d\sigma}{dQ^2} = \sum_{i,j} \sigma_V(Q^2, M_V^2) \int_\tau^1 \frac{dx_1}{x_1} \int_{\frac{\tau}{x_1}}^1 \frac{dx_2}{x_2} H_{ij}(x_1, x_2, \mu^2) \Delta_{ij}\left(\frac{\tau}{x_1 x_2}, \frac{Q^2}{\mu^2}\right), \tag{2.2.20}$$

where Δ_{ij} now stands for the coefficient function corresponding to the integrated cross section $d\sigma/dQ^2$.
Since the exact order α_s^2 corrections to this coefficient function are completely known see [24] ($\overline{\text{MS}}$-scheme) and [25] (DIS-scheme) one can now make a comparison between the exact DY cross section coming from the complete coefficient function and the approximate cross section due to the soft plus virtual gluon part. The full order α_s^2 contribution to the DY coefficient function requires besides the calculation of the subprocesses mentioned above the computation of the following two-to-three body partonic subprocesses. First we have the bremsstrahlungs correction to (2.2.16)

$$g + q(\bar{q}) \to V + q(\bar{q}) + g, \tag{2.2.21}$$

which entails the computation of the one-loop corrections to (2.2.16). In addition one has to add the subprocesses

$$q_1 + \bar{q}_2 \to V + q_1 + \bar{q}_2, \tag{2.2.22}$$

$$q(\bar{q}) + q(\bar{q}) \to V + q(\bar{q}) + q(\bar{q}), \tag{2.2.23}$$

and

$$g + g \to V + q + \bar{q}. \tag{2.2.24}$$

Reactions (2.2.21), (2.2.22), (2.2.23) and (2.2.24) contribute to the coefficient functions $\Delta_{gq}^{(2)}$, $\Delta_{q\bar{q}}^{(2)}$, $\Delta_{qq}^{(2)}$ and $\Delta_{gg}^{(2)}$ respectively. The exact result of the coefficient function calculated up to order α_s^2 for $d\sigma/dQ^2$ gives an indication about the validity of the soft plus virtual gluon approximation of $d^2\sigma/dQ^2 dx_F$ (or $d^2\sigma/dQ^2 dy$) for which a complete order α_s^2 calculation is still missing. In [25] one has made a detailed analysis of this approximation for the total cross section of W- and Z- production which is derived from (2.2.20) by integrating $d\sigma/dQ^2$ over Q^2. From this analysis one infers that the approximation works quite well in order α_s as well as in order α_s^2 when $M_V^2/S > 0.01$ provided the DY coefficient function is computed in the DIS-scheme. This implies that in practice one can only apply it to the cross section measured at the Sp$\bar{\text{p}}$S ($\sqrt{S} = 0.63\,\text{TeV}$). The reason that this happens in the DIS-scheme is purely accidental. It originates from the large coefficient of the delta-function $\delta(1-x)$ appearing in $\Delta_{q\bar{q}}(x)$ which is small in the $\overline{\text{MS}}$-scheme. Apparently the combination of the anomalous dimension (Altarelli-Parisi splitting function) and

the remaining part of the coefficient function is very small in the DIS-scheme. It is expected that the approximation will even work better when $\tau = Q^2/S \to 1$, a condition which is satisfied by fixed target experiments. In this case the phase space of the multi partonic final state in the above reactions will be reduced so that only soft gluons or fermion pairs with low invariant mass can be radiated off. Their contributions manifest themselves by large logarithms of the type $(\ln^k(1-x)/(1-x))_+$ which appear in the coefficient function in the DIS- as well as in the $\overline{\text{MS}}$-scheme. Notice that the above analysis holds if the mass factorization scale μ is chosen to be $\mu^2 = Q^2$. Therefore it is not impossible that the above conclusions have to be altered when a scale completely different from $\mu^2 = Q^2$ is adopted.
Finally one has to bear in mind that a complete next-to-next-to-leading order analysis cannot be carried out yet because the appropriate parton densities are not available. The latter can be attributed to the fact that the three-loop contributions to the Altarelli-Parisi splitting functions or the anomalous dimensions have not been calculated up to so far. Therefore the analysis of the order α_s^2 corrected result for $d\sigma/dQ^2$ has to be considered with caution. This holds even more for the order α_s^2 corrected differential distribution $d^2\sigma/dQ^2dx_F$ or $d^2\sigma/dQ^2dy$.

2.3 Results

In this section we start with a discussion of the validity of the soft plus virtual gluon ($S+V$) approximation of the order α_s^2 correction to $d^2\sigma/dQ^2dx_F$ (2.2.2). This is done by making a comparison with the integrated cross section $d\sigma/dQ^2$ (2.2.19) for which the coefficient function is completely known up to order α_s^2. Then we include this approximation in our analysis of the fixed target muon pair data published in [20]-[23]. In particular we show that this correction partially accounts for the difference in the normalization between the data in [20]-[23] and the order α_s corrected cross section calculated in [17, 18, 27, 28].

2.3.1 The validity of the soft plus virtual gluon approximation

The calculation of the cross sections $d\sigma/dQ^2$ (2.2.19) and $d^2\sigma/dQ^2dx_F$ (2.2.2) will be performed in the DIS- as well as in the $\overline{\text{MS}}$-scheme chosen for the coefficient functions as well as for the parton densities. The coefficient functions for $d\sigma/dQ^2$ up to order α_s^2 can be found in [24] ($\overline{\text{MS}}$-scheme) and [25] (DIS-scheme). The coefficient functions for $d^2\sigma/dQ^2dx_F$ corrected up to order α_s are obtained from [17, 18, 27] (DIS-scheme) and [28] ($\overline{\text{MS}}$-scheme). The order α_s^2 contribution as far as the soft plus virtual gluon part is concerned has been calculated in [26] and is presented in both schemes in a more amenable form in appendix B. For the next-to-leading order nucleon parton densities we have chosen the MRS(D-) set [29] for which a DIS- ($\Lambda = 230\,\text{MeV}$) and an $\overline{\text{MS}}$-version ($\Lambda = 215\,\text{MeV}$) exist. Further we use the two-loop ($\overline{\text{MS}}$-scheme) corrected running coupling constant with the number of light flavours $n_f = 4$ and the QCD scale is the same as chosen for the MRS(D-)

set. For the pion densities we take the leading log parametrization (DO1) in [30]. Using this set one could only fit the old lepton-pair data (for references see [30]) by allowing an arbitrary normalization (or K-factor) with respect to the leading order theoretical DY cross section. In this section it is shown that this factor can be partially explained by including higher order QCD corrections. Next-to-leading (NLO) order parton densities for the pion exist in [28] and [31] but they are only presented in the $\overline{\text{MS}}$-scheme. Also here one has to use an arbitrary K-factor to fit the data which is smaller than found for the leading order process since a part of the normalization is accounted for by the order α_s corrections. Because of the missing (NLO) parton densities of the pion in the DIS-scheme we prefer to use the leading log parametrization in [30]. Finally we choose the factorization scale μ to be equal to the renormalization scale where $\mu^2 = Q^2$.
The plots will be presented at three different fixed target energies given by $\sqrt{S} = 15.4\,; 21.8$ and $38.8\,\text{GeV}$. At the first energy i.e. $\sqrt{S} = 15.4\,\text{GeV}$ one has observed muon pairs produced in the reactions $\bar{p} + W \to \mu^+\mu^- + \text{“}X\text{”}$ and $\pi^- + W \to \mu^+\mu^- + \text{“}X\text{”}$ measured by the E537 group [20]. The second experiment is carried out at $\sqrt{S} = 21.8\,\text{GeV}$ by the E615 [21] group where the same lepton pair is measured in the reaction $\pi^- + W \to \mu^+\mu^- + \text{“}X\text{”}$. Finally we discuss the E772 experiment [22, 23] at $\sqrt{S} = 38.8\,\text{GeV}$ where the reaction $p + N \to \mu^+\mu^- + \text{“}X\text{”}$ is studied where N is either represented by the isoscalar targets ${}^2H$ and C or by W (tungsten) which has a large neutron excess. Here we will only make a comparison with the ${}^2H$-data. In the case of the E537, E615 experiments W is given by $Z/A = 0.405$ whereas E772 used tungsten with $Z/A = 0.409$. Here Z and A denote the charge and atomic number of the nucleus respectively. Finally notice that at the above energies we can safely neglect the contributions coming from the Z-boson in (2.2.5) since the virtual photon dominates the cross section.

Discussion of the $S + V$ approximation in the case of $d\sigma/dQ^2$

Let us first start with the discussion of the $S + V$ approximation to the coefficient function corresponding to $d\sigma/dQ^2$. The soft plus virtual gluon part of the coefficient function, which only appears in $\Delta_{q\bar{q}}$, can be written as

$$\Delta_{q\bar{q}}^{S+V}(x, Q^2, \mu^2) = \delta(1-x) + \sum_{i=1}^{\infty} \left(\frac{\alpha_s(\mu^2)}{4\pi}\right)^i \Bigg[\sum_{j=0}^{2i-1} a_j^{(i)}(Q^2, \mu^2) \left(\frac{\ln^j(1-x)}{1-x}\right)_+ + \delta(1-x) b^{(i)}(Q^2, \mu^2) \Bigg], \tag{2.3.1}$$

where the logarithms have to be interpreted in the distributional sense (see [17]). The coefficients $a_j^{(i)}$ and $b^{(i)}$ depend on Q^2 and the factorization scale μ^2. The above coefficients can be read off the explicit form of (2.3.1) given by eqs. (B.3), (B.8) in [24] and (A.3), (A.8) in [25]. In order to test the $S + V$ approximation to the DY

cross section we study the following ratios

$$R^{(1)}(\sqrt{\tau}) = \frac{\dfrac{d\sigma^{(0)}}{dm} + \dfrac{d\sigma^{S+V,(1)}}{dm}}{\dfrac{d\sigma^{(0)}}{dm} + \dfrac{d\sigma^{(1)}}{dm}}, \tag{2.3.2}$$

and

$$R^{(2)}(\sqrt{\tau}) = \frac{\dfrac{d\sigma^{(0)}}{dm} + \dfrac{d\sigma^{(1)}}{dm} + \dfrac{d\sigma^{S+V,(2)}}{dm}}{\dfrac{d\sigma^{(0)}}{dm} + \dfrac{d\sigma^{(1)}}{dm} + \dfrac{d\sigma^{(2)}}{dm}}. \tag{2.3.3}$$

In the above expressions $d\sigma^{(i)}/dm$ ($m = \sqrt{Q^2}$) denotes the $\mathcal{O}(\alpha_s^i)$ contribution to the DY cross section containing the exact $\mathcal{O}(\alpha_s^i)$ part of the coefficient function where all partonic subprocesses are included. The quantities $d\sigma^{S+V,(i)}/dm$ stand for the $\mathcal{O}(\alpha_s^i)$ contribution to the cross sections where only the soft plus virtual gluon part of the coefficient function according to (2.3.1) is taken into account.

In fig. 2.1 we have plotted $R^{(1)}(\sqrt{\tau})$ and $R^{(2)}(\sqrt{\tau})$ in the DIS-scheme for the $\sqrt{\tau}$-ranges explored by the three experiments mentioned above. From the figure we infer that the $S+V$ approximation overestimates the exact cross section by less than 10% at small $\sqrt{\tau}$-values. At large $\sqrt{\tau}$-values this becomes better which is to be expected since in the limit $\tau \to 1$ the approximation becomes equal to the exact correction. In this limit hard gluon radiation and all other partonic subprocesses like quark-gluon scattering are suppressed because of the reduction in phase space. By comparing $R^{(2)}(\sqrt{\tau})$ with $R^{(1)}(\sqrt{\tau})$ we observe a slight improvement when higher order corrections are included in the denominator as well as in the numerator. In fig. 2.2 we did the same as in fig. 2.1 but now for the $\overline{\text{MS}}$-scheme. Here we observe that the $S+V$ approximation underestimates the exact DY cross section by more than 10% in particular when the C.M. energy $\sqrt{S}$ is small like in the case of E537 ($\sqrt{S} = 15.4\,\text{GeV}$) or E615 ($\sqrt{S} = 21.8\,\text{GeV}$). Furthermore $R^{(2)}(\sqrt{\tau})$ (2.3.3) becomes worse than $R^{(1)}(\sqrt{\tau})$ (2.3.2) in particular in the low $\sqrt{\tau}$-region. Hence we can conclude that for $d\sigma/dm$ the $S+V$ approximation works better in the DIS-scheme than in the $\overline{\text{MS}}$-scheme.

Discussion of the $S+V$ approximation in the case of $d^2\sigma/dmdx_F$

In the case of the double differential cross section $d^2\sigma/dmdx_F$ ($m = \sqrt{Q^2}$) the exact order α_s^2 contribution to the coefficient function is not known so that one can only make a comparison on the order α_s level. The $S+V$ part of the coefficient function, of which the explicit form is given up to order α_s^2 in appendices A and B, becomes

$$\Delta_{q\bar{q}}^{S+V}(t_1, t_2, x_1, x_2, Q^2, \mu^2) = \frac{1}{x_1 + x_2}\Big[\delta(t_1 - x_1)\,\delta(t_2 - x_2)$$

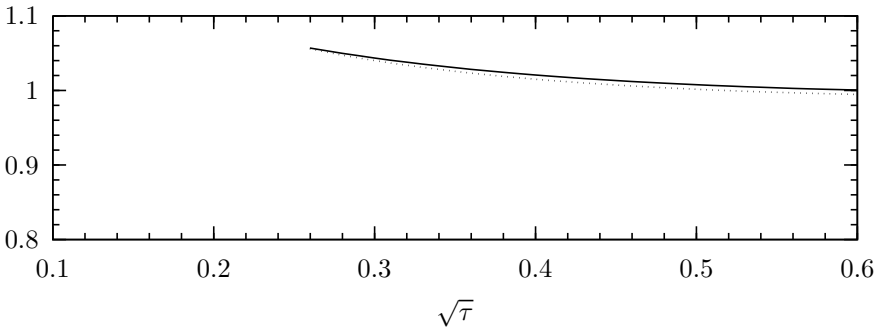

(a) $\sqrt{S} = 15.4\,\text{GeV}$ ($0.26 < \sqrt{\tau} < 0.60$, E537).

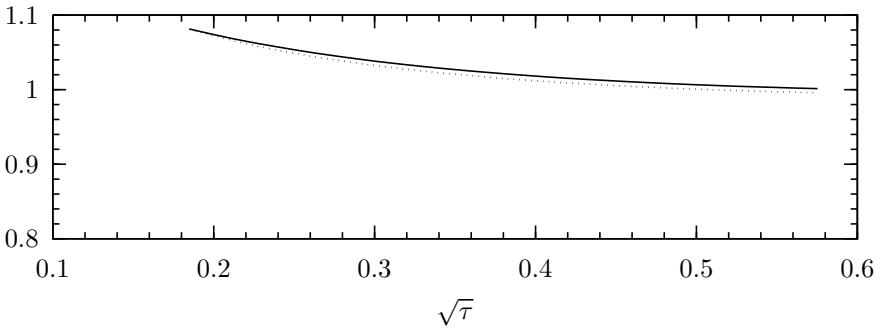

(b) $\sqrt{S} = 21.8\,\text{GeV}$ ($0.185 < \sqrt{\tau} < 0.575$, E615).

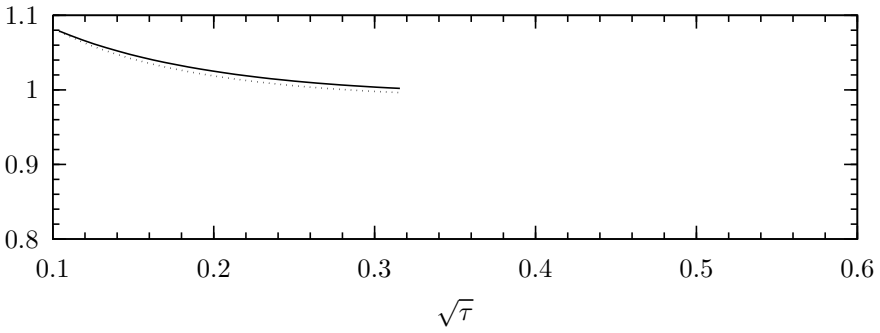

(c) $\sqrt{S} = 38.8\,\text{GeV}$ ($0.125 < \sqrt{\tau} < 0.342$, E772).

Figure 2.1: *The ratios $R^{(1)}(\sqrt{\tau})$ (2.3.2) and $R^{(2)}(\sqrt{\tau})$ (2.3.3) presented in the DIS-scheme. Solid line: $R^{(1)}(\sqrt{\tau})$; dotted line: $R^{(2)}(\sqrt{\tau})$.*

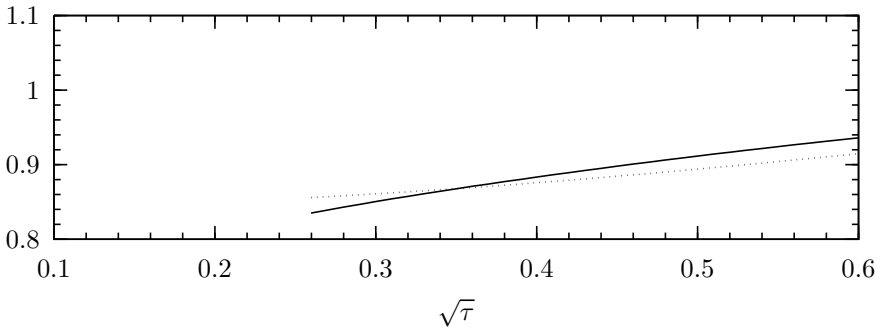

(a) $\sqrt{S} = 15.4\,\text{GeV}$ ($0.26 < \sqrt{\tau} < 0.60$, E537).

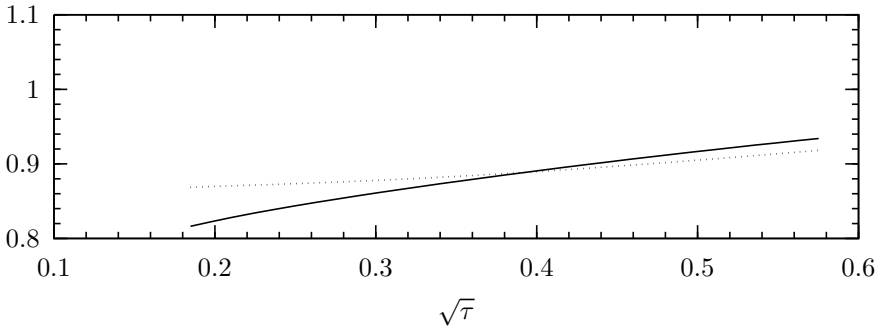

(b) $\sqrt{S} = 21.8\,\text{GeV}$ ($0.185 < \sqrt{\tau} < 0.575$, E615).

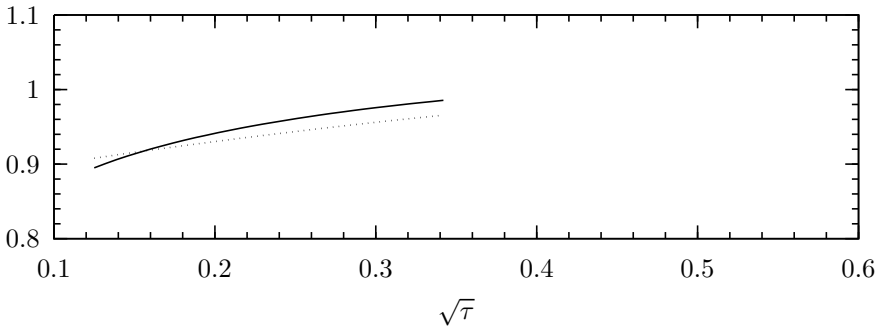

(c) $\sqrt{S} = 38.8\,\text{GeV}$ ($0.125 < \sqrt{\tau} < 0.342$, E772).

Figure 2.2: *The ratios $R^{(1)}(\sqrt{\tau})$ (2.3.2) and $R^{(2)}(\sqrt{\tau})$ (2.3.3) presented in the $\overline{\text{MS}}$-scheme. Solid line: $R^{(1)}(\sqrt{\tau})$; dotted line: $R^{(2)}(\sqrt{\tau})$.*

$$+\sum_{i=1}^{\infty}\left(\frac{\alpha_s(\mu^2)}{4\pi}\right)^i\Bigg\{\sum_{\substack{k,l\\ k+l\le 2i-2}} a_{kl}^{(i)}(Q^2,\mu^2)\left(\frac{\ln^k(t_1/x_1-1)}{t_1-x_1}\right)_+\left(\frac{\ln^l(t_2/x_2-1)}{t_2-x_2}\right)_+$$

$$+\delta(t_1-x_1)\sum_{\substack{k,l\\ k+l\le 2i-1}} b_{kl}^{(i)}(Q^2,\mu^2)\left(\frac{\ln^k(t_2/x_2-1)}{t_2-x_2}\right)_+\ln^l\frac{1-x_1}{x_1}$$

$$+\delta(t_2-x_2)\sum_{\substack{k,l\\ k+l\le 2i-1}} b_{kl}^{(i)}(Q^2,\mu^2)\left(\frac{\ln^k(t_1/x_1-1)}{t_1-x_1}\right)_+\ln^l\frac{1-x_2}{x_2}$$

$$+\delta(t_1-x_1)\delta(t_2-x_2)\sum_{\substack{k,l\\ k+l\le 2i}} c_{kl}^{(i)}(Q^2,\mu^2)\ln^k\frac{1-x_1}{x_1}\ln^l\frac{1-x_2}{x_2}\Bigg\}\Bigg] \qquad (2.3.4)$$

where the definitions for the distributions indicated by a plus sign can be found in appendix A.

To study the $S+V$ approximation we define an analogous quantity as given for $d\sigma/dm$ in (2.3.2). In the subsequent figures we plot the ratio

$$d\,R^{(1)}(\sqrt{\tau},x_F)=\frac{\dfrac{d^2\sigma^{(0)}}{dmdx_F}+\dfrac{d^2\sigma^{S+V,(1)}}{dmdx_F}}{\dfrac{d^2\sigma^{(0)}}{dmdx_F}+\dfrac{d^2\sigma^{(1)}}{dmdx_F}}, \qquad (2.3.5)$$

where the meaning of $d^2\sigma^{(i)}/dmdx_F$ and $d^2\sigma^{S+V,(i)}/dmdx_F$ is the same as for $d\sigma^{(i)}/dm$ and $d\sigma^{S+V,(i)}/dm$ defined below (2.3.3). Notice that here we cannot present $d\,R^{(2)}(\sqrt{\tau},x_F)$ because the exact cross section $d^2\sigma^{(2)}/dmdx_F$ is still unknown.

Starting with the DIS-scheme we have plotted $d\,R^{(1)}(\sqrt{\tau},x_F)$ at $\sqrt{S}=15.4\,\mathrm{GeV}$ (E537) for three representative $\sqrt{\tau}$-values as a function of x_F in fig. 2.3. From this figure one infers that at small $\sqrt{\tau}$ around $x_F=0$ the approximate cross section overestimates the exact one by about 20%. This value is much larger than in the case of the integrated cross section $d\sigma/dm$ where it was at maximum 10%. The approximation becomes better when either $|x_F|$ or $\sqrt{\tau}$ gets larger.

The overestimation is even bigger when the energy increases. This can be observed in fig. 2.4 ($\sqrt{S}=21.8\,\mathrm{GeV}$, E615) or fig. 2.5 ($\sqrt{S}=38.8\,\mathrm{GeV}$, E772). Here one overestimates the exact cross section at small $\sqrt{\tau}$-values even by 25%. If we repeat our calculations in the $\overline{\mathrm{MS}}$-scheme we observe a considerable improvement of the $S+V$ approximation to the double differential cross section (see figs. 2.6-2.8).

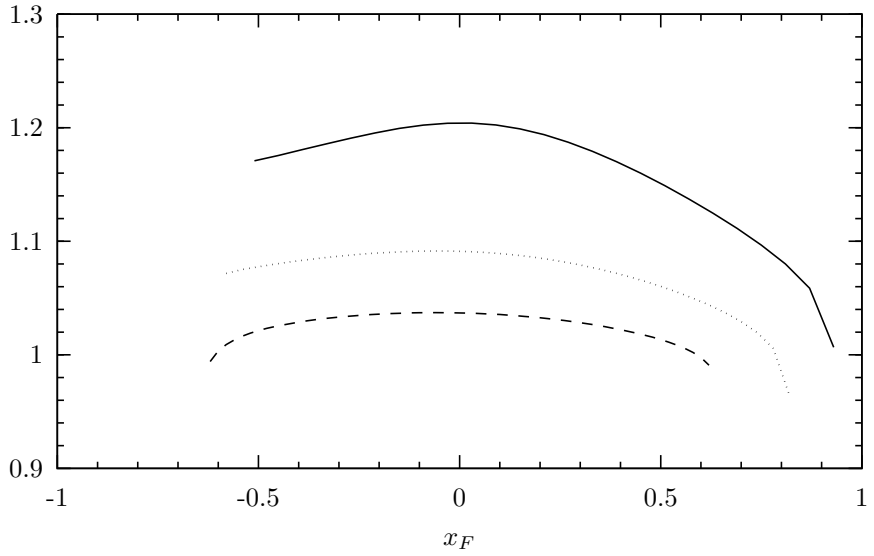

Figure 2.3: *The ratio* $d\,R^{(1)}(\sqrt{\tau}, x_F)$ *(2.3.5) presented in the DIS-scheme for* $\pi^- + W \to \mu^+\mu^- +$ *"X" at* $\sqrt{S} = 15.4\,GeV$ *(E537). Solid line:* $\sqrt{\tau} = 0.25$*; dotted line:* $\sqrt{\tau} = 0.42$*; dashed line:* $\sqrt{\tau} = 0.60$.

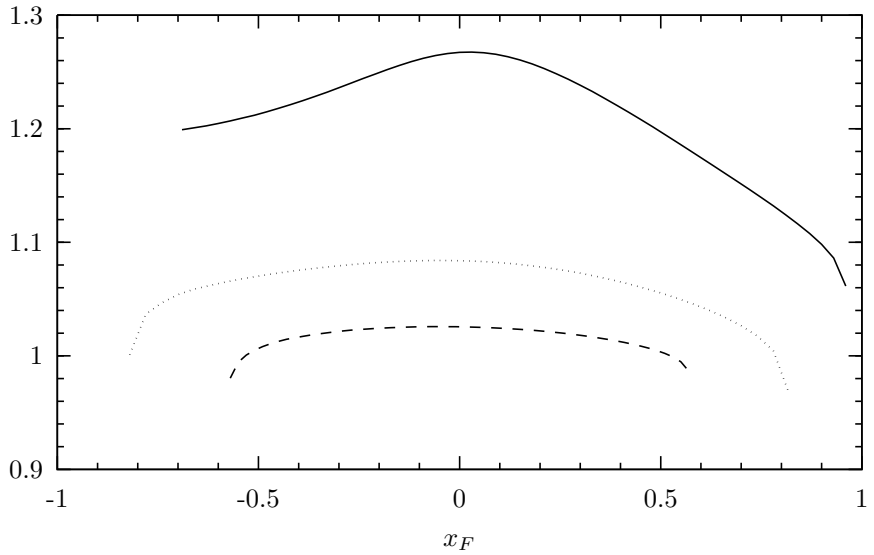

Figure 2.4: *The ratio* $d\,R^{(1)}(\sqrt{\tau}, x_F)$ *(2.3.5) presented in the DIS-scheme for* $\pi^- + W \to \mu^+\mu^- +$ *"X" at* $\sqrt{S} = 21.8\,GeV$ *(E615). Solid line:* $\sqrt{\tau} = 0.18$*; dotted line:* $\sqrt{\tau} = 0.42$*; dashed line:* $\sqrt{\tau} = 0.65$.

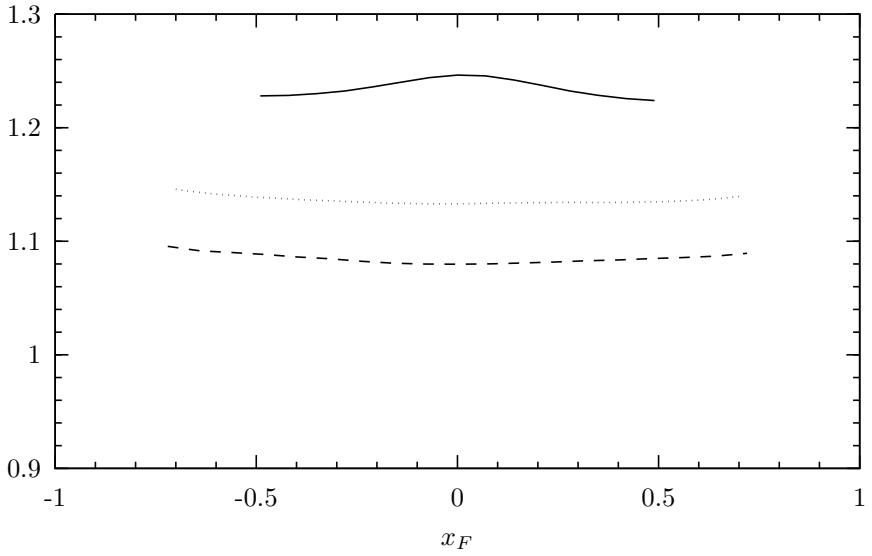

Figure 2.5: *The ratio* $d\,R^{(1)}(\sqrt{\tau}, x_F)$ *(2.3.5) presented in the DIS-scheme for* $p + {}^2H \to \mu^+\mu^- +$ *"X" at* $\sqrt{S} = 38.8\,GeV$ *(E772). Solid line:* $\sqrt{\tau} = 0.13$*; dotted line:* $\sqrt{\tau} = 0.23$*; dashed line:* $\sqrt{\tau} = 0.34$*.*

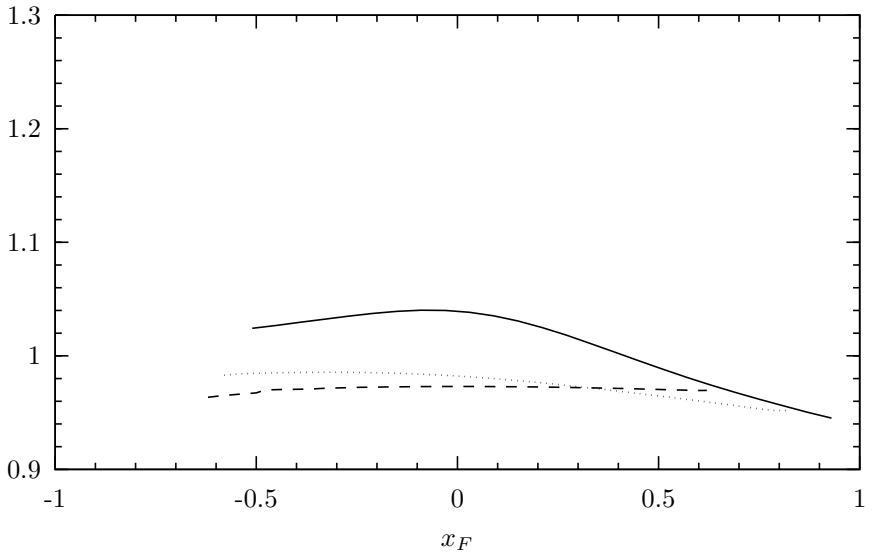

Figure 2.6: *The ratio* $d\,R^{(1)}(\sqrt{\tau}, x_F)$ *(2.3.5) presented in the* $\overline{\text{MS}}$*-scheme for* $\pi^- + W \to \mu^+\mu^- +$ *"X" at* $\sqrt{S} = 15.4\,GeV$ *(E537). Solid line:* $\sqrt{\tau} = 0.25$*; dotted line:* $\sqrt{\tau} = 0.42$*; dashed line:* $\sqrt{\tau} = 0.60$*.*

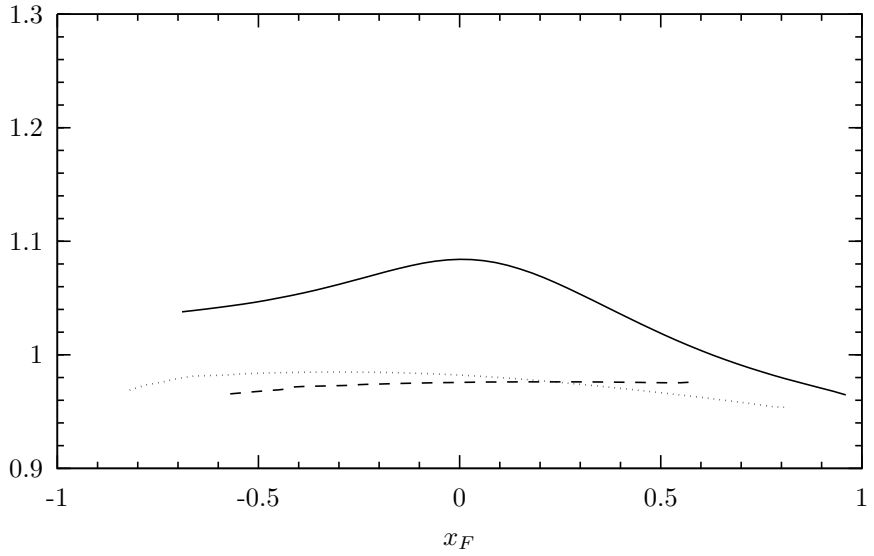

Figure 2.7: *The ratio* $d\,R^{(1)}(\sqrt{\tau}, x_F)$ *(2.3.5) presented in the* $\overline{\text{MS}}$*-scheme for* $\pi^- + W \to \mu^+\mu^- +$ *"X" at* $\sqrt{S} = 21.8\,GeV$ *(E615). Solid line:* $\sqrt{\tau} = 0.18$*; dotted line:* $\sqrt{\tau} = 0.42$*; dashed line:* $\sqrt{\tau} = 0.65$.

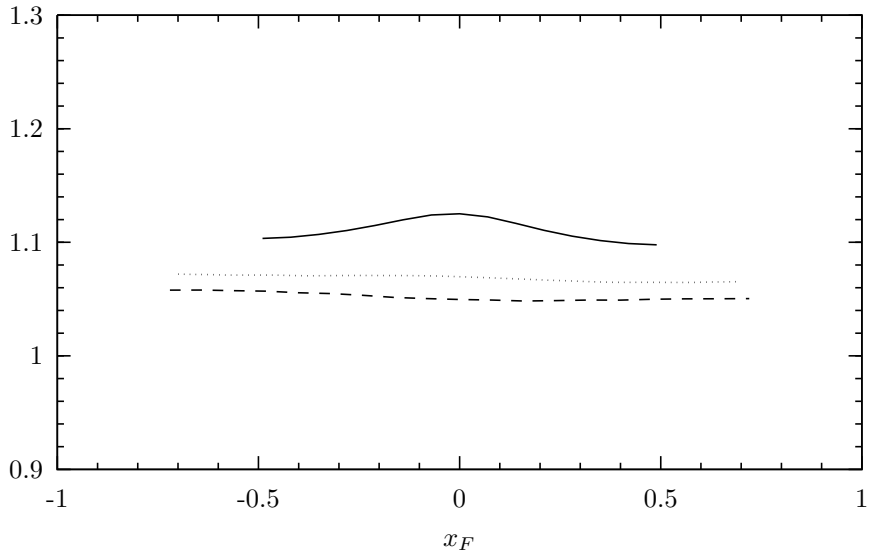

Figure 2.8: *The ratio* $d\,R^{(1)}(\sqrt{\tau}, x_F)$ *(2.3.5) presented in the* $\overline{\text{MS}}$*-scheme for* $p + {}^2H \to \mu^+\mu^- +$ *"X" at* $\sqrt{S} = 38.8\,GeV$ *(E772). Solid line:* $\sqrt{\tau} = 0.13$*; dotted line:* $\sqrt{\tau} = 0.23$*; dashed line:* $\sqrt{\tau} = 0.34$.

Although like in the case of $d\sigma/dm$ the approximation underestimates the cross section at high $\sqrt{\tau}$-values the difference with the exact one is less than 5%.

Conclusion

Summarizing our findings we conclude that in the case of the DIS-scheme the $S+V$ approximation works better for $d\sigma/dm$ than for $d^2\sigma/dmdx_F$ whereas for the $\overline{\text{MS}}$-scheme just the opposite is happening, except for $\tau \to 1$ where $R^{(1)}(\sqrt{\tau})$ and $d\,R^{(1)}(\sqrt{\tau}, x_F)$ become close to 1 independent of the chosen scheme. Further from figs. 2.3-2.8 it appears that when $d^2\sigma^{S+V,(1)}/dmdx_F$ is integrated over x_F according to (2.2.19) we get a result which differs from the one obtained from $d\sigma^{S+V,(1)}/dm$ in (2.2.20) in particular at small $\sqrt{\tau}$. On the first sight this is surprising because one expects the same cross section $d\sigma/dm$ independent of the order of integration. However both procedures only lead to the same answer for $d\sigma/dm$ when the full coefficient functions are inserted in the equations for $d^2\sigma/dmdx_F$ (2.2.2) and $d\sigma/dm$ (2.2.20). If we limit ourselves to the $S+V$ part of the coefficient functions as given in (2.3.1) and (2.3.4) then the two procedures to compute $d\sigma/dm$ only provides us with the same answer when $\tau \to 1$. This we have also checked for the order α_s^2 $S+V$ contribution. Therefore the expression in (2.3.1) is not the integrated form of equation (2.3.4) except if $\tau \to 1$. This explains why at large τ $R^{(1)}(\sqrt{\tau})$ (2.3.2) and $d\,R^{(1)}(\sqrt{\tau}, x_F)$ (2.3.5) are roughly the same and equal to 1 irrespective of the chosen scheme. The above properties of the $S+V$ approximation also reveal that if $\sqrt{\tau}$ becomes much smaller than 1 one has to be cautious in predicting the still unknown $d\,R^{(2)}(\sqrt{\tau}, x_F)$ from the values obtained for the known $R^{(2)}(\sqrt{\tau})$ (2.3.3) and $d\,R^{(1)}(\sqrt{\tau}, x_F)$ (2.3.5). In the subsequent part of this work we will use as a guiding principle that as long as $|d\,R^{(1)}(\sqrt{\tau}, x_F) - 1| < 0.1$ we expect that the $S+V$ approximation of the second order contribution to $d^2\sigma/dmdx_F$ will be very close to the exact result. If $|d\,R^{(1)}(\sqrt{\tau}, x_F) - 1| > 0.2$ then one should not trust this approximation and one has to rely on the predictions obtained from the first order corrected cross section. This implies that for the experiments discussed in this chapter one can make a reasonable prediction for the second order correction as long as $\sqrt{\tau} > 0.3$.

2.3.2 The order $\mathcal{O}(\alpha_s^2)$ contributions at fixed target energies

After having discussed the validity of the above approach at fixed target energies we will now make a comparison with the data of the E537 [20], E615 [21] and E772 [22, 23] experiments. For that purpose we compute the Born cross section $d^2\sigma_0/dmdx_F$, the order α_s corrected exact cross section $d^2\sigma_1/dmdx_F$ and the order α_s^2 corrected cross section $d^2\sigma_2/dmdx_F$. Notice that in the latter only the contribution due to the coefficient function $\Delta_{q\bar{q}}^{S+V}$ (2.3.4) (see appendix B) has been included because the other contributions are still missing. The computations have been carried out in the DIS-scheme. The results for the $\overline{\text{MS}}$-scheme will be shortly commented upon at the end of this section.

Starting with the experiment E537 ($\sqrt{S} = 15.4\,\text{GeV}$) we have plotted the quantity

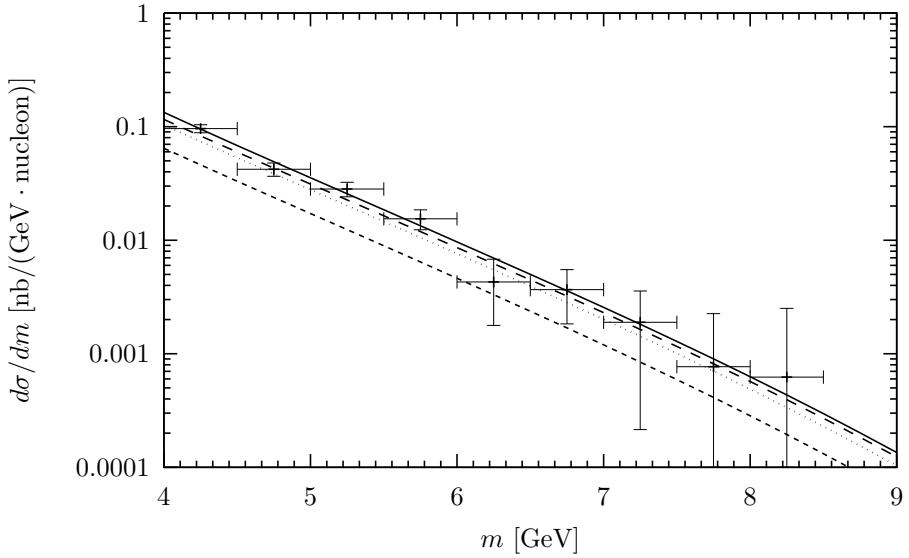

Figure 2.9: *$d\sigma/dm$ (2.3.6) for the reaction $\bar{p}+W \to \mu^+\mu^- +$ "X" at $\sqrt{S} = 15.4$ GeV. The data are obtained from the E537 experiment [20]. Dashed line: Born; dotted line: $\mathcal{O}(\alpha_s)$ (DIS); solid line: $\mathcal{O}(\alpha_s^2)$ (DIS); long dashed line: $\mathcal{O}(\alpha_s^2)$ ($\overline{\text{MS}}$).*

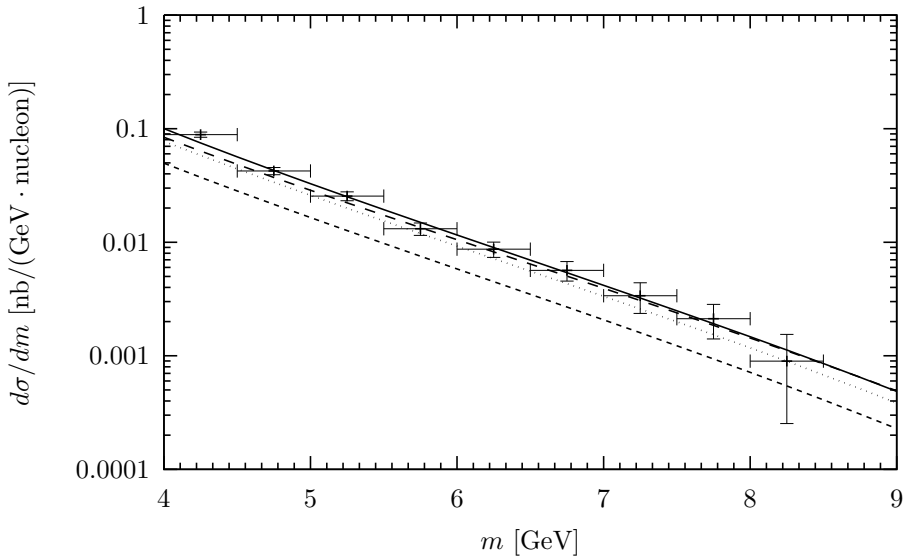

Figure 2.10: *$d\sigma/dm$ (2.3.6) for the reaction $\pi^- + W \to \mu^+\mu^- +$ "X" at $\sqrt{S} = 15.4$ GeV. The data are obtained from the E537 experiment [20]. Dashed line: Born; dotted line: $\mathcal{O}(\alpha_s)$ (DIS); solid line: $\mathcal{O}(\alpha_s^2)$ (DIS); long dashed line: $\mathcal{O}(\alpha_s^2)$ ($\overline{\text{MS}}$).*

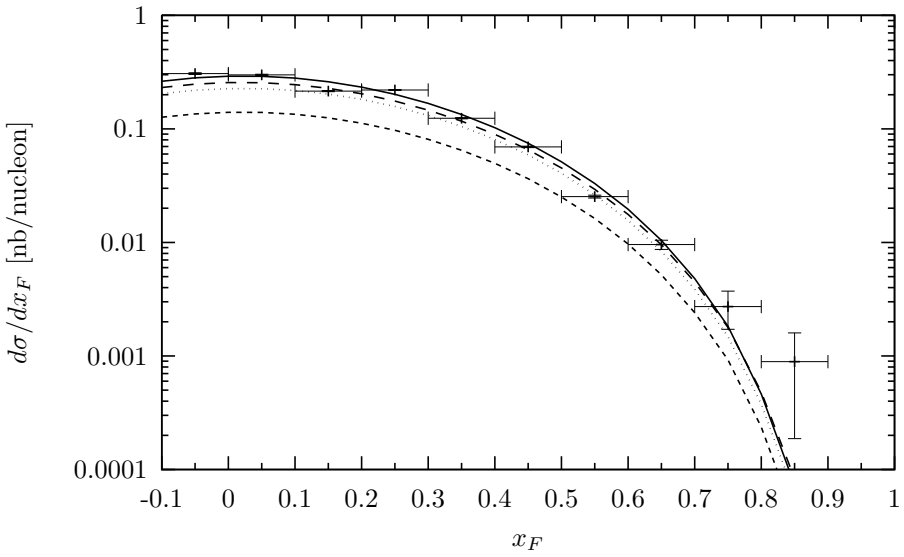

Figure 2.11: *$d\sigma/dx_F$ (2.3.7) for the reaction $\bar{p} + W \to \mu^+\mu^- +$ "X" at $\sqrt{S} = 15.4$ GeV. The data are obtained from the E537 experiment [20]. Dashed line: Born; dotted line: $\mathcal{O}(\alpha_s)$ (DIS); solid line: $\mathcal{O}(\alpha_s^2)$ (DIS); long dashed line: $\mathcal{O}(\alpha_s^2)$ ($\overline{\text{MS}}$).*

$$\frac{d\sigma}{dm} = \int_0^{1-\tau} dx_F \, \frac{d^2\sigma}{dm dx_F}, \tag{2.3.6}$$

in figs. 2.9 and 2.10 for the reactions $\bar{p} + W \to \mu^+\mu^- +$ "X" and $\pi^- + W \to \mu^+\mu^- +$ "X" respectively. Notice that x_F in [20] is defined as $x_F = 2p_L/[(1-\tau)\sqrt{S}]$ which differs from the usual definition in [17, 18, 27, 28]. Since the higher order QCD corrections are calculated for $d^2\sigma/dmdx_F$ with x_F defined in 2.2.3 and the cross section is not a Lorentz invariant we had to change the x_F-bins in table III of [20] according to our definition above. Figs. 2.9 and 2.10 reveal that the data are in agreement with the order α_s as well as with the order α_s^2 corrected cross section but lie above the result given by the Born approximation. The difference between the latter and the data is observed when we consider the quantity

$$\frac{d\sigma}{dx_F} = \int_{4.0}^{9.0} dm \, \frac{d^2\sigma}{dm dx_F}, \tag{2.3.7}$$

which is presented in figs. 2.11 and 2.12 for the above two reactions. Even the order α_s corrected cross section lies below the data for $x_F < 0.6$ as can be seen in fig. 2.12. On the other hand the order α_s^2 corrected cross section is in agreement with experiment over the whole x_F range.
The second experiment, E615 [21] also studies the reaction $\pi^- + W \to \mu^-\mu^+ +$ "X" but now for $\sqrt{S} = 21.8\,\text{GeV}$. In fig. 2.13 we have compared the quantity $d\sigma/d\sqrt{\tau} = \sqrt{S}\, d\sigma/dm$ with the data where $d\sigma/dm$ is defined in the same way as in (2.3.6). Apart from the bump, which is due to the Υ resonance at about $\sqrt{\tau} = 0.43$, the order α_s^2 corrected cross section reasonably describes the experimental results whereas the Born and the order α_s prediction fall below the data. The importance of the order

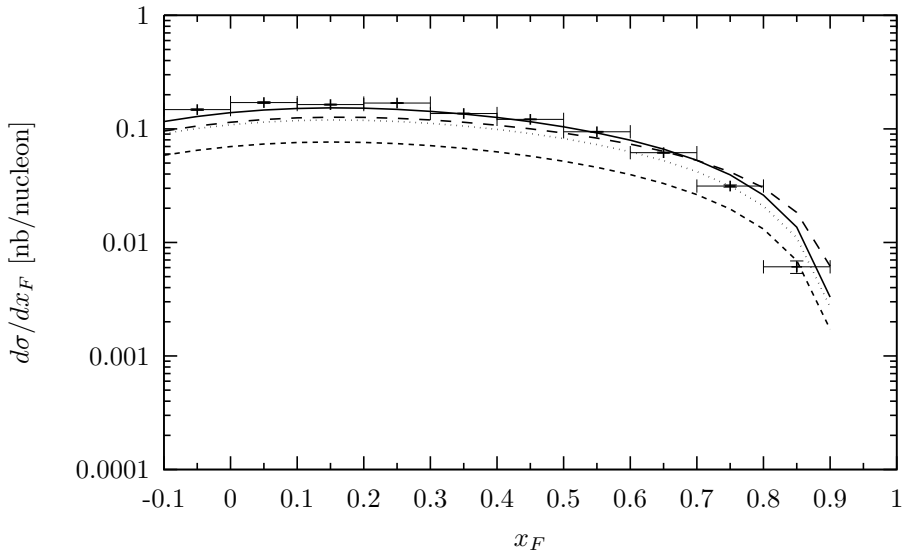

Figure 2.12: *$d\sigma/dx_F$ (2.3.7) for the reaction $\pi^- + W \to \mu^+\mu^- +$ "X" at $\sqrt{S} = 15.4$ GeV. The data are obtained from the E537 experiment [20]. Dashed line: Born; dotted line: $\mathcal{O}(\alpha_s)$ (DIS); solid line: $\mathcal{O}(\alpha_s^2)$ (DIS); long dashed line: $\mathcal{O}(\alpha_s^2)$ ($\overline{\text{MS}}$).*

α_s^2 contribution is also revealed when we study the double differential cross section

$$\frac{d^2\bar{\sigma}}{d\sqrt{\tau}dx_F} = \frac{1}{\sqrt{\tau_2} - \sqrt{\tau_1}} \int_{\sqrt{\tau_1}}^{\sqrt{\tau_2}} d\sqrt{\tau}\, \frac{d^2\sigma}{d\sqrt{\tau}dx_F}, \tag{2.3.8}$$

for various x_F regions, see figs. 2.14-2.19. The curves predicted by the Born and the order α_s corrections all lie below the data. For $\sqrt{\tau} > 0.277$ even the order α_s^2 contribution is not sufficient to close the gap between theory and experiment. This is due to the presence of the Υ in the region $0.323 < \sqrt{\tau} < 0.599$ which has not been subtracted from the data. The discrepancy between the order α_s^2 corrected cross section and the data becomes even more clear when we plot the K-factor (fig. 2.20) defined by

$$K_i(\sqrt{\tau}) = \frac{\displaystyle\int_0^{1-\tau} dx_F \frac{d^2\sigma_i}{d\sqrt{\tau}dx_F}}{\displaystyle\int_0^{1-\tau} dx_F \frac{d^2\sigma_0}{d\sqrt{\tau}dx_F}}, \tag{2.3.9}$$

in fig. 2.20 and compare the above expression with the experimental K-factor which is given by

$$K_{\text{exp}}(\sqrt{\tau}) = \frac{\displaystyle\int_0^{1-\tau} dx_F \frac{d^2\sigma_{\text{exp}}}{d\sqrt{\tau}dx_F}}{\displaystyle\int_0^{1-\tau} dx_F \frac{d^2\sigma_0}{d\sqrt{\tau}dx_F}}, \tag{2.3.10}$$

where $d^2\sigma_i/d\sqrt{\tau}dx_F$ denotes the order α_s^i corrected cross section. Fig. 2.20 shows that neither K_1 nor K_2 fit the data. The second order corrected K-factor is closer

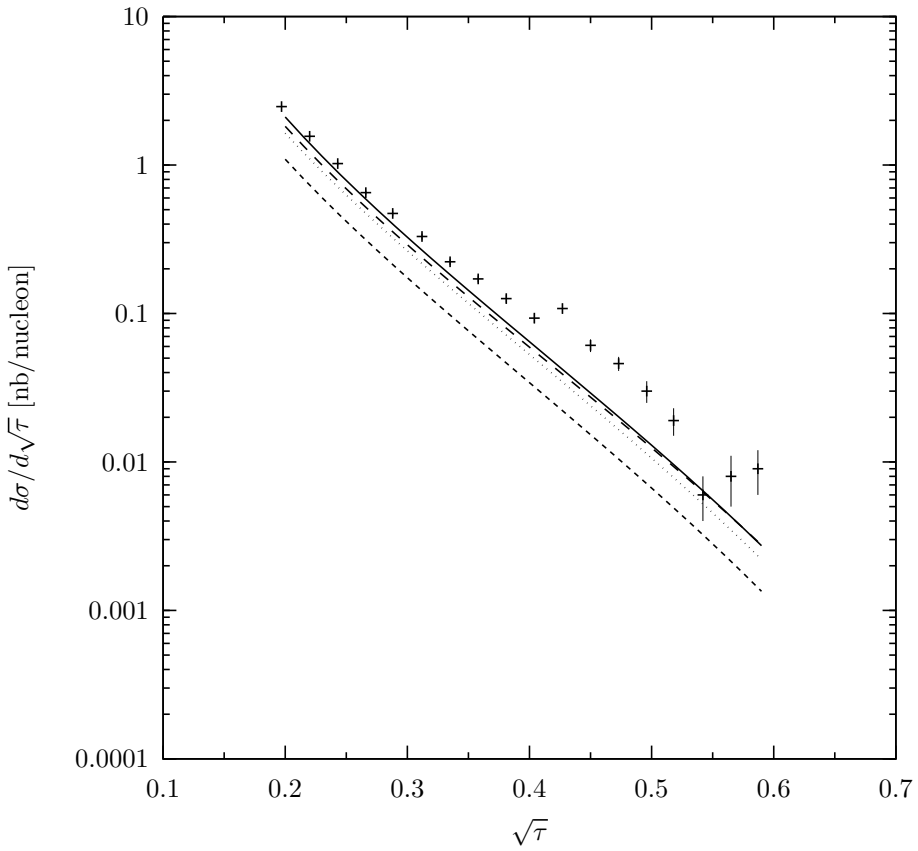

Figure 2.13: *$d\sigma/d\sqrt{\tau} = \sqrt{S}d\sigma/dm$ (see (2.3.6)) for the reaction $\pi^- + W \to \mu^+\mu^- +$ "X" at $\sqrt{S} = 21.8\,GeV$. The data are obtained from the E615 experiment [21]. Dashed line: Born; dotted line: $\mathcal{O}(\alpha_s)$ (DIS); solid line: $\mathcal{O}(\alpha_s^2)$ (DIS); long dashed line: $\mathcal{O}(\alpha_s^2)$ ($\overline{\text{MS}}$).*

to the data in the small $\sqrt{\tau}$-region. It is a pity that due to the presence of the Υ in the data it is difficult to compare theory with experiment in particular in those regions of $\sqrt{\tau}$ where the $S+V$ approximation is supposed to work.
Finally we also made a comparison with the data obtained by the E772 experiment for the reaction $p + {}^2H \to \mu^+\mu^- +$ "X" carried out at $\sqrt{S} = 38.8\,\text{GeV}$. The main goal of this experiment was to find a charge asymmetry in the sea-quark densities of the nucleon i.e. $\bar{u}(x) \neq \bar{d}(x)$. Here we are also interested whether the data obtained for $m^3 d^2\sigma/dmdx_F$ are in agreement with the order α_s^2 corrected DY cross section. In fig. 2.21 we have plotted the data for $m = 8.15\,\text{GeV}$ and compared them with the predictions given by the Born, the order α_s corrected and the order α_s^2 corrected cross section. The figure shows that the order α_s^2 corrections are needed to bring theory into agreement with the data. Notice that at this m-value one obtains $\sqrt{\tau} = 0.21$ which is quite small for the $S+V$ approximation so that the result has to be interpreted with care. In the next figure (fig. 2.22) we study the effect of the higher order QCD corrections on the suppression of the cross section near $x_F = 0.0$ which is caused by the difference between the up-sea and down-sea quark densities.

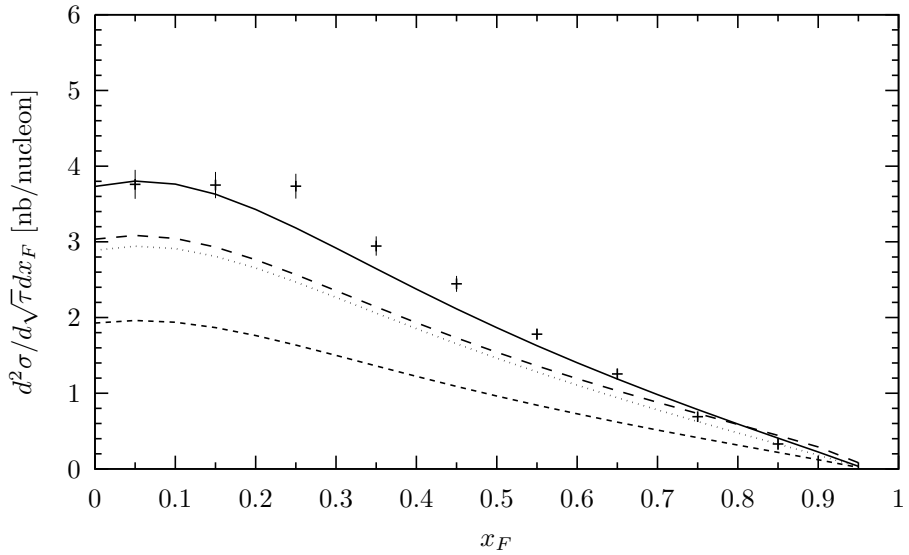

Figure 2.14: $d^2\bar{\sigma}/d\sqrt{\tau}dx_F$ *(2.3.8) with* $0.185 < \sqrt{\tau} < 0.231$ *for the reaction* $\pi^- + W \to \mu^+\mu^- +$ *"X" at* $\sqrt{S} = 21.8\,GeV$. *The data are obtained from the E615 experiment [21]. Dashed line: Born; dotted line:* $\mathcal{O}(\alpha_s)$ *(DIS); solid line:* $\mathcal{O}(\alpha_s^2)$ *(DIS); long dashed line:* $\mathcal{O}(\alpha_s^2)$ *(*$\overline{\text{MS}}$*).*

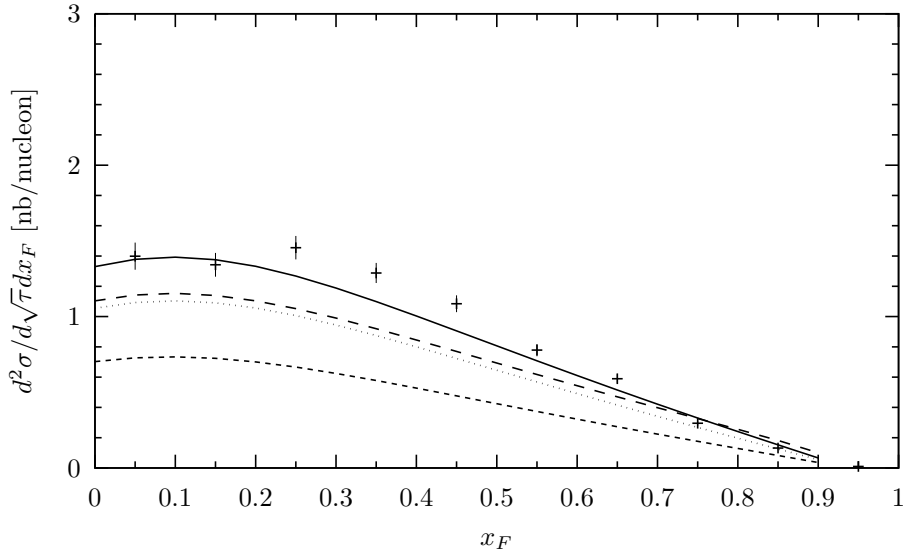

Figure 2.15: $d^2\bar{\sigma}/d\sqrt{\tau}dx_F$ *(2.3.8) with* $0.231 < \sqrt{\tau} < 0.277$ *for the reaction* $\pi^- + W \to \mu^+\mu^- +$ *"X" at* $\sqrt{S} = 21.8\,GeV$. *The data are obtained from the E615 experiment [21]. Dashed line: Born; dotted line:* $\mathcal{O}(\alpha_s)$ *(DIS); solid line:* $\mathcal{O}(\alpha_s^2)$ *(DIS); long dashed line:* $\mathcal{O}(\alpha_s^2)$ *(*$\overline{\text{MS}}$*).*

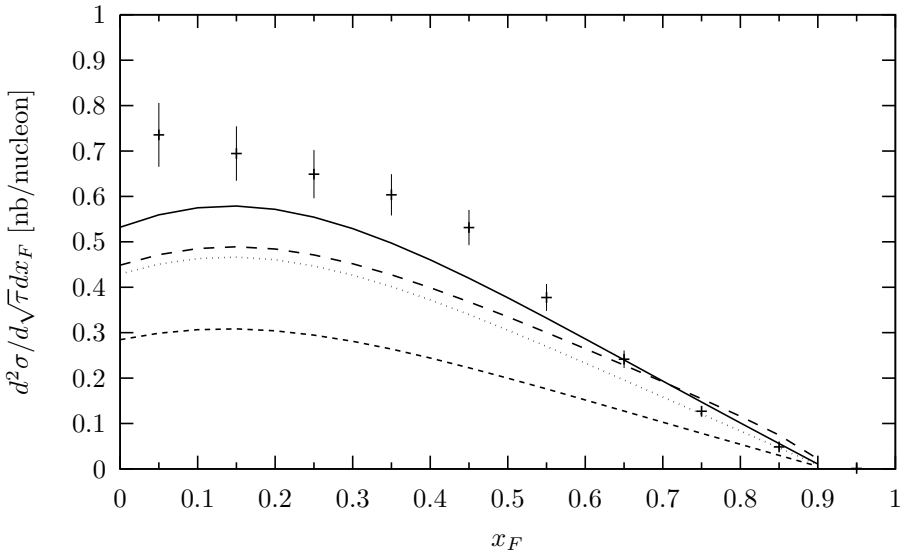

Figure 2.16: $d^2\bar{\sigma}/d\sqrt{\tau}dx_F$ *(2.3.8) with* $0.277 < \sqrt{\tau} < 0.323$ *for the reaction* $\pi^- + W \to \mu^+\mu^- +$ *"X" at* $\sqrt{S} = 21.8\,GeV$. *The data are obtained from the E615 experiment [21]. Dashed line: Born; dotted line:* $\mathcal{O}(\alpha_s)$ *(DIS); solid line:* $\mathcal{O}(\alpha_s^2)$ *(DIS); long dashed line:* $\mathcal{O}(\alpha_s^2)$ *(*$\overline{\text{MS}}$*).*

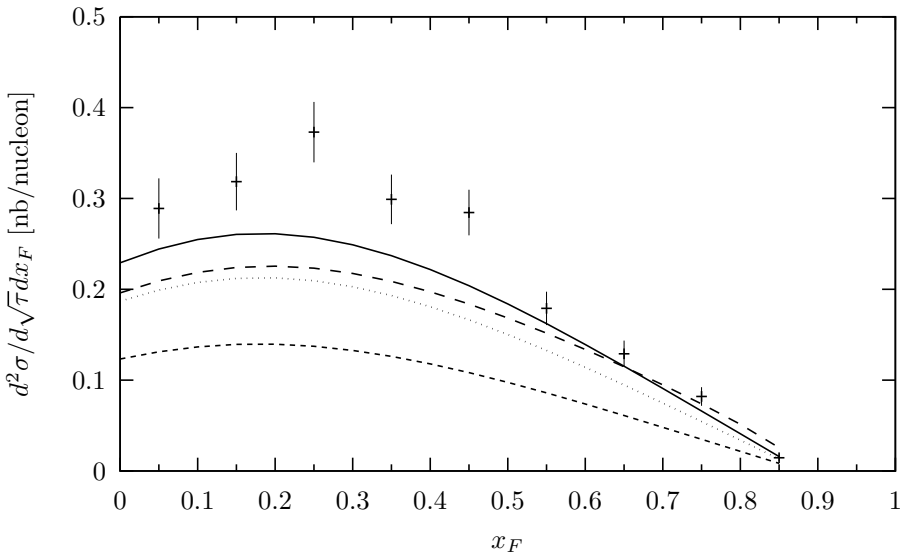

Figure 2.17: $d^2\bar{\sigma}/d\sqrt{\tau}dx_F$ *(2.3.8) with* $0.323 < \sqrt{\tau} < 0.369$ *for the reaction* $\pi^- + W \to \mu^+\mu^- +$ *"X" at* $\sqrt{S} = 21.8\,GeV$. *The data are obtained from the E615 experiment [21]. Dashed line: Born; dotted line:* $\mathcal{O}(\alpha_s)$ *(DIS); solid line:* $\mathcal{O}(\alpha_s^2)$ *(DIS); long dashed line:* $\mathcal{O}(\alpha_s^2)$ *(*$\overline{\text{MS}}$*).*

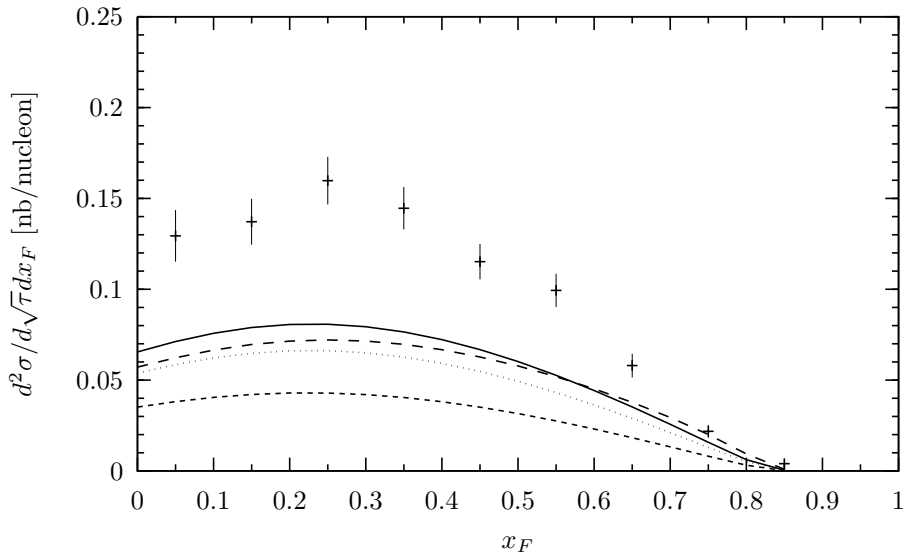

Figure 2.18: $d^2\bar{\sigma}/d\sqrt{\tau}dx_F$ *(2.3.8) with* $0.369 < \sqrt{\tau} < 0.484$ *for the reaction* $\pi^- + W \to \mu^+\mu^- +$ *"X" at* $\sqrt{S} = 21.8\,GeV$. *The data are obtained from the E615 experiment [21]. Dashed line: Born; dotted line:* $\mathcal{O}(\alpha_s)$ *(DIS); solid line:* $\mathcal{O}(\alpha_s^2)$ *(DIS); long dashed line:* $\mathcal{O}(\alpha_s^2)$ *(*$\overline{\text{MS}}$*).*

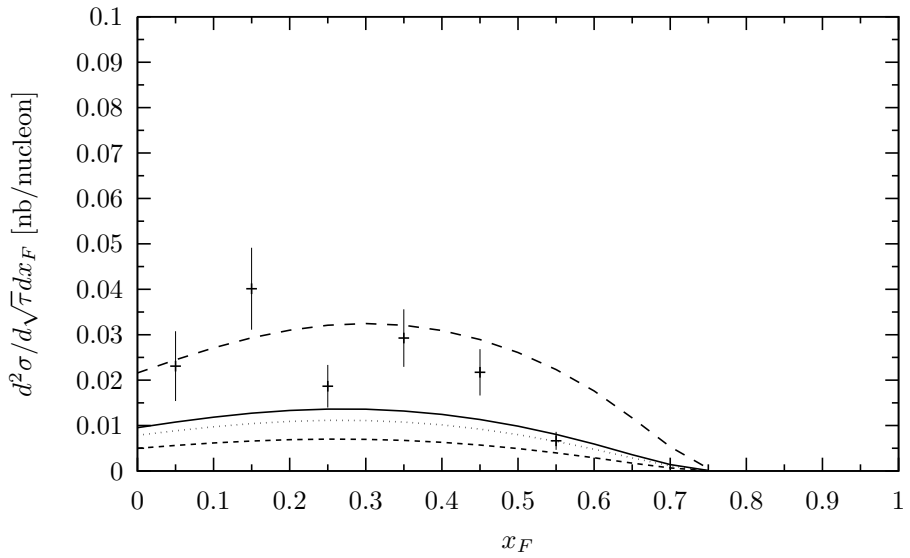

Figure 2.19: $d^2\bar{\sigma}/d\sqrt{\tau}dx_F$ *(2.3.8) with* $0.484 < \sqrt{\tau} < 0.599$ *for the reaction* $\pi^- + W \to \mu^+\mu^- +$ *"X" at* $\sqrt{S} = 21.8\,GeV$. *The data are obtained from the E615 experiment [21]. Dashed line: Born; dotted line:* $\mathcal{O}(\alpha_s)$ *(DIS); solid line:* $\mathcal{O}(\alpha_s^2)$ *(DIS); long dashed line:* $\mathcal{O}(\alpha_s^2)$ *(*$\overline{\text{MS}}$*).*

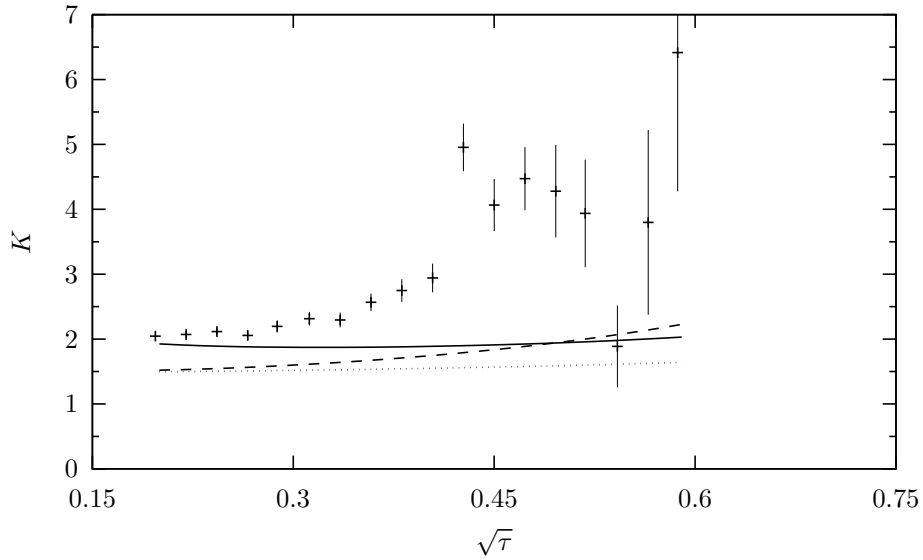

Figure 2.20: *Order α_s^i corrected K-factor denoted by K_i (2.3.9) compared with the experimental K-factor (2.3.10) for the reaction $\pi^- + W \to \mu^+\mu^- +$ "X" at $\sqrt{S} =$ 21.8 GeV. The data are obtained from the E615 experiment [21]. Dotted line: K_1 (DIS); solid line: K_2 (DIS); long dashed line: K_2 ($\overline{\text{MS}}$).*

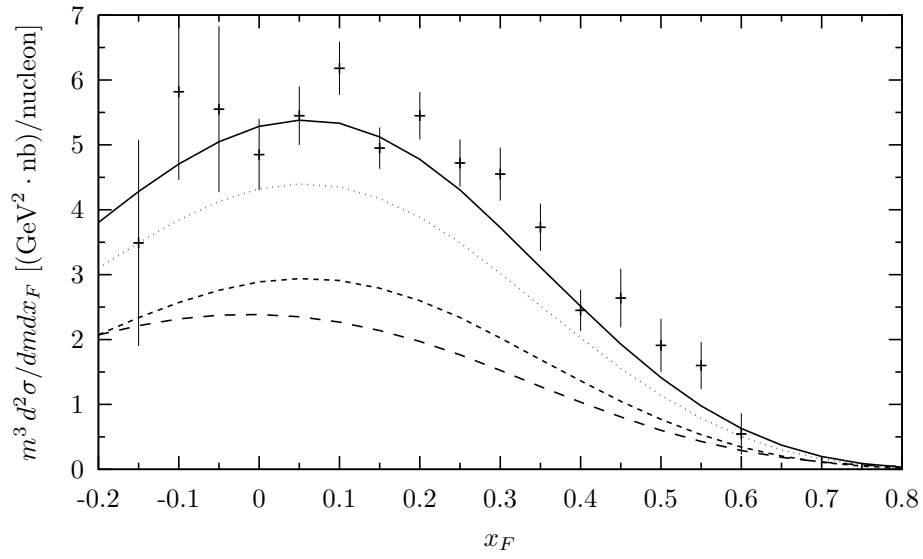

Figure 2.21: $m^3\, d^2\sigma/dmdx_F$ *for the reaction* $p + {}^2H \to \mu^+\mu^- +$ "X" *at* $\sqrt{S} =$ 38.8 GeV *and* $m = 8.15$ GeV. *The data are obtained from the E772 experiment [23]. Dashed line: Born; dotted line: $\mathcal{O}(\alpha_s)$ (DIS); solid line: $\mathcal{O}(\alpha_s^2)$ (DIS); long dashed line: $\mathcal{O}(\alpha_s^2)$ ($\overline{\text{MS}}$).*

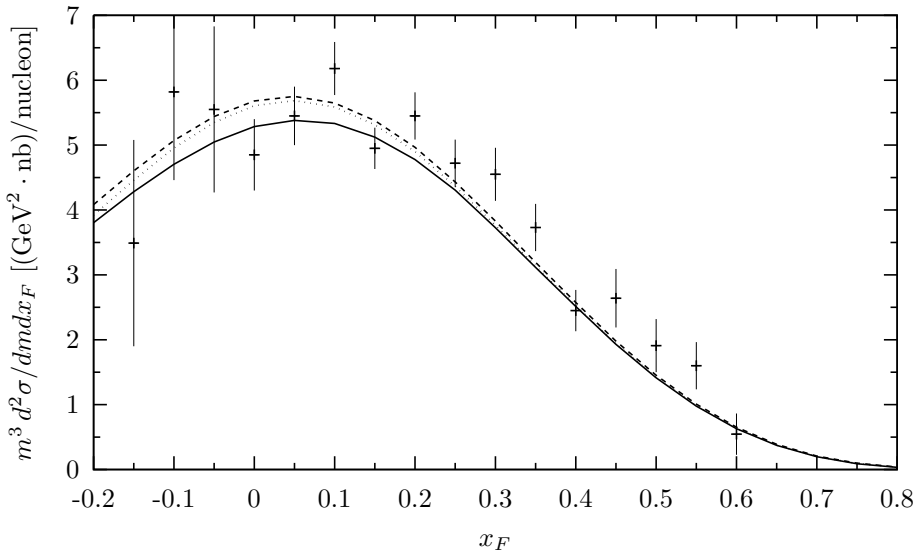

Figure 2.22: *Parton density dependence of $m^3\, d^2\sigma/dmdx_F$ corrected up to order α_s^2 for the reaction $p + {}^2H \to \mu^+\mu^- +$ "X" at $\sqrt{S} = 38.8\ GeV$ and $m = 8.15\ GeV$. The data are obtained from the E772 experiment [23]. Solid line: MRS(S0); dotted line: MRS(D0); dashed line: MRS(D-).*

Notice that the pp reaction is symmetric whereas the pn reaction is asymmetric around $x_F = 0.0$ irrespective whether there is charge asymmetry or not. Therefore the pn reaction leads to an x_F asymmetry even for isoscalar targets like ${}^2H$. In fig. 2.22 we have presented the order α_s^2 corrected cross section for three different parton density sets for the nucleon. They are given by MRS(S0) and MRS(D0) where the former has a symmetric sea ($\bar{u}(x) = \bar{d}(x)$) whereas the latter contains an asymmetric sea ($\bar{u}(x) \neq \bar{d}(x)$) parametrization. For comparison we have also shown MRS(D-) which only differs from MRS(D0) that the gluon and sea densities have a much steeper small x-behavior (lipatov-pomeron) than the ones given by MRS(D0) and MRS(S0) (non perturbative pomeron). Fig. 2.22 reveals that there is hardly any suppression of the cross section for $x_F < 0$ while going from the symmetric sea (MRS(S0)) to the asymmetric sea (MRS(D0)) parametrization so that both parton density sets are in agreement with the data.
If other parton densities are used like those discussed in [23] the suppression for $x_F < 0$ can be much larger. For the MRS-set it appears that a change in the small x-behavior of the parton densities leads to a larger suppression of the cross section (compare MRS(D0) with MRS(D-)) than the introduction of a charge asymmetry in the sea-quarks (MRS(S0) versus MRS(D0)).
In addition to the calculations performed in the DIS-scheme we have also presented in figs. 2.9-2.21 the order α_s^2 corrected cross section computed in the $\overline{\text{MS}}$-scheme. Although the latter is an improvement with respect to the order α_s corrected result it is smaller than the cross section computed in the DIS-scheme except when x_F is large. This is not surprising because figs. 2.6-2.8 already indicate that the approximation underestimates the exact cross section in the case of the $\overline{\text{MS}}$-scheme.

2.4 Summary

Summarizing the main results of this chapter we can conclude that up to the order α_s level the soft plus virtual gluon contribution gives a fairly good approximation of the exact DY cross section $d^2\sigma/dmdx_F$. Therefore we expect that this approximation will also work for the α_s^2 correction as long as the cross section is computed at fixed target energies and for $\sqrt{\tau} > 0.3$. In this τ-region we expect that all other partonic subprocesses are suppressed due to the reduction in phase space. This expectation is corroborated by a thorough analysis of the second order contribution to $d\sigma/dm$ for which the exact coefficient function is known. Because of the missing pieces in the order α_s^2 contribution to the coefficient function corresponding to the cross section $d^2\sigma/dmdx_F$ and the absence of the next-to-next-to-leading order parton densities we have to rely on the order α_s^2 soft plus virtual gluon approximation to make a comparison with the data. Using this approach we can show that a part of the discrepancy between the data and the order α_s corrected cross section can be attributed to the higher order soft plus virtual gluon contributions.

Appendix A

In this appendix we will present the order α_s contributions to the coefficient functions corresponding to $d^2\sigma/dQ^2dx_F$ coming from the partonic subprocesses in (2.2.15) and (2.2.16). Although these processes have been calculated in the DIS-scheme in [17, 18] (see also [27]) and the $\overline{\text{MS}}$-scheme [28] we have some different definitions for the distributions and we have a small disagreement with the coefficient function for the qg subprocess in [28]. Moreover we want to give a clear definition for the soft plus virtual $(S+V)$ gluon part of the coefficient function corresponding to the $q\bar{q}$ subprocess.
We have recalculated the double differential cross section $d^2\sigma/dQ^2dx_F$ for the partonic subprocesses 2.2.15 and 2.2.16. After performing the mass factorization in the $\overline{\text{MS}}$-scheme the coefficients $\Delta_{ij}^{(1)}$ (see the definition in 2.2.12) read as follows

$$\Delta_{q\bar{q}}^{(1)}(t_1,t_2,x_1,x_2,Q^2,\mu^2) = C_F\frac{\delta(t_1-x_1)\delta(t_2-x_2)}{x_1+x_2}\Bigg[$$

$$\left\{4\ln\frac{(1-x_1)(1-x_2)}{x_1x_2}+6\right\}\ln\frac{Q^2}{\mu^2}-16+12\zeta(2)+2\ln^2\frac{(1-x_1)(1-x_2)}{x_1x_2}\Bigg]$$

$$+C_F\frac{\delta(t_1-x_1)}{x_1+x_2}\Bigg[\left\{\left(\frac{4}{t_2-x_2}\right)_+-2\frac{t_2+x_2}{t_2^2}\right\}\ln\frac{Q^2}{\mu^2}+\left(\frac{4}{t_2-x_2}\right)_+\ln\frac{1-x_1}{x_1}$$

$$+4\left(\frac{\ln(t_2/x_2-1)}{t_2-x_2}\right)_++\frac{4}{t_2-x_2}\ln\frac{x_1+x_2}{x_1+t_2}+2\frac{t_2-x_2}{t_2^2}$$

$$-2\frac{t_2+x_2}{t_2^2}\ln\frac{(x_1+x_2)(1-x_1)(t_2-x_2)}{x_1x_2(t_2+x_1)}\Bigg]+[t_1\leftrightarrow t_2,x_1\leftrightarrow x_2]$$

$$+ C_F \frac{1}{x_1+x_2}\left[\frac{4}{(t_1-x_1)_+(t_2-x_2)_+} - 2\frac{t_2+x_2}{t_2^2}\left(\frac{1}{t_1-x_1}\right)_+\right.$$

$$- 2\frac{t_1+x_1}{t_1^2}\left(\frac{1}{t_2-x_2}\right)_+ - \frac{4}{(t_2+x_1)(t_1+x_2)} + \frac{2}{t_2(t_1+x_2)} + \frac{2}{t_1(t_2+x_1)}$$

$$\left. - \frac{2x_1}{t_2^2(t_1+x_2)} - \frac{2x_2}{t_1^2(t_2+x_1)} + \frac{2(x_1+x_2)(t_1^2+t_2^2)}{t_1^2t_2^2(t_1+t_2)}\right], \tag{A.1}$$

where the color factor C_F is given by $C_F = (N^2-1)/2N$ (QCD : $N = 3$). In this appendix and in the next one the distributions indicated by a plus sign in the denominator are defined as

$$\int_{x_k}^1 dt_k \left(\frac{\ln^i(t_k/x_k-1)}{t_k-x_k}\right)_+ f(t_k) = \int_{x_k}^1 dt_k \frac{\ln^i(t_k/x_k-1)}{t_k-x_k}(f(t_k)-f(x_k)), \tag{A.2}$$

$$\int_{x_1}^1 dt_1 \int_{x_2}^1 dt_2 \left(\frac{\ln^i(t_1/x_1-1)}{t_1-x_1}\right)_+ \left(\frac{\ln^j(t_2/x_2-1)}{t_2-x_2}\right)_+ f(t_1,t_2)$$

$$= \int_{x_1}^1 dt_1 \int_{x_2}^1 dt_2 \frac{\ln^i(t_1/x_1-1)}{t_1-x_1}\frac{\ln^j(t_2/x_2-1)}{t_2-x_2}(f(t_1,t_2)-f(x_1,t_2).$$

$$- f(t_1,x_2)+f(x_1,x_2)) \tag{A.3}$$

Expression (A.1) for $\Delta_{q\bar{q}}^{(1)}$ is in agreement with eq. (A.4) in [28]. Notice that the authors in [28] give a different definition for the distributions. This leads to a difference between (A.2) and eq. (A.12) in [28] which equals

$$\int_{x_k}^1 dt_k \frac{\ln t_k/x_k}{t_k-x_k} f(x_k) = f(x_k)\left[\frac{1}{2}\ln^2 x_k + \mathrm{Li}_2(1-x_k)\right]. \tag{A.4}$$

where the dilogarithmic function $\mathrm{Li}_2(x)$ is defined by

$$\mathrm{Li}_2(x) = -\int_0^x \frac{dt}{t}\ln(1-t). \tag{A.5}$$

The expression between the square brackets in (A.4), multiplied by two, has to be added to the coefficient of the $\delta(t_1-x_1)\delta(t_2-x_2)$ term in eq. (A.4) of [28] so that one obtains the same result as we have in (A.1) above.
The soft plus virtual gluon part of $\Delta_{q\bar{q}}^{(1)}$ is defined by isolating the double singular terms in (A.1) of the types $\delta(t_1-x_1)\delta(t_2-x_2)$, $\delta(t_1-x_1)\left(\frac{1}{t_2-x_2}\right)_+$, $\delta(t_2-x_2)\left(\frac{1}{t_1-x_1}\right)_+$ and $\left(\frac{1}{t_1-x_1}\right)_+\left(\frac{1}{t_2-x_2}\right)_+$. Hence we obtain

$$\Delta_{q\bar{q}}^{S+V,(1)}(t_1,t_2,x_1,x_2,Q^2,\mu^2) = C_F\frac{\delta(t_1-x_1)\delta(t_2-x_2)}{x_1+x_2}\left[\right.$$

$$\left\{4\ln\frac{(1-x_1)(1-x_2)}{x_1x_2}+6\right\}\ln\frac{Q^2}{\mu^2}-16+12\zeta(2)+2\ln^2\frac{(1-x_1)(1-x_2)}{x_1x_2}\Bigg]$$
$$+C_F\frac{\delta(t_1-x_1)}{x_1+x_2}\left[\left(\frac{4}{t_2-x_2}\right)_+\ln\frac{Q^2}{\mu^2}+\left(\frac{4}{t_2-x_2}\right)_+\ln\frac{1-x_1}{x_1}\right.$$
$$\left.+4\left(\frac{\ln(t_2/x_2-1)}{t_2-x_2}\right)_+\right]+[t_1\leftrightarrow t_2,x_1\leftrightarrow x_2]$$
$$+C_F\frac{1}{x_1+x_2}\left[\frac{4}{(t_1-x_1)_+(t_2-x_2)_+}\right], \tag{A.6}$$

where we have taken the residues at $t_k=x_k$.
For the gq subprocess we obtain the coefficient function

$$\Delta_{gq}^{(1)}(t_1,t_2,x_1,x_2,Q^2,\mu^2)=T_f\frac{\delta(t_2-x_2)}{x_1+x_2}\left[\left\{2\frac{x_1^2+(t_1-x_1)^2}{t_1^3}\right\}\ln\frac{Q^2}{\mu^2}\right.$$
$$\left.+2\frac{x_1^2+(t_1-x_1)^2}{t_1^3}\ln\frac{(x_1+x_2)(1-x_2)(t_1-x_1)}{x_1x_2(t_1+x_2)}+\frac{4x_1(t_1-x_1)}{t_1^3}\right]$$
$$+T_f\frac{1}{x_1+x_2}\left[2\frac{x_1^2+(t_1-x_1)^2}{t_1^3}\left(\frac{1}{t_2-x_2}\right)_+-2\frac{x_2^2+(t_1+x_2)^2}{t_1^3(t_2+x_1)}\right.$$
$$+4\frac{x_1+x_2}{t_1^2t_2}-4\frac{x_1x_2(x_1+x_2)}{t_1^3t_2^2}-4\frac{x_1^2-x_2^2}{t_1^3t_2}+2\frac{(x_1+x_2)(t_2-x_2)(t_2+x_1)}{t_1t_2^2(t_1+t_2)^2}$$
$$\left.+4\frac{x_1x_2(x_1+x_2)}{t_1^2t_2^2(t_1+t_2)}\right], \tag{A.7}$$

and

$$\Delta_{qg}^{(1)}(t_1,t_2,x_1,x_2,Q^2,\mu^2)=\Delta_{gq}^{(1)}(t_2,t_1,x_2,x_1,Q^2,\mu^2), \tag{A.8}$$

where $T_f=1/2$.
There is a discrepancy between our answer in (A.7) and the one given in eq. (A.8) of [28]. The difference between their result and ours equals $2\frac{x_1^2+(t_1-x_1)^2}{t_1^3}$. This discrepancy can be attributed to the procedure that in n-dimensional regularization before mass factorization the cross section with one gluon in the initial state has to be divided by $n-2$ in order to average over the initial gluon polarizations. Only in this case one can combine the coefficient functions with the parton densities of which the scale evolution is determined by the two-loop anomalous dimensions (or Altarelli-Parisi splitting functions) calculated in the literature (see e.g. [32]). The expression in eq. (A.8) of [28] can be only obtained if the polarization average factor is a $1/2$ instead of $1/(n-2)$. In the latter case one has to modify the two-loop anomalous dimensions via a finite renormalization. However the MRS parton densities in [29]

were constructed using the anomalous dimensions in [32] so that one has to divide the parton cross section by $n-2$ and not by 2. The choice of the polarization average factor shows up again when we want to present the coefficient functions in the DIS-scheme. The results in the DIS-scheme are obtained by performing a finite mass factorization. The coefficient functions in the two schemes are related by

$$\Delta_{ij}(t_1,t_2,x_1,x_2,Q^2,\mu^2)\big|_{\rm DIS} = \sum_{k,l}\int_{x_1}^1 du_1\int_{x_2}^1 du_2\Gamma_{ki}\left(\frac{u_1}{t_1}\right)\Gamma_{lj}\left(\frac{u_2}{t_2}\right)\cdot$$

$$\cdot\Delta_{kl}(u_1,u_2,x_1,x_2,Q^2,\mu^2)\big|_{\overline{\rm MS}}\,. \tag{A.9}$$

Up to order α_s, $\Gamma_{qq}(x)$ and $\Gamma_{qg}(x)$ are given by

$$\begin{aligned}\Gamma_{qq}(x) &= \delta(1-x)+\frac{\alpha_s}{4\pi}C_F\left[4\left(\frac{\ln(1-x)}{1-x}\right)_+ - 2(1+x)\ln(1-x)+6+4x\right.\\ &\left. -2\frac{1+x^2}{1-x}\ln x-\left(\frac{3}{1-x}\right)_+ +\delta(1-x)(-9-4\zeta(2))\right],\end{aligned} \tag{A.10}$$

$$\Gamma_{qg}(x)=\frac{\alpha_s}{4\pi}T_f\left[2\left\{x^2+(1-x)^2\right\}\ln\frac{1-x}{x}+16x(1-x)-2\right]. \tag{A.11}$$

Expressions (A.10) and (A.11) are in agreement with $C^{(1)}_{F,2}$ and $C^{(1)}_{G,2}$ in appendix I of [33]. Notice that the authors in [28] used a $\Gamma_{qg}(x)$ where $16x(1-x)-2$ is replaced by $12x(1-x)$ which is obtained when the gluon polarization average factor is taken to be $1/2$ instead of $1/(n-2)$. See the discussion above.
The coefficient functions in the DIS-scheme read

$$\begin{aligned}\Delta^{(1)}_{q\bar q}(t_1,t_2,x_1,x_2,Q^2,\mu^2) &= C_F\frac{\delta(t_1-x_1)\delta(t_2-x_2)}{x_1+x_2}\left[4\ln\frac{1-x_1}{x_1}\ln\frac{1-x_2}{x_2}\right.\\ &\left.+\left\{4\ln\frac{(1-x_1)(1-x_2)}{x_1x_2}+6\right\}\ln\frac{Q^2}{\mu^2}+2+20\zeta(2)+3\ln\frac{(1-x_1)(1-x_2)}{x_1x_2}\right]\\ &+C_F\frac{\delta(t_1-x_1)}{x_1+x_2}\left[\left\{\left(\frac{4}{t_2-x_2}\right)_+-2\frac{t_2+x_2}{t_2^2}\right\}\ln\frac{Q^2}{\mu^2}\right.\\ &+\left(4\ln\frac{1-x_1}{x_1}+3\right)\left(\frac{1}{t_2-x_2}\right)_+ +\frac{4}{t_2-x_2}\ln\frac{x_1+x_2}{x_1+t_2}\\ &\left.-2\frac{t_2+x_2}{t_2^2}\ln\frac{(x_1+x_2)(1-x_1)}{x_1(t_2+x_1)}-\frac{4}{t_2}-6\frac{x_2}{t_2^2}\right]+[t_1\leftrightarrow t_2,x_1\leftrightarrow x_2]\\ &+C_F\frac{1}{x_1+x_2}\left[\frac{4}{(t_1-x_1)_+(t_2-x_2)_+}-2\frac{t_2+x_2}{t_2^2}\left(\frac{1}{t_1-x_1}\right)_+\right.\end{aligned}$$

$$- 2\frac{t_1+x_1}{t_2^2}\left(\frac{1}{t_2-x_2}\right)_+ - \frac{4}{(t_2+x_1)(t_1+x_2)} + \frac{2}{t_2(t_1+x_2)} + \frac{2}{t_1(t_2+x_1)}$$

$$- 2\frac{x_1}{t_2^2(t_1+x_2)} - 2\frac{x_2}{t_1^2(t_2+x_1)} + 2\frac{(x_1+x_2)(t_1^2+t_2^2)}{t_1^2t_2^2(t_1+t_2)}\Bigg]. \tag{A.12}$$

The soft plus virtual gluon part is obtained in the same way as discussed in the case of the $\overline{\rm MS}$-scheme

$$\Delta_{q\bar{q}}^{S+V,(1)}(t_1,t_2,x_1,x_2,Q^2,\mu^2) = C_F\frac{\delta(t_1-x_1)\delta(t_2-x_2)}{x_1+x_2}\left[4\ln\frac{1-x_1}{x_1}\ln\frac{1-x_2}{x_2}\right.$$

$$\left.\left\{4\ln\frac{(1-x_1)(1-x_2)}{x_1x_2}+6\right\}\ln\frac{Q^2}{\mu^2}+2+20\zeta(2)+3\ln\frac{(1-x_1)(1-x_2)}{x_1x_2}\right]$$

$$+ C_F\frac{\delta(t_1-x_1)}{x_1+x_2}\left[\left\{\left(\frac{4}{t_2-x_2}\right)_+\right\}\ln\frac{Q^2}{\mu^2}\right.$$

$$\left.+\left(4\ln\frac{1-x_1}{x_1}+3\right)\left(\frac{1}{t_2-x_2}\right)_+\right] + [t_1\leftrightarrow t_2, x_1\leftrightarrow x_2]$$

$$+ C_F\frac{1}{x_1+x_2}\left[\frac{4}{(t_1-x_1)_+(t_2-x_2)_+}\right]. \tag{A.13}$$

The coefficient function for the subprocess with the gluon in the initial state becomes

$$\Delta_{qg}^{(1)}(t_1,t_2,x_1,x_2,Q^2,\mu^2) = T_f\frac{\delta(t_2-x_2)}{x_1+x_2}\left[\left\{2\frac{x_1^2+(t_1-x_1)^2}{t_1^3}\right\}\ln\frac{Q^2}{\mu^2}\right.$$

$$\left.+2\frac{x_1^2+(t_1-x_1)^2}{t_1^3}\ln\frac{(x_1+x_2)(1-x_2)}{x_2(t_1+x_2)}+\frac{2}{t_1}-12\frac{x_1(t_1-x_1)}{t_1^3}\right]$$

$$+ T_f\frac{1}{x_1+x_2}\left[2\frac{x_1^2+(t_1-x_1)^2}{t_1^3}\left(\frac{1}{t_2-x_2}\right)_+ - 2\frac{x_2^2+(t_1+x_2)^2}{t_1^3(t_2+x_1)}\right.$$

$$+4\frac{x_1+x_2}{t_1^2t_2} - 4\frac{x_1x_2(x_1+x_2)}{t_1^3t_2^2} - 4\frac{x_1^2-x_2^2}{t_1^3t_2} + 2\frac{(x_1+x_2)(t_2-x_2)(t_2+x_1)}{t_1t_2^2(t_1+t_2)^2}$$

$$\left.+4\frac{x_1x_2(x_1+x_2)}{t_1^2t_2^2(t_1+t_2)}\right], \tag{A.14}$$

where $\Delta_{qg}^{(1)}$ is related to $\Delta_{gq}^{(1)}$ via relation (A.8).

We have explicitly checked that if the above coefficient functions are inserted in (2.2.2) and the integrals over x_F are performed according to (2.2.19) one gets the same answer as given by $d\sigma/dm$ (2.2.20) with the coefficient functions obtained from [24, 25]. The coefficient functions for $d^2\sigma/dQ^2dy$ have not been explicitly listed here but are present in our computer program DIFDY. In the case of $d^2\sigma/dQ^2dy$ we agree

with the results for the $\overline{\rm MS}$-scheme published in [28] except for $1/2t_1$ in eq. (A.20) which has to be replaced by $\frac{x_1(t_1-x_1)}{t_1^3}$. This difference follows again from taking the average over the initial gluon polarizations as discussed for $\Delta_{gq}^{(1)}$ above. Our results for the DIS-scheme agree with those presented in the appendix of [27]. Notice that the soft plus virtual gluon part of $\Delta_{q\bar{q}}^{(1)}$ for $d^2\sigma/dQ^2dy$ can be obtained from (A.6) and (A.13) by multiplication with $x_1 + x_2$.

Appendix B

The order α_s^2 contribution to the coefficient function in the $S + V$ approximation has been calculated in [26]. Including the mass factorization parts represented by $\ln(Q^2/\mu^2)$ and rewriting the coefficient function in a more amenable form as presented for the first order correction in appendix A it reads in the $\overline{\rm MS}$-scheme as follows

$$
\begin{aligned}
\Delta_{q\bar{q}}^{S+V,(2)}(t_1,t_2,x_1,x_2,Q^2,\mu^2) = \frac{\delta(t_1-x_1)\delta(t_2-x_2)}{x_1+x_2}\Bigg[\\
C_F^2\Bigg\{\Bigg[18 - 8\zeta(2) + 8\left(P^2(x_1)+P^2(x_2)\right) + 24\left(P(x_1)+P(x_2)\right) \\
+ 16P(x_1)P(x_2)\Bigg] L_\mu^2 + \Big[-93 + 60\zeta(2) + 80\zeta(3) + 8\left(P^3(x_1)+P^3(x_2)\right) \\
+ 24\left(P^2(x_1)P(x_2) + P(x_1)P^2(x_2)\right) + 24P(x_1)P(x_2) \\
+ 12\left(P^2(x_1)+P^2(x_2)\right) + (-64+16\zeta(2))(P(x_1)+P(x_2))\Big] L_\mu \\
+ \frac{511}{4} - 128\zeta(2) - 60\zeta(3) + \frac{304}{9}\zeta^2(2) + 2\left(P^4(x_1)+P^4(x_2)\right) \\
+ 8\left(P^3(x_1)P(x_2) + P(x_1)P^3(x_2)\right) + 12P^2(x_1)P^2(x_2) \\
+ (-32+8\zeta(2))\left(P^2(x_1)+P^2(x_2)\right) + (-64+16\zeta(2))P(x_1)P(x_2) \\
+ 32\zeta(3)(P(x_1)+P(x_2))\Bigg\} \\
+ C_AC_F\Bigg\{\Bigg[-11 - \frac{22}{3}(P(x_1)+P(x_2))\Bigg] L_\mu^2 + \Bigg[\frac{193}{3} - 22\zeta(2) - 24\zeta(3) \\
- \frac{22}{3}\left(P^2(x_1)+P^2(x_2)\right) + \left(\frac{268}{9} - 8\zeta(2)\right)(P(x_1)+P(x_2))
\end{aligned}
$$

$$
- \frac{44}{3}P(x_1)P(x_2)\Big] L_\mu - \frac{1535}{12} + \frac{860}{9}\zeta(2) + \frac{172}{3}\zeta(3) - \frac{52}{5}\zeta^2(2)
$$

$$
- \frac{22}{9}\left(P^3(x_1) + P^3(x_2)\right) - \frac{22}{3}\left(P^2(x_1)P(x_2) + P(x_1)P^2(x_2)\right)
$$

$$
+ \left(\frac{134}{9} - 4\zeta(2)\right)\left(P^2(x_1) + P^2(x_2)\right) + \left(\frac{268}{9} - 8\zeta(2)\right)P(x_1)P(x_2)
$$

$$
+ \left(-\frac{808}{27} + \frac{44}{3}\zeta(2) + 28\zeta(3)\right)\left(P(x_1) + P(x_2)\right)\Big\}
$$

$$
+ n_f C_F \Big\{ \Big[2 + \frac{4}{3}(P(x_1) + P(x_2))\Big] L_\mu^2 + \Big[- \frac{34}{3} + 4\zeta(2) + \frac{4}{3}\Big(P^2(x_1)
$$

$$
+ P^2(x_2) \Big) + \frac{8}{3}P(x_1)P(x_2) - \frac{40}{9}(P(x_1) + P(x_2)) \Big] L_\mu + \frac{127}{6} - \frac{152}{9}\zeta(2)
$$

$$
+ \frac{8}{3}\zeta(3) + \frac{4}{9}\left(P^3(x_1) + P^3(x_2)\right) + \frac{4}{3}\left(P^2(x_1)P(x_2) + P(x_1)P^2(x_2)\right)
$$

$$
- \frac{40}{9}P(x_1)P(x_2) - \frac{20}{9}\left(P^2(x_1) + P^2(x_2)\right) + \left(\frac{112}{27} - \frac{8}{3}\zeta(2)\right)(P(x_1)
$$

$$
+ P(x_2)) \Big\} \Big]
$$

$$
+ \frac{\delta(t_1 - x_1)}{x_1 + x_2} \Big[C_F^2 \Big\{ \Big[16(D_1(t_2) + P(x_1)D_0(t_2)) + 24D_0(t_2) \Big] L_\mu^2
$$

$$
+ \Big[24D_2(t_2) + 48P(x_1)D_1(t_2) + 24P^2(x_1)D_0(t_2) + 24(D_1(t_2)
$$

$$
+ P(x_1)D_0(t_2)) + (-64 + 16\zeta(2))D_0(t_2) \Big] L_\mu + 8D_3(t_2)
$$

$$
+ 24P(x_1)D_2(t_2) + 24P^2(x_1)D_1(t_2) + 8P^3(x_1)D_0(t_2) + (-64
$$

$$
+ 16\zeta(2))(D_1(t_2) + P(x_1)D_0(t_2)) + 32\zeta(3)D_0(t_2) \Big\}
$$

$$
+ C_A C_F \Big\{ \Big[-\frac{22}{3}D_0(t_2)\Big] L_\mu^2 + \Big[-\frac{44}{3}D_1(t_2) - \frac{44}{3}P(x_1)D_0(t_2)
$$

$$
+ \left(\frac{268}{9} - 8\zeta(2)\right)D_0(t_2)\Big] L_\mu - \frac{22}{3}D_2(t_2) - \frac{44}{3}P(x_1)D_1(t_2)
$$

$$
\begin{aligned}
&- \frac{22}{3}P^2(x_1)D_0(t_2) + \left(\frac{268}{9} - 8\zeta(2)\right)(D_1(t_2) + P(x_1)D_0(t_2)) \\
&+ \left(-\frac{808}{27} + \frac{44}{3}\zeta(2) + 28\zeta(3)\right)D_0(t_2)\Bigg\} \\
&+ n_f C_F \Bigg\{\left[\frac{4}{3}D_0(t_2)\right]L_\mu^2 + \left[\frac{8}{3}(D_1(t_2) + P(x_1)D_0(t_2)) - \frac{40}{9}D_0(t_2)\right]L_\mu \\
&+ \frac{4}{3}D_2(t_2) + \frac{8}{3}P(x_1)D_1(t_2) + \frac{4}{3}P^2(x_1)D_0(t_2) - \frac{40}{9}(D_1(t_2) \\
&+ P(x_1)D_0(t_2)) + \left(\frac{112}{27} - \frac{8}{3}\zeta(2)\right)D_0(t_2)\Bigg\}\Bigg] + [t_1 \leftrightarrow t_2, x_1 \leftrightarrow x_2] \\
&+ \frac{1}{x_1 + x_2}\Bigg[C_F^2\Bigg\{\Bigg[16D_0(t_1)D_0(t_2)\Bigg]L_\mu^2 + \Bigg[48(D_1(t_1)D_0(t_2) \\
&+ D_0(t_1)D_1(t_2)) + 24D_0(t_1)D_0(t_2)\Bigg]L_\mu + 48D_1(t_1)D_1(t_2) \\
&+ 24(D_2(t_1)D_0(t_2) + D_0(t_1)D_2(t_2)) + (-64 + 16\zeta(2))D_0(t_1)D_0(t_2)\Bigg\} \\
&+ C_A C_F\Bigg\{\left[-\frac{44}{3}D_0(t_1)D_0(t_2)\right]L_\mu - \frac{44}{3}(D_1(t_1)D_0(t_2) + D_0(t_1)D_1(t_2)) \\
&+ \left(\frac{268}{9} - 8\zeta(2)\right)D_0(t_1)D_0(t_2)\Bigg\} \\
&+ n_f C_F\Bigg\{\left[\frac{8}{3}D_0(t_1)D_0(t_2)\right]L_\mu + \frac{8}{3}(D_1(t_1)D_0(t_2) + D_0(t_1)D_1(t_2)) \\
&- \frac{40}{9}D_0(t_1)D_0(t_2)\Bigg\}\Bigg]. \qquad \text{(B.1)}
\end{aligned}
$$

Here the color factors are given by $C_A = N$, $C_F = (N^2-1)/2N$ (QCD : $N = 3$) and n_f denotes the number of light flavours. In the above expression we have introduced the following shorthand notations

$$P^i(x_k) = \ln^i\left(\frac{1 - x_k}{x_k}\right) \qquad \text{(B.2)}$$

$$D_i(t_k) = \left(\frac{\ln^i\left(\frac{t_k}{x_k} - 1\right)}{t_k - x_k}\right)_+ \qquad \text{(B.3)}$$

$$L_\mu^i = \ln^i \frac{Q^2}{\mu^2} \tag{B.4}$$

In the DIS-scheme the above coefficient function becomes

$$\begin{aligned}
\Delta_{q\bar{q}}^{S+V,(2)}(t_1,t_2,x_1,x_2,Q^2,\mu^2) = \frac{\delta(t_1-x_1)\delta(t_2-x_2)}{x_1+x_2}\Bigg[\\
C_F^2\Bigg\{\Bigg[18-8\zeta(2)+8\left(P^2(x_1)+P^2(x_2)\right)+24\left(P(x_1)+P(x_2)\right) \\
+16P(x_1)P(x_2)\Bigg]L_\mu^2+\Bigg[15+84\zeta(2)+48\zeta(3)+12\left(P^2(x_1)+P^2(x_2)\right) \\
+16\left(P^2(x_1)P(x_2)+P(x_1)P^2(x_2)\right)+48P(x_1)P(x_2) \\
+(26+64\zeta(2))(P(x_1)+P(x_2))\Bigg]L_\mu+14\zeta(2)+72\zeta(3)+\frac{964}{5}\zeta^2(2) \\
+12\left(P^2(x_1)P(x_2)+P(x_1)P^2(x_2)\right)+8P^2(x_1)P^2(x_2) \\
+(17+80\zeta(2))P(x_1)P(x_2)+\left(\frac{9}{2}-8\zeta(2)\right)\left(P^2(x_1)+P^2(x_2)\right) \\
+\left(\frac{15}{2}+36\zeta(2)+24\zeta(3)\right)(P(x_1)+P(x_2))\Bigg\} \\
+C_AC_F\Bigg\{\Bigg[-11-\frac{22}{3}(P(x_1)+P(x_2))\Bigg]L_\mu^2+\Bigg[\frac{193}{3}-22\zeta(2)-24\zeta(3) \\
-\frac{22}{3}\left(P^2(x_1)+P^2(x_2)\right)+\left(\frac{268}{9}-8\zeta(2)\right)(P(x_1)+P(x_2)) \\
-\frac{44}{3}P(x_1)P(x_2)\Bigg]L_\mu+\frac{215}{9}+\frac{2366}{9}\zeta(2)-36\zeta(3)-\frac{194}{5}\zeta^2(2) \\
-\frac{22}{3}\left(P^2(x_1)P(x_2)+P(x_1)P^2(x_2)\right)-\frac{11}{2}\left(P^2(x_1)+P^2(x_2)\right) \\
+\left(\frac{57}{2}-12\zeta(3)\right)(P(x_1)+P(x_2))+\left(\frac{268}{9}-8\zeta(2)\right)P(x_1)P(x_2)\Bigg\} \\
+n_fC_F\Bigg\{\Bigg[2+\frac{4}{3}(P(x_1)+P(x_2))\Bigg]L_\mu^2+\Bigg[-\frac{34}{3}+4\zeta(2) \\
+\frac{4}{3}\left(P^2(x_1)+P^2(x_2)\right)+\frac{8}{3}P(x_1)P(x_2)-\frac{40}{9}(P(x_1)+P(x_2))\Bigg]L_\mu-\frac{38}{9}
\end{aligned}$$

$$
\begin{aligned}
&- \frac{380}{9}\zeta(2) - \frac{40}{9}P(x_1)P(x_2) + \frac{4}{3}\left(P^2(x_1)P(x_2) + P(x_1)P^2(x_2)\right) \\
&+ \left(P^2(x_1) + P^2(x_2)\right) - 5(P(x_1) + P(x_2))\Big\}\Big] \\
&+ \frac{\delta(t_1 - x_1)}{x_1 + x_2}\Big[C_F^2\Big\{\Big[16(D_1(t_2) + P(x_1)D_0(t_2)) + 24D_0(t_2)\Big]L_\mu^2 \\
&+ \Big[32P(x_1)D_1(t_2) + 16P^2(x_1)D_0(t_2) + 24D_1(t_2) + 48P(x_1)D_0(t_2) \\
&+ (26 + 64\zeta(2))D_0(t_2)\Big]L_\mu + 16P^2(x_1)D_1(t_2) + (9 - 16\zeta(2))D_1(t_2) \\
&+ 24P(x_1)D_1(t_2) + 12P^2(x_1)D_0(t_2) + (17 + 80\zeta(2))P(x_1)D_0(t_2)) \\
&+ \left(\frac{15}{2} + 36\zeta(2) + 24\zeta(3)\right)D_0(t_2)\Big\} \\
&+ C_A C_F\Big\{\Big[-\frac{22}{3}D_0(t_2)\Big]L_\mu^2 + \Big[-\frac{44}{3}D_1(t_2) - \frac{44}{3}P(x_1)D_0(t_2) \\
&+ \left(\frac{268}{9} - 8\zeta(2)\right)D_0(t_2)\Big]L_\mu - \frac{44}{3}P(x_1)D_1(t_2) - \frac{22}{3}P^2(x_1)D_0(t_2) \\
&- 11D_1(t_2) + \left(\frac{268}{9} - 8\zeta(2)\right)P(x_1)D_0(t_2) + \left(\frac{57}{2} - 12\zeta(3)\right)D_0(t_2)\Big\} \\
&+ n_f C_F\Big\{\Big[\frac{4}{3}D_0(t_2)\Big]L_\mu^2 + \Big[\frac{8}{3}(D_1(t_2) + P(x_1)D_0(t_2)) - \frac{40}{9}D_0(t_2)\Big]L_\mu \\
&+ \frac{8}{3}P(x_1)D_1(t_2) + \frac{4}{3}P^2(x_1)D_0(t_2) + 2D_1(t_2) - \frac{40}{9}P(x_1)D_0(t_2) \\
&- 5D_0(t_2)\Big\}\Big] + [t_1 \leftrightarrow t_2, x_1 \leftrightarrow x_2] \\
&+ \frac{1}{x_1 + x_2}\Big[C_F^2\Big\{\Big[16D_0(t_1)D_0(t_2)\Big]L_\mu^2 + \Big[32(D_1(t_1)D_0(t_2) \\
&+ D_0(t_1)D_1(t_2)) + 48D_0(t_1)D_0(t_2)\Big]L_\mu + 32D_1(t_1)D_1(t_2) \\
&+ 24(D_1(t_1)D_0(t_2) + D_0(t_1)D_1(t_2)) + (17 + 80\zeta(2))D_0(t_1)D_0(t_2)\Big\}
\end{aligned}
$$

$$
\begin{aligned}
&+ C_A C_F \left\{ \left[-\frac{44}{3} D_0(t_1) D_0(t_2) \right] L_\mu - \frac{44}{3} (D_1(t_1) D_0(t_2) + D_0(t_1) D_1(t_2)) \right. \\
&\left. + \left(\frac{268}{9} - 8\zeta(2) \right) D_0(t_1) D_0(t_2) \right\} \\
&+ n_f C_F \left\{ \left[\frac{8}{3} D_0(t_1) D_0(t_2) \right] L_\mu + \frac{8}{3} (D_1(t_1) D_0(t_2) + D_0(t_1) D_1(t_2)) \right. \\
&\left. - \frac{40}{9} D_0(t_1) D_0(t_2) \right\} \Bigg] . \qquad \text{(B.5)}
\end{aligned}
$$

If one chooses the renormalization scale μ_R unequal to the mass factorization scale μ one has to add the following term to the expressions in (B.1) and (B.5)

$$
\beta_0 \frac{\alpha_s(\mu_R^2)}{4\pi} \ln \frac{\mu_R^2}{\mu^2} \Delta_{q\bar{q}}^{S+V,(1)}(t_1, t_2, x_1, x_2, Q^2, \mu^2) \qquad \text{(B.6)}
$$

where β_0 is the lowest order coefficient in the β-function given by

$$
\beta_0 = \frac{11}{3} C_A - \frac{2}{3} n_f \qquad \text{(B.7)}
$$

and $\Delta_{qq}^{S+V,(1)}$ can be found in (A.1) for the $\overline{\text{MS}}$-scheme and in (A.13) for the DIS-scheme.
The coefficient functions for the cross section $d^2\sigma/dQ^2dy$ can be very easily derived from the above expression by multiplying the coefficient functions in (B.1), (B.5) and (B.6) by the factor $x_1 + x_2$.

References

[1] S.D. Drell and T.M. Yan, Phys. Rev. Lett. **25** (1970) 316. 13

[2] See section C of "Heavy-ion collisions" in the proceedings of the Large Hadron Collider Workshop, Aachen, 4-9 October 1990. Editors: G. Jarlskog and D. Rein, vol III p.1057-1234. 13

[3] G. Parisi, Phys. Lett. **90B** (1980) 295.

[4] G. Sterman, Nucl. Phys. **281** (1987) 310.

[5] D. Appell, P. Mackenzie and G. Sterman, Nucl. Phys. **B309** (1988) 259.

[6] S. Catani and L. Trentadue, Nucl. Phys. **B327** (1989) 323, *ibid.* Nucl. Phys. **B353** (1991) 183. 13

[7] H. Contapanagos and G. Sterman, Nucl. Phys. **B419** (1994) 77. 14

[8] P.M. Stevenson, Phys. Rev. **D23** (1981) 2916. 14

[9] G. Grunberg, Phys. Lett. **95B** (1980) 70, Erratum Phys. Lett. **110B** (1982) 501. 14

[10] S.J. Brodsky, G.P. Lepage and P.B. Mackenzie, Phys. Rev. **D28** (1983) 228. 7, 14

[11] J.H. Christenson *et al.*, Phys. Rev. Lett. **25** (1970) 1523. 14

[12] L.M. Lederman, Phys. Rep. **26** (1976) 149;
N.S. Craigie, Phys. Rep. **47** (1978) 1. 14

[13] J. Badier *et al.* (NA3 Collaboration), Phys. Lett. **89B** (1979) 145. 14

[14] R. Barate *et al.*, Phys. Rev. Lett. **43** (1979) 1541. 14

[15] G. Matthiae, Riv. Nuovo Cim. vol. 4, Nb.3 (1981) 1;
R. Stroynowski, Phys. Rep. **71** (1981) 1;
I.R. Kenyon, Rep. on Progr. in Phys. **45** (1982) 1261. 7, 14, 17

[16] J. Kubar-Andre and F.E. Paige, Phys. Rev. **D19** (1979) 221. 17, 19, 20, 30, 38, 94

[17] G. Altarelli, R.K. Ellis, and G. Martinelli, Nucl. Phys. **B157** (1979) 461. 17, 19, 30, 38

[18] J. Kubar, M. le Bellac, J.L. Meunier and G. Plaut, Nucl. Phys. **B175** (1980) 251. 14, 17, 95

[19] B. Humpert, and W.L. van Neerven, Nucl. Phys. **B184** (1981) 225. 14, 19, 20, 28, 29, 30, 31

[20] E. Anassontzis *et al.* (E537 Collaboration), Phys. Rev. **D38** (1988) 1377. 20, 28, 30, 32, 33, 34, 35, 36

[21] J.S. Conway *et al.* (E615 Collaboration), Phys. Rev. **D39** (1989) 92. 20, 28

[22] D.M. Alde *et al.* (E772 Collaboration), Phys. Rev. Lett. **64** (1990) 2479. 14, 19, 20, 28, 36, 37

[23] P.L. McGaughey *et al.* (E772 Collaboration), Phys. Rev. Lett. **69** (1992) 1726. 7, 14, 18, 19, 20, 42, 51, 52, 53, 61, 63, 64, 66

[24] R. Hamberg, W.L. van Neerven, and T. Matsuura, Nucl. Phys. **B359** (1991) 343. 14, 18, 19, 20, 42, 51, 52, 53, 63, 64

[25] W.L. van Neerven, and E.B. Zijlstra, Nucl. Phys. **B382** (1992) 11. 7, 14, 17, 19, 43, 51, 86

[26] T. Matsuura, and W.L. van Neerven, Z. Phys. **C38** (1988) 623;
T. Matsuura, S.C. van der Marck, and W.L. van Neerven, Nucl. Phys. **B319** (1989) 570, *ibid.* Phys. Lett. **B211** (1988) 171. 17, 19, 30, 38, 43

[27] P. Aurenche and P. Chiappetta, Z. Phys. **C34** (1987) 201. 17, 19, 20, 30, 38, 39, 40, 41, 43

[28] P.J. Sutton, A.D. Martin, R.G. Roberts, W.J. Stirling, Phys. Rev. **D45** (1992) 2349. 19, 40

[29] A.D. Martin, W.J. Stirling and R.G. Roberts, Phys. Rev. **D47** (1993) 867, *ibid.* Phys. Lett. **306B** (1993) 145, Erratum Phys. Lett. **309B** (1993) 492. 20

[30] J.F. Owens, Phys. Rev. **D30** (1984) 943. 20

[31] M. Glück, E. Reya, A. Vogt, Z. Phys. **C53** (1992) 651. 40, 41

[32] W. Furmanski, and R. Petronzio, Phys. Lett. **97B** (1980) 437. 41

[33] W. Furmanski, and R. Petronzio, Z. Phys. **C11** (1982) 293.

3 Heavy flavour contributions to the Drell-Yan cross section

3.1 Introduction

The production cross sections for the electroweak vector bosons W and Z in hadron–hadron collisions as described by the Drell-Yan (DY) [1] mechanism provides us with a beautiful test of perturbative QCD. One of the reasons is that the total cross section can be calculated in next-to-next-to leading order in perturbative QCD [2, 3] a result which is very hard to achieve for other processes in hadron-hadron collisions. Another advantage of this process is that on the Born level it is purely electroweak in origin for which the theory is in an excellent shape. Hence each deviation of the cross section from the Born approximation can be attributed to QCD effects. Therefore the Drell-Yan (DY) process belongs to the same class as deep inelastic lepton hadron scattering and electron–positron collisions where QCD corrections can be measured with much higher accuracy than in other reactions.
Besides the total cross section for vector boson production and the cross section $d\sigma/dm$ where m denotes the lepton pair invariant mass order α_s^2 corrections due to soft plus virtual gluon contributions have been calculated in [4] to the differential distributions $d^2\sigma/dmdx_F$ and $d^2\sigma/dmdy$. Here the quantities x_F and y denote the fraction of the longitudinal momentum of the lepton pair with respect to the center of mass (CM) momentum and the rapidity respectively.
Furthermore one has computed the full order α_s correction to the single vector boson inclusive cross sections $d^3\sigma/dmdx_Fdp_T$ or $d^3\sigma/dmdydp_T$ [5] where p_T denotes the transverse momentum of the vector boson. All the above calculations have been performed under the assumption that the quarks, appearing in the partonic subprocesses contributing to the DY process, are massless. This is a reasonable assumption for the light quarks u, d, and s and even for c since the masses of the W and Z are large compared with the masses of the above quarks. However this assumption is doubtful for the bottom quark and it is certainly wrong for the top quark since recent experiments [6] indicate that $m_t > M_W$, M_Z. Therefore we cannot neglect the masses of the bottom and top in the final state of the partonic subprocesses in particular if the collider CM energy is small like in the case of the $Sp\bar{p}S$ ($\sqrt{s} = 0.63\,\text{TeV}$) or the TEVATRON ($\sqrt{s} = 1.8\,\text{TeV}$). Maybe for some partonic subprocesses one can apply the zero mass approximation for the bottom quark at LHC ($\sqrt{s} = 16\,\text{TeV}$) as we will show later on. Contrary to the final state

we will omit the bottom and top quarks in the initial state because we assume that the bottom and top densities in the hadron are negligibly small.
The calculation of the contribution of heavy flavours to the DY cross section has been performed for Z-production in [7]. It contained all one-loop and two-loop corrections which are characteristic of Z-production but do not contribute to W-production or processes with a photon in the intermediate state. They are characterized by the triangular heavy flavour-loop insertions containing the Adler-Bell-Jackiw anomaly which has to cancel while adding top and bottom loops. This work was extended in [8] by including the interference terms originating from the final and initial state radiation of the vector boson in the process $q + \bar{q} \to Z + Q + \bar{Q}$ (with $Q = b$, t). All other production mechanisms, which also show up for W-production and processes with a photon in the intermediate state, have not been considered yet. The contributions to Z-production considered in [7, 8] all show up on the order α_s^2 level and amount to about 0.1 percent of the Born approximation which means that they are experimentally unobservable.
In this thesis we want to complete the above analysis by including all remaining Feynman graphs which also contribute to lepton pair production with a W or a photon in the intermediate state. Apart of some additional two-loop graphs they contain the contribution of the partonic subprocesses $q_1 + \bar{q}_2 \to V + Q_1 + \bar{Q}_2$ and $g + g \to V + Q_1 + \bar{Q}_2$ with $V = \gamma$, Z, W and $Q_i = b$, t. Like the corrections discussed in [7, 8] they all contribute to the DY cross section on the order α_s^2 level.
This chapter will be organized as follows. In section 2 we present the partonic cross sections corresponding to the subprocesses which contribute to heavy flavours plus vector boson production. Furthermore we show that in the case the vector boson mass becomes much larger than the heavy flavour mass one can find explicit analytic results. In section 3 we compute the heavy flavour contributions to vector boson production at current and future hadron-hadron colliders. In particular a comparison will be made between the order α_s^2 corrections due to light partons (quarks and gluons), calculated previously in [2, 3], and the contributions due to bottom and top quarks presented in this chapter. Finally in Appendix A we give an explicit formula for the two-loop vertex correction which was not computed in [7, 8].

3.2 The order α_s^2 corrections to the DY cross section due to heavy flavour production

In this section we present the partonic cross sections of heavy flavour production contributing to the Drell-Yan (DY) process which is given by

$$\begin{aligned} H_1 + H_2 \quad &\to \quad V + \text{“}X\text{”} \\ &\qquad \hookrightarrow \ell_1 + \ell_2, \end{aligned} \tag{3.2.1}$$

where H_1, H_2 denote the incoming hadrons and V stands for one of the vector bosons of the standard electroweak model (γ, Z or W) which subsequently decays

in the lepton pair ℓ_1, ℓ_2.
The heavy flavours in the final state are given by Q_1 and Q_2 respectively and the symbol "X" denotes any inclusive final hadronic state. In lowest order of the electroweak and strong coupling constants the above reaction receives contributions of the following parton subprocesses

$$i(k_1) + j(k_2) \to V(q) + Q_1(p_1) + \bar{Q}_2(p_2), \tag{3.2.2}$$

with i, $j = q$, $\bar{q}$, g. Here q stands for the light quarks given by u, d, s, and c whereas the heavy quarks are represented by t and b. Notice that in this chapter we study heavy flavour production at large hadron collider energies so that the charm can be treated as a light quark which mass can be neglected. In addition to reaction (3.2.2) we include the virtual corrections due to heavy flavour loops which contribute to the subprocesses

$$i(k_1) + j(k_2) \quad \to \quad V(q), \tag{3.2.3}$$

$$i(k_1) + j(k_2) \quad \to \quad V(q) + l(k_3), \tag{3.2.4}$$

with $l = q$, $\bar{q}$, g. The most of these virtual corrections reveal the presence of the triangle fermion loops giving rise to the well known Adler-Bell-Jackiw anomaly which has to cancel between the top and bottom contributions. They have been treated in [7, 8] in the case of $V = Z$. Here below we will add the contributions due to gluon self energies containing the heavy quark loop which also appear when V is represented by γ and W.
In the subsequent part of this chapter we are interested in the following parton cross section

$$\frac{d\hat{\sigma}_{ij}^V}{dQ^2} = \hat{\tau}\, \sigma_V(Q^2, M_V^2)\, \hat{W}_{ij}^V(\hat{\tau}, Q^2, m_1^2, m_2^2), \qquad \hat{\tau} = \frac{Q^2}{\hat{s}}, \tag{3.2.5}$$

receiving contributions from the reactions (3.2.2)-(3.2.4) (i, $j = q$, $\bar{q}$, g). The quantity σ_V represents the pointlike DY cross section and the kinematical variables $\sqrt{\hat{s}}$ ($\hat{s} = (k_1 + k_2)^2$) and $\sqrt{Q^2}$ stand for the C.M. energy and the lepton pair invariant mass respectively. In addition to the above variables the DY structure function, denoted by $\hat{W}_{ij}^V$, also depends on the heavy flavour masses m_1 and m_2. The pointlike cross section refers to the reaction

$$q_1 + \bar{q}_2 \to V \to \ell_1 + \bar{\ell}_2, \tag{3.2.6}$$

and is given by (see [2, 3])

$$\sigma_\gamma(Q^2) \;=\; \frac{1}{N}\,\frac{4\pi\alpha^2}{3Q^4}, \tag{3.2.7}$$

$$\sigma_Z(Q^2, M_Z^2) \;=\; \frac{1}{N}\,\frac{\pi\alpha}{4M_Z \sin^2\theta_W \cos^2\theta_W}\,\frac{\Gamma_{Z\to\ell\bar{\ell}}}{(Q^2 - M_Z^2)^2 + M_Z^2\Gamma_Z^2}, \tag{3.2.8}$$

$$\sigma_W(Q^2, M_W^2) \;=\; \frac{1}{N}\,\frac{\pi\alpha}{M_W \sin^2\theta_W}\,\frac{\Gamma_{W\to\ell\bar{\nu}}}{(Q^2 - M_W^2)^2 + M_W^2\Gamma_W^2}. \tag{3.2.9}$$

For completeness we also give the formula for the $\gamma - Z$ interference

$$\sigma_{\gamma Z}(Q^2, M_Z^2) = \frac{1}{N}\frac{\pi\alpha^2}{6}\frac{1-4\sin^2\theta_W}{\sin^2\theta_W\cos^2\theta_W}\frac{1}{Q^2}\frac{Q^2-M_Z^2}{(Q^2-M_Z^2)^2+M_Z^2\Gamma_Z^2}. \tag{3.2.10}$$

In the above expression θ_W denotes the electroweak angle. Furthermore Γ_Z and Γ_W represent the total width of the Z and W boson respectively (sum over all decay channels) and $N = 3$ ($SU(N)$, colour). The partial widths due to the leptonic decay of the Z and W are given by

$$\Gamma_{Z\to\ell\bar{\ell}} = \frac{\alpha M_Z(1+(1-4\sin^2\theta_W)^2)}{48\sin^2\theta_W\cos^2\theta_W}, \tag{3.2.11}$$

$$\Gamma_{W\to\ell\bar{\nu}_\ell} = \frac{\alpha M_W}{12\sin^2\theta_W}. \tag{3.2.12}$$

In the case of W- and Z-production the total cross section can be obtained using the narrow width approximation while integrating (3.2.5) over Q^2, i.e.

$$\frac{1}{(Q^2-M_V^2)^2+M_V^2\Gamma_V^2} \to \frac{\pi}{M_V\Gamma_V}\,\delta(Q^2-M_V^2). \tag{3.2.13}$$

The total rates $\hat{\sigma}_{ij}^V$ (sum over all leptonic and hadronic decay channels) are now given by

$$\hat{\sigma}_{ij}^Z = \frac{1}{N}\frac{\pi^2\alpha}{4\sin^2\theta_W\cos^2\theta_W}\frac{1}{\hat{s}}\hat{W}_{ij}^Z(M_Z^2/\hat{s}, M_Z^2, m^2, m^2), \tag{3.2.14}$$

$$\hat{\sigma}_{ij}^W = \frac{1}{N}\frac{\pi^2\alpha}{\sin^2\theta_W}\frac{1}{\hat{s}}\hat{W}_{ij}^W(M_W^2/\hat{s}, M_W^2, m_1^2, m_2^2). \tag{3.2.15}$$

When we consider the reaction where the vector boson decays into a specific lepton pair ℓ_1, $\bar{\ell}_2$ $\hat{\sigma}_{ij}^V$ in expressions (3.2.14), (3.2.15) has to be replaced by

$$\hat{\sigma}_{ij}^{V\to\ell_1\bar{\ell}_2} = \hat{\sigma}_{ij}^V\, B(V\to\ell_1\bar{\ell}_2), \tag{3.2.16}$$

where $B(V\to\ell_1\bar{\ell}_2)$ stands for the branching ratio

$$B(V\to\ell_1\bar{\ell}_2) = \frac{\Gamma_{V\to\ell_1\bar{\ell}_2}}{\Gamma_V}. \tag{3.2.17}$$

Notice that all particles into which the vector bosons decay are taken to be massless which is a good approximation since $M_Z >> m_b$ and the top is too heavy to appear in the decay products.
Further since the electroweak radiative corrections to $\sin^2\theta_W$ are non negligible it is better to replace $\sin^2\theta_W$ appearing in the denominators of the above expressions by

$$\sin^2\theta_W = \frac{\pi\alpha}{G_F\sqrt{2}M_W^2}, \tag{3.2.18}$$

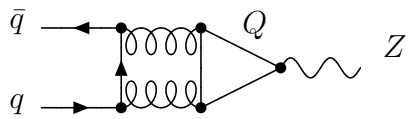

Figure 3.1: *Two-loop graph, containing the heavy flavours in the triangular subloop, which contributes to the subprocess* $q + \bar{q} \to Z$ *(3.2.22).*

where $G_F = 1.1667 \cdot 10^{-5}\,\mathrm{GeV}^{-2}$ (Fermi constant) whereas in the numerators we have put $\sin^2\theta_W = 0.2258$.
The above definitions imply that the vector- and axial-vector couplings describing the strength of the coupling of the vector bosons to the quarks are hidden in the definition for $\hat{W}_{ij}^V$ in (3.2.5). The same also holds for the elements of the Kobayashi-Maskawa matrix, denoted by $V_{q_1\bar{q}_2}$, which we approximate by retaining the Cabibbo angles only and putting the remaining angles and phases equal to zero.
In the case of the Born process as given by reaction (3.2.6) the DY-structure function becomes

$$\hat{W}_{q\bar{q}}^V = |V_{q_1\bar{q}_2}|^2 \left(\left(v_q^V\right)^2 + \left(a_q^V\right)^2 \right) \delta(1-\hat{\tau}), \tag{3.2.19}$$

with $V_{q_1\bar{q}_2} = 1$ in the case $V = \gamma,\ Z$. The vector- and axial-vector couplings are equal to

$$\begin{array}{ll}
v_u^\gamma = \frac{2}{3} & , a_u^\gamma = 0, \\
v_d^\gamma = -\frac{1}{3} & , a_d^\gamma = 0, \\
v_u^Z = 1 - \frac{8}{3}\sin^2\theta_W & , a_u^Z = -1, \\
v_d^Z = -1 + \frac{4}{3}\sin^2\theta_W & , a_d^Z = 1, \\
v_u^W = v_d^W = \frac{1}{\sqrt{2}} & , a_u^W = a_d^W = -\frac{1}{\sqrt{2}}.
\end{array} \tag{3.2.20}$$

We will now list all order α_s^2 parton cross sections due to heavy flavour production contributing to reaction (3.2.1).
We start with the two-loop corrections to the Born process

$$q_1 + \bar{q}_2 \to V, \tag{3.2.21}$$

which are presented by the graphs in Figs. 3.1 and 3.2. The first one (Fig. 3.1) contains a heavy quark in the triangular loop and it only contributes to Z-production. The W does not contribute because of charge conservation and the same holds for the photon due to charge conjugation (Furry's theorem). The DY structure function is equal to [7]-[9]

$$W_{q\bar{q}}^Z = \delta(1-\hat{\tau})\, a_q^Z a_Q^Z\, C_F T_f\, \frac{1}{2} \left(\frac{\alpha_s}{\pi}\right)^2 \Bigg[$$

$$\theta(Q^2 - 4m^2) G_1(m^2/Q^2) + \theta(4m^2 - Q^2) G_2(m^2/Q^2) \Bigg], \tag{3.2.22}$$

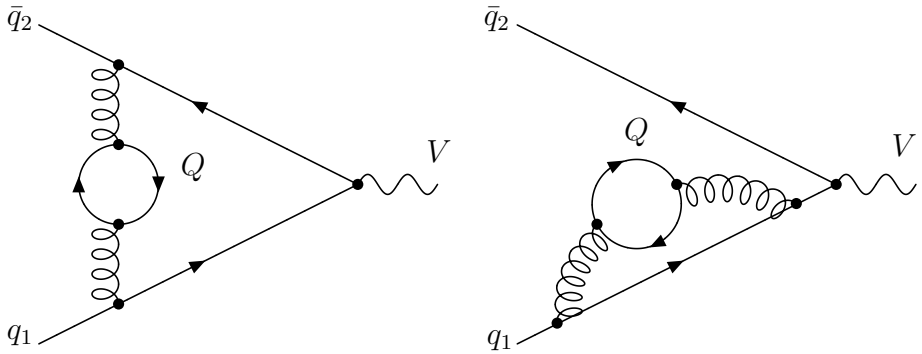

Figure 3.2: *Two-loop graphs, containing the heavy flavours in the gluon self energy, which contributes to the subprocess* $q + \bar{q} \to V$ *(3.2.23).*

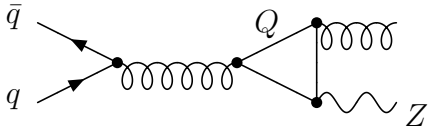

Figure 3.3: *One-loop graph with the heavy flavours in the triangle contributing to the subprocess* $q + \bar{q} \to Z + g$ *(3.2.26).*

where C_F and T_f are the $SU(N)$ colour factors: $C_F = \frac{N^2-1}{2N}$, $T_f = \frac{1}{2}$ and $q = u$, d, s, c , $Q = b$, t. The functions G_1 and G_2 are given in Eqs. (2.8) and (2.9) of [8] respectively. Notice that in expression (3.2.22) one has to sum over b and t in order to cancel the Adler-Bell-Jackiw axial anomaly.
The second two-loop correction to (3.2.21) is given by the vertex correction in Fig. 3.2. It contains the heavy quark loop contribution to the gluon self energy insertion in the vertex graph. The DY structure function becomes

$$W^V_{q\bar{q}} = \delta(1-\hat{\tau})\ |V_{q_1\bar{q}_2}|^2 \left(\left(v^V_q\right)^2 + \left(a^V_q\right)^2 \right) C_F T_f \frac{1}{8} \left(\frac{\alpha_s}{\pi}\right)^2 F(Q^2, m^2), \quad (3.2.23)$$

where $F(Q^2, m^2)$ can be found in (A.1) (also see [10]). The above expression contributes for all vector bosons and $V_{q_1\bar{q}_2} = 1$ when $V = \gamma$, Z.

Next we have the one-loop corrections to the two-to-two body processes (see Figs. 3.3 and 3.4)

$$q + \bar{q} \ \to \ g + V, \quad (3.2.24)$$

$$g + q(\bar{q}) \ \to \ q(\bar{q}) + V. \quad (3.2.25)$$

They all contain the triangle heavy quark loop insertion which only contributes to Z-production for the same reasons as mentioned above (3.2.22). For process (3.2.24)

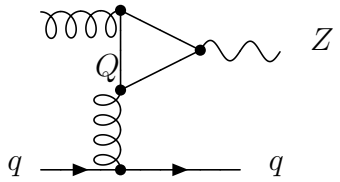

Figure 3.4: *One-loop graph with the heavy flavours in the triangle contributing to the subprocess* $g + q(\bar{q}) \to Z + q(\bar{q})$ *(3.2.27).*

(Fig. 3.3) the DY structure function reads

$$\hat{W}^Z_{q\bar{q}} = a^Z_q a^Z_Q C_F T_f \frac{1}{2}\left(\frac{\alpha_s}{\pi}\right)^2 \left[\frac{1+\hat{\tau}}{1-\hat{\tau}}\left\{-2+2\hat{\tau}\left(J_1(4m^2/\hat{s}) - J_1(4m^2/Q^2)\right)\right\}\right.$$
$$\left. -\frac{4m^2}{\hat{s}}\left(J_2(4m^2/\hat{s}) - J_2(4m^2/Q^2)\right)\right], \tag{3.2.26}$$

where J_1 and J_2 are given in Eqn. (2.12) of [8].
For process (3.2.25) (Fig. 3.4) we have the expression

$$\hat{W}^Z_{qg} = a^Z_q a^Z_Q T_f^2 \frac{1}{2}\left(\frac{\alpha_s}{\pi}\right)^2 \left[\theta(Q^2-4m^2)H_1(\hat{s},Q^2,m^2)\right.$$
$$\left. +\theta(4m^2-Q^2)H_2(\hat{s},Q^2,m^2)\right], \tag{3.2.27}$$

with H_1 and H_2 defined in (2.18) and (2.19) of [8] respectively. Like for the DY structure function in (3.2.22) the above expressions (3.2.26) and (3.2.27) have to be summed over b and t in order to cancel the axial anomaly.

The next contributions are given by the two to three body reactions (see Figs. 3.5 and 3.6)

$$q(k_1) + \bar{q}(k_2) \to V(q) + Q_1(p_1) + \bar{Q}_2(p_2), \tag{3.2.28}$$

$$g(k_1) + g(k_2) \to V(q) + Q_1(p_1) + \bar{Q}_2(p_2). \tag{3.2.29}$$

Since experiments indicate that $m_t > m_b + M_W$ [6] W-production has to be treated in a way which differs from the usual procedure applied to Z- and γ-production. This is due to the instability of the top quark appearing in the internal lines of the Feynman graphs in Figs. 3.5 and 3.6 corresponding to the reactions

$$q + \bar{q} \to t + \bar{t} \tag{3.2.30}$$
$$\hookrightarrow W^+ + b,$$

$$q + \bar{q} \to \bar{t} + t \tag{3.2.31}$$

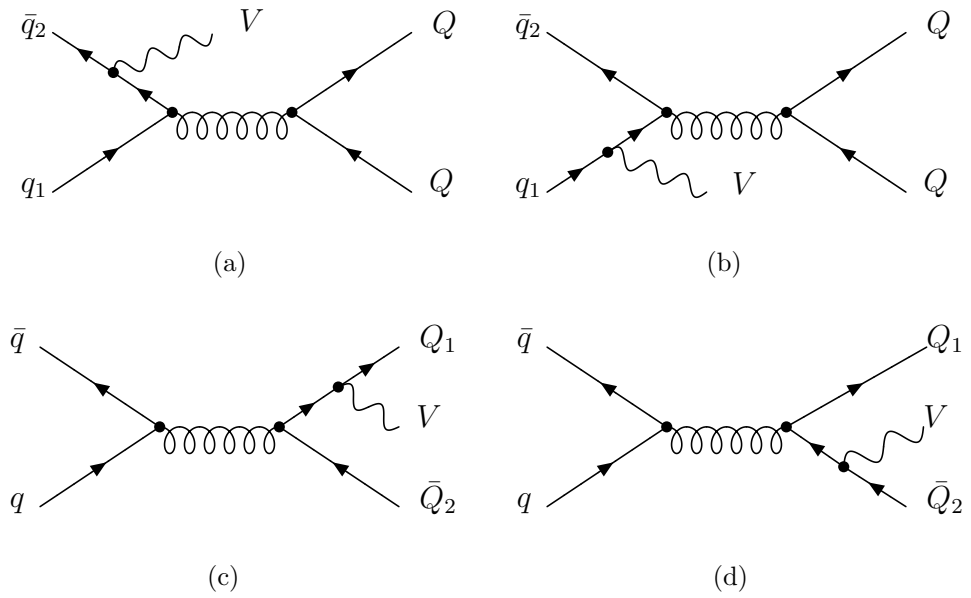

Figure 3.5: *Diagrams contributing to the subprocess* $q + \bar{q} \to V + Q_1 + \bar{Q}_2$*; a, b: initial state radiation; c, d: final state radiation (3.2.34).*

$$\begin{aligned} & \hookrightarrow W^- + \bar{b}, \\ g + g \;\to\; & t + \bar{t} \\ & \hookrightarrow W^+ + b, \end{aligned} \tag{3.2.32}$$

$$\begin{aligned} g + g \;\to\; & \bar{t} + t \\ & \hookrightarrow W^- + \bar{b}. \end{aligned} \tag{3.2.33}$$

In this case the internal top quark line cannot be described by an ordinary Feynman propagator anymore. Therefore it has to be treated as a resonance which implies that the top quark propagator has to be replaced by a Breit-Wigner form. However this procedure leads to a violation of gauge invariance which is hard to remedy. In the case of the total cross section (3.2.15) one can resort to an approximation which will be presented at the end of this section.
Starting with Z- and γ-production which is described by the Feynman diagrams in Figs. 3.5 and 3.6 the DY structure function is given by

$$\hat{W}_{ij}^V = K_{ij} \frac{1}{8\pi} \left(\frac{\alpha_s}{4\pi}\right)^2 \frac{1}{\hat{s}} \int d\hat{t}_1 \int d\hat{u}_1 \, \lambda^{1/2} \left(1, \frac{m_1^2}{\hat{s}_4}, \frac{m_2^2}{\hat{s}_4}\right) \cdot$$

$$\cdot \int_0^\pi d\phi \int_0^\pi d\theta \, \sin\theta \, \left|\mathcal{M}_{ij}^V\right|^2, \tag{3.2.34}$$

where $(i,\, j) = (q,\, \bar{q})$ or $(g,\, g)$. The symbol K_{ij} denotes the colour factor which is given by $K_{q\bar{q}} = C_F T_f$ and $K_{gg} = T_f^2$. In the definition of $\hat{W}_{ij}^V$ an average over the

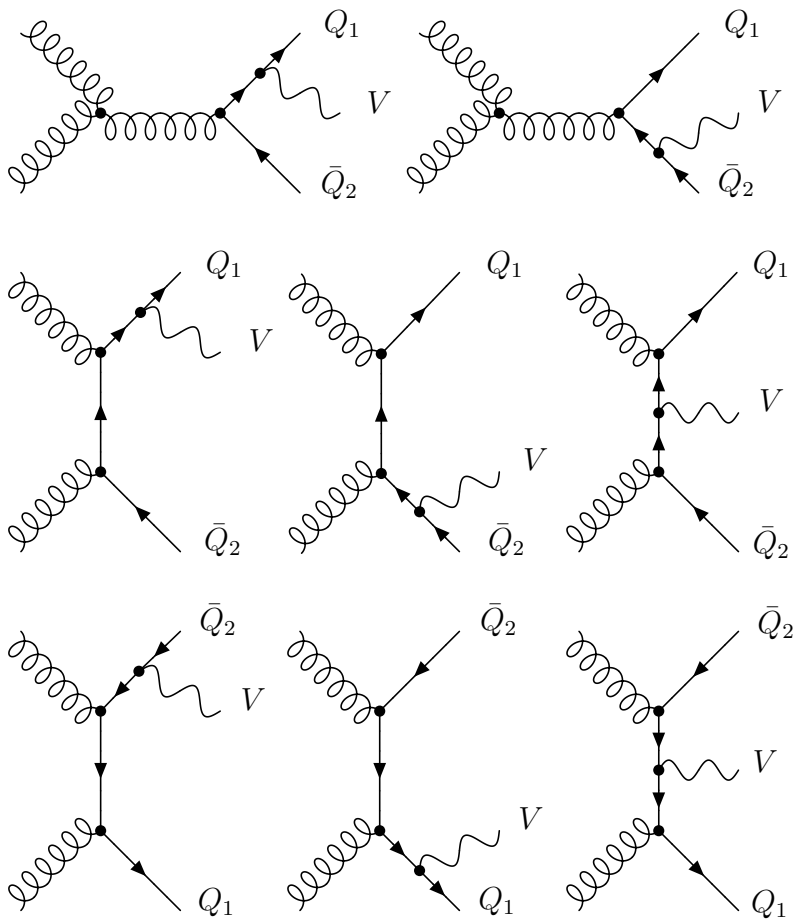

Figure 3.6: *Diagrams contributing to the subprocess* $g + g \to V + Q_1 + \bar{Q}_2$ *(3.2.34).*

initial spins and a sum over the final spins is understood. The Källen function is defined by $\lambda(x, y, z) = x^2 + y^2 + z^2 - 2xy - 2xz - 2yz$ and the kinematical invariants $\hat{s}_4$, $\hat{t}_1$, and $\hat{u}_1$ are given by (see (3.2.28) and (3.2.29))

$$\hat{s}_4 = (p_1 + p_2)^2, \quad \hat{t}_1 = (k_2 - q)^2, \quad \hat{u}_1 = (k_1 - q)^2. \tag{3.2.35}$$

In addition to the above invariants the matrix element squared $\left|\mathcal{M}_{ij}^V\right|^2$ depends on other kinematical variables which are analogous to the ones defined in Eqn. (4.2) of [11]. After having performed the traces the computation of $\left|\mathcal{M}_{ij}^V\right|^2$requires an intensive partial fractioning before the angular integration can be carried out. The angular integrals can be found in Appendix C of [11]. Notice that in the definition of $|\mathcal{M}|^2$ we have removed all the strong and electroweak coupling constants described by g_s, e, and g as defined in sections 10.6 and 14.5 of [12]. This also includes the typical factors which appear in the vertices like $-ig_s\gamma_\mu T_a$, $-iev_q^\gamma\gamma_\mu$, $-\frac{ig}{2}V_{q_1\bar{q}_2}\gamma_\mu(v_q^W + \gamma_5 a_q^W)$ and $-\frac{ig}{4\cos\theta_W}\gamma_\mu(v_q^Z + \gamma_5 a_q^Z)$ (see Eqn. (3.2.20)). Here $V_{q_1\bar{q}_2}$ denotes the Kobayashi-Maskawa matrixelement where only the Cabibbo angle θ_C

has been put to be unequal to zero. All these factors are absorbed in the definition of the pointlike cross sections $\sigma_V(Q^2, M_V^2)$ as presented in (3.2.7)-(3.2.9) except for the Cabibbo angles and the couplings v_q^V and a_q^V (3.2.20) which remain in $\hat{W}_{ij}^V$. In the case the vector boson couples to massless quarks they can be factored out too like in (3.2.19) but for massive quarks like the heavy flavours they remain in $\left|\mathcal{M}_{ij}^V\right|^2$. In the case $Q^2 >> m^2$ ($m_1 = m_2 = m$) one can obtain analytic expressions for the DY structure functions $\hat{W}_{q\bar{q}}^V$ and $\hat{W}_{gg}^V$. For process (3.2.28) where the vector boson is radiated off the incoming light quark lines (see Figs. 3.5a,b) one obtains *

$$
\begin{aligned}
W_{q\bar{q}}^{V,(1)}\left(\hat{\tau}, \frac{Q^2}{m^2}\right) &= |V_{q_1\bar{q}_2}|^2 \left\{\left(v_q^V\right)^2 + \left(a_q^V\right)^2\right\} C_F T_f \left(\frac{\alpha_s}{4\pi}\right)^2 \left[\frac{8}{3}\frac{1+\hat{\tau}^2}{1-\hat{\tau}} \ln^2\frac{Q^2}{m^2}\right. \\
&+ \left\{\frac{1+\hat{\tau}^2}{1-\hat{\tau}}\left(\frac{32}{3}\ln(1-\hat{\tau}) - \frac{32}{3}\ln\hat{\tau} - \frac{80}{9}\right) - \frac{32}{3}(1-\hat{\tau})\right\} \ln\frac{Q^2}{m^2} \\
&+ \frac{1+\hat{\tau}^2}{1-\hat{\tau}}\left(\frac{32}{3}\ln^2(1-\hat{\tau}) - \frac{64}{3}\ln\hat{\tau}\ln(1-\hat{\tau}) + \frac{28}{3}\ln^2\hat{\tau} - \frac{160}{9}\ln(1-\hat{\tau})\right. \\
&+ \left.\frac{160}{9}\ln\hat{\tau} - \frac{8}{3}\mathrm{Li}_2(1-\hat{\tau}) - \frac{32}{3}\zeta(2) + \frac{448}{27}\right) - \frac{16}{3}(1-\hat{\tau})\left(4\ln(1-\hat{\tau})\right. \\
&\left.\left. - 4\ln\hat{\tau} - \frac{19}{3}\right) - \frac{16}{3}\ln\hat{\tau} + \frac{8}{3}(1+\hat{\tau})\left(\mathrm{Li}_2(1-\hat{\tau}) + \frac{1}{2}\ln^2\hat{\tau}\right)\right].
\end{aligned}
\tag{3.2.36}
$$

If the parton cross section (3.2.5) is convoluted by the parton densities in order to compute the hadronic cross sections, as will be discussed in the next section, one approaches a singularity at $\hat{\tau} = 1$. In this case one cannot neglect the mass m in the denominator anymore. The resulting terms which even can go as a power of the type $\ln^3(Q^2/m^2)$ will be partially cancelled by similar terms arising in the vertex correction (3.2.23) (see (A.3)). They all can be described by an expression proportional to a delta function which has to be added to expression (3.2.36). This expression reads as follows

$$
\begin{aligned}
\hat{W}_{q\bar{q}}^{V,(2)}\left(\hat{\tau}, \frac{Q^2}{m^2}\right) &= |V_{q_1\bar{q}_2}|^2 \left\{\left(v_q^V\right)^2 + \left(a_q^V\right)^2\right\} C_F T_f \left(\frac{\alpha_s}{4\pi}\right)^2 \delta(1-\hat{\tau}) \left[4\ln^2\frac{Q^2}{m^2}\right. \\
&\left. - \frac{68}{3}\ln\frac{Q^2}{m^2} + \frac{32}{3}\zeta(3) - 16\zeta(2) + \frac{454}{9}\right].
\end{aligned}
\tag{3.2.37}
$$

Furthermore one has to replace in (3.2.36) the singular terms of the type $\ln^i(1-\hat{\tau})/(1-\hat{\tau})$ by $(\ln^i(1-\hat{\tau})/(1-\hat{\tau}))_+$ with the definition

$$
\int_0^1 dx \left(\frac{\ln^i(1-x)}{1-x}\right)_+ f(x) = \int_0^1 dx \frac{\ln^i(1-x)}{1-x}\left(f(x) - f(1)\right). \tag{3.2.38}
$$

*The polylogarithms of the type $\mathrm{Li}_n(x)$, $S_{n,p}(x)$ are defined in [13].

When the vector boson is radiated off the final state (see Figs. 3.5c,d) one finds in the limit $Q^2 >> m^2$

$$\hat{W}_{q\bar{q}}^{V,(3)}\left(\hat{\tau},\frac{Q^2}{m^2}\right) = |V_{q_1\bar{q}_2}|^2\left\{\left(v_Q^V\right)^2+\left(a_Q^V\right)^2\right\} C_F T_f \left(\frac{\alpha_s}{4\pi}\right)^2 \Bigg[(1+\hat{\tau})^2 \Bigg\{ - \frac{32}{3}\mathrm{Li}_2(-\hat{\tau}) - \frac{16}{3}\zeta(2) + \frac{8}{3}\ln^2\hat{\tau} - \frac{32}{3}\ln\hat{\tau}\,\ln(1+\hat{\tau}) \Bigg\} + \frac{8}{3}(3+4\hat{\tau}+3\hat{\tau}^2)\ln\hat{\tau} + \frac{40}{3}(1-\hat{\tau}^2) \Bigg]. \tag{3.2.39}$$

Finally in the case of Z-production one can also find an asymptotic expression for the interference terms between diagrams 3.5a,b and 3.5c,d. It is given by [2, 8]

$$\hat{W}_{q\bar{q}}^{Z,(4)}\left(\hat{\tau},\frac{Q^2}{m^2}\right) = a_q^Z a_Q^Z\, C_F T_f \left(\frac{\alpha_s}{4\pi}\right)^2 \left[16\frac{1+\hat{\tau}^2}{1-\hat{\tau}}\ln\hat{\tau} + 32\hat{\tau}\ln\hat{\tau} + 16(3-\hat{\tau}) \right]. \tag{3.2.40}$$

For the gluon-gluon fusion process (3.2.29) (see Fig. 3.6) one finds the following asymptotic expression

$$\hat{W}_{gg}^{V,(1)}\left(\hat{\tau},\frac{Q^2}{m^2}\right) = |V_{q_1\bar{q}_2}|^2\left\{\left(v_Q^V\right)^2+\left(a_Q^V\right)^2\right\} T_f^2 \left(\frac{\alpha_s}{4\pi}\right)^2 \Bigg\{ \Bigg[- \Big(8(1+4\hat{\tau} + 4\hat{\tau}^2)\ln\hat{\tau} + 16(1-\hat{\tau})(1+3\hat{\tau}) \Big) \ln^2\frac{Q^2}{m^2} + \Bigg\{ - 32(1+4\hat{\tau}+4\hat{\tau}^2)\cdot \cdot \Big(\mathrm{Li}_2(1-\hat{\tau}) + \ln\hat{\tau}\,\ln(1-\hat{\tau}) - \frac{1}{4}\ln^2\hat{\tau} \Big) - 64(1-\hat{\tau})(1+3\hat{\tau})\ln(1-\hat{\tau}) + 8(1+8\hat{\tau}-4\hat{\tau}^2)\ln\tau + 4(1-\hat{\tau})(7+67\hat{\tau}) \Bigg\} \ln\frac{Q^2}{m^2} + 4(1+4\hat{\tau}+4\hat{\tau}^2)\cdot \Big(16\mathrm{Li}_3(1-\hat{\tau}) - 4\mathrm{Li}_2(1-\hat{\tau})\,\ln\hat{\tau} - 16\mathrm{Li}_2(1-\hat{\tau})\,\ln(1-\hat{\tau}) + 4\ln^2\hat{\tau}\,\ln(1-\hat{\tau}) - 8\ln^2(1-\hat{\tau})\,\ln\hat{\tau} \Big) + 4(1+\hat{\tau}) \Big(8\mathrm{Li}_2(-\hat{\tau}) + 8\ln\hat{\tau}\,\ln(1+\hat{\tau}) \Big) + 4(1+\hat{\tau})^2 \Big(- 16S_{1,2}(-\hat{\tau}) - 16\mathrm{Li}_2(-\hat{\tau})\ln(1+\hat{\tau}) - 8\zeta(2)\ln(1+\hat{\tau}) + 12\ln^2\hat{\tau}\,\ln(1+\hat{\tau}) - 8\ln^2(1+\hat{\tau})\,\ln\hat{\tau} \Big) - 32(1+10\hat{\tau} + 7\hat{\tau}^2)\,S_{1,2}(1-\hat{\tau}) - 32(1+2\hat{\tau}-\hat{\tau}^2)\mathrm{Li}_3(-\hat{\tau}) - 16(1+2\hat{\tau}-2\hat{\tau}^2)\zeta(3)$$

$$
\begin{aligned}
&- 16(5+4\hat{\tau}-14\hat{\tau}^2)\mathrm{Li}_2(1-\hat{\tau}) + 32(2+4\hat{\tau}+\hat{\tau}^2)\mathrm{Li}_2(-\hat{\tau})\ln\hat{\tau} + 16\zeta(2)\cdot \\
&(3+10\hat{\tau}+10\hat{\tau}^2)\ln\hat{\tau} + 16(5+9\hat{\tau}-12\hat{\tau}^2)\zeta(2) - \frac{8}{3}(3+8\hat{\tau}+8\hat{\tau}^2)\ln^3\hat{\tau} \\
&- 8(3+7\hat{\tau}+4\hat{\tau}^2)\ln^2\hat{\tau} - 64(1-\hat{\tau})(1+3\hat{\tau})\ln^2(1-\hat{\tau}) + 16(1+8\hat{\tau} \\
&- 4\hat{\tau}^2)\ln\hat{\tau}\,\ln(1-\hat{\tau}) - 4(23+64\hat{\tau}-105\hat{\tau}^2)\ln\hat{\tau} + 8(1-\hat{\tau})(7+67\hat{\tau})\cdot \\
&\cdot\ln(1-\hat{\tau}) - 8(1-\hat{\tau})(16+49\hat{\tau})\Big] \\
&+ \frac{N^2}{N^2-1}\Bigg[4(1+\hat{\tau})^2\Bigg\{16S_{1,2}(-\hat{\tau}) + 24\mathrm{Li}_3(-\hat{\tau}) + 16\zeta(3) \\
&+ \frac{16}{3}\mathrm{Li}_2(-\hat{\tau}) - 24\mathrm{Li}_2(-\hat{\tau})\ln\hat{\tau} + 16\mathrm{Li}_2(-\hat{\tau})\ln(1+\hat{\tau}) + 8\zeta(2)\ln(1+\hat{\tau}) \\
&+ \frac{8}{3}\zeta(2) - 12\ln^2\hat{\tau}\,\ln(1+\hat{\tau}) + 8\ln^2(1+\hat{\tau})\,\ln\hat{\tau} + \frac{16}{3}\ln\hat{\tau}\,\ln(1+\hat{\tau})\Bigg\} \\
&- 32(1-\hat{\tau})^2 S_{1,2}(1-\hat{\tau}) + \frac{8}{3}(-2+2\hat{\tau}+25\hat{\tau}^2)\ln^2\hat{\tau} - \frac{8}{3}(6+38\hat{\tau} \\
&+ 75\hat{\tau}^2)\ln\hat{\tau} - \frac{1}{3}(1-\hat{\tau})(188+764\hat{\tau})\Bigg]\Bigg\}. \qquad (3.2.41)
\end{aligned}
$$

As we will see in the next section some of the above approximation turn out to be very useful for Z-production accompanied with $b\bar{b}$ quarks because $Q^2 = M_Z^2 >> m_b^2$. As has been discussed below (3.2.29) W-production has to be treated in a different way as has been done above for Z- and γ-production. Here one has to make a distinction between initial and final state emission of the W-boson. In the case the W-boson is radiated off from a light quark in the initial state, described by the graphs in Figs. 3.5a,b, the DY structure function is given by $\hat{W}_{q\bar{q}}^W$ in (3.2.34). However if the W-boson is the decay product of the top or anti-top quark in the final state like in Figs. 3.5c,d or Fig. 3.6 one has to resort to different methods. In this chapter we are only interested in the total cross section. Hence we can follow the same procedure as is outlined in (3.2.13)-(3.2.15). First we neglect the graphs where the W is emitted from the bottom quark because the latter is far off-shell and apply the narrow width approximation to the Breit-Wigner form of the top quark in reactions (3.2.30) and (3.2.31). This is a reasonable approach because the width of the top $\Gamma_t = 1.41\,\mathrm{GeV}$[†] is much smaller than its mass $m_t = 174\,\mathrm{GeV}$ [6]. Following the above procedure for W-production in quark-antiquark annihilation the total cross section is then given by

$$\sigma_{q\bar{q}}^W = \sigma_{\mathrm{tot}}(q\bar{q} \to t\bar{t})\,B(t \to Wb), \qquad (3.2.42)$$

[†] Γ_t is related to m_t using the formulae in [14].

with $B(t \to Wb) \approx 1$ and $\sigma_{\rm tot}(q\bar{q} \to t\bar{t})$ [15, 16] is equal to

$$\sigma_{\rm tot}(q\bar{q} \to t\bar{t}) = \frac{4\pi}{3}\,\alpha_s^2\,\frac{1}{N}\,C_F T_f\,\frac{1}{\hat{s}}\sqrt{1-\frac{4m^2}{\hat{s}}}\,\left(1+\frac{2m^2}{\hat{s}}\right). \tag{3.2.43}$$

In the case of the gluon-gluon fusion process (3.2.29) we proceed in the same way. Neglecting the emission of the W from the bottom quark and applying the narrow width approximation to reactions (3.2.32), (3.2.33) we get

$$\sigma_{gg}^W = \sigma_{\rm tot}(gg \to t\bar{t})\,B(t \to Wb), \tag{3.2.44}$$

where $\sigma_{\rm tot}(gg \to t\bar{t})$ is given by [15, 16]

$$\begin{aligned}\sigma_{\rm tot}(gg \to t\bar{t}) = 4\pi\alpha_s^2\,\frac{1}{N}\,T_f^2\,\frac{1}{\hat{s}}\Bigg[\Bigg\{ &-\left(1+\frac{4m^2}{\hat{s}}\right)\sqrt{1-\frac{4m^2}{\hat{s}}} \\ &+\left(1+\frac{4m^2}{\hat{s}}-\frac{8m^4}{\hat{s}^2}\right)\ln y(\hat{s})\Bigg\} + \frac{N^2}{N^2-1}\Bigg\{-\left(\frac{2}{3}+\frac{10}{3}\frac{m^2}{\hat{s}}\right)\sqrt{1-\frac{4m^2}{\hat{s}}} \\ &+\frac{8m^4}{\hat{s}^2}\ln y(\hat{s})\Bigg\}\Bigg],\end{aligned} \tag{3.2.45}$$

with

$$y(\hat{s}) = \frac{1+\sqrt{1-4m^2/\hat{s}}}{1-\sqrt{1-4m^2/\hat{s}}}. \tag{3.2.46}$$

3.3 Hadronic cross sections

In this section we want to discuss the heavy flavour (b and t) contribution to the total cross section of W- and Z-production at large hadron colliders. The energies and the colliders under study are given by $\sqrt{s} = 0.63\,\text{TeV}$ ($Sp\bar{p}S$, $p\bar{p}$), $\sqrt{s} = 1.8\,\text{TeV}$ (TEVATRON, $p\bar{p}$) and $\sqrt{s} = 16\,\text{TeV}$ (LHC, pp). Investigated will be the part of the total cross section constituted by the heavy flavour contribution. We also want to know how the latter, which is of order α_s^2, compares with the light parton contribution calculated in the same order of perturbation theory which has been studied in the past (see [2, 3]). Finally we want to study the validity of the approximation for the total cross section of $H_1 + H_2 \to Z + b + \bar{b}$ obtained from the formulae in (3.2.36)-(3.2.41) which are calculated in the limit $M_Z^2 >> m_b^2$.
The hadronic cross section is related to the partonic cross section (3.2.5) through the relation

$$\begin{aligned}\frac{d\sigma^V}{dQ^2} = \sum_{i,j}\int_0^1 dy_1\int_0^1 dy_2\int_0^1 dz\,\delta(\tau - y_1y_2z)\,y_1y_2\,f_i^{H_1}(y_1,\mu^2)\,f_j^{H_2}(y_2,\mu^2)\cdot \\ \cdot\frac{d\hat{\sigma}_{ij}^V}{dQ^2}(Q^2/y_1y_2s, Q^2, m_1^2, m_2^2, \mu^2),\end{aligned} \tag{3.3.1}$$

subprocess	equation	σ^Z (nb)
$q+\bar{q} \to Z$	(3.2.22)	$3.13 \cdot 10^{-3}$
$q+\bar{q} \to Z$	(3.2.23)	$1.40 \cdot 10^{-4}$
$q+\bar{q} \to Z+g$	(3.2.26)	$1.13 \cdot 10^{-4}$
$g+q(\bar{q}) \to Z+q(\bar{q})$	(3.2.27)	$-1.77 \cdot 10^{-5}$
$q+\bar{q} \to Z+b+\bar{b}$	(3.2.34)	$1.47 \cdot 10^{-3}$
$q+\bar{q} \to Z+t+\bar{t}$	(3.2.34)	$1.35 \cdot 10^{-11}$
$g+g \to Z+b+\bar{b}$	(3.2.34)	$6.39 \cdot 10^{-5}$
$g+g \to Z+t+\bar{t}$	(3.2.34)	$1.25 \cdot 10^{-16}$
$\sigma^Z(b,t)$		$4.90 \cdot 10^{-3}$
$\sigma^Z(u,d,s,c,g) = 1.54\,(\text{Born}) + 0.41\,(\mathcal{O}(\alpha_s)) + 0.10\,(\mathcal{O}(\alpha_s^2)) = 2.05$		

Table 3.1: *Contributions to the total cross section for Z-production at $\sqrt{s} = 0.63$ TeV ($\alpha_s(M_Z) = 0.107$).*

where $f_i^H(y,\mu^2)$ denotes the density of parton i inside the hadron H which depends aside from y also on the factorization (renormalization) scale μ. Notice that for convenience we have put the renormalization scale equal to the factorization scale. In the case heavy flavour production is treated in lowest order, as we do in this chapter, $d\hat{\sigma}/dQ^2$ is independent of the factorization scale (Born approximation). However since this approximation is of order α_s^2 it does depend on the renormalization scale. In the case of light partons in the initial and final state one has to perform mass factorization to $d\hat{\sigma}_{ij}/dQ^2$ in order to remove the collinear divergences and this quantity has to be replaced by the DY coefficient function which has been calculated up to order α_s^2 in [2, 3]. Therefore in addition to the renormalization scale the latter also depends on the factorization scale.
In our calculations we have chosen the $\overline{\text{MS}}$-scheme for the coupling constant α_s as well as for the DY-coefficient function calculated up to order α_s^2 in [2]. For the parton densities we have chosen the $\overline{\text{MS}}$-version of the set MRS(H) [17] with $\Lambda^{(4)}_{\overline{\text{MS}}} = 230\,\text{MeV}$. Furthermore we use the two-loop corrected running coupling constant α_s with the QCD scale Λ mentioned above. Since we only consider top and bottom quark production we have put the number of light flavours equal to four, i.e. $n_f = 4$. Finally we have set the factorization (renormalization) scale $\mu^2 = Q^2$ where $Q^2 = M_V^2$. For the electroweak parameters we have taken the following values: $M_Z = 91.196\,\text{GeV}$, $M_W = 80.24\,\text{GeV}$, $G_F = 1.1667 \cdot 10^{-5}\,\text{GeV}^{-2}$, $\sin^2\theta_W = 0.2258$ and $\sin^2\theta_C = 0.0484$. The masses of the heavy flavours are given by $m_b = 5\,\text{GeV}$ and $m_t = 174\,\text{GeV}$.

subprocess	equation	σ^Z (nb)
$q+\bar{q}\to Z$	(3.2.22)	$5.33\cdot 10^{-3}$
$q+\bar{q}\to Z$	(3.2.23)	$4.86\cdot 10^{-4}$
$q+\bar{q}\to Z+g$	(3.2.26)	$3.67\cdot 10^{-4}$
$g+q(\bar{q})\to Z+q(\bar{q})$	(3.2.27)	$-1.61\cdot 10^{-4}$
$q+\bar{q}\to Z+b+\bar{b}$	(3.2.34)	$8.57\cdot 10^{-3}$
$q+\bar{q}\to Z+t+\bar{t}$	(3.2.34)	$3.58\cdot 10^{-6}$
$g+g\to Z+b+\bar{b}$	(3.2.34)	$4.71\cdot 10^{-3}$
$g+g\to Z+t+\bar{t}$	(3.2.34)	$5.50\cdot 10^{-8}$
$\sigma^Z(b,t)$		$1.93\cdot 10^{-2}$
$\sigma^Z(u,d,s,c,g)=5.34\,(\text{Born})+1.05\,(\mathcal{O}(\alpha_s))+0.17\,(\mathcal{O}(\alpha_s^2))=6.56$		

Table 3.2: *Contributions to the total cross section for Z-production at $\sqrt{s}=1.8$ TeV ($\alpha_s(M_Z)=0.107$).*

subprocess	equation	σ^Z (nb)
$q+\bar{q}\to Z$	(3.2.22)	$1.21\cdot 10^{-2}$
$q+\bar{q}\to Z$	(3.2.23)	$5.02\cdot 10^{-3}$
$q+\bar{q}\to Z+g$	(3.2.26)	$8.06\cdot 10^{-4}$
$g+q(\bar{q})\to Z+q(\bar{q})$	(3.2.27)	$-1.57\cdot 10^{-3}$
$q+\bar{q}\to Z+b+\bar{b}$	(3.2.34)	$9.28\cdot 10^{-2}$
$q+\bar{q}\to Z+t+\bar{t}$	(3.2.34)	$3.17\cdot 10^{-4}$
$g+g\to Z+b+\bar{b}$	(3.2.34)	$5.85\cdot 10^{-1}$
$g+g\to Z+t+\bar{t}$	(3.2.34)	$9.23\cdot 10^{-4}$
$\sigma^Z(b,t)$		$6.95\cdot 10^{-1}$
$\sigma^Z(u,d,s,c,g)=55.2\,(\text{Born})+7.45\,(\mathcal{O}(\alpha_s))-0.09\,(\mathcal{O}(\alpha_s^2))=62.6$		

Table 3.3: *Contributions to the total cross section for Z-production at $\sqrt{s}=16$ TeV ($\alpha_s(M_Z)=0.107$).*

3.3.1 Heavy flavour contributions to $d\sigma/dQ^2$ for Z-production

To calculate the total cross section for Z-production we have integrated expression (3.3.1) over Q^2 and used the narrow width approximation (3.2.14). In tables 3.1-3.3 we have listed the various contributions coming from the partonic subprocesses discussed in the previous section and compared them with the light parton cross section corrected up to order α_s^2. The tables reveal that at smaller energies, i.e.

$\sqrt{s} = 0.63\,\text{TeV}$ the total heavy flavour cross section is dominated by the vertex correction (3.2.22) given by Fig. 3.1 and the subprocess $q + \bar{q} \to Z + b + \bar{b}$ (3.2.34) depicted in Fig. 3.5. As we will show later on the importance of the last process is wholly due to initial state radiation (Figs. 3.5a,b). At larger energies like $\sqrt{s} = 1.8\,\text{TeV}$ also the process $g + g \to Z + b + \bar{b}$ (3.2.34) (Fig. 3.6) becomes important. The latter even overwhelms the other reactions when $\sqrt{s} = 16\,\text{TeV}$ (LHC). This can be traced back to the gluon density which steeply rises at very small $\tau = M_V^2/s$. Finally we observe that the processes with top quarks in the final state are completely unimportant which is due to the limited phase space available even for energies as large as $\sqrt{s} = 16\,\text{TeV}$ (LHC).
The reason that the virtual correction in Fig. 3.1 plays an important role can be inferred from the expression in (3.2.22). Here the first term G_1 only contributes in the case of the bottom loop ($M_Z^2 > 4m_b^2$) whereas the second term G_2 only contributes for the top loop ($M_Z^2 < 4m_t^2$). In [8] it has been shown that for $Q^2 >> m^2$ the function G_1 vanishes like

$$G_1\left(\frac{m^2}{Q^2}\right) \sim \mathcal{O}\left(\frac{m^2}{Q^2}\right), \tag{3.3.2}$$

whereas the function G_2 has the following asymptotic behavior for $m^2 >> Q^2$

$$G_2\left(\frac{m^2}{Q^2}\right) \sim -3\ln\frac{Q^2}{m^2} - 2\zeta(2) + \frac{21}{2} + \mathcal{O}\left(\frac{Q^2}{m^2}\right), \tag{3.3.3}$$

which means that this correction is dominated by the top-loop contribution.
In tables 3.1-3.3 we have also listed the results coming from the light parton contribution calculated in [2]. We observe that the heavy flavour part of the DY cross section is very small and it amounts to 0.2% ($\sqrt{s} = 0.63\,\text{TeV}$), 0.3% ($\sqrt{s} = 1.8\,\text{TeV}$), 1% ($\sqrt{s} = 16\,\text{TeV}$) of the light quark contribution. Even if we compare the heavy flavour part, which is an order α_s^2 correction, with the corresponding light parton contribution in the same order of perturbation theory one discovers that it is very small except when the energy gets very large. It amounts to 5% ($\sqrt{s} = 0.63\,\text{TeV}$), 11% ($\sqrt{s} = 1.8\,\text{TeV}$), and 770% (absolute value) ($\sqrt{s} = 16\,\text{TeV}$) of the α_s^2 correction to the cross section which is due to light partons. This means that only at LHC energies heavy flavour production is more important than the light parton subprocesses contributing in order α_s^2.

3.3.2 Heavy flavour contributions to $d\sigma/dQ^2$ for W-production

For the W-cross section we proceed in the same way as for Z-production except that here we also have to make the narrow width approximation for the top quark. This is needed when the W is radiated off the top-quark in the final state exhibited by the graphs in Figs. 3.5c,d and 3.6. Furthermore the graphs containing the triangle heavy flavour loop like Figs. 3.1, 3.3, and 3.4 do not contribute. The results are given in tables 3.4-3.6. Like in the case of Z-production the process $q_1 + \bar{q}_2 \to W + b + \bar{b}$ (3.2.34)

subprocess	equation	σ^W (nb)
$q_1 + \bar{q}_2 \to W$	(3.2.23)	$1.32 \cdot 10^{-3}$
$q_1 + \bar{q}_2 \to W + b + \bar{b}$	(3.2.34)	$4.11 \cdot 10^{-3}$
$q_1 + \bar{q}_2 \to W + t + \bar{t}$	(3.2.34)	$1.94 \cdot 10^{-11}$
$q + \bar{q} \to t(\bar{t}) + \bar{t}(t)$ $\hookrightarrow W^+(W^-) + b(\bar{b})$	(3.2.42)	$1.43 \cdot 10^{-6}$
$g + g \to t(\bar{t}) + \bar{t}(t)$ $\hookrightarrow W^+(W^-) + b(\bar{b})$	(3.2.44)	$1.52 \cdot 10^{-9}$
$\sigma^W(b,t)$		$5.43 \cdot 10^{-3}$
$\sigma^W(u,d,s,c,g) = 5.09\,(\text{Born}) + 1.34\,(\mathcal{O}(\alpha_s)) + 0.33\,(\mathcal{O}(\alpha_s^2)) = 6.76$		

Table 3.4: *Contributions to the total cross section for $W^+ + W^-$-production at $\sqrt{s} = 0.63$ TeV ($\alpha_s(M_W) = 0.109$).*

subprocess	equation	σ^W (nb)
$q_1 + \bar{q}_2 \to W$	(3.2.23)	$4.67 \cdot 10^{-3}$
$q_1 + \bar{q}_2 \to W + b + \bar{b}$	(3.2.34)	$2.51 \cdot 10^{-2}$
$q_1 + \bar{q}_2 \to W + t + \bar{t}$	(3.2.34)	$6.36 \cdot 10^{-6}$
$q + \bar{q} \to t(\bar{t}) + \bar{t}(t)$ $\hookrightarrow W^+(W^-) + b(\bar{b})$	(3.2.42)	$1.10 \cdot 10^{-3}$
$g + g \to t(\bar{t}) + \bar{t}(t)$ $\hookrightarrow W^+(W^-) + b(\bar{b})$	(3.2.44)	$1.28 \cdot 10^{-4}$
$\sigma^W(b,t)$		$3.10 \cdot 10^{-2}$
$\sigma^W(u,d,s,c,g) = 18.0\,(\text{Born}) + 3.47\,(\mathcal{O}(\alpha_s)) + 0.50\,(\mathcal{O}(\alpha_s^2)) = 22.0$		

Table 3.5: *Contributions to the total cross section for $W^+ + W^-$-production at $\sqrt{s} = 1.8$ TeV ($\alpha_s(M_W) = 0.109$).*

(Figs. 3.5a,b) is dominant at lower energies although also the vertex correction (3.2.23) contributes a little bit. When the energy gets larger like in the case of LHC also the process $g + g \to t + \bar{t}$ with $t \to W^+ b$ and $\bar{t} \to W^- \bar{b}$ (3.2.44) (Fig. 3.6) becomes important due to the gluon density which becomes very large at small $\tau = M_W^2/s$. As in Z-production the heavy flavours give a small contribution to the W-cross section. The latter is of the same magnitude as in the Z-cross section and it amounts to 0.1% ($\sqrt{s} = 0.63$ TeV), 0.1% ($\sqrt{s} = 1.8$ TeV), and 0.2% ($\sqrt{s} = 16$ TeV) of the light parton contribution. If we make a comparison with the order α_s^2 part of the light parton contribution these numbers become 2%, 6%, and 90% respectively which are however smaller than in the case of Z-production.

subprocess	equation	σ^W (nb)
$q_1 + \bar{q}_2 \to W$	(3.2.23)	$4.79 \cdot 10^{-2}$
$q_1 + \bar{q}_2 \to W + b + \bar{b}$	(3.2.34)	$2.76 \cdot 10^{-1}$
$q_1 + \bar{q}_2 \to W + t + \bar{t}$	(3.2.34)	$6.26 \cdot 10^{-4}$
$q + \bar{q} \to t(\bar{t}) + \bar{t}(t)$ $\hookrightarrow W^+(W^-) + b(\bar{b})$	(3.2.42)	$2.00 \cdot 10^{-2}$
$g + g \to t(\bar{t}) + \bar{t}(t)$ $\hookrightarrow W^+(W^-) + b(\bar{b})$	(3.2.44)	$1.77 \cdot 10^{-1}$
$\sigma^W(b,t)$		$5.22 \cdot 10^{-1}$
$\sigma^W(u,d,s,c,g) = 185\,(\text{Born}) + 24.8\,(\mathcal{O}(\alpha_s)) - 0.6\,(\mathcal{O}(\alpha_s^2)) = 209$		

Table 3.6: *Contributions to the total cross section for $W^+ + W^-$-production at $\sqrt{s} = 16$ TeV ($\alpha_s(M_W) = 0.109$).*

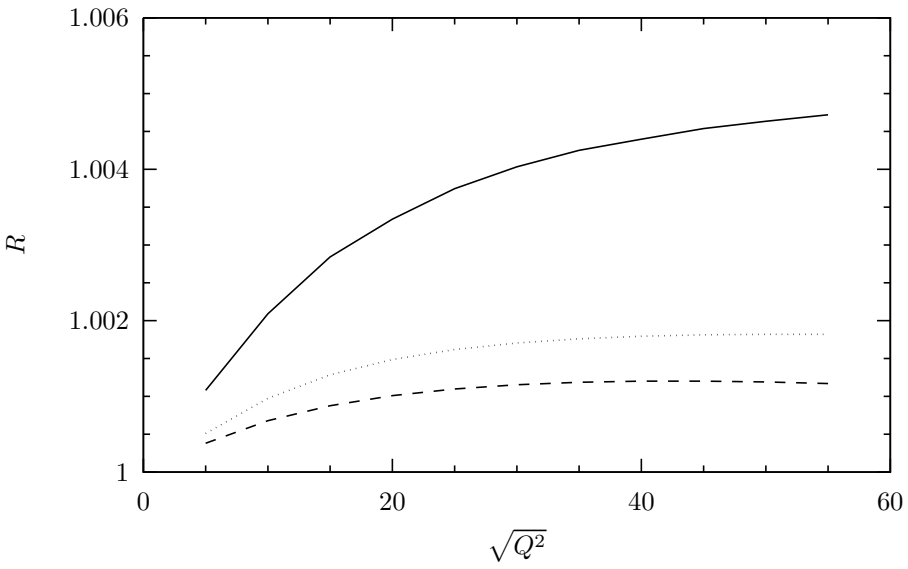

Figure 3.7: *The heavy flavour content, represented by R (3.3.4), of the cross section $d\sigma/dQ^2$ for the processes: $p + \bar{p} \to \gamma^* +$ "X" $\sqrt{s} = 0.63$ TeV (solid line), $\sqrt{s} = 1.8$ TeV (dotted line) and $p + p \to \gamma^* +$ "X" $\sqrt{s} = 16$ TeV (dashed line).*

3.3.3 Heavy flavour contributions to $d\sigma/dQ^2$ for $\sqrt{Q^2} < 60$ GeV

Besides vector boson production we have also studied the heavy flavour part of the DY cross section $d\sigma/dQ^2$ at small Q^2 ($\sqrt{Q^2} < 60$ GeV) where the virtual photon

	$B_Z\,\sigma^Z$ (pb)	$B_W\,\sigma^W$ (pb)
UA1	$58.6 \pm 7.8 \pm 8.4$	$609 \pm 41 \pm 94$
UA2	$65.6 \pm 4.0 \pm 3.8$	$682 \pm 12 \pm 40$
$B_V\,\sigma^V(u,d,s,c,g)$	68.7	737
$B_V\,\sigma^V(b,t)$	0.164	0.592

Table 3.7: *$B_Z\,\sigma^Z$ and $B_W\,\sigma^W$ for the $Sp\bar{p}S$ [18, 19] with $B_Z \equiv B(Z \to e^+\,e^-) = 3.35 \cdot 10^{-2}$ and $B_W \equiv B(W \to e\nu_e) = 0.109$, $\sqrt{s} = 0.63$ TeV.*

	$B_Z\,\sigma^Z$ (nb)	$B_W\,\sigma^W$ (nb)
CDF	$0.214 \pm 0.011 \pm 0.020$	$2.20 \pm 0.04 \pm 0.20$
$B_V\,\sigma^V(u,d,s,c,g)$	0.220	2.40
$B_V\,\sigma^V(b,t)$	$6.47 \cdot 10^{-4}$	$3.38 \cdot 10^{-3}$

Table 3.8: *$B_Z\,\sigma^Z$ and $B_W\,\sigma^W$ for the TEVATRON [20] with $B_Z \equiv B(Z \to e^+\,e^-) = 3.35 \cdot 10^{-2}$ and $B_W \equiv B(W \to e\nu_e) = 0.109$, $\sqrt{s} = 1.8$ TeV.*

dominates the cross section. In Fig. 3.7 we have plotted the ratio R

$$R(Q^2) = \frac{\frac{d\sigma}{dQ^2}(u,d,s,c,g) + \frac{d\sigma}{dQ^2}(t,b)}{\frac{d\sigma}{dQ^2}(u,d,s,c,g)}, \tag{3.3.4}$$

at three different energies, i.e. $\sqrt{s} = 0.63, 1.8, 16\,\text{TeV}$. Like in the case of Z- and W-boson production the contribution of the heavy flavours to the DY cross section is very small. When the energy increases it grows from 0.1% to 0.5% of the part constituted by the light parton contributions.

3.3.4 Contributions of the heavy flavours to the total cross section for *Z*- and *W*-production

Using the MRS(H) [17] parton densities we also calculate the cross sections for Z- and W-production where the lepton pair into which the vector boson decays is measured. The results are presented in table 3.7 ($Sp\bar{p}S$, $\sqrt{S} = 0.63\,\text{TeV}$) and table 3.8 (TEVATRON, $\sqrt{s} = 1.8\,\text{TeV}$). They are obtained by multiplying the total cross sections σ^Z and σ^W in tables 3.1 to 3.6 by the branching ratios $B(Z \to e^+\,e^-) = 3.35 \cdot 10^{-2}$ and $B(W \to e\nu_e) = 0.109$ respectively. Furthermore we have also listed the experimental data obtained from the groups UA1 [18], UA2 [19] ($Sp\bar{p}S$) and CDF [20] (TEVATRON). As is expected from the previous discussion the contribution from the heavy flavours b and t to the cross section is extremely small when compared with the light parton part.

$\sqrt{s} = 0.63$ TeV			
	σ^Z_{exact} (nb)		$\sigma^Z_{\text{app.}}$ (nb)
$q + \bar{q} \to Z + b + \bar{b}$	$1.58 \cdot 10^{-3}$	(3.2.23), (3.2.34)	$1.11 \cdot 10^{-3}$ (3.2.36), (3.2.37)
	$2.41 \cdot 10^{-6}$	(3.2.34)	$2.48 \cdot 10^{-6}$ (3.2.39)
	$-9.09 \cdot 10^{-6}$	(3.2.34)	$-1.26 \cdot 10^{-5}$ (3.2.40)
$g + g \to Z + b + \bar{b}$	$6.39 \cdot 10^{-5}$	(3.2.34)	$5.80 \cdot 10^{-5}$ (3.2.41)
$\sqrt{s} = 1.8$ TeV			
	σ^Z_{exact} (nb)		$\sigma^Z_{\text{app.}}$ (nb)
$q + \bar{q} \to Z + b + \bar{b}$	$8.88 \cdot 10^{-3}$	(3.2.23), (3.2.34)	$7.40 \cdot 10^{-3}$ (3.2.36), (3.2.37)
	$4.31 \cdot 10^{-5}$	(3.2.34)	$4.35 \cdot 10^{-5}$ (3.2.39)
	$-1.40 \cdot 10^{-5}$	(3.2.34)	$-2.14 \cdot 10^{-5}$ (3.2.40)
$g + g \to Z + b + \bar{b}$	$4.71 \cdot 10^{-3}$	(3.2.34)	$4.56 \cdot 10^{-3}$ (3.2.41)
$\sqrt{s} = 16$ TeV			
	σ^Z_{exact} (nb)		$\sigma^Z_{\text{app.}}$ (nb)
$q + \bar{q} \to Z + b + \bar{b}$	$9.54 \cdot 10^{-2}$	(3.2.23), (3.2.34)	$8.01 \cdot 10^{-2}$ (3.2.36), (3.2.37)
	$5.93 \cdot 10^{-4}$	(3.2.34)	$5.97 \cdot 10^{-4}$ (3.2.39)
	$-6.88 \cdot 10^{-6}$	(3.2.34)	$-2.30 \cdot 10^{-5}$ (3.2.40)
$g + g \to Z + b + \bar{b}$	$5.85 \cdot 10^{-1}$	(3.2.34)	$5.77 \cdot 10^{-1}$ (3.2.41)

Table 3.9: *Comparison of the exact versus approximate cross sections for Z- and $b\bar{b}$-production ($\alpha_s(M_Z) = 0.107$).*

3.3.5 The asymptotic region where $m^2 << Q^2$

Before concluding this section we have also studied the cross sections obtained from (3.2.36)-(3.2.41) which are derived in the limit $Q^2 >> m^2$. In practice these formulae are only applicable to the reaction $H_1 + H_2 \to Z + b + \bar{b}$ where $M_Z^2 >> m_b^2$. This inequality does not apply to top production also when the Z is replaced by the W. In the case a photon appears in the intermediate state the above formulae are also not very useful because in the region $Q^2 >> m^2$ the production rate is too low. In table 3.9 we have compared the results obtained from the exact cross section

represented by (3.2.23), (3.2.34) with those predicted by the asymptotic formulae in (3.2.36)-(3.2.41). First the table shows that the whole contribution to the cross section of the subprocess $q + \bar{q} \to Z + b + \bar{b}$ is given by the initial state radiation of the Z-boson as depicted in Figs. 3.5a,b which also includes the virtual contribution in Fig. 3.2. This is due to the large logarithmic terms $\ln^k(Q^2/m^2)$ which show up in (3.2.36) and (3.2.37). Furthermore the approximations to the initial state radiation process work rather well in particularly when the energy increases. The difference between the exact (3.2.23), (3.2.34) and the approximate cross sections (3.2.36), (3.2.37) amounts to 30% ($\sqrt{s} = 0.63\,\text{TeV}$), 17% ($\sqrt{s} = 1.8\,\text{TeV}$) and 16% ($\sqrt{s} = 16\,\text{TeV}$) of the exact value. The main reason for the difference is that the cubic logarithmic term $\ln^3(Q^2/m^2)$, arising in the exact expressions (3.2.23), (3.2.34) in the limit $Q^2 >> m^2$, will only cancel when m^2 is taken to be really small with respect to Q^2. This is apparently not the case for $Q^2 = M_Z^2$ and $m^2 = m_b^2$. Therefore the sum of the two exact expressions is not quite equal to the sum of the approximations (3.2.36) and (3.2.37) which behaves asymptotically like $\ln^2(Q^2/m^2)$. In practice the asymptotic limit is only reached for $m^2 < 1\text{GeV}^2$ which is an order of magnitude less than $m^2 = (5\,\text{GeV})^2$. A similar problem shows up in the contribution originating from the interference between initial state (Figs. 3.5a,b) and final state (Figs. 3.5c,d) radiation of the vector boson. In spite of the fact that here no large logarithms of the type $\ln^k(Q^2/m^2)$ appear in the final expression (3.2.40) the various integrals contributing to the interference term contain these type of logarithms so that in this case one observes an incomplete cancellation too. From table 3.9 we infer that the approximation to the interference term is not so bad when $\sqrt{s} = 0.63\,\text{TeV}$ but it becomes worse at higher energies. Apart from the incomplete cancellation mentioned above this is also due to the fact that the quality of the approximation depends on the values for $\hat{s} = y_1 y_2 s$ in the partonic cross section $d\hat{\sigma}/dQ^2$ (3.3.1). When the energy $\sqrt{s}$ increases it may happen that the product of the parton densities in (3.3.1) probe the $\hat{s}$-region where the approximation fails. Fortunately the interference term gives a negligible contribution to the cross section of $q + \bar{q} \to Z + b + \bar{b}$. The latter also holds for the final state radiation of the Z-boson as depicted by the graphs in Figs. 3.5c,d. However here the approximation to the the cross section (3.2.34) as given by (3.2.39) becomes excellent which is independent of the energies under consideration. The most simple explanation for this phenomenon is that here large logarithms of the type $\ln^k(Q^2/m^2)$ neither appear in the final result (3.2.39) nor in the separate integrals contributing to this expression. Therefore in this case no cancellation of large logarithmic terms has to occur. Finally table 3.9 reveals that the approximation to the cross section of the gluon-gluon fusion process $g + g \to Z + b + \bar{b}$ (Fig. 3.6) turns out to be very good for all energies under consideration. Although the approximate cross section (3.2.41) behaves quadratically in $\ln(Q^2/m^2)$ it is closer to the exact result as discovered for the initial state radiation of the Z-boson in $q + \bar{q} \to Z + b + \bar{b}$. This is mainly due to the fact that in the former process no cancellation of leading logarithmic terms occur.

In general we can conclude that irrespective of the energies considered the approxi-

mations work rather well for Z-production accompanied by bottom quarks although this statement is more valid for $g+g \to Z+b+\bar{b}$ (Fig. 3.6) than for $q+\bar{q} \to Z+b+\bar{b}$ (Fig. 3.5). Since the large logarithms $\ln^k(Q^2/m^2)$ dominate the cross sections for $\sqrt{s} > 1.8\,\text{TeV}$ the bottom can be treated as a light quark. Further we have also studied the limit $Q^2 >> m^2$ for the charmed quark cross sections. In this case the approximations (3.2.36)-(3.2.41) are even better than for bottom production. This even holds for $\sqrt{s} = 0.63\,\text{TeV}$. The logarithms of the type $\ln(Q^2/m^2)$ dominate the charm and bottom cross sections and they give rise to large corrections. Therefore they have to be removed by mass factorization and subsequently to be absorbed, after resummation via the renormalization group equations, into the charm and bottom densities in the hadron.

3.4 Conclusions

Summarizing the content of this chapter we have computed all order α_s^2 contributions to the DY cross section which can be attributed to heavy flavours. All virtual as well as radiative processes have been considered. In this way we have extended the work done in [7, 8] where only the contributions characteristic for Z-production have been considered.
From the results obtained in this chapter one can conclude that the contributions of the heavy flavours b and t to the DY cross section in particularly to vector boson production are very small. They are on the one percent level in the case of Z-production provided the energy is very large which will only happen when the LHC is put into operation. Furthermore we have shown that for $\sqrt{s} > 1.8\,\text{TeV}$ the cross sections (3.2.36)-(3.2.41) derived in the limit $Q^2 >> m^2$ can be applied to Z-$b\bar{b}$-production. This means that the bottom quark can be treated as a light flavour at large collider energies. The heavy flavour cross sections will only become observable if the vector boson as well as the heavy quarks are detected. This will happen for the LHC where the process $p+p \to Z+b+\bar{b}$ constitutes an important background for Higgs production [21].

Appendix A

The two-loop vertex correction $F(Q^2, m^2)$

In this appendix we present the two-loop vertex correction defined by $F(Q^2, m^2)$ in (3.2.23). It contains the gluon self energy contribution with the heavy flavours appearing in the subloop (Fig. 3.2). The vertex correction reads

$$F(Q^2,m^2) = -\left(\frac{440}{9}\frac{m^2}{Q^2} + \frac{530}{27}\right)\ln\frac{Q^2}{m^2} + x\left(\frac{184}{9}\frac{m^2}{Q^2} + \frac{76}{9}\right)\cdot$$

$$\left(2\text{Li}_2\left(\frac{x-1}{x+1}\right) - 2\zeta(2) + \frac{1}{2}\ln^2\frac{x-1}{x+1}\right) + \left(16\frac{m^4}{Q^4} - \frac{8}{3}\right)\cdot$$

$$\left(-2\mathrm{Li}_3\left(\frac{x-1}{x+1}\right) + 2\zeta(3) - \frac{1}{6}\ln^3\frac{x-1}{x+1} + 2\zeta(2)\ln\frac{x-1}{x+1}\right) + \frac{952}{9}\frac{m^2}{Q^2}$$

$$+\frac{3355}{81}, \tag{A.1}$$

where

$$x = \sqrt{1+4\frac{m^2}{Q^2}}. \tag{A.2}$$

Further the following asymptotic expansions turn out to be useful. In the limit $m^2 << Q^2$ one obtains the expansion

$$F(Q^2,m^2) \underset{m\to 0}{=} -\frac{4}{9}\ln^3\frac{Q^2}{m^2} + \frac{38}{9}\ln^2\frac{Q^2}{m^2} + \left(\frac{16}{3}\zeta(2) - \frac{530}{27}\right)\ln\frac{Q^2}{m^2}$$

$$+\frac{3355}{81} - \frac{152}{9}\zeta(2) - \frac{16}{3}\zeta(3). \tag{A.3}$$

In the case that $m^2 >> Q^2$ the vertex correction behaves like

$$F(Q^2,m^2) \underset{m\to\infty}{=} \frac{Q^2}{m^2}\left(\frac{176}{225} - \frac{8}{45}\ln\frac{Q^2}{m^2}\right), \tag{A.4}$$

which shows that heavy flavours decouple from $F(Q^2,m^2)$ when the quark mass gets infinite.

References

[1] S.D. Drell and T.M. Yan, Phys. Rev. Lett. **25** (1970) 316. 7, 14, 18, 19, 20, 42, 51, 52, 53, 61, 63, 64, 66

[2] R. Hamberg, W.L. van Neerven, and T. Matsuura, Nucl. Phys. **B359** (1991) 343. 14, 18, 19, 20, 42, 51, 52, 53, 63, 64

[3] W.L. van Neerven, and E.B. Zijlstra, Nucl. Phys. **B382** (1992) 11. 7, 14, 17, 19, 43, 51, 86

[4] T. Matsuura, and W.L. van Neerven, Z. Phys. **C38** (1988) 623;
T. Matsuura, S.C. van der Marck, and W.L. van Neerven, Nucl. Phys. **B319** (1989) 570;
P.J. Rijken and W.L. van Neerven, Phys. Rev. **D51** (1995) 44. 51

[5] P.B. Arnold and M.H. Reno, Nucl. Phys. **B319** (1989) 37, Erratum Nucl. Phys. **B330** (1990) 284;
R.J. Gonsalves, J. Pawłowski and C.F. Wai, Phys. Rev. **D40** (1989) 2245. 4, 51, 57, 62

[6] F. Abe *et al.* (CDF Collaboration), Phys. Rev. **D50** (1994) 2966. 8, 52, 53, 55, 72

[7] D.A. Dicus and S.S.D. Willenbrock, Phys. Rev. **D34** (1986) 148. 52, 53, 56, 57, 61, 66, 72

[8] R.J. Gonsalves, C.M. Hung and J. Pawłowski, Phys. Rev. **D46** (1992) 4930. 55

[9] B.A. Kniehl and J.H. Kühn, Nucl. Phys. **B329** (1990) 547. 56

[10] G.J.H. Burgers, Phys. Lett. **B164** (1985) 167. 59, 92

[11] W. Beenakker, H. Kuijf, W.L. van Neerven, and J. Smith, Phys. Rev. **D40** (1989) 54. 59

[12] D. Bailin and A. Love, "Introduction to Gauge Field Theory", Revised edition 1993, J.W. Arrowsmith, Ltd. Bristol. 60

[13] L. Lewin, "Polylogarithms and Associated Functions" (North Holland, Amsterdam 1983);
R. Barbieri, J.A. Mignaco, and E. Remiddi, Nuovo Cim. **11A** (1972) 824;
A. Devoto, and D.W. Duke, Riv. Nuovo Cim. **7-6** (1984) 1. 62

[14] A. Denner and T. Sack, Nucl. Phys. **B358** (1991) 46. 63

[15] L.M. Jones and H. Wyld, Phys. Rev. **D17** (1978) 782;
M. Glück, J.F. Owens and E. Reya, Phys. Rev. **D17** (1978) 2324;
J. Babcock, D. Sivers and S. Wolfram, Phys. Rev. **D18** (1978) 162;
H. Georgi *et al.*, Ann. Phys. (NY) 114 (1978) 273;
B.L. Combridge, Nucl. Phys. **B151** (1979) 429;
K. Hagiwara and T. Yoshino, Phys. Lett. **80B** (1979) 282. 63

[16] E. Laenen, J. Smith and W.L. van Neerven, Nucl. Phys. **B369** (1992) 543. 64, 69

[17] A.D. Martin, W.J. Stirling and R.G. Roberts, Phys. Rev. **D50** (1994) 6734. 69

[18] C. Albajar *et al.* (UA1 Collaboration), Phys. Lett. **B253** (1991) 503. 69

[19] J. Alitti *et al.* (UA2 Collaboration), Phys. Lett. **B256** (1991) 365. 69

[20] F. Abe *et al.* (CDF Collaboration), Phys. Rev. Lett. **69** (1992) 28. 72

[21] J.F. Gunion, H.E. Haber, G. Kane and S. Dawson, "The Higgs Hunter's Guide", Frontiers in Physics, Addison-Wesley Pub. Co. 1990.

4 Order $\mathcal{O}(\alpha_s^2)$ contributions to hadron production in electron–positron annihilation

4.1 Introduction

Semi-leptonic processes represented by electron-positron annihilation into hadrons, deep inelastic lepton-hadron scattering and the Drell-Yan process have provided us with the most valuable testing grounds for perturbative quantum chromodynamics (QCD). Perturbative calculations in next-to-leading order, and in some cases even to higher order, give a good explanation of numerous quantities measured in various experiments [1]. The reason for these successes originates from the experimental as well as theoretical characteristics of the above reactions. From the experimental viewpoint semi-leptonic reactions provide us with an overwhelming amount of data and in the case of electron–positron annihilation into hadrons and deep inelastic lepton-hadron scattering the background is fully under control. Therefore the systematical and statistical errors are very small. From the theoretical viewpoint we want to mention the following features. First, the Born approximation to semi-leptonic cross sections is of purely electroweak origin so that it is independent of the strong coupling constant α_s. Since the electroweak standard model is tested up to about a few permille by the LEP1-experiments [2] each deviation from the Born approximation is due to the strong interactions. Second, if one limits oneself to the computation of semi-inclusive or inclusive quantities, like structure functions or total cross sections, the final hadronic state is completely integrated over and we do not have to care about problems as jet definition or hadronization effects. The third feature is that it is possible to extend the calculation of the QCD corrections to the above integrated quantities beyond next-to-leading order. Examples are the order α_s^2 contributions to the coefficient functions corresponding to the Drell-Yan cross section $d\sigma/dQ^2$ [3] and the deep inelastic structure functions $F_k(x, Q^2)$ [4] where Q^2 denotes the virtuality of the electroweak vector bosons γ, Z, W. Order α_s^3 corrections are even known for sum rules $\int_0^1 dx\, x^{n-1} F_k(x, Q^2)$ $(n \leq 10)$ [5] and the total cross section $\sigma_{\rm tot}(e^+ e^- \to \text{“hadrons”})$ [6]. The reason that these higher order corrections are much easier to compute than those encountered in e.g. hadron-hadron collisions (except for the Drell-Yan process) can be attributed to the simplicity of

the phase space integrals and the virtual corrections appearing in semi-leptonic processes. Moreover if one integrates in the latter processes over the total hadronic state one can use alternative methods to evaluate the Feynman diagrams (see e.g. [7]), which are not applicable to hadron-hadron reactions or to more exclusive semi-leptonic processes.
In the past the order α_s^2 contributions to the coefficient functions have been calculated for the Drell-Yan cross section $d\sigma/dQ^2$ [3] and the deep inelastic structure functions $F_k(x, Q^2)$ [4]. However the same corrections were not computed for the fragmentation functions showing up in the process $e^+ e^- \to H +$ "X" where H is the detected hadron ($H = \pi^{\pm}, K^{\pm}, P, \bar{P}$) and "$X$" stands for any inclusive hadronic state. These corrections are needed because of the large amount of data which have been collected over the past ten years. One has studied the above process over a wide range of energies of many different $e^+ e^-$-colliders. Data have been obtained from DASP ($\sqrt{s} = 5.2$ GeV) [8], ARGUS ($\sqrt{s} = 10$ GeV) [9], TASSO ($\sqrt{s} = 22, 35, 45$ GeV) [10], MARK II [11] and TPC/2γ ($\sqrt{s} = 29$ GeV) [12], CELLO ($\sqrt{s} = 35$ GeV) [13], AMY ($\sqrt{s} = 55$ GeV) [14] and the LEP experiments DELPHI [15], ALEPH [16], OPAL [17, 18] ($\sqrt{s} = 91.2$ GeV). In particular the last two experiments found a discrepancy between the measured longitudinal fragmentation function $F_L(x, Q^2)$ and its theoretical prediction computed up to order α_s. They also obtained data for σ_L and σ_T separately and the latter collaboration even made a measurement of σ_A for the first time. The separation of σ_L and σ_T is important because the former cross section enables us to extract the strong coupling constant α_s and allows us to determine the gluon fragmentation density $D_g(x)$ with a much higher degree of accuracy as could be done before. Furthermore the measurement of σ_A provides us with information on hadronization effects [19] since the QCD corrections are very small. We want to fill in this gap in our knowledge by presenting the order α_s^2 contributions to the longitudinal ($F_L(x, Q^2)$), transverse ($F_T(x, Q^2)$) and asymmetric fragmentation ($F_A(x, Q^2)$) functions and discuss their phenomenological implications. Although a complete next-to-next-to-leading (NNLO) order analysis of the transverse (and also asymmetric) fragmentation function is not possible, since we do not know the three-loop order timelike DGLAP [20] splitting functions, one can still study the effect of the order α_s^2 corrected coefficient functions. Furthermore one can obtain the transverse cross section σ_T for which analysis the DGLAP splitting functions are not needed so that the former is factorization scheme independent. The sum of the transverse (σ_T) and the longitudinal (σ_L) cross sections yield $\sigma_{\rm tot}(e^+ e^- \to$ "hadrons"). It turns out that the $\sigma_{\rm tot}$ presented in this thesis is in agreement with the order α_s^2 corrected result quoted in the literature [21] providing us with a very strong check on our calculations.
This chapter will be organized as follows. In section 2 we introduce our notations of the fragmentation functions and the corresponding cross sections. In section 3 we give an outline of the calculations of the parton subprocesses contributing to the process $e^+ e^- \to H +$ "X" up to order α_s^2. In section 4 we perform the renormalization and mass factorization of the partonic quantities providing us with the longitudinal and transverse coefficient functions. The discussion of our results will be presented

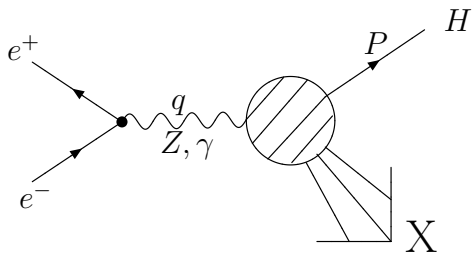

Figure 4.1: *Kinematics of the process* $e^+ e^- \to H +$ *"X".*

in section 5 (longitudinal and transverse fragmentation functions) and in section 6 (asymmetric fragmentation function) and a comparison with data coming from recent and past experiments on electron-positron annihilation will be made. The long expressions obtained for the order α_s^2 corrected coefficient functions are presented in the $\overline{\text{MS}}$-scheme and the A- (annihilation) scheme in appendix A and appendix B respectively.

4.2 Single particle inclusive cross sections

In this chapter we want to study the QCD corrections to the single particle inclusive process (see fig. 4.1)

$$e^+ + e^- \to \gamma, Z \to H + \text{"}X\text{"}, \tag{4.2.1}$$

where "X" denotes any inclusive final hadronic state and H represents either a specific charged outgoing hadron or a sum over all charged hadron species. The unpolarized differential cross section of the above process is given by [19, 22]

$$\frac{d^2\sigma^H}{dx\, d\cos\theta} = \frac{3}{8}(1+\cos^2\theta)\frac{d\sigma_T^H}{dx} + \frac{3}{4}\sin^2\theta\frac{d\sigma_L^H}{dx} + \frac{3}{4}\cos\theta\frac{d\sigma_A^H}{dx}. \tag{4.2.2}$$

The Bjorken scaling variable x is defined by

$$x = \frac{2pq}{Q^2}, \quad q^2 = Q^2 > 0, \quad 0 < x \leq 1, \tag{4.2.3}$$

where p and q are the four-momenta of the produced particle H and the virtual vector boson (γ, Z) respectively. In the centre of mass (CM) frame of the electron–positron pair the variable x can be interpreted as a fraction of the beam energy carried away by the hadron H. The variable θ denotes the angle of emission of particle H with respect to the electron beam direction in the CM frame. The transverse, longitudinal and asymmetric cross sections in (4.2.2) are defined by σ_T^H, σ_L^H, and σ_A^H respectively. The latter only shows up if the intermediate vector boson is given by the Z-boson and is absent in purely electromagnetic annihilation.
In the QCD improved parton model which describes the production of the parton

denoted by p and its subsequent fragmentation into hadron H, the cross sections σ_k^H $(k = T, L, A)$ can be expressed as follows

$$\frac{d\sigma_k^H}{dx} = \int_x^1 \frac{dz}{z} \left[\sigma_{\rm tot}^{(0)}(Q^2) \left\{ D_{\rm S}^H\left(\frac{x}{z}, M^2\right) \mathbb{C}_{k,q}^{\rm S}(z, Q^2/M^2) + D_g^H\left(\frac{x}{z}, M^2\right) \cdot \right.\right.$$

$$\left.\left. \cdot \mathbb{C}_{k,g}^{\rm S}(z, Q^2/M^2) \right\} + \sum_{p=1}^{n_f} \sigma_p^{(0)}(Q^2)\, D_{{\rm NS},p}^H\left(\frac{x}{z}, M^2\right) \mathbb{C}_{k,q}^{\rm NS}(z, Q^2/M^2) \right], \quad (4.2.4)$$

for $k = T, L$. In the case of the asymmetric cross section we have

$$\frac{d\sigma_A^H}{dx} = \int_x^1 \frac{dz}{z} \left[\sum_{p=1}^{n_f} A_p^{(0)}(Q^2) D_{A,p}^H\left(\frac{x}{z}, M^2\right) \mathbb{C}_{A,q}^{\rm NS}(z, Q^2/M^2) \right]. \quad (4.2.5)$$

In the formulae (4.2.4) and (4.2.5) we have introduced the following notations. The function $D_g^H(z, M^2)$ denotes the gluon fragmentation density corresponding to the hadron of species H. The same notation holds for the quark and anti-quark fragmentation densities which are given by $D_p^H(z, M^2)$ and $D_{\bar{p}}^H(z, M^2)$ respectively. Further we have defined the singlet (S) and non-singlet (NS, A) combinations of quark fragmentation densities. They are given by

$$D_{\rm S}^H(z, M^2) = \frac{1}{n_f} \sum_{p=1}^{n_f} \left(D_p^H(z, M^2) + D_{\bar{p}}^H(z, M^2) \right), \quad (4.2.6)$$

$$D_{{\rm NS},p}^H(z, M^2) = D_p^H(z, M^2) + D_{\bar{p}}^H(z, M^2) - D_{\rm S}^H(z, M^2), \quad (4.2.7)$$

$$D_{A,p}^H(z, M^2) = D_p^H(z, M^2) - D_{\bar{p}}^H(z, M^2). \quad (4.2.8)$$

The index p stands for the quark species and n_f denotes the number of light flavours. Assuming that the charm and the bottom quark can be treated as massless we can put $n_f = 5$ and the indices $p = 1, 2, 3, 4, 5$ stand for $p = u, d, s, c, b$. Further the variable M appearing in $D_p^H(z, M^2)$ stands for the mass factorization scale which for convenience has been put equal to the renormalization scale. The pointlike cross section of the process

$$e^+ + e^- \to p + \bar{p}, \quad (4.2.9)$$

which shows up in (4.2.4) is equal to

$$\sigma_p^{(0)}(Q^2) = \frac{4\pi\alpha^2}{3Q^2} N \left[e_\ell^2 e_p^2 + \frac{2Q^2(Q^2 - M_Z^2)}{|Z(Q^2)|^2} e_\ell e_p C_{V,\ell} C_{V,p} + \frac{(Q^2)^2}{|Z(Q^2)|^2} \cdot \right.$$

$$\left. \cdot (C_{V,\ell}^2 + C_{A,\ell}^2)(C_{V,p}^2 + C_{A,p}^2) \right], \quad (4.2.10)$$

$$\sigma_{\rm tot}^{(0)}(Q^2) = \sum_{p=1}^{n_f} \sigma_p^{(0)}(Q^2), \quad (4.2.11)$$

with

$$Z(Q^2) = Q^2 - M_Z^2 + iM_Z\Gamma_Z. \tag{4.2.12}$$

Here N stands for the number of colours ($N = 3$) and M_Z, Γ_Z denote the mass and width of the Z-boson respectively. For the latter we have used the narrow width approximation. Furthermore we have neglected all quark masses in (4.2.10). The charges of the lepton and the up and down quarks are given by

$$e_\ell = -1, \qquad e_u = \frac{2}{3}, \qquad e_d = -\frac{1}{3}. \tag{4.2.13}$$

The vector- and axial-vector coupling constants of the Z-boson to the lepton and quarks are equal to

$$\begin{aligned} &C_{A,\ell} = \frac{1}{2\sin 2\theta_W}, && C_{V,\ell} = -C_{A,\ell}\,(1 - 4\sin^2\theta_W), \\ &C_{A,u} = -C_{A,d} = -C_{A,\ell}, && \\ &C_{V,u} = C_{A,\ell}\,(1 - \frac{8}{3}\sin^2\theta_W), && C_{V,d} = -C_{A,\ell}\,(1 - \frac{4}{3}\sin^2\theta_W), \end{aligned} \tag{4.2.14}$$

where θ_W denotes the weak mixing angle.
The electroweak coupling constants also appear in the asymmetry factor $A_p^{(0)}$ (4.2.5) which is given by

$$A_p^{(0)} = \frac{4\pi\alpha^2}{3Q^2} N \left[\frac{2Q^2(Q^2 - M_Z^2)}{|Z(Q^2)|^2}\, e_\ell e_p C_{A,\ell} C_{A,p} + 4\frac{(Q^2)^2}{|Z(Q^2)|^2}\, C_{A,\ell} C_{A,p} C_{V,\ell} C_{V,p} \right]. \tag{4.2.15}$$

The QCD corrections in (4.2.4), (4.2.5) are described by the coefficient functions $\mathbb{C}_{k,\ell}^r$ ($k = T, L, A$; $\ell = q, g$) which can be distinguished with respect to the flavour group $SU(n_f)$ in a singlet ($r = \mathrm{S}$) and a non-singlet part ($r = \mathrm{NS}$). They depend on the factorization scale M and in order α_s^2 on the number of flavours n_f. As will be shown later on the gluonic coefficient function only receives contributions from flavour singlet channel partonic subprocesses so that we can drop the superscript S on $\mathbb{C}_g$. However the quark coefficient functions can be of flavour singlet as well as flavour non-singlet origin. Up to first order in the strong coupling constant α_s it turns out that $\mathbb{C}_{k,q}^{\mathrm{NS}} = \mathbb{C}_{k,q}^{\mathrm{S}}$. However in higher order both quantities start to deviate from each other. Hence we define the purely singlet coefficient function $\mathbb{C}_{k,q}^{\mathrm{PS}}$ via

$$\mathbb{C}_{k,q}^{\mathrm{S}} = \mathbb{C}_{k,q}^{\mathrm{NS}} + \mathbb{C}_{k,q}^{\mathrm{PS}}. \tag{4.2.16}$$

Like $\mathbb{C}_{k,g}$ the purely singlet coefficient function only receives contributions from the flavour singlet channel partonic subprocesses which for the first time show up in order α_s^2.
Using charge conjugation invariance of the strong interactions one can show that $\mathbb{C}_{k,q}^r = \mathbb{C}_{k,\bar{q}}^r$ ($r = \mathrm{S}, \mathrm{NS}$; $k = T, L$), $\mathbb{C}_{A,q}^{\mathrm{NS}} = -\mathbb{C}_{A,\bar{q}}^{\mathrm{NS}}$ and $\mathbb{C}_{A,q}^{\mathrm{PS}} = \mathbb{C}_{A,g} = 0$. This implies

that to σ_A^H (4.2.5) only non-singlet channel partonic subprocesses can contribute. Another important property of the coefficient functions is that they do not depend on the probe γ or Z or on the electroweak couplings given in (4.2.13), (4.2.14) so that one can extract the overall pointlike cross section $\sigma_p^{(0)}$ (4.2.10) or the asymmetry factor $A_p^{(0)}$ (4.2.15). However this is only true if all quark masses are equal to zero and if one sums over all quark members in one family provided the latter appear in the inclusive state of the partonic subprocess (see section 4).
From (4.2.2) we can derive the total hadronic cross section

$$\sigma_{\rm tot}(Q^2) = \frac{1}{2}\sum_H \int_0^1 dx \int_{-1}^1 d\cos\theta \left(x \frac{d^2\sigma^H}{dx\, d\cos\theta} \right) = \sigma_T(Q^2) + \sigma_L(Q^2), \quad (4.2.17)$$

with

$$\sigma_k(Q^2) = \frac{1}{2}\sum_H \int_0^1 dx\, x \frac{d\sigma_k^H}{dx}, \quad (k = T, L, A), \quad (4.2.18)$$

where one has summed over all types of outgoing hadrons H. Hence we obtain the result

$$\sigma_{\rm tot}(Q^2) = R_{ee}\, \sigma_{\rm tot}^{(0)}(Q^2), \quad (4.2.19)$$

where R_{ee} represents the QCD corrections to the pointlike total cross section $\sigma_{\rm tot}^{(0)}(Q^2)$. At this moment the perturbation series of R_{ee} is already known up to order α_s^3 [6]. Up to order α_s^2 it reads [21]

$$R_{ee} = 1 + \frac{\alpha_s}{4\pi} C_F\, [3] + \left(\frac{\alpha_s}{4\pi}\right)^2 \left[C_F^2 \left\{ -\frac{3}{2} \right\} + C_A C_F \left\{ -11 \ln \frac{Q^2}{M^2} - 44\zeta(3) + \frac{123}{2} \right\} + n_f C_F T_f \left\{ 4 \ln \frac{Q^2}{M^2} + 16\zeta(3) - 22 \right\} \right]. \quad (4.2.20)$$

In section 4.4 we also want to present the coefficient functions $\mathbb{C}_{k,\ell}$ up to order α_s^2 and show that they lead to the same R_{ee} as calculated in the literature (see section 4.5).
Finally we also define the transverse, longitudinal and asymmetric fragmentation functions $F_k^H(x, Q^2)$*

$$F_k^H(x, Q^2) = \frac{1}{\sigma_{\rm tot}^{(0)}(Q^2)} \frac{d\sigma_k^H}{dx}, \quad k = (T, L, A). \quad (4.2.21)$$

Further the total fragmentation function is given by

$$F^H(x, Q^2) = F_L^H(x, Q^2) + F_T^H(x, Q^2). \quad (4.2.22)$$

*Notice that we make a distinction in nomenclature between the fragmentation densities D_p^H and the fragmentation functions F_k^H.

In the case the virtual photon dominates the annihilation process (4.2.1) one observes that, apart from the charge squared e_p^2 in (4.2.10) ($p = u, d$), the above structure functions are just the timelike photon analogues of the ones measured in deep inelastic electron–proton scattering. When the Z-boson contributes we will define in section 4.4 for each combination of the electroweak coupling constants in (4.2.10) a separate structure function. However for the discussion of our results in section 4.5 this distinction will not be needed.

4.3 Fragmentation coefficient functions in e^+e^- annihilation up to order α_s^2

In this section we will give an outline of the calculation of the order α_s^2 corrections to the fragmentation coefficient functions. The procedure is analogous to the one presented for the calculation of the Drell-Yan process in [3] and the deep inelastic lepton-hadron reaction in [4]. The coefficient functions originate from the following reaction

$$V(q) \to \text{“}p(k_0)\text{”} + p_1(k_1) + p_2(k_2) + \cdots + p_\ell(k_\ell), \tag{4.3.1}$$

where $V = \gamma, Z$ and “p” denotes the detected parton which fragments into the hadron H. The process (4.3.1) is inclusive with respect to the partons p_i ($i = 1, 2, \ldots, \ell$) so that one has to integrate over all momenta indicated by k_i. Notice that the first part of reaction (4.2.1) i.e. $e^+e^- \to V$ is not relevant for the determination of the coefficient function. Up to order α_s^2 all parton subprocesses represented by (4.3.1) are listed in table 4.1. Notice that because of the charge conjugation invariance of the strong interactions the processes where an anti-quark is detected do not have to be considered (see the remarks below (4.2.16)). From the amplitude $M_\mu(\ell)$ describing process (4.3.1) one obtains the parton structure tensor (indicated by a hat)

$$\hat{W}_{\mu\nu}^{(V,V')}(p,q) = \frac{z^{n-3}}{4\pi} \sum_{\ell=1}^{\infty} \int \mathrm{dPS}^{(\ell)}\, M_\mu^V(\ell)\, M_\nu^{V'}(\ell)^*. \tag{4.3.2}$$

Here $\int \mathrm{dPS}^{(\ell)}$ denotes the k-body phase space integral defined by

$$\int \mathrm{dPS}^{(\ell)} = \left\{ \prod_{j=1}^{\ell} \int \frac{d^n k_j}{(2\pi)^{n-1}}\, \delta^+(k_j^2) \right\} (2\pi)^n\, \delta^{(n)}(q - k_0 - \sum_{i=1}^{\ell} k_i), \tag{4.3.3}$$

$$\delta^+(k_j^2) = \theta(k_j^0)\, \delta(k_j^2), \tag{4.3.4}$$

and μ and ν stand for the Lorentz indices of the vector bosons V and V' respectively with $V = \gamma, Z$ and $V' = \gamma, Z$. Further we have defined the partonic scaling variable

$$z = \frac{2k_o q}{Q^2}, \tag{4.3.5}$$

figure	Parton subprocesses			
4.2	α_s^0:	$V \to$	$q + \bar{q}$	
4.3	α_s:	$V \to$	$q + \bar{q}$	(one-loop correction)
4.4		$V \to$	"q" $+ \bar{q} + g$	
4.4		$V \to$	$q + \bar{q} +$ "g"	
4.5	α_s^2	$V \to$	$q + \bar{q}$	(two-loop correction)
4.6		$V \to$	"q" $+ \bar{q} + g$	(one-loop correction)
4.7		$V \to$	"q" $+ \bar{q} + g + g$	
4.6		$V \to$	$q + \bar{q} +$ "g"	(one-loop correction)
4.7		$V \to$	$q + \bar{q} +$ "g" $+ g$	
4.8		$V \to$	"q" $+ \bar{q} + q' + \bar{q}'$	

Table 4.1: *List of parton subprocesses in $e^+ e^-$ annihilation up to order α_s^2.*

and the factor z^{n-3} in (4.3.2) originates from the n-dimensional phase space of the detected parton p (4.3.1). It appears in the definition of the cross sections $d\hat{\sigma}_{k,p}/dz$ which are the partonic analogues of the hadronic cross sections in (4.2.2). The former are proportional to the functions $\hat{\mathcal{F}}_{k,p}$ defined below.
To regularize the ultraviolet (U), infrared (IR) and collinear (C) divergences showing up in expression (4.3.2) we have chosen the method of n-dimensional regularization. Therefore the phase space integral in (4.3.3) is generalized to n dimensions so that the above divergences show up as pole terms of the type $(1/\varepsilon)^m$ with $\varepsilon = n-4$. The calculation of the matrix elements $M_\mu(k)\, M_\nu(k)^*$ was performed in n dimensions using the algebraic manipulation program FORM [23]. After having computed the traces we have to integrate the matrix elements over all internal loop and final state momenta where the momentum k_0 of the detected parton is kept fixed. In this chapter we take all partons to be massless. The case of massive quarks is discussed in [19] where their contributions are presented up to order α_s.
The parton structure tensor in (4.3.2) can be also written as

$$\hat{W}_{\mu\nu}^{(V,V')}(k_0, q) = \frac{1}{4\pi} \sum_{\ell=1}^{\infty} \int \mathrm{dPS}^{(\ell)} \, \langle 0 |\, \hat{J}_\mu^{(V)}(0) \,| p, \{p_\ell\} \rangle \, \langle p, \{p_\ell\} |\, \hat{J}_\nu^{(V')}(0) \,| 0 \rangle,$$

(4.3.6)

where $\hat{J}_\mu^{(V)}$ is the electroweak partonic current corresponding to the vector boson V. Using Lorentz covariance and CP invariance (4.3.6) can be written as follows

$$\hat{W}_{\mu\nu}^{(V,V')}(k_0,q) = (v_{q_1}^{(V)}v_{q_2}^{(V')} + a_{q_1}^{(V)}a_{q_2}^{(V')}) \left[(k_{0\mu} - \frac{k_0q}{q^2}q_\mu)(k_{0\nu} - \frac{k_0q}{q^2}q_\nu) \frac{q^4}{(k_0q)^3} \cdot \right.$$

$$\cdot \hat{\mathcal{F}}_{L,p}(z,Q^2) - \left(g_{\mu\nu} - \frac{1}{k_0q}(k_0^\mu q^\nu + q^\mu k_0^\nu) + \frac{q^2}{(k_0q)^2}k_{0\mu}k_{0\nu} \right) \frac{q^2}{2k_0q} \cdot$$

$$\left. \cdot \hat{\mathcal{F}}_{T,p}(z,Q^2) \right] - (v_{q_1}^{(V)}a_{q_2}^{(V')} + a_{q_1}^{(V)}v_{q_2}^{(V')})\, i\epsilon_{\mu\nu\alpha\beta}k_0^\alpha q^\beta \frac{q^2}{2(k_0q)^2}\, \hat{\mathcal{F}}_{A,p}(z,Q^2).$$

(4.3.7)

We will call $\hat{\mathcal{F}}_{k,p}(z,Q^2)$ $(p = q,g)$ the parton fragmentation functions which describe the Born reaction plus the higher order QCD corrections represented by the parton subprocesses in table 4.1. The vector and axial-vector couplings of the quark q interacting with the vector boson V are given by $v_q^{(V)}$ and $a_q^{(V)}$ respectively. In the standard model they read

$$\begin{aligned}
v_u^{(\gamma)} &= \tfrac{2}{3}, & a_u^{(\gamma)} &= 0,\\
v_d^{(\gamma)} &= -\tfrac{1}{3}, & a_d^{(\gamma)} &= 0,\\
v_u^{(Z)} &= \tfrac{1}{2} - \tfrac{4}{3}\sin^2\theta_W, & a_u^{(Z)} &= \tfrac{1}{2},\\
v_d^{(Z)} &= -\tfrac{1}{2} + \tfrac{2}{3}\sin^2\theta_W, & a_u^{(Z)} &= -\tfrac{1}{2}.
\end{aligned} \tag{4.3.8}$$

As we have already mentioned in section 4.2 below (4.2.16) in the case of massless quarks the electroweak factors can be completely factorized out of the radiative corrections according to (4.3.7) so that $\hat{\mathcal{F}}_{k,p}$ $(k = T,L,A)$ do not depend on them. Therefore we can also put them all equal to $1/\sqrt{2}$ without affecting the parton fragmentation functions. Hence the latter are obtained via the following projections

$$\hat{\mathcal{F}}_{T,p}(z,Q^2) = \frac{1}{n-2}\left(-\frac{2k_0q}{q^2}\hat{W}^\mu{}_\mu - \frac{2}{k_0q}k_0^\mu k_0^\nu \hat{W}_{\mu\nu} \right), \tag{4.3.9}$$

$$\hat{\mathcal{F}}_{L,p}(z,Q^2) = \frac{1}{k_0q}k_0^\mu k_0^\nu \hat{W}_{\mu\nu}, \tag{4.3.10}$$

$$\hat{\mathcal{F}}_{A,p}(z,Q^2) = -\frac{2}{q^2}\frac{1}{(n-2)(n-3)} i\epsilon^{\mu\nu\alpha\beta}k_{0\alpha}q_\beta \hat{W}_{\mu\nu}, \tag{4.3.11}$$

where according to the prescription in [24] we have contracted the Levi-Civita tensors $\epsilon^{\mu\nu\alpha\beta}$ in n-dimensions. The computation of the asymmetric fragmentation function

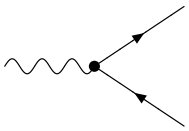

Figure 4.2: *Born contribution given by the subprocess $V \to$ "q" $+ \bar{q}$.*

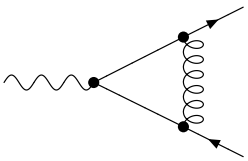

Figure 4.3: *One-loop correction to the subprocess $V \to$ "q"$+\bar{q}$. Graphs with external self energies are omitted since they do not contribute in the case of massless quarks.*

involves the prescription of the γ_5-matrix and the Levi-Civita tensor in n-dimensions. We will come back to this in section 4.3.3.

We will now discuss the QCD corrections order by order in perturbation theory. In zeroth order in α_s (see fig. 4.2) we obtain the simple parton model results

$$\hat{\mathcal{F}}_{T,q}^{(0)} = \hat{\mathcal{F}}_{A,q}^{(0)} = \delta(1-z), \quad \hat{\mathcal{F}}_{T,g}^{(0)} = 0; \quad \hat{\mathcal{F}}_{L,q}^{(0)} = \hat{\mathcal{F}}_{L,g}^{(0)} = 0. \tag{4.3.12}$$

4.3.1 The first order results

The first order corrections denoted by $\hat{\mathcal{F}}_{k,i}^{(1)}$ $(k = T, L, A; i = q, g)$ have been calculated in the literature [25, 26, 19]. In the case of n-dimensional regularization they are computed up to finite terms in the limit $\varepsilon \to 0$ and can be found in [19, 26]. Since the mass factorization has to be carried out up to order α_s^2 one also needs those terms in $\hat{\mathcal{F}}_{k,i}^{(1)}(z, Q^2, \varepsilon)$ which are proportional to ε. Therefore we have repeated the

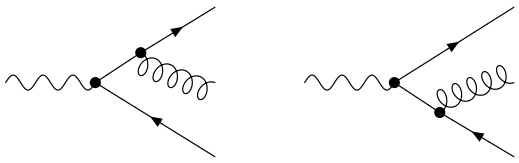

Figure 4.4: *Graphs contributing to the subprocess $V \to$ "q" $+ \bar{q} + g$ and $V \to$ "g" $+ q + \bar{q}$.*

calculation of the graphs in fig. 4.3 and 4.4 and the results can be presented in the following form

$$\hat{\mathcal{F}}_{L,q}^{(1)} = \left(\frac{\hat{\alpha}_s}{4\pi}\right) S_\varepsilon \left(\frac{Q^2}{\mu^2}\right)^{\varepsilon/2} \left[\, \bar{c}_{L,q}^{(1)} + \varepsilon\, a_{L,q}^{(1)} \,\right], \tag{4.3.13}$$

$$\hat{\mathcal{F}}_{T,q}^{(1)} = \left(\frac{\hat{\alpha}_s}{4\pi}\right) S_\varepsilon \left(\frac{Q^2}{\mu^2}\right)^{\varepsilon/2} \left[\, P_{qq}^{(0)} \frac{1}{\varepsilon} + \bar{c}_{T,q}^{(1)} + \varepsilon\, a_{T,q}^{(1)} \,\right], \tag{4.3.14}$$

$$\hat{\mathcal{F}}_{A,q}^{(1)} = \left(\frac{\hat{\alpha}_s}{4\pi}\right) S_\varepsilon \left(\frac{Q^2}{\mu^2}\right)^{\varepsilon/2} \left[\, P_{qq}^{(0)} \frac{1}{\varepsilon} + \bar{c}_{A,q}^{(1)} + \varepsilon\, a_{A,q}^{(1)} \,\right], \tag{4.3.15}$$

$$\hat{\mathcal{F}}_{L,g}^{(1)} = \left(\frac{\hat{\alpha}_s}{4\pi}\right) S_\varepsilon \left(\frac{Q^2}{\mu^2}\right)^{\varepsilon/2} \left[\, \bar{c}_{L,g}^{(1)} + \varepsilon\, a_{L,g}^{(1)} \,\right], \tag{4.3.16}$$

$$\hat{\mathcal{F}}_{T,g}^{(1)} = \left(\frac{\hat{\alpha}_s}{4\pi}\right) S_\varepsilon \left(\frac{Q^2}{\mu^2}\right)^{\varepsilon/2} \left[\, 2P_{gq}^{(0)} \frac{1}{\varepsilon} + \bar{c}_{T,g}^{(1)} + \varepsilon\, a_{T,g}^{(1)} \,\right]. \tag{4.3.17}$$

The pole terms $1/\varepsilon$ stand for the collinear divergence in the final state and μ^2 and S_ε are artefacts of n-dimensional regularization. The mass parameter μ originates from the dimensionality of the gauge coupling constant in n dimensions and should not be confused with the renormalization scale R and the mass factorization scale M. The spherical factor S_ε is defined by

$$S_\varepsilon = \exp\left[\frac{1}{2}\varepsilon(\gamma_E - \ln 4\pi)\right]. \tag{4.3.18}$$

Further $\hat{\alpha}_s$ denotes the bare coupling constant and $P_{ij}^{(0)}$ ($i,j = q,\bar{q},g$) stand for the lowest order contribution to the DGLAP splitting functions [20]. Using our convention they are presented in eqs. (2.13)-(2.16) of [3]. Notice that in lowest order there is no difference in the expressions for $P_{ij}^{(0)}$ found for the deep inelastic structure functions (spacelike process) and those appearing in the fragmentation functions (timelike process). In next-to-leading order the DGLAP splitting functions are different for spacelike and timelike processes as will be shown later on.
The coefficients $\bar{c}_{k,i}^{(1)}$, presented in the $\overline{\text{MS}}$-scheme, are already calculated in the literature [25, 26, 19] (see also appendix A). Furthermore we also have to compute the coefficients $a_{k,i}^{(1)}$ (proportional to ε), since they are needed for the mass factorization which has to be carried out up to order α_s^2. The results are

$$a_{L,q}^{(1)} = C_F\, \{-1 + \ln(1-z) + 2\ln z\}, \tag{4.3.19}$$

$$a_{T,q}^{(1)} = C_F \left\{ \left(\frac{\ln^2(1-z)}{1-z}\right)_+ - \frac{3}{2}\left(\frac{\ln(1-z)}{1-z}\right)_+ + \left(\frac{7}{2} - 3\zeta(2)\right)\left(\frac{1}{1-z}\right)_+ \right.$$
$$\left. - \frac{1}{2}(1+z)\ln^2(1-z) + 2\frac{1+z^2}{1-z}\ln z \ln(1-z) + 2\frac{1+z^2}{1-z}\ln^2 z \right.$$

$$- 3\frac{1}{1-z}\ln z + \frac{3}{2}(1-z)\ln(1-z) + 3(1-z)\ln z - \frac{3}{2} + \frac{5}{2}z$$

$$+ \frac{3}{2}(1+z)\zeta(2) + \delta(1-z)\left(9 - \frac{33}{4}\zeta(2)\right)\Bigg\}, \tag{4.3.20}$$

$$a_{A,q}^{(1)} = C_F\Bigg\{\left(\frac{\ln^2(1-z)}{1-z}\right)_+ - \frac{3}{2}\left(\frac{\ln(1-z)}{1-z}\right)_+ + \left(\frac{7}{2} - 3\zeta(2)\right)\left(\frac{1}{1-z}\right)_+$$

$$- \frac{1}{2}(1+z)\ln^2(1-z) + 2\frac{1+z^2}{1-z}\ln z\ln(1-z) + 2\frac{1+z^2}{1-z}\ln^2 z$$

$$- 3\frac{1}{1-z}\ln z + \frac{1}{2}(1-z)\ln(1-z) + (1-z)\ln z - \frac{3}{2} + \frac{1}{2}z$$

$$+ \frac{3}{2}(1+z)\zeta(2) + \delta(1-z)\left(9 - \frac{33}{4}\zeta(2)\right)\Bigg\}, \tag{4.3.21}$$

$$a_{L,g}^{(1)} = C_F\left\{4\frac{1-z}{z}(\ln(1-z) + 2\ln z - 2)\right\}, \tag{4.3.22}$$

$$a_{T,g}^{(1)} = C_F\Bigg\{\left(\frac{2}{z} - 2 + z\right)(\ln^2(1-z) + 4\ln z\ln(1-z) + 4\ln^2 z - 3\zeta(2))$$

$$- 4\frac{1-z}{z}(\ln(1-z) + 2\ln z - 3) + 4z\Bigg\}. \tag{4.3.23}$$

4.3.2 Diagrams contributing at second order

The calculation of the order α_s^2 corrections proceeds in the following way. First we have the two-loop corrections to the quark-vector boson vertex represented by the graphs in fig. 4.5 which only contribute to $\hat{\mathcal{F}}_{T,q}^{(2)}$ and $\hat{\mathcal{F}}_{A,q}^{(2)}$. The two-loop vertex correction can be found in eq. (2.49) of [27] (see also appendix A of [28]). The result agrees with the one quoted in [29]. Notice that the first graph in fig. 4.5 does not contribute for $V = \gamma$ because of Furry's theorem. It only plays a role in the case $V = Z$ provided one sums over all flavours in a quark family in order to cancel the anomaly which originates from the triangle fermion sub-loop. Since all quarks are massless the final result for this graph is zero too even in the case of $V = Z$.

One-loop virtual corrections to three particle final state subprocesses

Next we have to compute the one-loop virtual corrections to the radiative process in fig. 4.4 which contribute to $\hat{\mathcal{F}}_{k,q}^{(2)}$ $(k = T, A, L)$ as well as $\hat{\mathcal{F}}_{k,g}^{(2)}$ $(k = T, L)$. The corresponding graphs are shown in fig. 4.6. Notice that we have omitted the diagrams with the self energy insertions on the external quark and gluon legs. Their contributions vanish because of the method of n-dimensional regularization and the

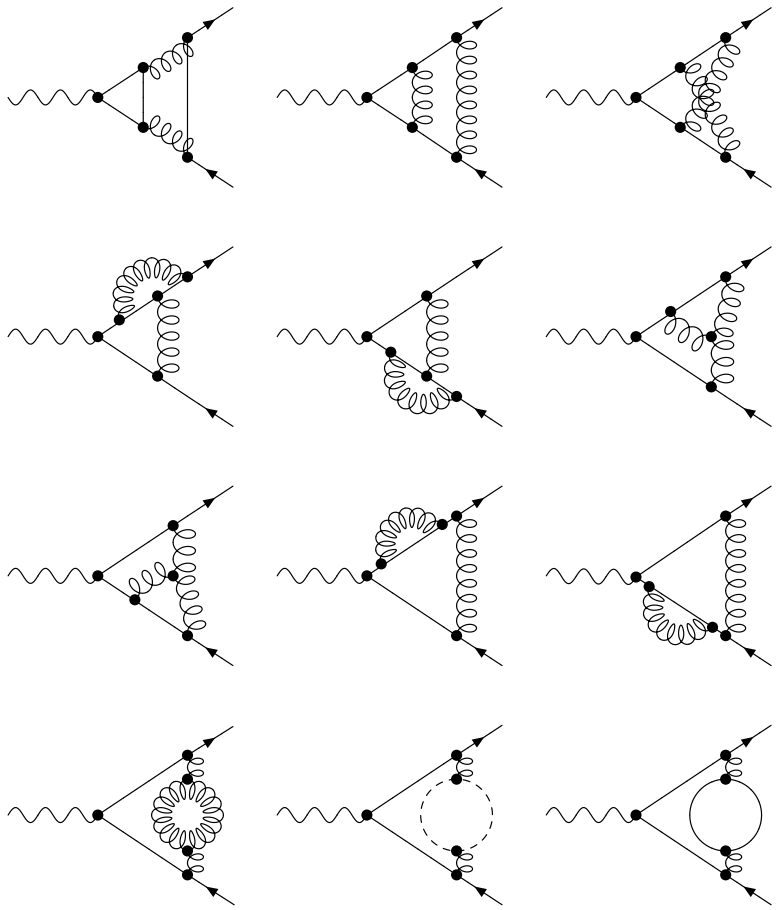

Figure 4.5: *Two-loop corrections to the subprocess $V \to$ "q"+$\bar{q}$. Graphs with external self energies are omitted since they do not contribute in the case of massless quarks.*

on-mass shell conditions $k_0^2 = k_\ell^2 = 0$. Another vanishing contribution happens for the last graph in fig. 4.6 when $V = \gamma$ because of Furry's theorem. In the case of $V = Z$ it only contributes when the quarks are massive. However here one has to sum over all members of a quark family in order to cancel the anomaly originating from the triangle fermion loop.
The amplitude of the parton subprocesses in fig. 4.6 will be denoted by $M(2)$ (see (4.3.1) where $\ell = 2$). The momenta of the incoming vector boson V and the outgoing partons are parameterized like

$$q = \sqrt{s}\,(1, \mathbf{0}_{n-1}),$$

$$k_0 = \frac{s - s_{12}}{2\sqrt{s}}\,(1, 1, \mathbf{0}_{n-2}),$$

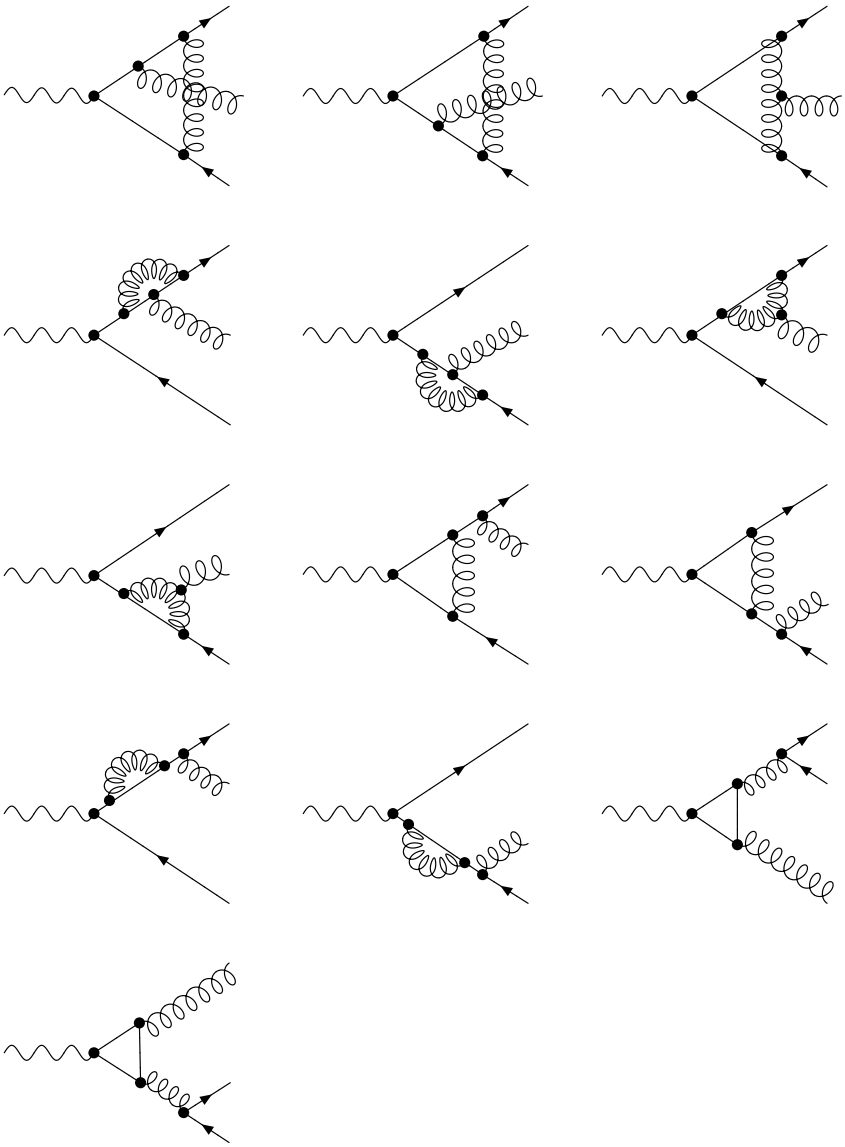

Figure 4.6: *One-loop corrections to the subprocesses $V \to$ "q" $+ \bar{q} + g$ and $V \to$ "g"$+q+\bar{q}$. Graphs with external self energies are omitted since they do not contribute in the case of massless quarks and gluons.*

$$k_1 = \frac{s - s_2}{2\sqrt{s}} \, (1, \cos\theta_1, \sin\theta_1, \mathbf{0}_{n-3}), \quad k_2 = q - k_0 - k_1, \tag{4.3.24}$$

where $\mathbf{0}_n$ stands for the n-dimensional null vector. The phase space integral in (4.3.2), (4.3.3) becomes

$$\int \mathrm{dPS}^{(2)} \; |M(2)|^2 = \frac{1}{8\pi} \, \frac{1}{\Gamma(1 + \frac{1}{2}\varepsilon)} \, \frac{1}{(4\pi)^{\varepsilon/2}} \, s^{\varepsilon/2} (1 - z)^{\varepsilon/2}.$$

$$\cdot \int_0^1 dy\, y^{\varepsilon/2}(1-y)^{\varepsilon/2}\, |M(2)|^2\,. \tag{4.3.25}$$

Here we have defined the Lorentz invariants

$$s = Q^2, \quad s_1 = (k_0+k_1)^2, \quad s_2 = (k_0+k_2)^2, \quad s_{12} = (k_1+k_2)^2, \tag{4.3.26}$$

with $s = s_1 + s_2 + s_{12}$. The parameterization of (4.3.25) follows from momentum conservation and the on-shell condition $k_0^2 = k_\ell^2 = 0$. Hence we get

$$\cos\theta_1 = \frac{s_2 s_{12} - s_1 s}{(s-s_{12})(s-s_2)}, \quad s_1 = z(1-y)s, \quad s_{12} = (1-z)s, \quad s_2 = zys. \tag{4.3.27}$$

The Feynman integrals corresponding to the one-loop graphs which contribute to $M(2)$ in (4.3.25) contain loop momenta in the numerator. They can be reduced to scalar one-loop integrals using an n-dimensional extension of the reduction program in [30]. The expressions for these scalar integrals which are valid for all n can be found in appendix D of [28]. The phase space integrals which emerge from the computation of $|M(2)|^2$ are very numerous so that we cannot present them in this thesis. They are calculated algebraically using the program FORM [23].

Parton subprocesses with four particles in the final state

The most difficult and laborious part of the calculation can be attributed to the parton subprocesses (4.3.1) where one has to integrate over three partons in the final state (see also table 4.1). These parton subprocesses are depicted in figs. 4.7, 4.8 providing us with the amplitude $M(3)$ (see (4.3.1) where $\ell = 3$). The graphs in fig. 4.7 determine $\hat{\mathcal{F}}_{k,q}^{(2)}$ $(k = T, A, L)$ as well as $\hat{\mathcal{F}}_{k,g}^{(2)}$ $(k = T, L)$ whereas the graphs in fig. 4.8, which only contain quarks and anti-quarks in the final state, contribute to $\hat{\mathcal{F}}_{k,q}^{(2)}$ only. For the computation of the three body phase space integrals we choose the following parameterization for the momenta of the virtual vector boson V and the outgoing partons (see [29])

$$\begin{aligned}
q &= \sqrt{s}\,(1, \mathbf{0}_{n-1}),\\
k_0 &= \left(\frac{s_{023}-s_{23}}{2\sqrt{s_{23}}}\right)(1, 1, \mathbf{0}_{n-2}),\\
k_1 &= \left(\frac{s_{123}-s_{23}}{2\sqrt{s_{23}}}\right)(1, \cos\chi, \sin\chi, \mathbf{0}_{n-3}),\\
k_2 &= \frac{1}{2}\sqrt{s_{23}}(1, \cos\theta_1, \sin\theta_1\cos\theta_2, \sin\theta_1\sin\theta_2, \mathbf{0}_{n-4}),\\
k_3 &= \frac{1}{2}\sqrt{s_{23}}(1, -\cos\theta_1, -\sin\theta_1\cos\theta_2, -\sin\theta_1\sin\theta_2, \mathbf{0}_{n-4}),
\end{aligned} \tag{4.3.28}$$

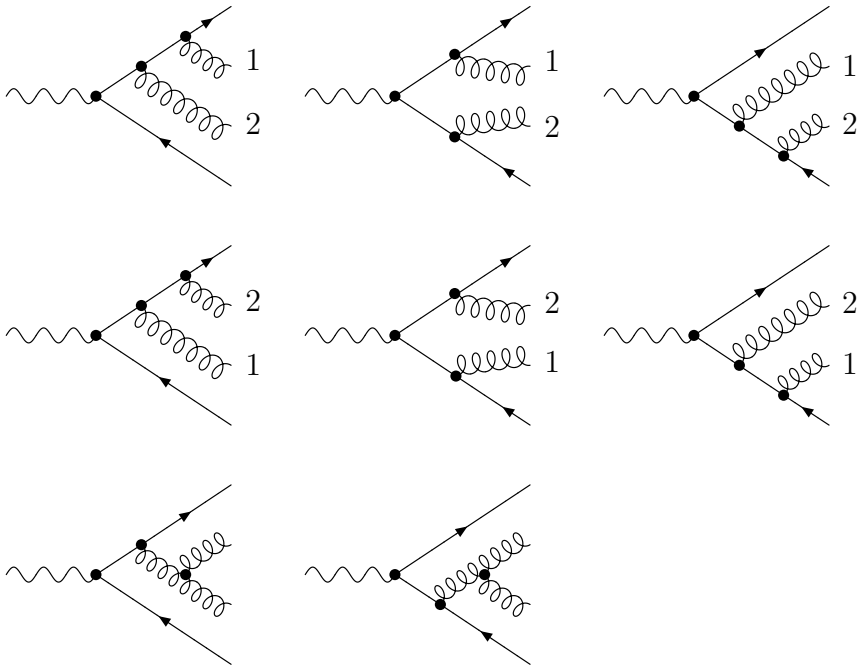

Figure 4.7: *Graphs contributing to the subprocesses $V \to$ "q" $+ \bar{q} + g + g$ and $V \to$ "g" $+ q + \bar{q} + g$.*

where we have defined the invariants

$$s_{ij} = (k_i + k_j)^2, \quad s_{ijm} = (k_i + k_j + k_m)^2, \quad s = q^2. \tag{4.3.29}$$

From momentum conservation and the on-mass shell conditions one can derive

$$1 - \cos\chi = \frac{2s_{23}(s + s_{23} - s_{023} - s_{123})}{(s_{023} - s_{23})(s_{123} - s_{23})}. \tag{4.3.30}$$

The three-body phase space integral in (4.3.2), (4.3.3) can be expressed as

$$\begin{aligned}\int \mathrm{dPS}^{(3)}\ |M(3)|^2 = {} & \frac{1}{2^8\pi^4}\,\frac{1}{\Gamma(1+\varepsilon)}\,\frac{1}{(4\pi)^\varepsilon}\,s^{1+\varepsilon}\,z^{1+\varepsilon/2}(1-z)^{1+\varepsilon}\cdot \\ & \cdot\int_0^1 dy_1 \int_0^1 dy_2\, y_1^{1+\varepsilon}(1-y_1)^{\varepsilon/2}\,y_2^{\varepsilon/2}(1-y_2)^{\varepsilon/2}\,(1-y_2(1-z))^{-\varepsilon-2}\cdot \\ & \cdot\int_0^\pi d\theta_1\,(\sin\theta_1)^{1+\varepsilon}\int_0^\pi d\theta_2\,(\sin\theta_2)^{\varepsilon}\ |M(3)|^2\,,\end{aligned} \tag{4.3.31}$$

where the invariants in (4.3.29) depend on z, y_1, and y_2 in the following way

$$\begin{aligned}& s_{023} = \frac{y_1 z s}{1 - y_2(1-z)}, \quad s_{123} = (1-z)s, \quad s_{23} = \frac{z(1-z)y_1y_2s}{1-y_2(1-z)}, \\ & 2k_0q = zs, \quad s_{01} = z(1-y_1)s.\end{aligned} \tag{4.3.32}$$

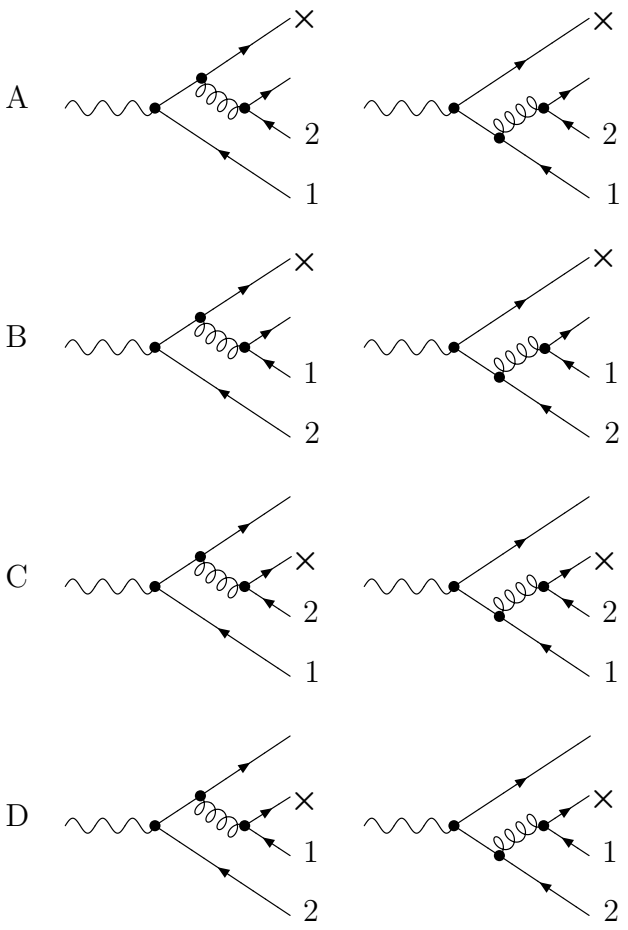

Figure 4.8: *Graphs contributing to the subprocess $V \to$ "q" $+ \bar{q}(1) + q + \bar{q}(2)$. The cross ($\times$) indicates that the process is exclusive with respect to the quark denoted by "q". If $\bar{q}(1) \neq \bar{q}(2)$ only combinations A and C have to be considered. When $\bar{q}(1) = \bar{q}(2)$ combinations B and D have to be added to A and C.*

Before we can perform the angular integrations the matrix element $|M(3)|^2$ has to be decomposed via partial fractioning in terms which have the general form

$$T^{n_1 n_2 n_3 n_4} = (s_{i_1 j_1})^{n_1} (s_{i_2 j_2})^{n_2} (s_{i_3 j_3})^{n_3} (s_{i_4 j_4})^{n_4},$$

$$n_i = \cdots, 2, 1, 0, -1, -2, \cdots. \tag{4.3.33}$$

The decomposition can be done in such a way that one invariant e.g. $s_{i_1 j_1}$ in the product (4.3.33) depends on the polar angle θ_1 whereas an other invariant e.g. $s_{i_2 j_2}$ contains the polar angle θ_1 as well as the azimuthal angle θ_2. The remaining invariants i.e. $s_{i_3 j_3}$ and $s_{i_4 j_4}$ do not depend on the angles.
Sometimes it happens that the azimuthal angle θ_2 also appears in $s_{i_1 j_1}$. In this case one has to rotate the frame in (4.3.28) so that $s_{i_1 j_1}$ becomes independent of the

azimuthal angle. This is always possible because the phase space integral (4.3.4) is Lorentz invariant. The angular integrals take the form

$$I_{\varepsilon}^{(i,j)} = \int_0^{\pi} d\theta_1 \int_0^{\pi} d\theta_2 \frac{(\sin\theta_1)^{1+\varepsilon}\,(\sin\theta_2)^{\varepsilon}}{(a+b\cos\theta_1)^i\,(A+B\cos\theta_1+C\sin\theta_1\cos\theta_2)^j}, \quad (4.3.34)$$

where a, b, A, B, and C are functions of the kinematical invariants s, s_{123}, s_{023}, s_{23} (4.3.32). These integrals can be found in appendix C of [31]. However they have to be extended by including terms which are proportional to ε^k where the degree k has to be larger than the one appearing in the integrals of [31]. This is necessary because these terms contribute due to the appearance of high power singularities $(1/\varepsilon)^k$ in the phase space integral (4.3.31). The n-dimensional expression for (4.3.34) becomes very cumbersome if $a^2 \neq b^2$ and $A^2 \neq B^2 + C^2$. Fortunately this situation can be avoided when one chooses the frame presented in (4.3.28). In this frame the worst case is given by $a^2 \neq b^2$, $A^2 = B^2 + C^2$ or $a^2 = b^2$, $A^2 \neq B^2 + C^2$. These type of integrals have to be partially done by hand before one can algebraically evaluate expression (4.3.31) using the program FORM [23]. The angular integrals are easy to perform when $a^2 = b^2$ and $A^2 = B^2 + C^2$ because they can be expressed into a hypergeometric function ${}_2F_1(\alpha, \beta; \gamma; x)$ [32] (see [33]). Inserting the latter in (4.3.31) the remaining integrations are then again performed using the algebraic manipulation program FORM.

4.3.3 Prescription of the γ_5-matrix and the Levi-Civita tensor in n-dimensions

The computation of $\hat{\mathcal{F}}_{A,q}$ proceeds in the same way as has been done for $\hat{\mathcal{F}}_{k,q}$ ($k = T, L$) described in the previous section. In the calculation one has to deal with the presence of ultraviolet (UV), infrared (IR) and collinear (C) divergences which have to be regularized using the method of n-dimensional regularization. However there is one difference between the calculation of $\hat{\mathcal{F}}_{k,q}$ ($k = T, L$) on one hand and the computation of $\hat{\mathcal{F}}_{A,q}$ on the other hand. This difference is due to the appearance of the γ_5-matrix in the interference term $M_V M_A^* + M_A M_V^*$ where M_V and M_A stand for the vector and axial-vector amplitude of the above processes. Here one has to find an n-dimensional extension for the γ_5-matrix occuring in M_A. For our calculation we have adopted the prescription for γ_5 given by 't Hooft and Veltman [34] (see also Breitenlohner and Maison [35]). Since the axial vector vertex is represented by $\gamma_\mu\gamma_5$ one can simplify the traces using the identification

$$\gamma_\mu\gamma_5 = -\frac{i}{6}\epsilon_{\mu\alpha\beta\sigma}\gamma^\alpha\gamma^\beta\gamma^\sigma, \quad (4.3.35)$$

which yields the same result as the prescription of 't Hooft and Veltman as is shown in [36, 24]. Although this prescription is consistent it has one drawback namely that the non-singlet axial vector current is renormalized in spite of the fact that it is conserved. Hence for each virtual correction where the γ_5-matrix appears in the

loop one needs an additional renormalization constant to undo this unwanted effect. This constant has been calculated in [24] and reads up to order α_s^2

$$Z_A = 1 - \frac{\alpha_s}{4\pi} C_F \left[4 - 5\varepsilon \right] + \left(\frac{\alpha_s}{4\pi} \right)^2 \left[C_F^2 \left\{ 22 \right\} + C_A C_F \left\{ -\frac{44}{3\varepsilon} - \frac{107}{9} \right.\right.$$
$$\left.\left. + n_f C_F T_f \left\{ \frac{16}{3\varepsilon} + \frac{4}{9} \right\} \right] , \tag{4.3.36}$$

where the colour factors in QCD are given by $C_F = (N^2-1)/2N$, $C_A = N$, and $T_f = 1/2$ with $N = 3$ and the number of light flavours is denoted by n_f. The rest of the calculation proceeds in the same way as performed for the deep inelastic parton structure functions $\hat{\mathcal{F}}_{3,q}^{\rm NS}$ [4] which is the analogue of $\hat{\mathcal{F}}_{A,q}^{\rm NS}$. Apart from the check on the procedure outlined in [4] we will add a new one which has the advantage that we can get rid of the renormalization constant Z_A in (4.3.36) which is needed when the γ_5-matrix appears in the loop of the virtual Feynman graph. This check is based on the observation that the difference between the asymmetric and transverse parton cross sections does not contain the distributions denoted by $\delta(1-z)$ and $(\ln^k(1-z)/(1-z))_+$. These singular functions originate from the one- and two-loop corrections to the Born-process (fig. 4.2) and the contributions due to soft gluon and collinear fermion pair production in figures 4.4, 4.6-4.8. Hence these distributions cancel in $\hat{\mathcal{F}}_{A,q}^{\rm NS}(z,Q^2/\mu^2) - \hat{\mathcal{F}}_{T,q}^{\rm NS}(z,Q^2/\mu^2)$. Since the computation of $\hat{\mathcal{F}}_{T,q}^{\rm NS}$ does not involve the γ_5-matrix we can obtain $\hat{\mathcal{F}}_{A,q}^{\rm NS}$ from the difference $\hat{\mathcal{F}}_{A,q}^{\rm NS} - \hat{\mathcal{F}}_{T,q}^{\rm NS}$. The latter is only determined by the one-loop corrections to the regular part of the process in fig. 4.4 (hard gluon radiative part) and the regular part of the processes in fig. 4.7 and 4.8 (hard gluon radiation plus quark anti-quark production). Hence we only have to deal with the γ_5-matrix in the one-loop corrections to the process in fig. 4.4. However we have now checked that the following identity holds

$$Z_A \left[\left\{ M_V^{(1)^*} M_A^{(1)} + M_A^{(1)^*} M_V^{(1)} \right\} + \left\{ M_V^{(1)^*} M_A^{(3)} + M_V^{(3)^*} M_A^{(1)} + M_A^{(1)^*} M_V^{(3)} \right.\right.$$
$$\left.\left. + M_A^{(3)^*} M_V^{(1)} \right\} \right] = \left\{ M_V^{(1)^*} M_A^{(1)} + M_A^{(1)^*} M_V^{(1)} \right\} + \left\{ 2M_A^{(1)^*} M_V^{(3)} \right.$$
$$\left. + 2M_V^{(3)^*} M_A^{(1)} \right\} , \tag{4.3.37}$$

where $M_k^{(\ell)}$ is the order g^ℓ ($\alpha_s = g^2/4\pi$) contribution to the amplitude M_k ($k = V, A$). Here $M_V^{(\ell)}$ and $M_A^{(\ell)}$ denote the amplitudes where the quark is attached to the vector- and axial-vector current respectively so that $M_A^{(\ell)}$ contains the γ_5-matrix. The term between the first pair of curly brackets on the left-hand side of (4.3.37) originates from the purely radiative process (fig. 4.4) whereas the term in the second pair of curly brackets refers to the interference between the process in fig. 4.4 and the virtual corrections to the process it (fig. 4.6). The latter is represented by the amplitude

$M_k^{(3)}$ $(k = V, A)$. Equation (4.3.37) reveals that one can get rid of the renormalization constant Z_A by shifting the γ_5-matrix from $M_A^{(3)}$ to the amplitude $M_A^{(1)}$ of the radiative process in fig. 4.4 so that this matrix becomes harmless. Actually one can now also choose the naive γ_5-prescription without altering the final result.

4.3.4 Soft contributions to the parton fragmentation functions

Finally we would like to comment on a special type of term appearing in the transverse and asymmetric parton fragmentation functions $\hat{\mathcal{F}}_{k,q}(z, Q^2, \varepsilon)$ $(k = T, A)$. They only show up in the non-singlet part and the order α_s^m contribution takes the form

$$\hat{\mathcal{F}}_{T,q}^{(m)}(z, Q^2, \varepsilon) = \sum_{\ell=-1}^{2m-1} (1-z)^{\frac{m}{2}\varepsilon-1} \frac{f_\ell(z)}{\varepsilon^\ell}, \tag{4.3.38}$$

where $f_\ell(1)$ is finite. These type of terms originate from gluon bremsstrahlung (figs. 4.4, 4.6, 4.7) and gluon splitting into a quark–anti-quark pair (fig. 4.8). In the limit $z \to 1$ all gluons become soft and the angle between the quark and anti-quark pair goes to zero (collinear emission). In the next section expression (4.3.38) has to be convoluted with the so-called bare fragmentation densities $\hat{D}_q^H(z)$ (for the definition see section 4) which yields the integral

$$\sum_{\ell=-1}^{2m-1} \int_x^1 dz\, \hat{D}_q^H\left(\frac{x}{z}\right) (1-z)^{\frac{m}{2}\varepsilon-1} \frac{f_\ell(z)}{\varepsilon^\ell}. \tag{4.3.39}$$

Inspection of the above integral reveals that at $z = 1$ one gets an additional pole term which means that we also have to compute $f_{-1}(1)$. Therefore for $z = 1$ the phase space integrals (4.3.31) have to be computed even up to one order higher in powers of ε than is needed for those which are integrable at $z = 1$. Since $f_\ell(z) - f_\ell(1)$ is integrable at $z = 1$ we can replace in (4.3.38) $f_\ell(z)$ by $f(1)$ and one only has to consider the integral

$$\hat{\mathcal{F}}_{k,q}^{(m)} = \sum_{\ell=-1}^{2m-1} \int_x^1 dz\, \hat{D}_q^H\left(\frac{x}{z}\right) (1-z)^{\frac{m}{2}\varepsilon-1} \frac{f_\ell(1)}{\varepsilon^\ell}, \quad k = T, A, \tag{4.3.40}$$

which can be written as

$$\hat{\mathcal{F}}_{k,q}^{(m)} = \sum_{\ell=-1}^{2m-1} \left[\int_x^1 dz\, (1-z)^{\frac{m}{2}\varepsilon-1} \frac{f_\ell(1)}{\varepsilon^\ell} \left\{ \hat{D}_q^H\left(\frac{x}{z}\right) - \hat{D}_q^H(x) \right\} \right.$$

$$\left. + \frac{2}{m} \varepsilon^{-\ell-1} \hat{D}_q^H(x) f_\ell(1) (1-x)^{\frac{m}{2}\varepsilon-1} \right], \quad k = T, A. \tag{4.3.41}$$

If we define the distribution (see [37])

$$\mathcal{D}_i(z) = \left(\frac{\ln^i(1-z)}{1-z} \right)_+, \tag{4.3.42}$$

by

$$\int_0^1 dz\, \mathcal{D}_i(z)\, g(z) = \int_0^1 dz\, \frac{\ln^i(1-z)}{1-z}\,(g(z)-g(1)), \tag{4.3.43}$$

one can rewrite (4.3.41) in the following way

$$\hat{\mathcal{F}}_{k,q}^{(m)} = \int_x^1 dz \left[\left\{ \sum_{\ell=0}^{2m-1} \frac{f_\ell(1)}{\varepsilon^\ell}\, \hat{D}_q^H\left(\frac{x}{z}\right) \sum_{i=0}^{\ell} \frac{1}{i!} \left(\frac{1}{2} m\varepsilon\right)^i \mathcal{D}_i(z) \right\} \right.$$

$$\left. + \hat{D}_q^H\left(\frac{x}{z}\right) \hat{\mathcal{F}}_{k,q}^{(m),\rm soft}(z) \right], \quad k = T, A, \tag{4.3.44}$$

where $\hat{\mathcal{F}}_{k,q}^{\rm soft}$ $(k = T, A)$ stands for the soft gluon bremsstrahlung contribution which is given by (see the definition in [38])

$$\hat{\mathcal{F}}_{k,q}^{(m),\rm soft} = \delta(1-z) \sum_{\ell=-1}^{2m-1} \frac{2}{m} \varepsilon^{-\ell-1}\, f_\ell(1), \quad k = T, A. \tag{4.3.45}$$

In order α_s^2 $(m = 2)$ the highest order pole term which can occur in (4.3.45) is represented by $1/\varepsilon^4$. The latter is cancelled by similar terms originating from the virtual gluon contributions given by the two-loop vertex corrections in fig. 4.5. Finally we want to emphasize that the type of singular terms in (4.3.38) only occur in $\hat{\mathcal{F}}_{k,q}^{\rm NS}$ $(k = T, A)$ and are absent in $\hat{\mathcal{F}}_{L,q}^{\rm NS}$ and $\hat{\mathcal{F}}_{k,q}^{\rm PS}$, $\hat{\mathcal{F}}_{k,g}$ $(k = q, g)$ † $(k = T, L)$.
Adding all virtual-, soft- and hard-gluon contributions, the IR divergences cancel while computing the parton structure functions $\hat{\mathcal{F}}_{k,p}(z, Q^2, \varepsilon)$ which is in agreement with the Bloch-Nordsieck theorem. The left-over divergences are removed by coupling constant renormalization and the C-divergences are factorized out of $\hat{\mathcal{F}}_{k,p}(z, Q^2, \varepsilon)$ leaving us with the coefficient functions which are finite in the limit $\varepsilon \to 0$. These two procedures will be carried out in the next section.

4.4 Determination of the coefficient functions in the $\overline{\rm MS}$- and the annihilation scheme (A-scheme)

In this section we determine the coefficient functions of the process (4.2.1) by applying coupling constant renormalization and mass factorization to the parton fragmentation functions $\hat{\mathcal{F}}_{k,p}$ $(p = q, g)$ which are computed up to order α_s^2 in the last section. These coefficient functions have to satisfy renormalization group equations. One can formally solve these equations order by order in α_s by writing the renormalization group functions like the beta-function $\beta(\alpha_s)$ and the anomalous dimension

†Notice that $\hat{\mathcal{F}}_{A,q}^{\rm PS} = \hat{\mathcal{F}}_{A,g} = 0$ because of charge conjugation invariance of the strong interactions.

$\gamma_{ij}(\alpha_s)$ $(i,j = q,g)$ as a power series in α_s. In this way one can algebraically express the coefficient functions into the coefficients of the power series. Using the mass factorization theorem which holds in every renormalizable field theory for all leading twist two contributions, one can also express the parton fragmentation functions $\hat{\mathcal{F}}_{k,p}$ into the same coefficients. Our calculations described in the last section have to satisfy the algebraic expressions of $\hat{\mathcal{F}}_{k,p}$ at least up to pole terms $(1/\varepsilon)^m$ which is a minimal requirement for the correctness of our results.
Before presenting the algebraic expressions for $\hat{\mathcal{F}}_{k,p}$ we have to decompose them according to the flavour symmetry group. Convoluting the parton structure tensor $\hat{W}_{\mu\nu}^{(V,V')}$ (4.3.7) with the bare parton fragmentation densities $\hat{D}_p^H(z)$ we obtain the following functions

$$F_k^{H,(V,V')}(x,Q^2) = \sum_{p=q,\bar{q},g} \sum_{q_1,q_2=1}^{n_f} (v_{q_1}^{(V)} v_{q_2}^{(V')} + a_{q_1}^{(V)} a_{q_2}^{(V')}) \cdot$$

$$\cdot \int_0^1 \frac{dz}{z} \hat{D}_p^H\left(\frac{x}{z}\right) \hat{\mathcal{F}}_{k,p}(z,Q^2,\varepsilon), \quad (k = T,L), \tag{4.4.1}$$

$$F_A^{H,(V,V')}(x,Q^2) = \sum_{p=q,\bar{q}} \sum_{q_1,q_2=1}^{n_f} (v_{q_1}^{(V)} a_{q_2}^{(V')} + a_{q_1}^{(V)} v_{q_2}^{(V')}) \cdot$$

$$\cdot \int_0^1 \frac{dz}{z} \hat{D}_p^H\left(\frac{x}{z}\right) \hat{\mathcal{F}}_{A,p}(z,Q^2,\varepsilon). \tag{4.4.2}$$

The reason that we call $\hat{D}_p^H$ 'bare', originates from the fact that the C-divergence which are removed from $\hat{\mathcal{F}}_{k,p}$ via mass factorization will be absorbed by $\hat{D}_p^H$ so that the latter are dressed up to the phenomenological fragmentation densities defined in (4.2.4), (4.2.5). The hadronic fragmentation functions defined in (4.2.21) are obtained by contracting the parton structure tensor $\hat{W}_{\mu\nu}^{(V,V')}$ (4.3.7), after convolution by $\hat{D}_p^H$, with the leptonic tensor due to the subprocess $e^+ + e^- \to V(V')$ where one also has to include the vector boson propagators given by $Z(Q^2)^{-1}$ in (4.2.12).
The contributions to $\hat{\mathcal{F}}_{k,p}$ $(p = q,g)$ can be distinguished in a flavour singlet (S) and a flavour non-singlet (NS) part. Equations (4.4.1), (4.4.2) can then be written as

$$F_k^{H,(V,V')}(x,Q^2) = \int_x^1 \frac{dz}{z} \Bigg[\sum_{p=1}^{n_f} (v_p^{(V)} v_p^{(V')} + a_p^{(V)} a_p^{(V')}) (\hat{D}_p^H\left(\frac{x}{z}\right) + \hat{D}_{\bar{p}}^H\left(\frac{x}{z}\right)) \cdot$$

$$\cdot \hat{\mathcal{F}}_{k,q}^{\mathrm{NS}}(z,Q^2,\varepsilon) + \left(\sum_{q_1=1}^{n_f} a_{q_1}^{(V')} \sum_{p=1}^{n_f} a_p^{(V)} + \sum_{q_1=1}^{n_f} a_{q_1}^{(V)} \sum_{p=1}^{n_f} a_p^{(V')} \right) (\hat{D}_p^H\left(\frac{x}{z}\right)$$

$$+ \hat{D}_{\bar{p}}^H\left(\frac{x}{z}\right)) \hat{\mathcal{F}}_{k,q}^{\prime,\mathrm{NS}}(z,Q^2,\varepsilon) + \sum_{q_1=1}^{n_f} (v_{q_1}^{(V)} v_{q_1}^{(V')} + a_{q_1}^{(V)} a_{q_1}^{(V')}) \Bigg\{ \frac{1}{n_f} \sum_{p=1}^{n_f} (\hat{D}_p^H\left(\frac{x}{z}\right)$$

$$+ \hat{D}_{\bar{p}}^{H}\left(\frac{x}{z}\right))\,\hat{\mathcal{F}}_{k,q}^{\text{PS}}(z,Q^2,\varepsilon) + \hat{D}_{g}^{H}\left(\frac{x}{z}\right)\,\hat{\mathcal{F}}_{k,g}(z,Q^2,\varepsilon)\Big\}\Big], \quad (k=T,L), \tag{4.4.3}$$

$$F_A^{H,(V,V')}(x,Q^2) = \int_x^1 \frac{dz}{z}\Big[\sum_{p=1}^{n_f}(v_p^{(V)}a_p^{(V')} + a_p^{(V)}v_p^{(V')})(\hat{D}_p^H\left(\frac{x}{z}\right) - \hat{D}_{\bar{p}}^H\left(\frac{x}{z}\right))\cdot$$

$$\cdot\hat{\mathcal{F}}_{A,q}^{\text{NS}}(z,Q^2,\varepsilon) + (\sum_{q_1=1}^{n_f} a_{q_1}^{(V')}\sum_{p=1}^{n_f} v_p^{(V)} + \sum_{q_1=1}^{n_f} a_{q_1}^{(V)}\sum_{p=1}^{n_f} v_p^{(V')})(\hat{D}_p^H\left(\frac{x}{z}\right)$$

$$- \hat{D}_{\bar{p}}^H\left(\frac{x}{z}\right))\,\hat{\mathcal{F}}_{A,q}^{\prime,\text{NS}}(z,Q^2,\varepsilon)\Big]. \tag{4.4.4}$$

Here we use the same notation as introduced above (4.2.9) where $p = 1,2,\ldots,n_f$ stands for $p = u,d,\ldots$. Further we have the relations

$$\hat{\mathcal{F}}_{k,q}^{(r)} = \hat{\mathcal{F}}_{k,\bar{q}}^{(r)}, \quad (k=T,L;r=\text{NS},\text{PS}), \tag{4.4.5}$$

$$\hat{\mathcal{F}}_{A,q}^{\text{NS}} = -\hat{\mathcal{F}}_{A,\bar{q}}^{\text{NS}}, \quad \hat{\mathcal{F}}_{A,q}^{\text{PS}} = \hat{\mathcal{F}}_{A,\bar{q}}^{\text{PS}} = 0, \quad \hat{\mathcal{F}}_{A,g} = 0. \tag{4.4.6}$$

Relations (4.4.5), (4.4.6) follow from charge conjugation invariance of the strong interactions. The parton fragmentation function $\hat{\mathcal{F}}_{k,q}^{\text{PS}}$ is called the purely singlet part for reasons we will explain below.
The function $\hat{\mathcal{F}}_{k,g}$ $(k=T,L)$, describing process (4.3.1) where the gluon is detected $(p=g)$, receives contributions from the graphs in figs. 4.4, 4.6, 4.7. Since the gluon is a flavour singlet $\hat{\mathcal{F}}_{k,g}$ belongs to the same representation. The quarks q_1 and q_2 in (4.4.1), which are directly coupled to the vector bosons V and V' respectively, automatically belong to the inclusive state when $p=g$ in reaction (4.3.1) so that the sums over q_1, q_2, and p in (4.4.1) have to be separately performed.
The non-singlet part $\hat{\mathcal{F}}_{k,q}^{\text{NS}}$ $(k=T,A,L)$ describing process (4.3.1) where the quark or anti-quark is detected ($p=q$ or $p=\bar{q}$), is determined by the graphs in figs. 4.2-4.8 except for the combinations C^2, D^2 and AD, BC (see below). Notice that groups B and D only contribute when the anti-quarks q_1 and q_2 are identical. In the case of the non-singlet contribution the quarks q_1 and q_2 can be identified with p (i.e. $p=q_1=q_2$) so that the sums over q_1, q_2, and p in (4.4.1) are now connected. The above diagrams also contribute to $\hat{\mathcal{F}}_{k,q}^{\text{S}}$ in the case of $k=T,L$ when they are projected on the singlet channel and the result is the same as the one obtained for $\hat{\mathcal{F}}_{k,q}^{\text{NS}}$ so that we can set $\hat{\mathcal{F}}_{k,q}^{\text{S}} = \hat{\mathcal{F}}_{k,q}^{\text{NS}}$. The groups C^2 and D^2 in fig. 4.8 only survive if they are projected on the singlet channel. This is because the detected quark p is only connected with the vector bosons V and V' via the exchange of a gluon which is a flavour singlet. To show this more explicitly we have drawn the cut graphs contributing to the parton structure tensor $\hat{W}_{\mu\nu}^{(V,V')}$ which originate from groups C and D in fig. 4.9. Because of the purely singlet nature the groups C and D only contribute to $\hat{\mathcal{F}}_{k,q}^{\text{S}}$ and their contribution will be called $\hat{\mathcal{F}}_{k,q}^{\text{PS}}$. Like in the case of $\hat{\mathcal{F}}_{k,g}$

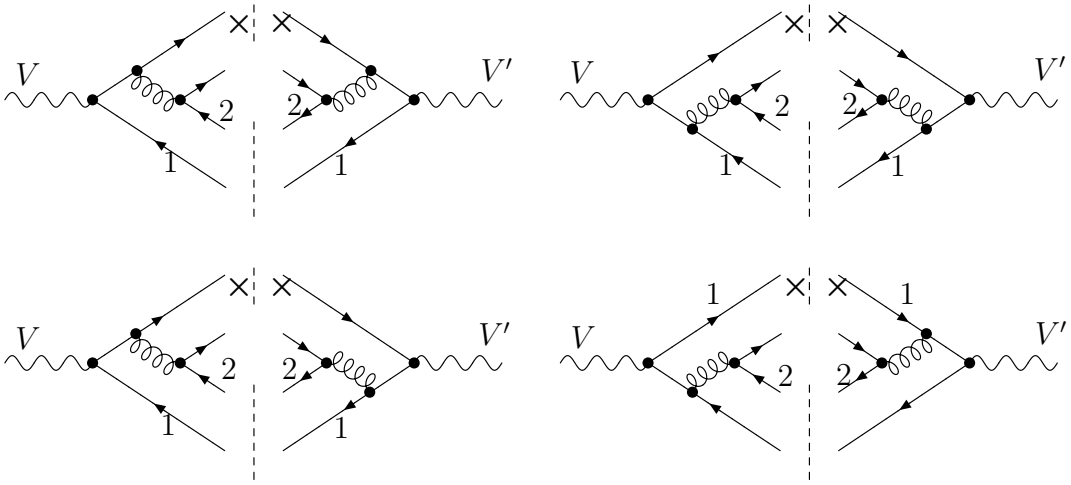

Figure 4.9: *Cut diagrams obtained from the groups C and D in fig. 4.8 contributing to the process* $V \to$ "q" $+ \bar{q}(1) + q + \bar{q}(2)$.

the quarks q_1, q_2 belong to the inclusive state since $p \neq q_1$, $p \neq q_2$. Therefore one can separately sum over p and q_1, q_2 which determines the factor of $\hat{\mathcal{F}}_{k,q}^{\mathrm{PS}}$ in (4.4.3). Finally we have a special non-singlet contribution which we will call $\hat{\mathcal{F}}_{k,q}^{\prime\mathrm{NS}}$ (4.4.3) ($k = T, L$) and $\hat{\mathcal{F}}_{A,q}^{\prime\mathrm{NS}}$ (4.4.4). The latter originates from the combinations AD and BC in fig. 4.8 which only appear in the case when the anti-quarks q_1 and q_2 are identical. The corresponding cut graphs are drawn in fig. 4.10. If one removes the dashed line, which indicates the integration over the momenta cut by that line, one obtains a closed fermion loop. This fermion loop, to which are attached two gluons and one vector boson V (V'), has the same properties as the triangular fermion loops inserted in the virtual diagrams of figs. 4.5, 4.6. In fig. 4.10 we have taken the example that the vector boson V' couples to the cut fermion loop via the quark q_1 whereas V couples to the detected quark p (see also (4.4.3), (4.4.4)). Like in the case of the triangle fermion loops in figs. 4.5, 4.6 only the axial vector current can couple to the cut fermion-loop which rules out $V' = \gamma$ so that only $V' = Z$ remains. Since $a_p^{(\gamma)} = a_{q_1}^{(\gamma)} = 0$ we have in (4.4.3) $V = Z$ whereas in (4.4.4) we either can get $V = \gamma$ or $V = Z$. Only when the above condition is satisfied the parton fragmentation functions $\hat{\mathcal{F}}_{k,q}^{\prime\mathrm{NS}}$ ($k = T, L$) and $\hat{\mathcal{F}}_{A,q}^{\prime\mathrm{NS}}$ can contribute to $F_k^{(Z,Z)}$ (4.4.3) and $F_A^{(V,Z)}$ ($V = \gamma, Z$) respectively. If we now in addition sum in fig. 4.10 over all quark flavours q_1 belonging to one family one gets $\sum_{q_1=u,d} a_{q_1}^{(Z)} = 0$ (see (4.3.8)) so that in this case the above contributions due to $\hat{\mathcal{F}}_{k,q}^{\prime\mathrm{NS}}$, $\hat{\mathcal{F}}_{A,q}^{\prime\mathrm{NS}}$ will vanish. Since one has to sum over all members of one family anyhow in order to cancel the anomaly appearing in the triangle fermion-loops in figs. 4.5, 4.6 we will do the same for the graphs in fig. 4.10. Therefore we do not have to calculate $\hat{\mathcal{F}}_{k,q}^{\prime\mathrm{NS}}$ and $\hat{\mathcal{F}}_{A,q}^{\prime\mathrm{NS}}$ and they will not be included in our phenomenological analysis in this thesis.

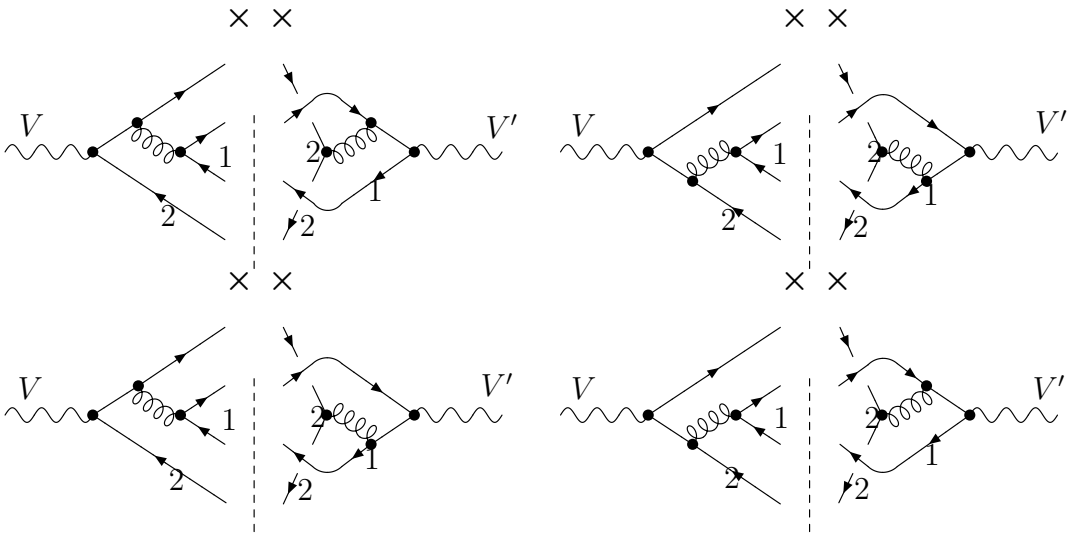

Figure 4.10: *Cut diagrams resulting from the combinations AD and BC in fig. 4.8 contributing to* $V \to$ *"q"* $+ \bar{q}(1) + q + \bar{q}(2)$ *in the case that* $\bar{q}(1) = \bar{q}(2)$.

Summarizing the above the singlet fragmentation function $\hat{\mathcal{F}}^{\rm S}_{k,q}$ $(k = T, L)$ receives two kinds of contributions and it can be written as

$$\hat{\mathcal{F}}^{\rm S}_{k,q} = \hat{\mathcal{F}}^{\rm NS}_{k,q} + \hat{\mathcal{F}}^{\rm PS}_{k,q}, \quad (k = T, L). \tag{4.4.7}$$

After having specified the various parts to the parton fragmentation functions we will now list them below. Starting with the non-singlet part the parton fragmentation function expanded in the bare coupling constant $\hat{\alpha}_s$read as follows

$$\hat{\mathcal{F}}^{\rm NS,(2)}_{L,q} = \left(\frac{\hat{\alpha}_s}{4\pi}\right)^2 S_\varepsilon^2 \left(\frac{Q^2}{\mu^2}\right)^\varepsilon \left[\frac{1}{\varepsilon} \left\{ -2\beta_0 \bar{c}^{(1)}_{L,q} + P^{(0)}_{qq} \otimes \bar{c}^{(1)}_{L,q} \right\} + \bar{c}^{\rm NS,nid,(2)}_{L,q} + \bar{c}^{\rm NS,id,(2)}_{L,q} - 2\beta_0 a^{(1)}_{L,q} + P^{(0)}_{qq} \otimes a^{(1)}_{L,q} \right], \tag{4.4.8}$$

$$\hat{\mathcal{F}}^{\rm NS,(2)}_{T,q} = \left(\frac{\hat{\alpha}_s}{4\pi}\right)^2 S_\varepsilon^2 \left(\frac{Q^2}{\mu^2}\right)^\varepsilon \left[\frac{1}{\varepsilon^2} \left\{ \frac{1}{2} P^{(0)}_{qq} \otimes P^{(0)}_{qq} - \beta_0 P^{(0)}_{qq} \right\} + \frac{1}{\varepsilon} \left\{ \frac{1}{2} (P^{(1),\rm NS}_{qq} + P^{(1),\rm NS}_{q\bar{q}}) - 2\beta_0 \bar{c}^{(1)}_{T,q} + P^{(0)}_{qq} \otimes \bar{c}^{(1)}_{T,q} \right\} + \bar{c}^{\rm NS,nid,(2)}_{T,q} + \bar{c}^{\rm NS,id,(2)}_{T,q} - 2\beta_0 a^{(1)}_{T,q} + P^{(0)}_{qq} \otimes a^{(1)}_{T,q} \right], \tag{4.4.9}$$

$$\hat{\mathcal{F}}^{\rm NS,(2)}_{A,q} = \left(\frac{\hat{\alpha}_s}{4\pi}\right)^2 S_\varepsilon^2 \left(\frac{Q^2}{\mu^2}\right)^\varepsilon \left[\frac{1}{\varepsilon^2} \left\{ \frac{1}{2} P^{(0)}_{qq} \otimes P^{(0)}_{qq} - \beta_0 P^{(0)}_{qq} \right\} + \frac{1}{\varepsilon} \left\{ \frac{1}{2} (P^{(1),\rm NS}_{qq}$$

$$- P_{q\bar{q}}^{(1),\mathrm{NS}}) - 2\beta_0 \bar{c}_{A,q}^{(1)} + P_{qq}^{(0)} \otimes \bar{c}_{A,q}^{(1)} \Big\} + \bar{c}_{A,q}^{\mathrm{NS,nid},(2)} - \bar{c}_{A,q}^{\mathrm{NS,id},(2)} - 2\beta_0 a_{A,q}^{(1)}$$

$$+ P_{qq}^{(0)} \otimes a_{A,q}^{(1)} \Big] . \tag{4.4.10}$$

The convolution symbol denoted by $\otimes$ is defined by

$$(f \otimes g)(z) = \int_0^1 dz_1 \int_0^1 dz_2 \, \delta(z - z_1 z_2) f(z_1) g(z_2). \tag{4.4.11}$$

The second order DGLAP splitting functions denoted by $P_{ij}^{(1)}$ $(i, j = q, g)$ are different for deep inelastic structure functions (spacelike process) and fragmentation functions (timelike process). For the latter case they have been calculated in [39, 40]. In order to solve the Altarelli-Parisi equations of the fragmentation densities D_p^H it is convenient to split them into two parts which in the $\overline{\mathrm{MS}}$-scheme are given by

$$P_{qq}^{\mathrm{NS},(1)}(z) = n_f C_F T_f \Big[- \frac{160}{9} \mathcal{D}_0(z) - \frac{16}{9} + \frac{176}{9} z - \frac{16}{3} \frac{1+z^2}{1-z} \ln z$$

$$- \delta(1-z)(\frac{4}{3} + \frac{32}{3}\zeta(2)) \Big]$$

$$+ C_F^2 \Big[\frac{1+z^2}{1-z} \ln z \, (12 + 16 \ln(1-z) - 16 \ln z) - 40(1-z)$$

$$- (28 + 12z) \ln z + 4(1+z) \ln^2 z + \delta(1-z)(3 - 24\zeta(2) + 48\zeta(3)) \Big]$$

$$+ C_A C_F \Big[(\frac{536}{9} - 16\zeta(2)) \mathcal{D}_0(z) + 8(1+z)\zeta(2) + 8(1+z) \ln z + \frac{212}{9}$$

$$- \frac{748}{9} z + \frac{1+z^2}{1-z} \Big(4 \ln^2 z + \frac{44}{3} \ln z \Big) + \delta(1-z)(\frac{17}{3} + \frac{88}{3}\zeta(2) - 24\zeta(3)) \Big] , \tag{4.4.12}$$

$$P_{q\bar{q}}^{\mathrm{NS},(1)}(z) = (C_F^2 - \frac{1}{2} C_A C_F) \Big[\frac{1+z^2}{1+z} \Big(8 \ln^2 z - 32 \ln z \ln(1+z) - 32 \mathrm{Li}_2(-z)$$

$$- 16\zeta(2) \Big) + 32(1-z) + 16(1+z) \ln z \Big] , \tag{4.4.13}$$

where $\mathrm{Li}_n(x)$ denote the polylogarithmic functions which can be found in [41]. The splitting function $P_{q\bar{q}}^{\mathrm{NS},(1)}$ (4.4.13) arises when the (anti) quarks p_1 and p_2 in reaction (4.3.1) become identical and it is only determined by the interference terms AB and CD in fig. 4.8. Like the splitting functions we have also decomposed the second

order coefficients $\bar{c}_{k,q}^{\text{NS},(2)}$ $(k = T, A, L)$ into two parts i.e. $\bar{c}_{k,q}^{\text{NS,nid},(2)}$ and $\bar{c}_{k,q}^{\text{NS,id},(2)}$. The latter is due to identical (anti) quark contributions and like $P_{q\bar{q}}$ it originates from combinations AB and CD in fig. 4.8. All coefficients $\bar{c}_{k,q}^{(i)}$ $(i = 0, 1)$ are computed in the $\overline{\text{MS}}$-scheme indicated by a bar and they show up in the perturbation series of the coefficient functions as we will see below. The coefficients $a_{k,q}^{(1)}$ are presented in (4.3.19), (4.3.20) and β_0 is the lowest order coefficient in the beta-function defined by

$$\beta(\alpha_s) = -2\alpha_s \left[\beta_0 \frac{\alpha_s}{4\pi} + \beta_1 \left(\frac{\alpha_s}{4\pi}\right)^2 + \cdots\right], \quad \beta_0 = \frac{11}{3} C_A - \frac{4}{3} T_f n_f, \tag{4.4.14}$$

where α_s now stands for the renormalized coupling (see below). The purely singlet contributions (see (4.4.7)) are given by

$$\hat{\mathcal{F}}_{L,q}^{\text{PS},(2)} = n_f \left(\frac{\hat{\alpha}_s}{4\pi}\right)^2 S_\varepsilon^2 \left(\frac{Q^2}{\mu^2}\right)^\varepsilon \left[\frac{1}{\varepsilon}\left\{\frac{1}{2} P_{qg}^{(0)} \otimes \bar{c}_{L,g}^{(1)}\right\} + \bar{c}_{L,q}^{\text{PS},(2)} + \frac{1}{2} P_{qg}^{(0)} \otimes a_{L,g}^{(1)}\right], \tag{4.4.15}$$

$$\hat{\mathcal{F}}_{T,q}^{\text{PS},(2)} = n_f \left(\frac{\hat{\alpha}_s}{4\pi}\right)^2 S_\varepsilon^2 \left(\frac{Q^2}{\mu^2}\right)^\varepsilon \left[\frac{1}{\varepsilon^2}\left\{\frac{1}{2} P_{gq}^{(0)} \otimes P_{qg}^{(0)}\right\} + \frac{1}{\varepsilon}\left\{\frac{1}{2} P_{qq}^{\text{PS},(1)} + \frac{1}{2} P_{qg}^{(0)} \otimes \bar{c}_{T,g}^{(1)}\right\} + \bar{c}_{T,q}^{\text{PS},(2)} + \frac{1}{2} P_{qg}^{(0)} \otimes a_{T,g}^{(1)}\right], \tag{4.4.16}$$

where $a_{L,g}^{(1)}$ and $a_{T,g}^{(1)}$ are presented in (4.3.22) and (4.3.23) respectively. The above expressions are determined by the combinations C^2 (non-identical (anti-) quarks) or C^2 and D^2 (identical (anti-) quarks) in fig. 4.8. The timelike splitting function $P_{qq}^{\text{PS},(1)}$ can be inferred from [39, 40] and it reads ($\overline{\text{MS}}$-scheme)

$$P_{qq}^{\text{PS},(1)}(z) = C_F T_f \left[-\frac{320}{9z} - 128 + 64z + \frac{896}{9} z^2 + 16(1+z)\ln^2 z - (80 + 144z + \frac{128}{3} z^2)\ln z\right]. \tag{4.4.17}$$

From (4.4.7) we can now also obtain the singlet parton fragmentation function $\hat{\mathcal{F}}_{k,q}^{\text{S},(2)}$ $(k = T, L)$. Adding eqs. (4.4.8) and (4.4.15) provides us with $\hat{\mathcal{F}}_{L,q}^{\text{S},(2)}$ whereas the sum of eqs. (4.4.9) and (4.4.16) leads to $\hat{\mathcal{F}}_{T,q}^{\text{S},(2)}$. In the same way we obtain from (4.4.12), (4.4.13) and (4.4.17) the singlet splitting function

$$P_{qq}^{\text{S},(1)} = P_{qq}^{\text{NS},(1)} + P_{q\bar{q}}^{\text{NS},(1)} + P_{qq}^{\text{PS},(1)}. \tag{4.4.18}$$

Finally the order α_s^2 contributions to $\hat{\mathcal{F}}_{k,g}$ become

$$\hat{\mathcal{F}}_{L,g}^{(2)} = n_f \left(\frac{\hat{\alpha}_s}{4\pi}\right)^2 S_\varepsilon^2 \left(\frac{Q^2}{\mu^2}\right)^\varepsilon \left[\frac{1}{\varepsilon} \left\{ -2\beta_0 \bar{c}_{L,g}^{(1)} + P_{gg}^{(0)} \otimes \bar{c}_{L,g}^{(1)} + 2P_{gq}^{(0)} \otimes \bar{c}_{L,q}^{(1)} \right\} \right.$$
$$\left. + \bar{c}_{L,g}^{(2)} - 2\beta_0 a_{L,g}^{(1)} + P_{gg}^{(0)} \otimes a_{L,g}^{(1)} + 2P_{gq}^{(0)} \otimes a_{L,q}^{(1)} \right], \tag{4.4.19}$$

$$\hat{\mathcal{F}}_{T,g}^{(2)} = n_f \left(\frac{\hat{\alpha}_s}{4\pi}\right)^2 S_\varepsilon^2 \left(\frac{Q^2}{\mu^2}\right)^\varepsilon \left[\frac{1}{\varepsilon^2} \left\{ P_{gq}^{(0)} \otimes (P_{gg}^{(0)} + P_{qq}^{(0)}) - 2\beta_0 P_{gq}^{(0)} \right\} \right.$$
$$+ \frac{1}{\varepsilon} \left\{ P_{gq}^{(1)} - 2\beta_0 \bar{c}_{T,g}^{(1)} + P_{gg}^{(0)} \otimes \bar{c}_{T,g}^{(1)} + 2P_{gq}^{(0)} \otimes \bar{c}_{T,q}^{(1)} \right\} + \bar{c}_{T,g}^{(2)} - 2\beta_0 a_{T,g}^{(1)}$$
$$\left. + P_{gg}^{(0)} \otimes a_{T,g}^{(1)} + 2P_{gq}^{(0)} \otimes a_{T,g}^{(1)} \right], \tag{4.4.20}$$

where the timelike splitting function $P_{gq}^{(1)}$ in the $\overline{\text{MS}}$-scheme can be found in [39, 40]. It is given by

$$P_{gq}^{(1)} = C_F^2 \left[-4 + 36z + (-64 + 4z)\ln z + 16z\ln(1-z) + (8-4z)\ln^2 z \right.$$
$$+ (\frac{16}{z} - 16 + 8z)\ln^2(1-z) + (\frac{64}{z} - 64 + 32z)\ln z \ln(1-z)$$
$$\left. + (\frac{128}{z} - 128 + 64z)\text{Li}_2(1-z) + (-\frac{128}{z} + 128 - 64z)\zeta(2) \right]$$
$$+ C_A C_F \left[\frac{136}{9z} + 40 - 8z - \frac{352}{9}z^2 + (-\frac{48}{z} + 64 + 72z + \frac{64}{3}z^2)\ln z \right.$$
$$- 16z\ln(1-z) - (\frac{32}{z} + 16 + 24z)\ln^2 z + (-\frac{16}{z} + 16 - 8z)\ln^2(1-z)$$
$$+ (-\frac{32}{z} + 32 - 16z)\ln z \ln(1-z) + (-\frac{128}{z} + 128 - 64z)\text{Li}_2(1-z)$$
$$+ (\frac{32}{z} + 32 + 16z)\text{Li}_2(-z) + (\frac{32}{z} + 32 + 16z)\ln z \ln(1+z) + (\frac{128}{z}$$
$$\left. - 96 + 64z)\zeta(2) \right]. \tag{4.4.21}$$

The pole terms $(1/\varepsilon)^m$ showing up in the parton fragmentation functions $\hat{\mathcal{F}}_{k,p}$ $(k = T, A, L;\ p = q, g)$ are due to UV and C-divergences. In order to get the coefficient functions corresponding to the fragmentation process (4.2.1) these singularities

have to be removed via coupling constant renormalization and mass factorization. The coupling constant renormalization can be achieved by replacing the bare (unrenormalized) coupling constant $\hat{\alpha}_s$ by

$$\frac{\hat{\alpha}_s}{4\pi} = \frac{\alpha_s(R^2)}{4\pi}\left(1 + \frac{\alpha_s(R^2)}{4\pi}\frac{2\beta_0}{\varepsilon}S_\varepsilon\left(\frac{R^2}{\mu^2}\right)^{\varepsilon/2}\right), \tag{4.4.22}$$

where R represents the renormalization scale. After having removed the UV singularities the remaining pole terms can be attributed to final state collinear divergence only because $\hat{\mathcal{F}}_{k,p}$ is a semi-inclusive quantity. The latter singularities are removed by mass factorization which proceeds in the following way

$$\hat{\mathcal{F}}^{\rm NS}_{k,q} = \Gamma^{\rm NS}_{qq} \otimes \mathbb{C}^{\rm NS}_{k,q}, \quad (k = T, L) \tag{4.4.23}$$

$$\hat{\mathcal{F}}^{\rm NS}_{A,q} = \Gamma^{\rm NS}_{A,qq} \otimes \mathbb{C}^{\rm NS}_{A,q}, \tag{4.4.24}$$

$$\hat{\mathcal{F}}^{\rm S}_{k,q} = \Gamma^{\rm S}_{qq} \otimes \mathbb{C}^{\rm S}_{k,q} + n_f\,\Gamma_{qg} \otimes \mathbb{C}_{k,g}, \tag{4.4.25}$$

$$\hat{\mathcal{F}}_{k,g} = 2\Gamma_{gq} \otimes \mathbb{C}^{\rm S}_{k,q} + \Gamma_{gg} \otimes \mathbb{C}_{k,g}, \tag{4.4.26}$$

with $\Gamma_{gq} = \Gamma_{g\bar{q}}$, $\Gamma_{qg} = \Gamma_{\bar{q}g}$. The quantities $\Gamma_{A,qq}$, Γ_{ij} are called transition functions in which all C-divergences are absorbed so that the fragmentation coefficient function $\mathbb{C}_{k,p}$ are finite. Both functions are expanded in the renormalized coupling constant $\alpha_s(R^2)$ and depend explicitly on the renormalization scale R and the factorization scale M which implies that they are scheme dependent. If we expand $\Gamma_{A,qq}$, Γ_{ij} in the unrenormalized coupling constant $\hat{\alpha}_s$ the expressions become very simple. Choosing the $\overline{\rm MS}$-scheme they take the following form

$$\overline{\Gamma}^{\rm NS}_{qq} = \mathbb{1} + \frac{\hat{\alpha}_s}{4\pi}\,S_\varepsilon\left(\frac{M^2}{\mu^2}\right)^{\varepsilon/2}\left[\frac{1}{\varepsilon}P^{(0)}_{qq}\right] + \left(\frac{\hat{\alpha}_s}{4\pi}\right)^2 S^2_\varepsilon\left(\frac{M^2}{\mu^2}\right)^{\varepsilon}\left[\frac{1}{\varepsilon^2}\left\{\frac{1}{2}P^{(0)}_{qq}\otimes P^{(0)}_{qq} - \beta_0 P^{(0)}_{qq}\right\} + \frac{1}{\varepsilon}\left\{\frac{1}{2}P^{\rm NS,(1)}_{qq} + \frac{1}{2}P^{\rm NS,(1)}_{q\bar{q}}\right\}\right], \tag{4.4.27}$$

$$\overline{\Gamma}^{\rm NS}_{A,qq} = \mathbb{1} + \frac{\hat{\alpha}_s}{4\pi}\,S_\varepsilon\left(\frac{M^2}{\mu^2}\right)^{\varepsilon/2}\left[\frac{1}{\varepsilon}P^{(0)}_{qq}\right] + \left(\frac{\hat{\alpha}_s}{4\pi}\right)^2 S^2_\varepsilon\left(\frac{M^2}{\mu^2}\right)^{\varepsilon}\left[\frac{1}{\varepsilon^2}\left\{\frac{1}{2}P^{(0)}_{qq}\otimes P^{(0)}_{qq} - \beta_0 P^{(0)}_{qq}\right\} + \frac{1}{\varepsilon}\left\{\frac{1}{2}P^{\rm NS,(1)}_{qq} - \frac{1}{2}P^{\rm NS,(1)}_{q\bar{q}}\right\}\right], \tag{4.4.28}$$

$$\overline{\Gamma}^{\rm S}_{qq} = \overline{\Gamma}^{\rm NS}_{qq} + 2n_f\,\overline{\Gamma}^{\rm PS}_{qq}, \tag{4.4.29}$$

$$\overline{\Gamma}^{\rm PS}_{qq} = \left(\frac{\hat{\alpha}_s}{4\pi}\right)^2 S^2_\varepsilon\left(\frac{M^2}{\mu^2}\right)^{\varepsilon}\left[\frac{1}{\varepsilon^2}\left\{\frac{1}{4}P^{(0)}_{gq}\otimes P^{(0)}_{qg}\right\} + \frac{1}{\varepsilon}\left\{\frac{1}{4}P^{\rm PS,(1)}_{qq}\right\}\right], \tag{4.4.30}$$

$$\overline{\Gamma}_{gq} = \frac{\hat{\alpha}_s}{4\pi} S_\varepsilon \left(\frac{M^2}{\mu^2}\right)^{\varepsilon/2} \left[\frac{1}{\varepsilon} P_{gq}^{(0)}\right] + \left(\frac{\hat{\alpha}_s}{4\pi}\right)^2 S_\varepsilon^2 \left(\frac{M^2}{\mu^2}\right)^{\varepsilon} \left[\frac{1}{\varepsilon}\left\{\frac{1}{2} P_{gq}^{(0)} \otimes \right.\right.$$
$$\left.\left. (P_{gg}^{(0)} + P_{qq}^{(0)}) - \beta_0 P_{gq}^{(0)} + \frac{1}{\varepsilon}\left\{\frac{1}{2} P_{gq}^{(1)}\right\}\right], \tag{4.4.31}$$

$$\overline{\Gamma}_{qg} = \frac{\hat{\alpha}_s}{4\pi} S_\varepsilon \left(\frac{M^2}{\mu^2}\right)^{\varepsilon/2} \left[\frac{1}{2\varepsilon} P_{qg}^{(0)}\right], \tag{4.4.32}$$

$$\overline{\Gamma}_{gg} = \mathbb{1} + \frac{\hat{\alpha}_s}{4\pi} S_\varepsilon \left(\frac{M^2}{\mu^2}\right)^{\varepsilon/2} \left[\frac{1}{\varepsilon} P_{gg}^{(0)}\right], \tag{4.4.33}$$

where the $\mathbb{1}$ in (4.4.27), (4.4.28) and (4.4.33) is a shorthand notation for $\delta(1-z)$. Notice that we have expanded the Γ_{ij} above in sufficiently higher order of α_s in order to get the coefficient functions finite. Therefore the computation of $\hat{\mathcal{F}}_{k,p}$ allows us to determine the DGLAP-splitting functions $P_{qq}^{\mathrm{NS},(1)}$, $P_{q\bar{q}}^{\mathrm{NS},(1)}$, $P_{qq}^{\mathrm{PS},(1)}$, and $P_{gq}^{(1)}$ in an alternative way which is different from the method used in [39, 40]. Further the transition functions satisfy the following relations which originate from energy momentum conservation

$$\int_0^1 dz\, z\, (\Gamma_{qq}^{\mathrm{S}}(z) + \Gamma_{gq}(z)) = 1, \tag{4.4.34}$$

$$\int_0^1 dz\, z\, (\Gamma_{gg}(z) + 2n_f\, \Gamma_{qg}(z)) = 1. \tag{4.4.35}$$

If we substitute $\hat{\mathcal{F}}_{k,p}$ (4.4.23) - (4.4.26) into eq. (4.4.3) the C-singularities are absorbed by the bare fragmentation densities $\hat{D}_p^H$ as follows

$$D_{\mathrm{NS},p}^H = \Gamma_{qq}^{\mathrm{NS}} \otimes \hat{D}_{\mathrm{NS},p}^H, \tag{4.4.36}$$

$$D_{A,p}^H = \Gamma_{A,qq}^{\mathrm{NS}} \otimes \hat{D}_{A,p}^H, \tag{4.4.37}$$

$$D_{\mathrm{S}}^H = \Gamma_{qq}^{\mathrm{S}} \otimes \hat{D}_{\mathrm{S}}^H + 2\Gamma_{gq} \otimes \hat{D}_g^H, \tag{4.4.38}$$

$$D_g^H = n_f\, \Gamma_{qg} \otimes \hat{D}_{\mathrm{S}}^H + \Gamma_{gg} \otimes \hat{D}_g^H, \tag{4.4.39}$$

Here $D_{\mathrm{NS},p}^H$ and D_{S}^H denote the non-singlet and singlet combinations of the parton fragmentation densities as defined in (4.2.6), (4.2.7). The same definition holds for the bare densities $\hat{D}_{\mathrm{NS},p}^H$ and $\hat{D}_{\mathrm{S}}^H$. Furthermore $D_{A,p}^H$ and $\hat{D}_{A,p}^H$ stand for the asymmetrical combinations as defined in (4.2.8). The densities $D_{\mathrm{NS},p}^H$, $D_{A,p}^H$, D_{S}^H, and D_g^H depend on the renormalization scale R and the mass factorization scale M which are usually set to be equal.
Substituting eqs. (4.4.23)-(4.4.26), (4.4.36)-(4.4.39) in (4.4.3)-(4.4.4) and using eq.

(4.4.7) we obtain after rearranging terms the structure function $F_k^{(V,V')}(x,Q^2)$ expressed into the renormalized parton fragmentation densities D_p^H and the fragmentation coefficient functions $\mathbb{C}_{k,p}$ $(p = q, g)$.

$$F_k^{(V,V')}(x,Q^2) = \int_x^1 \frac{dz}{z} \left[\sum_{p=1}^{n_f} (v_p^{(V)} v_p^{(V')} + a_p^{(V)} a_p^{(V')}) \left\{ D_{\rm S}^H \left(\frac{x}{z}, M^2\right) \cdot \right.\right.$$

$$\left. \cdot \mathbb{C}_{k,q}^{\rm S}(z, Q^2/M^2) + D_g^H \left(\frac{x}{z}, M^2\right) \mathbb{C}_g(z, Q^2/M^2) \right\}$$

$$\left. + \sum_{p=1}^{n_f} (v_p^{(V)} v_p^{(V')} + a_p^{(V)} a_p^{(V')}) \, D_{{\rm NS},p}^H \left(\frac{x}{z}, M^2\right) \mathbb{C}_{k,q}^{\rm NS}(z, Q^2/M^2) \right], \quad k = T, L, \tag{4.4.40}$$

$$F_A^{(V,V')}(x,Q^2) = \int_x^1 \frac{dz}{z} \sum_{p=1}^{n_f} (v_p^{(V)} a_p^{(V')} + a_p^{(V)} v_p^{(V')}) \, D_{A,p}^H \left(\frac{x}{z}, M^2\right) \cdot$$

$$\cdot \mathbb{C}_{A,q}^{\rm NS}(z, Q^2/M^2), \tag{4.4.41}$$

where we have chosen $R = M$.
Like the parton fragmentation functions $\hat{\mathcal{F}}_{k,p}$ in eqs. (4.4.8)-(4.4.20) we can express the coefficient functions $\mathbb{C}_{k,p}$ $(p = q, g)$ into the renormalization group coefficients. In the $\overline{\rm MS}$-scheme they take the following form. The non-singlet coefficient functions become

$$\overline{\mathbb{C}}_{L,q}^{\rm NS} = \frac{\alpha_s}{4\pi} \left[\bar{c}_{L,q}^{(1)} \right] + \left(\frac{\alpha_s}{4\pi}\right)^2 \left[\left\{ -\beta_0 \bar{c}_{L,q}^{(1)} + \frac{1}{2} P_{qq}^{(0)} \otimes \bar{c}_{L,q}^{(1)} \right\} L_M + \bar{c}_{L,q}^{{\rm NS},(2),{\rm nid}} \right.$$

$$\left. + \bar{c}_{L,q}^{{\rm NS},(2),{\rm id}} \right], \tag{4.4.42}$$

$$\overline{\mathbb{C}}_{T,q}^{\rm NS} = \mathbb{1} + \frac{\alpha_s}{4\pi} \left[\frac{1}{2} P_{qq}^{(0)} L_M + \bar{c}_{T,q}^{(1)} \right] + \left(\frac{\alpha_s}{4\pi}\right)^2 \left[\left\{ \frac{1}{8} P_{qq}^{(0)} \otimes P_{qq}^{(0)} \right.\right.$$

$$\left. - \frac{1}{4} \beta_0 P_{qq}^{(0)} \right\} L_M^2 + \left\{ \frac{1}{2} (P_{qq}^{(1),{\rm NS}} + P_{q\bar{q}}^{(1),{\rm NS}}) - \beta_0 \bar{c}_{T,q}^{(1)} + \frac{1}{2} P_{qq}^{(0)} \otimes \bar{c}_{T,q}^{(1)} \right\} L_M$$

$$\left. + \bar{c}_{T,q}^{{\rm NS},(2),{\rm nid}} + \bar{c}_{T,q}^{{\rm NS},(2),{\rm id}} \right], \tag{4.4.43}$$

$$\overline{\mathbb{C}}_{A,q}^{\rm NS} = \mathbb{1} + \frac{\alpha_s}{4\pi} \left[\frac{1}{2} P_{qq}^{(0)} L_M + \bar{c}_{A,q}^{(1)} \right] + \left(\frac{\alpha_s}{4\pi}\right)^2 \left[\left\{ \frac{1}{8} P_{qq}^{(0)} \otimes P_{qq}^{(0)} \right.\right.$$

$$- \frac{1}{4}\beta_0 P_{qq}^{(0)} \Big\} L_M^2 + \Big\{ \frac{1}{2}(P_{qq}^{(1),\mathrm{NS}} - P_{q\bar{q}}^{(1),\mathrm{NS}}) - \beta_0 \bar{c}_{A,q}^{(1)} + \frac{1}{2} P_{qq}^{(0)} \otimes \bar{c}_{A,q}^{(1)} \Big\} L_M$$

$$+ \bar{c}_{A,q}^{\mathrm{NS},(2),\mathrm{nid}} - \bar{c}_{A,q}^{\mathrm{NS},(2),\mathrm{id}} \Big] . \tag{4.4.44}$$

The singlet coefficient functions are given by

$$\overline{\mathbb{C}}_{k,q}^{\mathrm{S}} = \overline{\mathbb{C}}_{k,q}^{\mathrm{NS}} + \overline{\mathbb{C}}_{k,q}^{\mathrm{PS}}, \quad (k = T, L), \tag{4.4.45}$$

$$\overline{\mathbb{C}}_{L,q}^{\mathrm{PS}} = n_f \left(\frac{\alpha_s}{4\pi}\right)^2 \Big[\Big\{ \frac{1}{4} P_{qg}^{(0)} \otimes \bar{c}_{L,g}^{(1)} \Big\} L_M + \bar{c}_{L,q}^{\mathrm{PS},(2)} \Big] , \tag{4.4.46}$$

$$\overline{\mathbb{C}}_{T,q}^{\mathrm{PS}} = n_f \left(\frac{\alpha_s}{4\pi}\right)^2 \Big[\Big\{ \frac{1}{8} P_{gq}^{(0)} \otimes P_{qg}^{(0)} \Big\} L_M^2 + \Big\{ \frac{1}{2} P_{qq}^{\mathrm{PS},(1)} + \frac{1}{4} P_{qg}^{(0)} \otimes \bar{c}_{T,g}^{(1)} \Big\} L_M$$

$$+ \bar{c}_{T,q}^{\mathrm{PS},(2)} \Big] . \tag{4.4.47}$$

The gluon coefficient functions become

$$\overline{\mathbb{C}}_{L,g} = \frac{\alpha_s}{4\pi} \Big[\bar{c}_{L,g}^{(1)} \Big] + \left(\frac{\alpha_s}{4\pi}\right)^2 \Big[\Big\{ - \beta_0 \bar{c}_{L,g}^{(1)} + \frac{1}{2} P_{gg}^{(0)} \otimes \bar{c}_{L,g}^{(1)}$$

$$+ P_{gq}^{(0)} \otimes \bar{c}_{L,q}^{(1)} \Big\} L_M + \bar{c}_{L,g}^{(2)} \Big] , \tag{4.4.48}$$

$$\overline{\mathbb{C}}_{T,g} = \frac{\alpha_s}{4\pi} \Big[P_{gq}^{(0)} L_M + \bar{c}_{T,g}^{(1)} \Big] + \left(\frac{\alpha_s}{4\pi}\right)^2 \Big[\Big\{ \frac{1}{4} P_{gq}^{(0)} \otimes (P_{gg}^{(0)} + P_{qq}^{(0)})$$

$$- \frac{1}{2}\beta_0 P_{gq}^{(0)} \Big\} L_M^2 + \Big\{ P_{gq}^{(1)} - \beta_0 \bar{c}_{T,g}^{(1)} + \frac{1}{2} P_{gg}^{(0)} \otimes \bar{c}_{T,g}^{(1)} + P_{gq}^{(0)} \otimes \bar{c}_{T,q}^{(1)} \Big\} L_M$$

$$+ \bar{c}_{T,g}^{(2)} \Big] . \tag{4.4.49}$$

Further we have defined

$$\mathbb{1} \equiv \delta(1-z), \quad L_M = \ln \frac{Q^2}{M^2}, \quad \alpha_s \equiv \alpha_s(M^2). \tag{4.4.50}$$

In the case $M \neq R$ the resulting coefficient functions can be very easily derived from the above expressions (4.4.42)-(4.4.49) by replacing

$$\alpha_s(M^2) = \alpha_s(R^2) \left[1 + \frac{\alpha_s(R^2)}{4\pi} \beta_0 \ln \frac{R^2}{M^2} \right] . \tag{4.4.51}$$

The explicit expressions for the coefficient functions (4.4.42)-(4.4.49) are listed in appendix A.

Besides the $\overline{\rm MS}$-scheme one also can compute the coefficient functions in the so-called annihilation scheme (A-scheme) [19]. It is defined in such a way that F^H/R_{ee} (see (4.2.20), (4.2.22)) does not get any α_s corrections at $M^2 = R^2 = Q^2$. In the A-scheme the transition functions Γ_{ij} are related to the ones in the $\overline{\rm MS}$-scheme denoted by $\overline{\Gamma}_{ij}$ (see (4.4.27)-(4.4.33)) as follows

$$\Gamma_{qq}^{\rm NS} = Z_{qq}^{\rm NS}\,\overline{\Gamma}_{qq}^{\rm NS}, \quad \Gamma_{A,qq}^{\rm NS} = Z_{qq}^{\rm NS}\,\overline{\Gamma}_{A,qq}^{\rm NS}, \quad \Gamma_{ij} = Z_{ik}\,\overline{\Gamma}_{kj}, \tag{4.4.52}$$

where $Z_{qq}^{\rm NS}$, Z_{ik} are given by (see eqs. (2.61), (2.62) in [19])

$$Z_{qq}^{\rm NS} = R_{ee}^{-1}\,\overline{\mathbb{C}}_q^{\rm NS}, \tag{4.4.53}$$

$$Z = \begin{pmatrix} R_{ee}^{-1}\,\overline{\mathbb{C}}_q^{\rm S} & R_{ee}^{-1}\,\overline{\mathbb{C}}_g \\ 0 & 1 \end{pmatrix}. \tag{4.4.54}$$

The coefficient functions $\overline{\mathbb{C}}_\ell^{(r)}$ $(r = {\rm NS, S},\ \ell = q, g)$ correspond to the structure function F^H defined in (4.2.22) and they are given by

$$\overline{\mathbb{C}}_\ell^{(r)} = \overline{\mathbb{C}}_{T,\ell}^{(r)} + \overline{\mathbb{C}}_{L,\ell}^{(r)}. \tag{4.4.55}$$

The coefficient functions in the A-scheme, denoted by $\mathbb{C}_{k,p}$, are related to the ones presented in the $\overline{\rm MS}$-scheme in the following way $(k = T, L)$

$$\mathbb{C}_{k,q}^{\rm NS} = \left(Z_{qq}^{\rm NS}\right)^{-1}\,\overline{\mathbb{C}}_{k,q}^{\rm NS}, \tag{4.4.56}$$

$$\mathbb{C}_{A,q}^{\rm NS} = \left(Z_{qq}^{\rm NS}\right)^{-1}\,\overline{\mathbb{C}}_{A,q}^{\rm NS}, \tag{4.4.57}$$

$$\mathbb{C}_{k,i} = \left(Z^{-1}\right)_{ji}\,\overline{\mathbb{C}}_{k,j}, \tag{4.4.58}$$

Expanding all coefficient functions and R_{ee} in α_s the former take the following form in the A-scheme

$$\begin{aligned}\mathbb{C}_{L,q}^{\rm NS} = {} & \frac{\alpha_s}{4\pi}\left[\bar{c}_{L,q}^{(1)}\right] + \left(\frac{\alpha_s}{4\pi}\right)^2\left[\left\{-\beta_0\bar{c}_{L,q}^{(1)} + \frac{1}{2}P_{qq}^{(0)}\otimes\bar{c}_{L,q}^{(1)}\right\}L_M + \bar{c}_{L,q}^{(2),{\rm NS,nid}}\right. \\ & \left. + \bar{c}_{L,q}^{(2),{\rm NS,id}} + R^{(1)}\bar{c}_{L,q}^{(1)} - \bar{c}_q^{(1)}\otimes\bar{c}_{L,q}^{(1)}\right],\end{aligned} \tag{4.4.59}$$

$$\begin{aligned}\mathbb{C}_{T,q}^{\rm NS} = {} & \mathbb{1} + \frac{\alpha_s}{4\pi}\left[\frac{1}{2}P_{qq}^{(0)}L_M + R^{(1)}\mathbb{1} - \bar{c}_{L,q}^{(1)}\right] + \left(\frac{\alpha_s}{4\pi}\right)^2\left[\left\{\frac{1}{8}P_{qq}^{(0)}\otimes P_{qq}^{(0)}\right.\right. \\ & \left. - \frac{1}{4}\beta_0 P_{qq}^{(0)}\right\}L_M^2 + \left\{\frac{1}{2}(P_{qq}^{{\rm NS},(1)} + P_{q\bar{q}}^{{\rm NS},(1)}) - \beta_0\bar{c}_{T,q}^{(1)} + \frac{1}{2}R^{(1)}P_{qq}^{(0)}\right. \\ & \left.\left. - \frac{1}{2}P_{qq}^{(0)}\otimes\bar{c}_{L,q}^{(1)}\right\}L_M + R^{(2)}\mathbb{1} - \bar{c}_{L,q}^{{\rm NS},(2),{\rm nid}} - \bar{c}_{L,q}^{{\rm NS},(2),{\rm id}} - R^{(1)}\bar{c}_{L,q}^{(1)}\right.\end{aligned}$$

$$+ \bar{c}_q^{(1)} \otimes \bar{c}_{L,q}^{(1)} \Big] , \tag{4.4.60}$$

$$\mathbb{C}_{A,q}^{\rm NS} = \mathbb{1} + \frac{\alpha_s}{4\pi} \Big[\frac{1}{2} P_{qq}^{(0)} L_M + R^{(1)} . \mathbb{1} + \bar{c}_{A,q}^{(1)} - \bar{c}_q^{(1)} \Big] + \Big(\frac{\alpha_s}{4\pi}\Big)^2 \Big[\Big\{ \frac{1}{8} P_{qq}^{(0)} \otimes P_{qq}^{(0)} - \frac{1}{4} \beta_0 P_{qq}^{(0)} \Big\} L_M^2 + \Big\{ \frac{1}{2} (P_{qq}^{\rm NS,(1)} - P_{q\bar{q}}^{\rm NS,(1)}) - \beta_0 \bar{c}_{A,q}^{(1)} + \frac{1}{2} P_{qq}^{(0)} \otimes (R^{(1)} . \mathbb{1} - \bar{c}_q^{(1)} + \bar{c}_{A,q}^{(1)}) \Big\} L_M + R^{(2)} . \mathbb{1} + \bar{c}_{A,q}^{\rm NS,(2),nid} - \bar{c}_{A,q}^{\rm NS,(2),id} - \bar{c}_q^{(2)} + (\bar{c}_q^{(1)} - R^{(1)} . \mathbb{1}) \otimes (\bar{c}_q^{(1)} - \bar{c}_{A,q}^{(1)}) \Big] , \tag{4.4.61}$$

$$\mathbb{C}_{L,q}^{\rm PS} = n_f \Big(\frac{\alpha_s}{4\pi}\Big)^2 \Big[\Big\{ \frac{1}{4} P_{qg}^{(1)} \otimes \bar{c}_{L,g}^{(1)} \Big\} L_M + \bar{c}_{L,q}^{\rm PS,(2)} \Big] = \overline{\mathbb{C}}_{L,q}^{\rm PS}, \tag{4.4.62}$$

$$\mathbb{C}_{T,q}^{\rm PS} = n_f \Big(\frac{\alpha_s}{4\pi}\Big)^2 \Big[\Big\{ \frac{1}{8} P_{qg}^{(0)} \otimes P_{gq}^{(0)} \Big\} L_M^2 + \Big\{ \frac{1}{2} P_{qq}^{\rm PS,(1)} + \frac{1}{4} P_{qg}^{(0)} \otimes \bar{c}_{T,g}^{(1)} \Big\} L_M - \bar{c}_{L,q}^{\rm PS,(2)} \Big] , \tag{4.4.63}$$

$$\mathbb{C}_{L,g} = \frac{\alpha_s}{4\pi} \Big[\bar{c}_{L,g}^{(1)} \Big] + \Big(\frac{\alpha_s}{4\pi}\Big)^2 \Big[\Big\{ - \beta_0 \bar{c}_{L,g}^{(1)} + \frac{1}{2} P_{gg}^{(0)} \otimes \bar{c}_{L,g}^{(1)} + P_{gq}^{(0)} \otimes \bar{c}_{L,q}^{(1)} \Big\} L_M + \bar{c}_{L,g}^{(2)} - \bar{c}_g^{(1)} \otimes \bar{c}_{L,q}^{(1)} \Big] , \tag{4.4.64}$$

$$\mathbb{C}_{T,g} = \frac{\alpha_s}{4\pi} \Big[P_{gq}^{(0)} L_M - \bar{c}_{L,g}^{(1)} \Big] + \Big(\frac{\alpha_s}{4\pi}\Big)^2 \Big[\Big\{ \frac{1}{4} P_{gq}^{(0)} \otimes (P_{gg}^{(0)} + P_{qq}^{(0)}) - \frac{1}{2} \beta_0 P_{gq}^{(0)} \Big\} L_M^2 + \Big\{ P_{gq}^{(1)} - \beta_0 \bar{c}_{T,g}^{(1)} + \frac{1}{2} P_{gg}^{(0)} \otimes \bar{c}_{T,g}^{(1)} + P_{gq}^{(0)} \otimes \bar{c}_{T,q}^{(1)} - \frac{1}{2} P_{qq}^{(0)} \otimes \bar{c}_g^{(1)} \Big\} L_M - \bar{c}_{L,g}^{(2)} + \bar{c}_g^{(1)} \otimes \bar{c}_{L,q}^{(1)} \Big] , \tag{4.4.65}$$

where $\mathbb{1}$ is given by (4.4.50) and the coefficients $R^{(i)}$ show up in the perturbation series for R_{ee} (4.2.20):

$$R_{ee} = 1 + \frac{\alpha_s}{4\pi} R^{(1)} + \Big(\frac{\alpha_s}{4\pi}\Big)^2 R^{(2)} + \cdots . \tag{4.4.66}$$

Notice that we have expressed the above coefficient functions into the renormalization group coefficients $P_{ij}^{(1)}$, $\bar{c}_{k,p}^{(i)}$ presented in the $\overline{\rm MS}$-scheme. From (4.4.59)-(4.4.65)

we infer that at $Q^2 = M^2$ ($L_M = 0$) the coefficient functions in (4.4.55) become

$$\mathbb{C}_q^{\rm NS} = \mathbb{1}.R_{ee}, \quad \mathbb{C}_q^{\rm PS} = 0, \quad \mathbb{C}_g = 0. \tag{4.4.67}$$

In any scheme the coefficient functions satisfy the renormalization group equations

$$\left[\left\{ M\frac{\partial}{\partial M} + \beta(\alpha_s)\frac{\partial}{\partial \alpha_s} \right\} \delta_{ij} - \gamma_{ij}^{(m)} \right] \tilde{\mathbb{C}}_{k,i}^{(m)} = 0, \tag{4.4.68}$$

with $k = T, A, L$ and $i, j = q, g$. Further we have defined the Mellin transforms

$$\mathbb{C}_{k,i}^{(m)}(Q^2/M^2) = \int_0^1 dz\, z^{m-1}\, \mathbb{C}_{k,i}(z, Q^2/M^2), \tag{4.4.69}$$

$$\gamma_{ij}^{(m)} = -\int_0^1 dz\, z^{m-1}\, P_{ij}(z), \tag{4.4.70}$$

and introduced the following the notations

$$\tilde{\mathbb{C}}_{k,q}^{(m)} = \mathbb{C}_{k,q}^{(m)}, \quad \tilde{\mathbb{C}}_{k,g}^{(m)} = \frac{1}{2}\mathbb{C}_{k,g}^{(m)}. \tag{4.4.71}$$

The quantities $\gamma_{ij}^{(m)}$ are the anomalous dimensions corresponding with the timelike cut vertex operators of spin m. Like the timelike splitting functions P_{ij} they are scheme dependent. The relations between the anomalous dimensions obtained from different schemes can e.g. be found in eqs. (3.82)-(3.86) in [42].

4.5 Results for the longitudinal and transverse fragmentation functions

In this section we will discuss the order α_s^2 contributions to the longitudinal and transverse cross sections and their corresponding fragmentation functions. In particular we investigate how the leading order (LO) longitudinal quantities, which already exist in the literature [19], [24], [25], are modified by including the order α_s^2 contributions. We will do the same for the transverse quantities for which a next-to-leading order (NLO) result already exists. Further we study the dependence of the above quantities on the mass factorization scale M and the renormalization scale R and show that the sensitivity to these scales becomes less when higher order corrections are included. Before we proceed we want to emphasize that with all higher order QCD corrections at hand it is only possible to perform a full NLO analysis on the cross sections and the fragmentation functions. The order α_s^2 contributions also allow for a next-to-next-to-leading order (NNLO) analysis of the transverse cross section $\sigma_T(Q^2)$ but not for the transverse fragmentation function $F_T(x, Q^2)$. For the latter one also needs the three-loop timelike splitting functions which have not been calculated yet. Therefore the order α_s^2 contributions to $F_T(x, Q^2)$ have to be considered as an estimate of the NNLO result. Nevertheless we will use the notation F_T^{NNLO} to indicate the order α_s^2 corrected transverse structure function.

The longitudinal and transverse cross section $\sigma_k(Q^2)$ $(k = T,\ L)$ defined in (4.2.18) are obtained from the coefficient functions calculated in the previous sections as follows

$$\sigma_k(Q^2) = \sigma_{\rm tot}^{(0)}(Q^2) \int_0^1 dz\, z \left[\mathbb{C}_{k,q}^{\rm S}(z, Q^2/M^2) + \frac{1}{2}\mathbb{C}_{k,g}(z, Q^2/M^2) \right]. \tag{4.5.1}$$

The results are

$$\sigma_L(Q^2) = \sigma_{\rm tot}^{(0)}(Q^2) \left[\frac{\alpha_s(R^2)}{4\pi} C_F[3] + \left(\frac{\alpha_s(R^2)}{4\pi}\right)^2 \left[C_F^2 \left\{ -\frac{15}{2} \right\} + C_A C_F \left\{ \right.\right.\right.$$

$$\left.\left.\left. -11 \ln \frac{Q^2}{R^2} - \frac{24}{5}\zeta(3) + \frac{2023}{30} \right\} + n_f C_F T_f \left\{ 4 \ln \frac{Q^2}{R^2} - \frac{74}{3} \right\} \right] \right], \tag{4.5.2}$$

$$\sigma_T(Q^2) = \sigma_{\rm tot}^{(0)}(Q^2) \left[1 + \left(\frac{\alpha_s(R^2)}{4\pi}\right)^2 \left[C_F^2\{6\} + C_A C_F \left\{ -\frac{196}{5}\zeta(3) - \frac{178}{30} \right\} \right.\right.$$

$$\left.\left. + n_f C_F T_f \left\{ 16\zeta(3) + \frac{8}{3} \right\} \right] \right]. \tag{4.5.3}$$

Addition of σ_L and σ_T yields the well-known answer $\sigma_{\rm tot}(Q^2)$ (see (4.2.19) and (4.2.20)) which is in agreement with the literature [21] (see also [6]). Hence (4.5.2) and (4.5.3) provides us with a check on our calculation of the longitudinal and transverse coefficient functions. Notice that in lowest order $\sigma_{\rm tot}(Q^2)$ only receives a contribution from the transverse cross section (4.5.3) whereas the order α_s contribution can be only attributed to the longitudinal part in (4.5.2). In order α_s^2 both σ_L and σ_T contribute to $\sigma_{\rm tot}$.
Because of the high sensitivity of expression (4.5.2) to the value of α_s, the longitudinal cross section provides us with an excellent tool to measure the running coupling constant.

To illustrate the dependence of the cross sections on the running coupling constant we have plotted the ratios

$$R_L(Q^2) = \frac{\sigma_L(Q^2)}{\sigma_{\rm tot}(Q^2)} = \frac{\alpha_s(R^2)}{4\pi} C_F[3] + \left(\frac{\alpha_s(R^2)}{4\pi}\right) \left[C_F^2 \left\{ -\frac{33}{2} \right\} + C_A C_F \left\{ \right.\right.$$

$$\left.\left. -11 \ln \frac{Q^2}{R^2} - 44\zeta(3) + \frac{123}{2} \right\} + n_f C_F T_f \left\{ 4 \ln \frac{Q^2}{R^2} - \frac{74}{3} \right\} \right], \tag{4.5.4}$$

and

$$R_T(Q^2) = \frac{\sigma_T(Q^2)}{\sigma_{\rm tot}(Q^2)} = 1 - \frac{\sigma_L(Q^2)}{\sigma_{\rm tot}(Q^2)}, \tag{4.5.5}$$

as a function of Q (CM-energy of the e^+e^- system) in fig. 4.11 and fig. 4.12 respectively. In fig. 4.11 we have shown R_L corrected up to order α_s (R_L^{LO}) and R_L corrected up to order α_s^2 (R_L^{NLO}). For R_L^{LO} we have used as input the leading

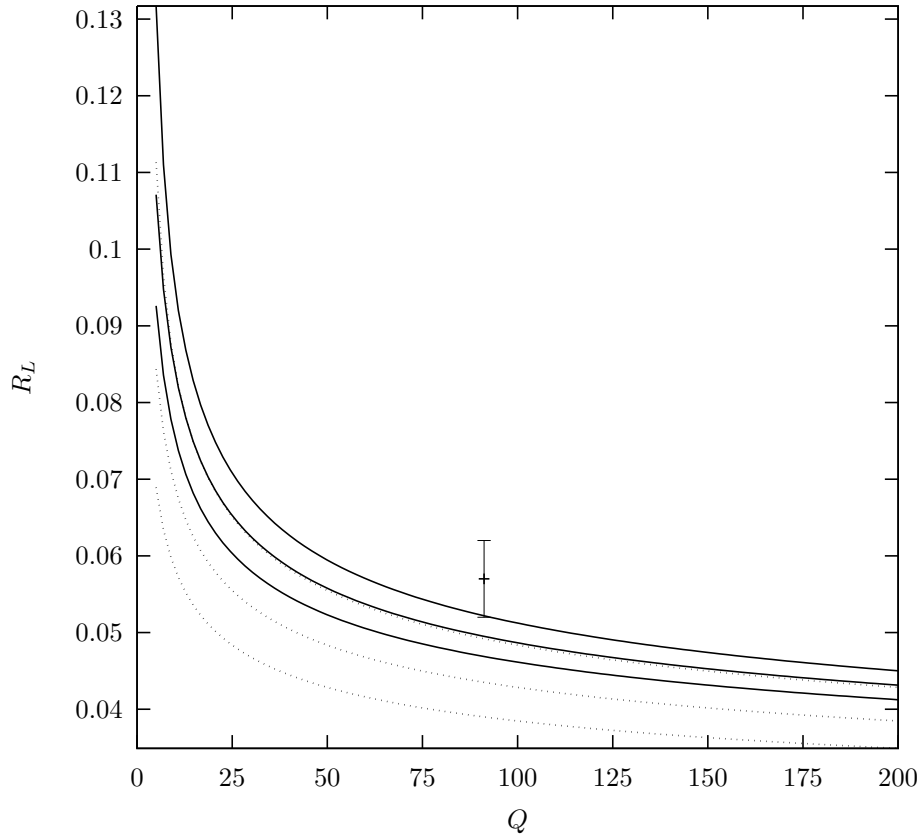

Figure 4.11: *The ratio* $R_L = \sigma_L/\sigma_{\rm tot}$. *Dotted lines:* R_L^{LO}; *solid lines:* R_L^{NLO}. *Lower curve:* $R = 2Q$; *middle curve:* $R = Q$; *upper curve:* $R = Q/2$. *The data point at* $Q = M_Z$ *is from OPAL [18].*

log running coupling constant $\alpha_s^{LL}(n_f, \Lambda_{LO}^{(n_f)}, R^2)$ with $n_f = 5$ and $\Lambda_{LO}^{(5)} = 108$ MeV ($\alpha_s^{LL}(M_Z) = 0.122$). The input parameters of R_L^{NLO} are given by the next-to-leading log running coupling constant $\alpha_s^{NLL}(n_f, \Lambda_{\overline{\rm MS}}^{(nf)}, R^2)$ with $n_f = 5$ and $\Lambda_{\overline{\rm MS}}^{(5)} = 227$ MeV ($\alpha_s^{NLL}(M_Z) = 0.118$). Further we have shown the variation of R_L on the renormalization scale R by choosing the values $R = Q/2,\ Q,\ 2Q$. Fig. 4.11 reveals that the order α_s^2 corrections are appreciable and they vary from 48% ($Q = 10$ GeV) down to 28% ($Q = 200$ GeV) with respect to the LO result. Furthermore one observes an improvement of the renormalization scale dependence while going from R_L^{LO} to R_L^{NLO}. In fig. 4.12 we have plotted R_T (4.5.5) up to first order (R_T^{NLO}) and up to second order (R_T^{NNLO}) in the running coupling constant. As input we have used for R_T^{NLO} and R_T^{NNLO} the coupling constants α_s^{LL} and α_s^{NLL} respectively. The features of fig. 4.12 are the same as those observed in fig. 4.11. In particular R_T^{NNLO} becomes less dependent on the renormalization scale as is shown for R^{NLO}. In figs. 4.11, 4.12 we have also presented the values R_L and R_T at $Q = M_Z$ measured by the OPAL-experiment [18] which are given by

$$R_L = 0.057 \pm 0.005, \tag{4.5.6}$$

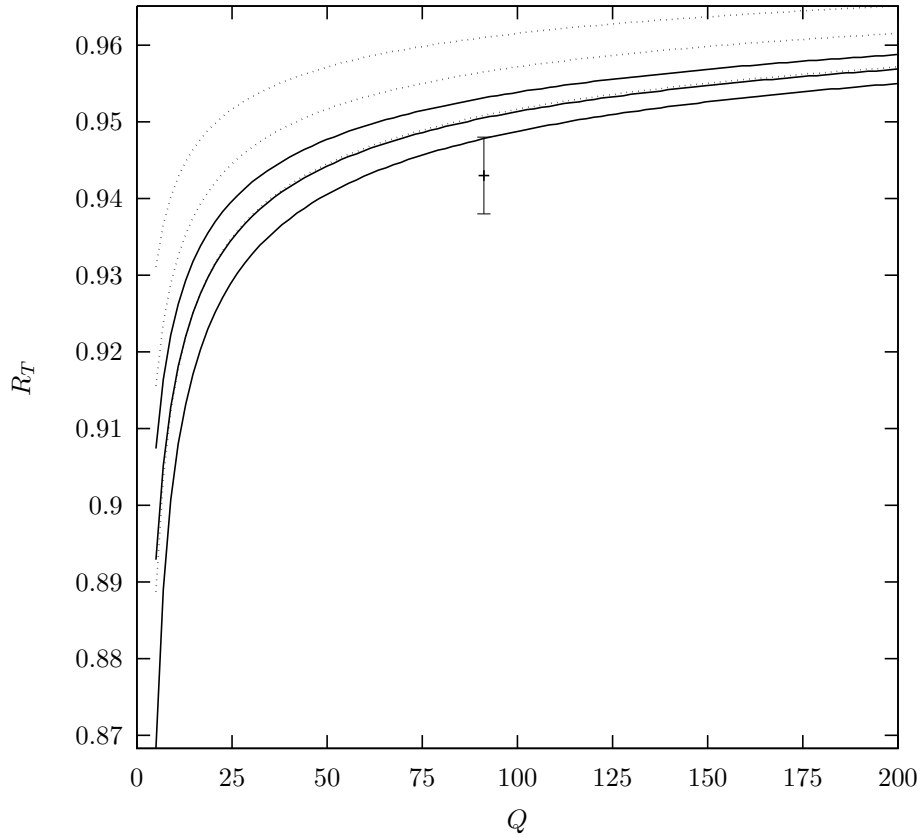

Figure 4.12: *The ratio $R_T = \sigma_T/\sigma_{\rm tot}$. Dotted lines: R_T^{NLO}; solid lines: R_T^{NNLO}. Lower curve: $R = Q/2$; middle curve: $R = Q$; upper curve: $R = 2Q$. The data point at $Q = M_Z$ is from OPAL [18].*

$$R_T = 0.943 \pm 0.005. \tag{4.5.7}$$

One observes a considerable improvement in the ratios R_k ($k = T,\ L$) when the order α_s^2 contributions are included. However there is still a little discrepancy between R_L^{NLO} and R_T^{NNLO}, taken at $R = Q = M_Z$, and the data. This can either be removed by choosing a larger $\Lambda_{\overline{\rm MS}}$ or by including the masses of the heavy quarks c and b in the calculation of the coefficient functions. Also a contribution of higher twist effects may not be negligible (see [19, 22]).
We now want to investigate the effect of the order α_s^2 contributions to the longitudinal and transverse fragmentation functions $F_L(x, Q^2)$ and $F_T(x, Q^2)$ as defined in (4.2.21).
For our analysis we have chosen the fragmentation density sets in [43], [44] which will be called BKK1 and BKK2 respectively. Notice that the range of validity of the fragmentation densities $D_p^H(z, M^2)$ in the BKK1-set is given by $0.1 < z < 0.9$ whereas those belonging to the BKK2-set are only reliable for $0.1 < z < 0.8$. Therefore the results obtained below for z-values outside these regions have to be interpreted with caution. The input parameters for α_s and the QCD scale Λ are the same as given

below (4.5.5) except for BKK1 [43] where one has chosen $\Lambda^{(5)}_{LO} = \Lambda^{(5)}_{\overline{\rm MS}} = 190$ MeV. The definitions for F_L^{LO} and F_L^{NLO} are the same as those given above for R_L^{LO} and R_L^{NLO} respectively. However for both F_T^{NLO} (order α_s corrected) and F_T^{NNLO} (order α_s^2 corrected) we use $\alpha_s^{NLL}(5, \Lambda^{(5)}_{\overline{\rm MS}}, R^2)$. In [43, 44] the fragmentation densities $D_p^H(z, M^2)$ have been determined for $H = \pi^+ + \pi^-$, $K^+ + K^-$ by fitting the total fragmentation function $F(x, Q^2) = \sum_H F^H(x, Q^2)$ (4.2.22) with $H = \pi^\pm$, $K^\pm$, P, $\bar{P}$ to the e^+e^- data in the range $5.2 < Q < 91.2$ GeV. Here the proton and anti-proton contributions to the fragmentation functions have been estimated like

$$F_k^{P+\bar{P}}(x, Q^2) = f(x)\, F_k^{\pi^+ + \pi^-}(x, Q^2), \tag{4.5.8}$$

with

$$f(x) = 0.16, \quad \text{in [43]}, \tag{4.5.9}$$

$$f(x) = 0.195 - 1.35\,(x - 0.35)^2, \quad \text{in [44]}. \tag{4.5.10}$$

Further we introduce the notation

$$F_k(x, Q^2) = \sum_H F_k^H(x, Q^2), \tag{4.5.11}$$

where we sum over $H = \pi^+,\ \pi^-,\ K^+,\ K^-,\ P,\ \bar{P}$.
Notice that $f(x)$ in (4.5.10) becomes negative when $x > 0.73$ so that $F_k^{P+\bar{P}}(x, Q^2)$ ceases to be valid above this x-value. In [43] (BKK1) the fit has been only made to the TPC/2γ-data [12] ($Q = 29$ GeV) whereas in [44] (BKK2) one also included the data coming from the ALEPH [16] and OPAL [17] collaboration. Since the range of Q-values covered by the BKK2 parametrization is larger than the one given by BKK1 the scale evolution of the fragmentation densities turns out to be better when the BKK2-set [44] is chosen. However this improvement goes at the expense of the description of the longitudinal fragmentation function $F_L(x, Q^2)$ as we will show below. For each set there exists a leading log and a next-to-leading log parametrization of $D_p^H(z, M^2)$ ($p = q, g$). The latter is presented in the $\overline{\rm MS}$-scheme so that we have to choose the corresponding coefficient functions in appendix A. Further we set the factorization scale M equal to the renormalization scale R.

In fig. 4.13 we have plotted $F_L(x, Q^2)$ in LO and NLO at $M = Q = M_Z$ and compared the results with the ALEPH [16] and OPAL [18] data. Here we have chosen the BKK1-set because the BKK2-set leads to a much worse result. The latter already happens in LO as was noticed in [44] where one had to choose a very small factorization scale. We observe that F_L^{LO} is below the data in particular in the small x-region. The agreement with the data becomes better when the order α_s corrections are included although at very small x F_L^{NLO} is still smaller than the values given by experiment. In the case of the BKK2-set (not shown in the figure) one gets a result which is far below the data. This was already noticed in fig. 5 of [44] where one had to choose a very small factorization scale M ($M = 20$ GeV) to bring F_L^{LO} in agreement with experiment. In NLO the discrepancy between F_L^{NLO}, in the case of BKK2, and the data becomes even larger which is due to the kaon contribution.

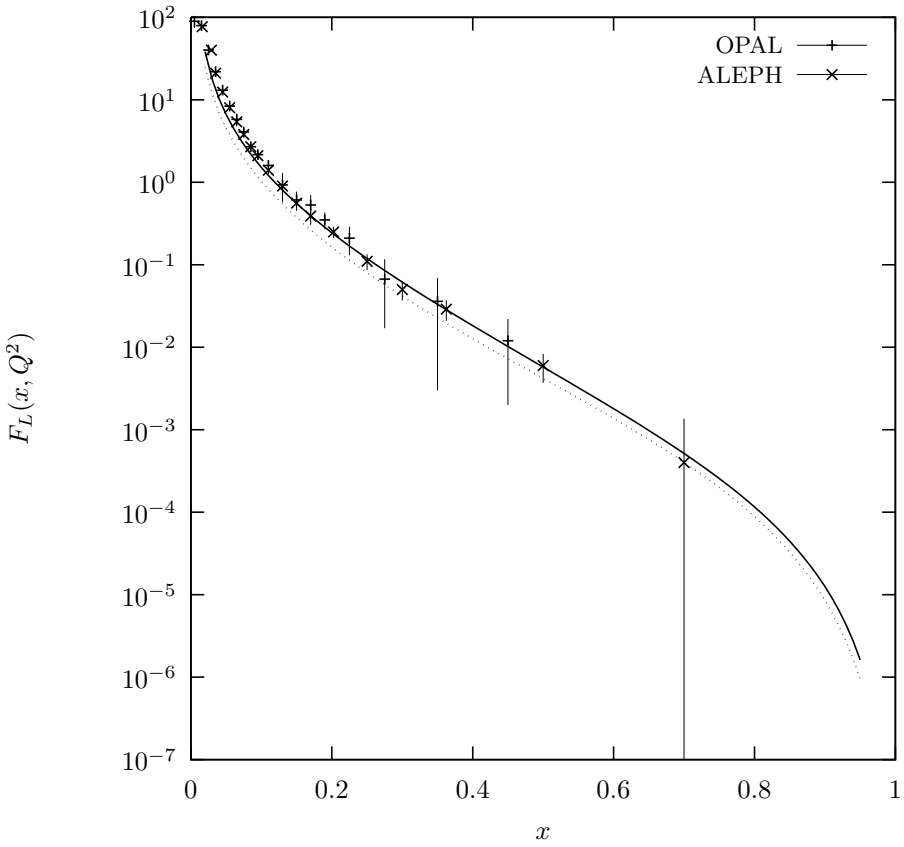

Figure 4.13: *The longitudinal fragmentation function $F_L(x,Q^2)$ at $M = Q = M_Z$. Dotted line: F_L^{LO}; solid line: F_L^{NLO}. The data are from ALEPH [16] and OPAL [18]. The fragmentation density set is BKK1 [43].*

It turns out that the convolution of $D_p^{K^++K^-}(z,M^2)$ with the order α_s^2 contribution from the coefficient functions given in (4.2.4), leads to a negative $F_L^{K^++K^-}$. This example illustrates the importance of the measurement of $F_L(x,Q^2)$ and the higher order corrections for the determination of the fragmentation densities. We have also shown the results for F_T^{NLO} and F_T^{NNLO} at $M = Q = M_Z$ in fig. 4.14 using the BKK1-set. Both fragmentation functions agree with the data except that F_T^{NNLO} gets a little bit worse at very small x. Furthermore F_T^{NLO} and F_T^{NNLO} hardly differ from each other which means that the order α_s^2 corrections are small. We do not expect that this will change when the three-loop splitting functions are included. One also notices that F_L constitutes the smallest part of the total fragmentation function $F = F_T + F_L$ which can be inferred from figs. 4.13, 4.14. This in particular holds at large x where $F_T >> F_L$. Hence a fit of the fragmentation densities to the data of F_T is not sufficient to give a precise prediction for F_L and one has to include the data of the latter to provide us with better fragmentation densities. This in particular holds for $D_g^H(z,M^2)$ in the small z-region. The order α_s^2 contribution to F_L will certainly change the parametrization of the gluon fragmentation density

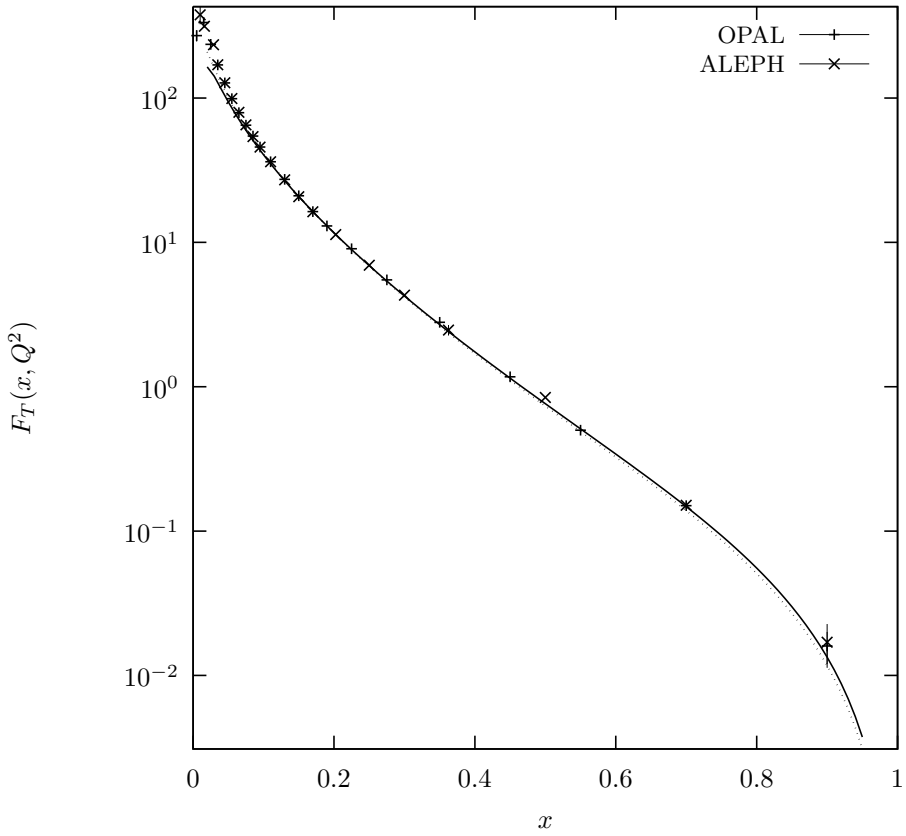

Figure 4.14: *The transverse fragmentation function* $F_T(x,Q^2)$ *at* $M = Q = M_Z$. *Dotted line:* F_T^{NLO}*; solid line:* F_T^{NNLO}. *The data are from ALEPH [16] and OPAL [18]. The fragmentation density set is BKK1 [43].*

given by ALEPH in [16] and OPAL in [18].
To illustrate the effect of the order α_s^2 contributions to the coefficient functions calculated in this chapter at various e^+e^- collider energies we have studied the K-factors

$$K_L^H = \frac{F_L^{H,NLO}(x,Q^2)}{F_L^{H,LO}(x,Q^2)}, \tag{4.5.12}$$

$$K_T^H = \frac{F_T^{H,NNLO}(x,Q^2)}{F_T^{H,NLO}(x,Q^2)}. \tag{4.5.13}$$

In fig. 4.15 we have plotted (4.5.12) for $H = \pi^+ + \pi^-$ at $Q = 5.2$, 10, 29, 35, 55, 91.2 GeV choosing the BKK2-set since the latter shows a better scale evolution. From fig. 4.15 one infers that the corrections are large at small x where they vary between 2 ($Q = 5.2$ GeV) and 1.4 ($Q = 91.1$ GeV). The corrections become smaller when x increases. A similar plot is made for $K_T^{\pi^+ + \pi^-}$ in fig. 4.16. Here the order α_s^2 corrections are much smaller than in the longitudinal case except at large x where

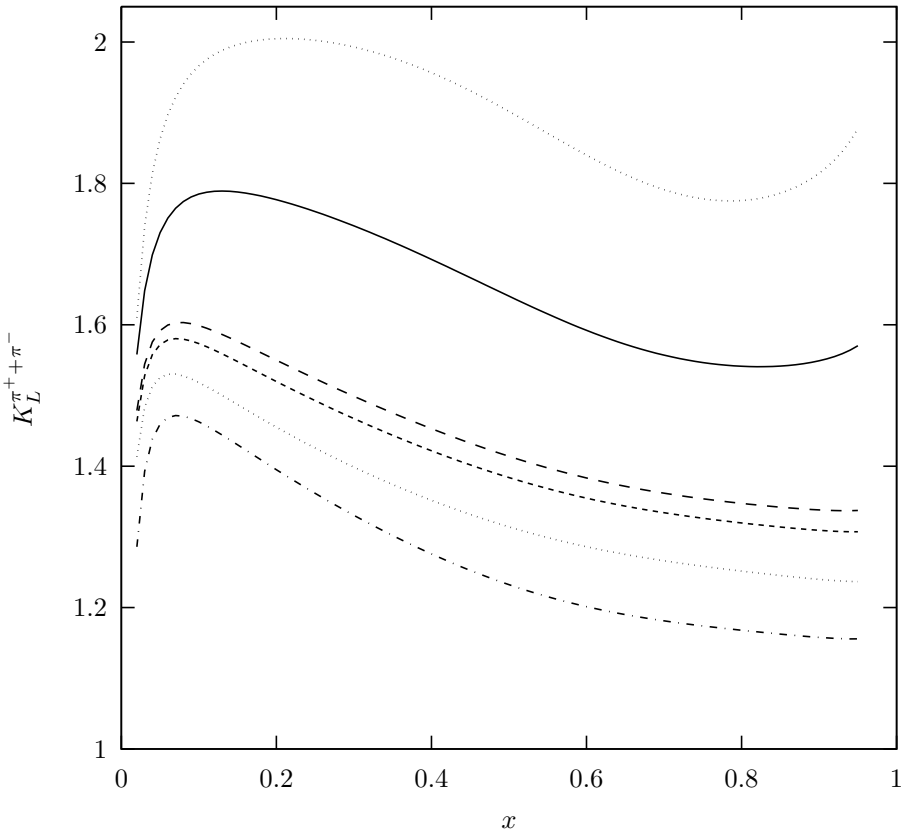

Figure 4.15: *The ratio $K_L^H = F_L^{H,NLO}/F_L^{H,LO}$ with $H = \pi^+ + \pi^-$ at $M = Q$ for different values of Q. Upper dotted line: $Q = 5.2$ GeV; solid line $Q = 10$ GeV; long dashed line: $Q = 29$ GeV; short dashed line: $Q = 35$ GeV; lower dotted line: $Q = 55$ GeV; dashed-dotted line: $Q = 91.2$ GeV. The fragmentation density set is BKK2 [44].*

they are of the same size. Furthermore at low x the order α_s^2 corrections become negative ($K_T^{\pi^+ + \pi^-} < 1$) which is already revealed by fig. 4.14 for $Q = M_Z$. Again the largest correction occurs at smallest Q. This can be mainly attributed to the running coupling constant which becomes large when Q gets small. Notice that the large corrections at small x have to be interpreted with care because of the uncertainties in the fragmentation densities $D_p^H(z, M^2)$ outside the region $0.1 < z < 0.8$.

In fig. 4.17 we investigate the dependence of K_T (4.5.13) on the specific set of fragmentation densities used. The same has been done for K_L (4.5.12) in fig. 4.18 where we compared the BKK1-set with the one in [19] which is presented in the A-scheme. It turns out that K_L^H is very sensitive to the parametrization of the fragmentation densities. Choosing the set in [19] and $M = Q = M_Z$ we observe that K_L is mildly dependent on x. Using the same input a similar observation can be made for K_T which shows a constant behaviour over the whole x-region (see fig. 4.17). On the other hand K_L (see fig. 2 in [45]) and K_T steeply rise when x tends to one if the BKK1 or BKK2 sets are chosen. Again we want to emphasize that the

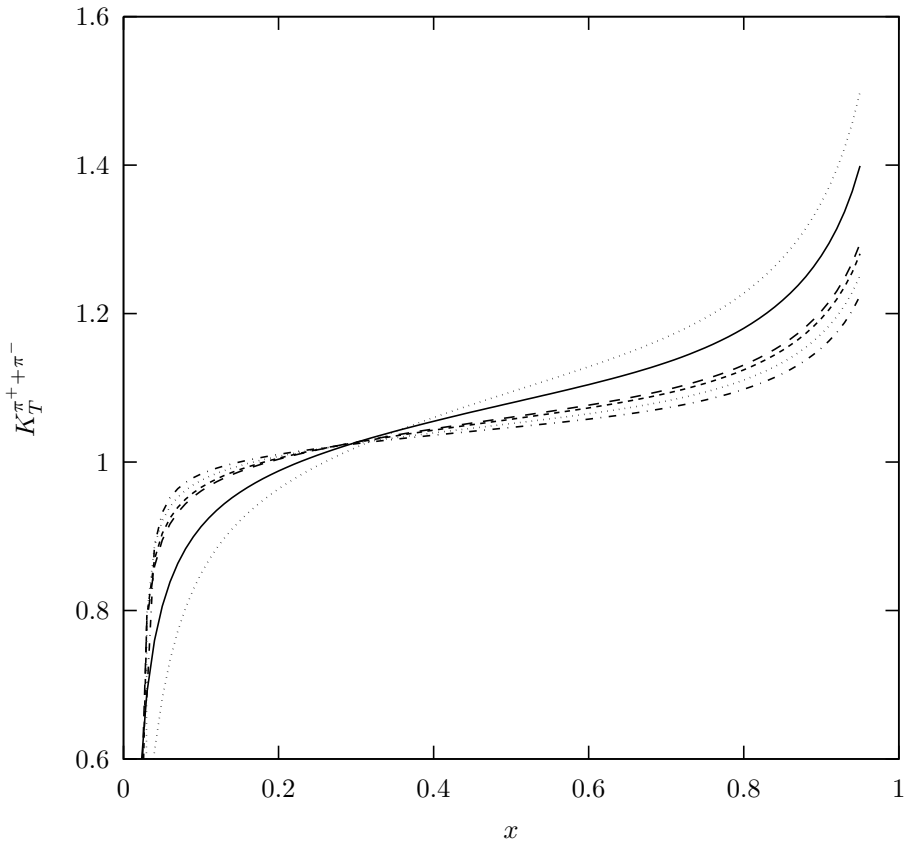

Figure 4.16: *The same as in fig. 4.20 but now for the ratio* $K_T^H = F_T^{H,NNLO}/F_T^{H,NLO}$ *with* $H = \pi^+ + \pi^-$.

fragmentation densities are badly known above $z = 0.9$ (BKK1) or $z = 0.8$ (BKK2) which in particular affects the large x-behaviour of the fragmentation functions. Bearing this in mind one may conclude that the K-factors heavily depend on the parametrization for the fragmentation densities which is intimately related to the chosen scheme ($\overline{\text{MS}}$ versus A).
In the next figures we study the factorization scale dependence of the fragmentation functions and show the decrease in sensitivity on the scale choice for M when higher order corrections are included.
In fig. 4.19 we have plotted $F_L^{NLO}(x, Q^2)$ at three different scales $M = Q/2,\ Q,\ 2Q$ where $Q = M_Z$. Like in fig. 4.13 we have chosen the BKK1-set since in this case we get agreement with the data. From fig. 4.19 one infers that the scale variation of F_L is small and that all scales describe the data rather well. To show the improvement in the scale dependence more clearly it is convenient to plot the following quantity

$$\Delta_k^r(x, Q^2) = \frac{\max\left(F_k^r(\frac{1}{2}Q), F_k^r(Q), F_k^r(2Q)\right) - \min\left(F_k^r(\frac{1}{2}Q), F_k^r(Q), F_k^r(2Q)\right)}{\text{average}\left(F_k^r(\frac{1}{2}Q), F_k^r(Q), F_k^r(2Q)\right)}, \tag{4.5.14}$$

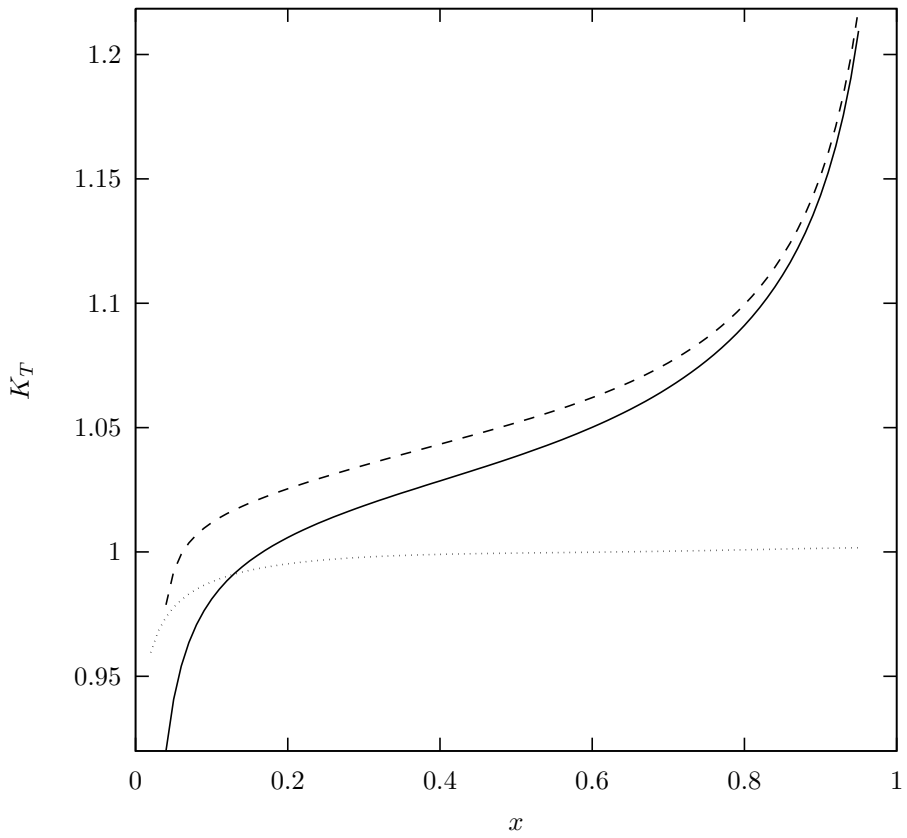

Figure 4.17: *The dependence of K_T on the fragmentation density sets at $M = Q = M_Z$. Dotted curve: set from [19]; solid curve: BKK1 [43]; dashed curve: BKK2 [44].*

for $r = LO,\ NLO,\ NNLO$ and $k = T,\ L$.

In fig. 4.20 one can see that $\Delta_L^{NLO} < \Delta_L^{LO}$ as long as $x > 0.1$ which implies that F_L^{NLO} is less sensitive to the scale M than F_L^{LO}. The same observation is made for F_T (fig. 4.21) and Δ_T (fig. 4.22). In fig. 4.21 we have plotted F_T^{NLO} at the same scales as above. At all three scales the data are described very well. In addition we also show F_T^{NNLO} for $M = Q = M_Z$. At very small x we found that $F_T^{NNLO} < F_T^{NLO}$ for all three scales and F_T^{NNLO} is also below the data. In fig. 4.22 we see again an improvement while going from LO to NNLO except when $x < 0.1$. The reason that for $x < 0.1$ the scale dependence of F_k^{NLO} $(k = T,\ L)$ is much larger than the one found in F_k^{LO} can be found in [43] where is stated that the scale evolution of the fragmentation densities is only reliable in the region $0.1 < x < 0.9$.

Finally we also study the scale dependence of the fragmentation functions at a lower energy. As an example we take the total fragmentation function F^H with $H = \pi^+ + \pi^-$ (4.2.22) and investigate its behaviour for different choices of the factorization scale M where again $M = Q/2,\ Q,\ 2Q$. Contrary to the previous plots we have chosen the BKK2-set which range of validity is bounded by $Q \leq 100$ GeV and $0.1 < x < 0.8$. Further we take $Q = 29$ GeV and compare the theoretical result

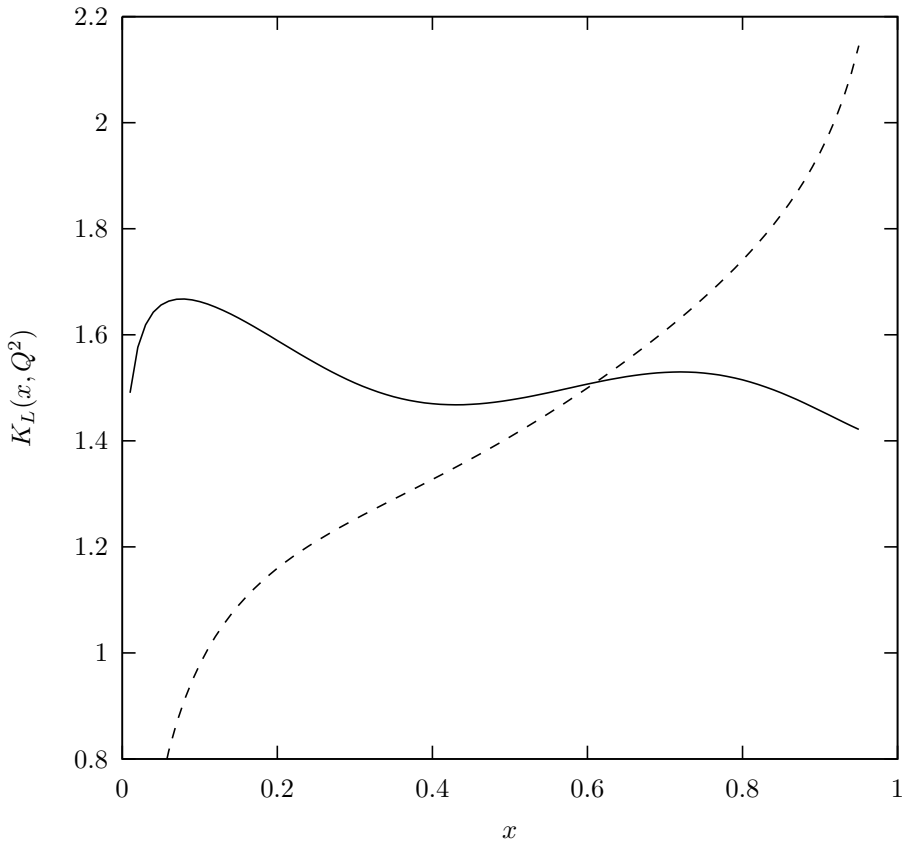

Figure 4.18: *The dependence of K_L on the fragmentation density sets at $M = Q = M_Z$. Dotted curve: set from [19]; solid curve: BKK1 [43]; dashed curve: BKK2 [44].*

with the TPC/2γ-data [12]. In fig. 4.23 we show $F^{H,NLO}$ at three different scales. The scale variation is small and only noticeable at large x. The data are very well described by $F^{H,NLO}$ at the three different scales except at very small x where the BKK2 parametrization is not reliable anymore. The same holds for $F^{H,NNLO}$ which hardly differs from $F^{H,NLO}$ so that even at lower energies the order α_s^2 corrections are very small. To show the improvement of the scale dependence in a better way we have plotted $\Delta^{H,LO}$, $\Delta^{H,NLO}$ and $\Delta^{H,NNLO}$ in fig. 4.24. A comparison with fig. 4.22 shows that there is essentially no difference between the Δ_k^r ($r = LO,\ NLO,\ NNLO$, $k = T,\ L$) taken at low ($Q = 29$ GeV) and high energies ($Q = M_Z = 91.2$ GeV).

4.5.1 Conclusions

Summarizing the results of this section we have computed the order α_s^2 contributions to the longitudinal and transverse coefficient functions. The effect of these contributions to the longitudinal and transverse cross sections are large which allow us for a better determination of the strong coupling constant α_s. The corrections to the longitudinal fragmentation function F_L^H are appreciable too which has important

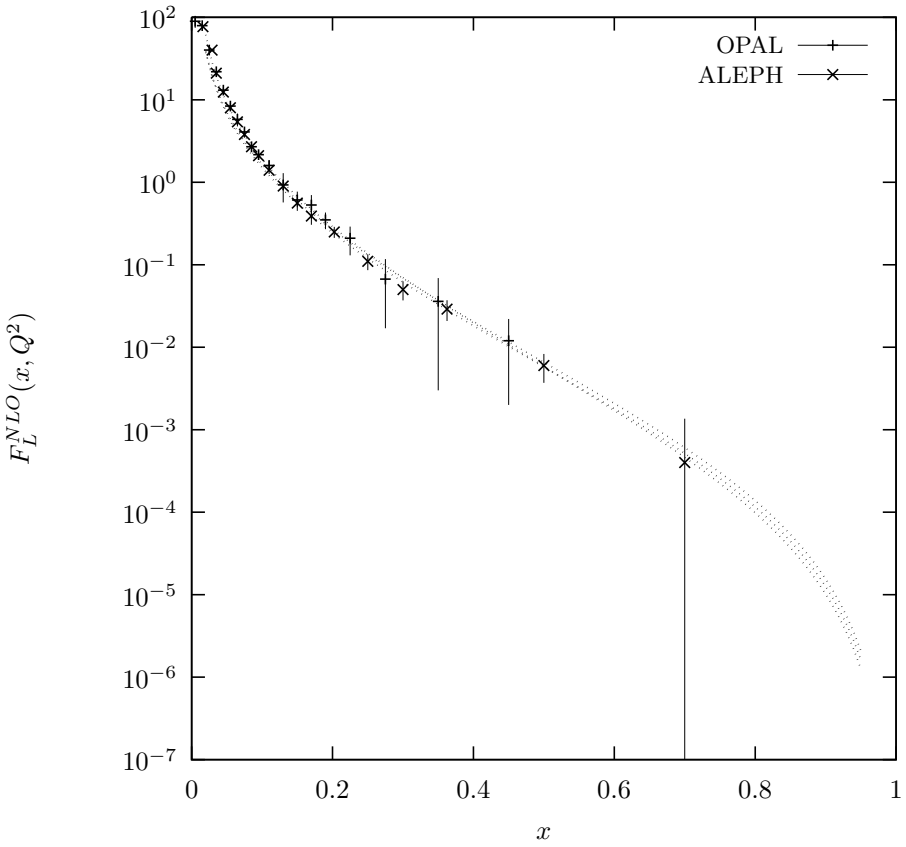

Figure 4.19: *The mass factorization scale dependence of F_L^{NLO} at $Q = M_Z$. Lower dotted curve: $M = 2Q$; middle dotted curve: $M = Q$; upper dotted curve: $M = Q/2$. The data are from ALEPH [16] and OPAL [18]. The fragmentation density set is BKK1 [43].*

consequences for the determination of the gluon fragmentation density $D_g^H(z, M^2)$. Furthermore one can now make a full NLO analysis of F_L^H. A NNLO description of the transverse structure function is still not possible because of the missing three-loop DGLAP splitting functions. However the order α_s^2 contributions from the coefficient functions indicate that probably the NNLO corrections are very small.

4.6 Results for the asymmetric fragmentation function

The first quantity we would like to study is the flavour asymmetry sum rule which is defined in eq. (2.23) of [19]. It is given by

$$\Sigma_A^Q = \sum_{H,f} A_f(Q^2) \int_0^1 dz_1 \; Q_H^{(f)} \left(D_f^H(z_1, \mu^2) - D_{\bar{f}}^H(z_1, \mu^2) \right) .$$

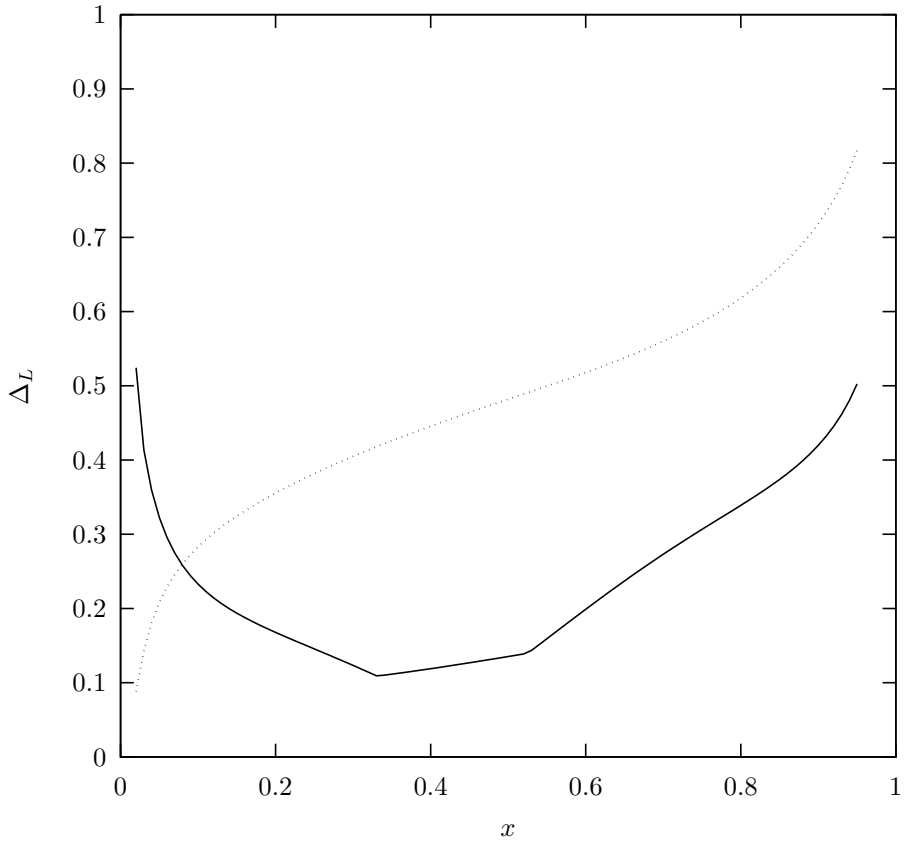

Figure 4.20: *Sensitivity of F_L^r ($r = LO,\ NLO$) to the mass factorization scale represented by Δ_L^r (4.5.14) at $Q = M_Z$. Dotted line: Δ_L^{LO}; solid line: Δ_L^{NLO}. The fragmentation density set is BKK1 [43].*

$$\cdot \int_0^1 dz_2\ \mathbb{C}_{A,q}^{\mathrm{NS}}(z_2, Q^2/\mu^2), \tag{4.6.1}$$

where $Q_H^{(f)}$ is a conserved additive quantity. The first moment of the non-singlet coefficient function calculated up to order α_s^2 is equal to

$$\int_0^1 dz_2\, \mathbb{C}_{A,q}^{\mathrm{NS}}(z_2, Q^2/\mu^2) = 1 - \left(\frac{\alpha_s(Q^2)}{4\pi}\right)^2 \left[\, 12\beta_0 C_F \zeta(3) \,\right] + \left(\frac{\alpha_s(Q^2)}{4\pi}\right)^3 \left[\, c_{A,q}^{(3)} \,\right], \tag{4.6.2}$$

where β_0 is the lowest order coefficient of the beta-function given by

$$\beta_0 = \frac{11}{3} C_A - \frac{4}{3} T_f n_f. \tag{4.6.3}$$

Notice that the first moments of $\mathbb{C}_{A,q}^{\mathrm{NS}}$ and $D_f^H - D_{\bar{f}}^H$ are separately scheme independent. Further there are no order α_s corrections to the first moment of $\mathbb{C}_{A,q}^{\mathrm{NS}}$ [19] and the order α_s^2 correction is proportional to β_0. A comparison between (4.6.2) and

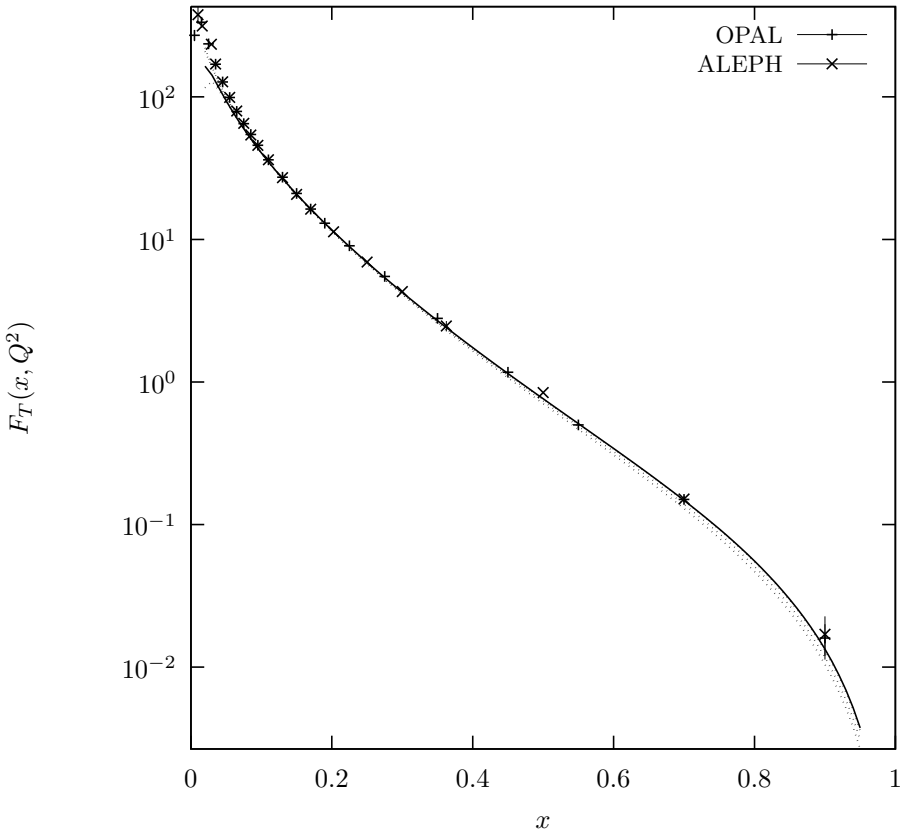

Figure 4.21: *The same as in fig. 4.19 but now for F_T^{NLO}. Also presented is the curve for F_T^{NNLO} (solid line).*

the order α_s^2 corrected $R_{ee} = \sigma_{\rm tot}(e^+ e^- \to X)/\sigma^{(0)}$ [6] reveals that the coefficients of the Riemann zeta-functions (here $\zeta(3)$ only) are exactly the same. Furthermore if one drops all rational numbers in R_{ee} one obtains exactly (4.6.2). Following the arguments in [46] one can make an interesting conjecture about the third order term $c_{A,q}^{(3)}$ which has not been calculated yet. Suppose that all rational numbers in $c_{A,q}^{(3)}$ are zero and that the coefficients of the Riemann zeta-functions $\zeta(n)$ (here $\zeta(3)$ and $\zeta(5)$) are the same as in R_{ee} then we can make the following conjecture

$$
\begin{aligned}
c_{A,q}^{(3)} = {} & C_A C_F^2 \left[-572\zeta(3) + 880\zeta(5) \right] + C_F C_A^2 \left[-\frac{10948}{9}\zeta(3) - \frac{440}{3}\zeta(5) \right] \\
& + C_F^2 T_f n_f \left[304\zeta(3) - 320\zeta(5) \right] + C_A C_F T_f n_f \left[\frac{7168}{9}\zeta(3) + \frac{160}{3}\zeta(5) \right] \\
& + C_F T_f^2 n_f^2 \left[-\frac{1216}{9}\zeta(3) \right] + \frac{n_f}{N} d_{abc} d_{abc} \left[-8\zeta(3) \right], \qquad (4.6.4)
\end{aligned}
$$

where d_{abc} denote the structure constants which emerge from the anti-commutation relations of the generators of the group $SU(N)$. We now want to study the effect of

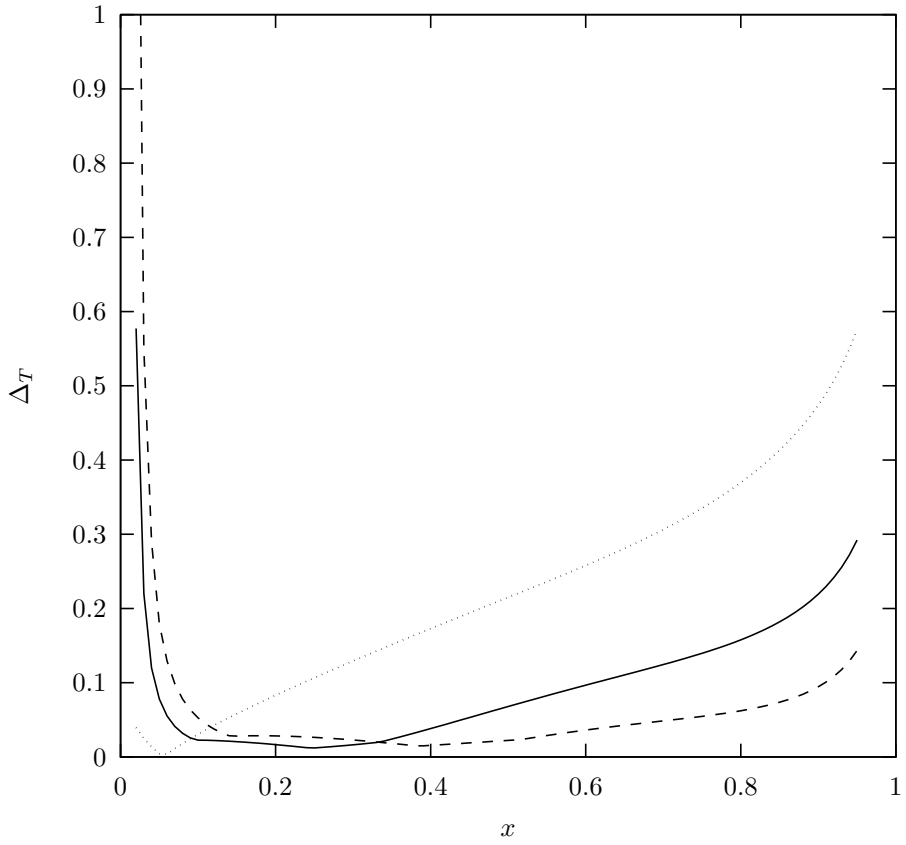

Figure 4.22: *The same as in fig. 4.20 but now for* Δ_T^r *(4.5.14). Also shown is* Δ_T^{NNLO} *(dashed line).*

the order α_s^2 correction on the asymmetric fragmentation function and compare the result with the OPAL data [18]. The fragmentation functions F_k^H will be defined by (see [18])

$$F_k^H(x,Q^2) = \frac{1}{\sigma_{\rm tot}} \frac{d\sigma_k^H(x,Q^2)}{dx}, \quad (k = T, L, A). \tag{4.6.5}$$

If we sum over all hadrons of species H we obtain the quantities

$$F_k(x,Q^2) = \sum_H F_k^H(x,Q^2), \quad (k = L, T), \tag{4.6.6}$$

$$F_A(x,Q^2) = \sum_H Q_H \, F_A^H(x,Q^2), \tag{4.6.7}$$

where the sum in (4.6.7) is taken over all charged hadrons. From (4.2.5) and (4.6.6) we infer that F_A gets only contributions from the valence fragmentation densities $D_{V,f}^H = D_f^H - D_{\bar f}^H$. Hence the measurement of F_A provides us with information about the x-behaviour of the valence fragmentation densities. Unfortunately the latter are not available yet. Therefore we have to resort to make an estimate of the

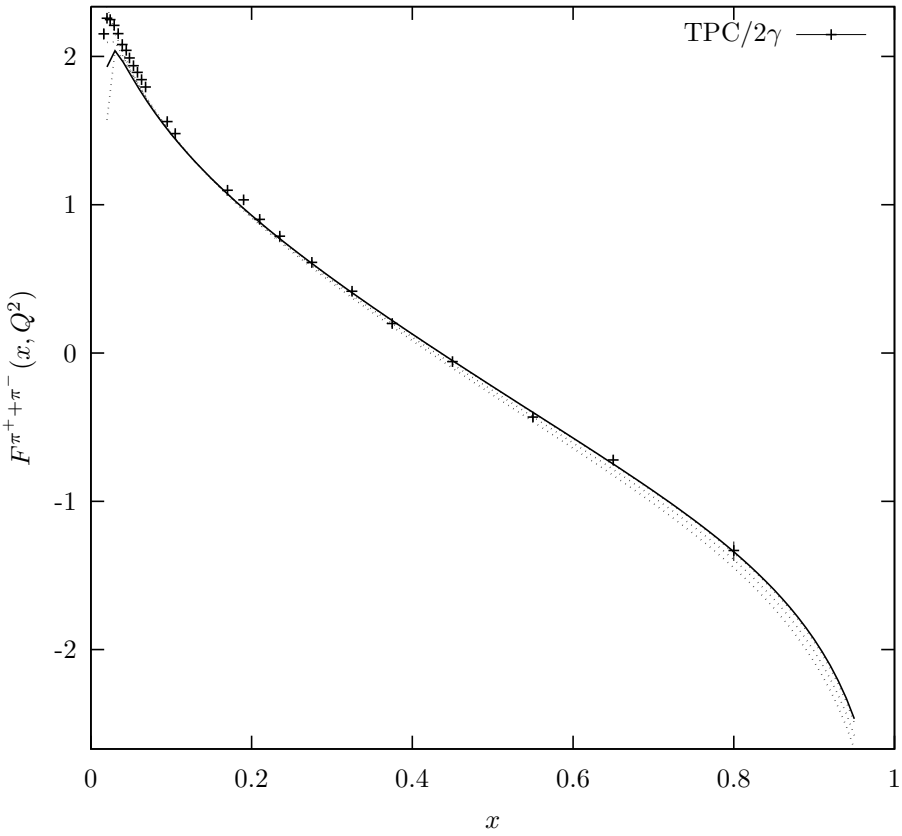

Figure 4.23: *The mass factorization scale dependence of the total fragmentation function $F^{H,NLO}$ with $H = \pi^+ + \pi^-$ at $Q = 29$ GeV. Lower dotted curve: $M = 2Q$; middle dotted curve: $M = Q$; upper dotted curve: $M = Q/2$; solid line: $F_T^{H,NNLO}$. The data are from TPC/2γ [12]. The fragmentation density set is BKK2 [44].*

quantities calculated below. Valence fragmentation densities are available in [43] for $H = \pi^+ + \pi^-$, $K^+ + K^-$ and $p + \bar{p}$ where they are parametrized in leading log (LL) and in next-to-leading log (NLL, $\overline{\text{MS}}$-scheme). Notice that in [43] the combination $F = F_T + F_L$ (4.6.6) for charged particles was analyzed so that one only gets information about $D_f^{H+\bar{H}} = D_{\bar{f}}^{H+\bar{H}}$. However in order to compute the asymmetric fragmentation function in (4.6.7) one needs information on D_f^H and $D_{\bar{f}}^H$ separately so that also $D_f^{H-\bar{H}}$, $D_{\bar{f}}^{H-\bar{H}}$ have to be determined. Because of this lack of information we have to make the following assumptions.
Let us first denote the up and down quark in each family by U and D respectively. For our calculation this means that $U = u$ (π^+, K^+) and $D = d$ (π^+) or $D = s$ (K^+). From [43] one infers for $H = \pi$, K

$$D_{V,U}^{H+\bar{H}} = D_{V,\bar{U}}^{H+\bar{H}} = D_{V,D}^{H+\bar{H}} = D_{V,\bar{D}}^{H+\bar{H}} \equiv D_V^{\langle H \rangle}. \tag{4.6.8}$$

We will now assume the following

$$D_{V,f}^H = D_V^{\langle H \rangle}, \quad f = U, D, \tag{4.6.9}$$

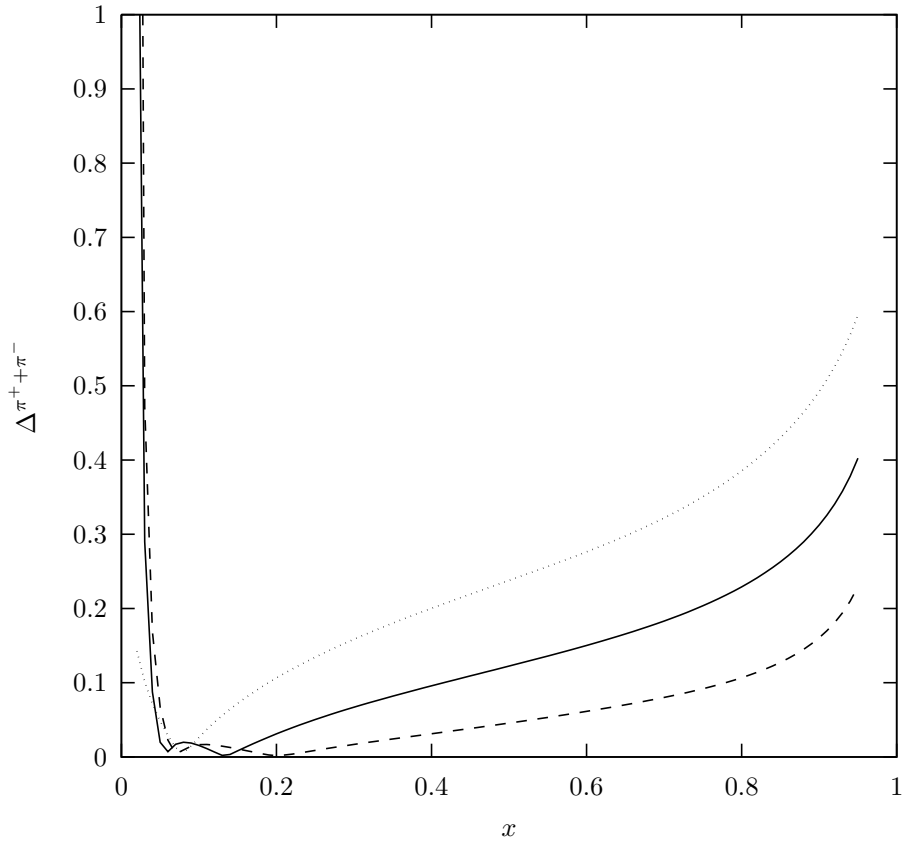

Figure 4.24: *Sensitivity of* $F^{H,r}$ *(*$r = LO,\ NLO,\ NNLO$*) to the mass factorization scale represented by* $\Delta^{H,r}$ *with* $H = \pi^+ + \pi^-$ *at* $Q = 29\ GeV$*. Dotted line:* $\Delta^{H,LO}$*; solid line:* $\Delta^{H,NLO}$*; dashed line:* $\Delta^{H,NNLO}$*. The fragmentation density set is BKK2 [44].*

provided f is a valence quark of the hadron H. Relation (4.6.9) also holds when on the lefthand side of this equation f is replaced by $\bar{f}$ or H by $\bar{H}$ as long as the above condition is satisfied. For the valence fragmentation function of the proton we assume

$$D^{p}_{V,f} = D^{\bar{p}}_{V,\bar{f}} = 0.16\, D^{\langle\pi\rangle}_{V}, \quad f = U, D, \tag{4.6.10}$$

provided f and $\bar{f}$ are the valence quarks of p and $\bar{p}$ respectively. The factor 0.16 originates from [43] where one has estimated $F^{p+\bar{p}} = 0.16\, F^{\pi^+ + \pi^-}$ with $F^{H+\bar{H}} = F_T^{H+\bar{H}} + F_L^{H+\bar{H}}$.
The structure function F_A^H in (4.6.7) can be inferred from (4.2.5) and (4.6.5) and we get

$$F_A^H(x,Q^2) = \frac{1}{\sigma_{\rm tot}} \int_x^1 \frac{dz}{z} \left[A_U(Q^2)\, D^H_{V,U}\left(\frac{x}{z},\mu^2\right) - A_D(Q^2)\, D^H_{V,D}\left(\frac{x}{z},\mu^2\right) \right] \cdot$$

$$\cdot \mathbb{C}^{\rm NS}_{A,q}(z, Q^2/\mu^2). \tag{4.6.11}$$

Choosing the valence fragmentation functions in [43] and making the assumptions in (4.6.9), (4.6.10) we compute F_A^H in (4.6.11) at the peak of the Z-resonance which implies the choice $Q^2 = M_Z^2$.
Since we have taken $D_{V,U}^H = D_{V,D}^H$ we observe that $F_A^H(Q^2, M_Z^2)$ is negative over the whole x-region. This property can be traced back to the value of the electroweak angle leading to $A_D(M_Z^2)/A_U(M_Z^2) \sim 2$. Therefore all hadrons with positive charge ($Q_H > 0$) give a negative contribution to $F_A(x, M_Z^2)$ (4.6.7). If $\bar{H}$ is the anti-particle of H we have the relation $F_A^{\bar{H}} = -F_A^H$. Because of $Q_{\bar{H}} = -Q_H$ in (4.6.7) the anti-particles $(\pi^-, K^-, \bar{p})$ also give a negative contribution to $F_A(x, Q^2)$. Therefore the parametrization in [43] predicts a negative $F_A(x, Q^2)$ (4.6.7) over the whole x-region at $Q^2 = M_Z^2$.
In our plots discussed below a comparison will be made with the OPAL data [18]. Further we take $\mu^2 = Q^2$ in (4.6.11) and $n_f = 5$. The running coupling constant is chosen to be $\alpha_s(M_Z^2) = 0.126$. Finally we want to emphasize that a full next-to-next-to-leading (NNLO) analysis of F_T and F_A is not possible yet because of the missing three-loop contributions to the DGLAP splitting functions. Therefore the order α_s^2 correction, which can be only attributed to the coefficient functions in (4.4.42), (4.4.49), have to be considered as an estimate.

In fig. 4.25 we have plotted F_A^{LO}, F_A^{NLO} and F_A^{NNLO} together with the OPAL data (see also fig. 4 in [18]). There is a difference between F_A^{LO} and F_A^{NLO} but the order α_s^2 corrections shown by F_A^{NNLO} are unobservable. Since the plots for F_A^{NLO} and F_A^{NNLO} are indistinguishable both are represented by the solid line in fig. 4.25. Furthermore the theoretical curves are above the data. In fig. 8 of [18] the OPAL-collaboration also presented the data for the ratio

$$R_A(x, Q^2) = \frac{F_A(x, Q^2)}{F(x, Q^2)}, \quad F(x, Q^2) = F_T(x, Q^2) + F_L(x, Q^2). \tag{4.6.12}$$

In fig. 4.26 these data are compared with the theoretical predictions R_A^{LO}, R_A^{NLO}, and R_A^{NNLO}. Here we see the same features as has been observed for F_A in fig. 4.25. As can be expected from the previous figure the plots for R_A^{NLO} and R_A^{NNLO}, both represented by the solid line in fig. 4.26, are almost identical since the order α_s^2 corrections are extremely small. However the difference between R_A^{LO} and R_A^{NLO} which is due to the order α_s corrections is visible. Also in the case of R_A (4.6.12) the data are below the theoretical predictions.
From the data one can infer the integrated fragmentation function for which the theoretical predictions corrected up to order α_s^2 are given below

$$\int_{0.1}^{1} dx\, F_A^{NNLO}(x, M_Z^2) = -0.016 \quad (-0.023), \tag{4.6.13}$$

$$\int_{0.1}^{1} dx\, \frac{1}{2} x\, F_A^{NNLO}(x, M_Z^2) = -0.0020 \quad (-0.0027). \tag{4.6.14}$$

The experimental values for (4.6.13) and (4.6.14) are -0.0229± 0.0044 and -0.00369± 0.00046 respectively. Since the fragmentation densities in [43] have a limited range

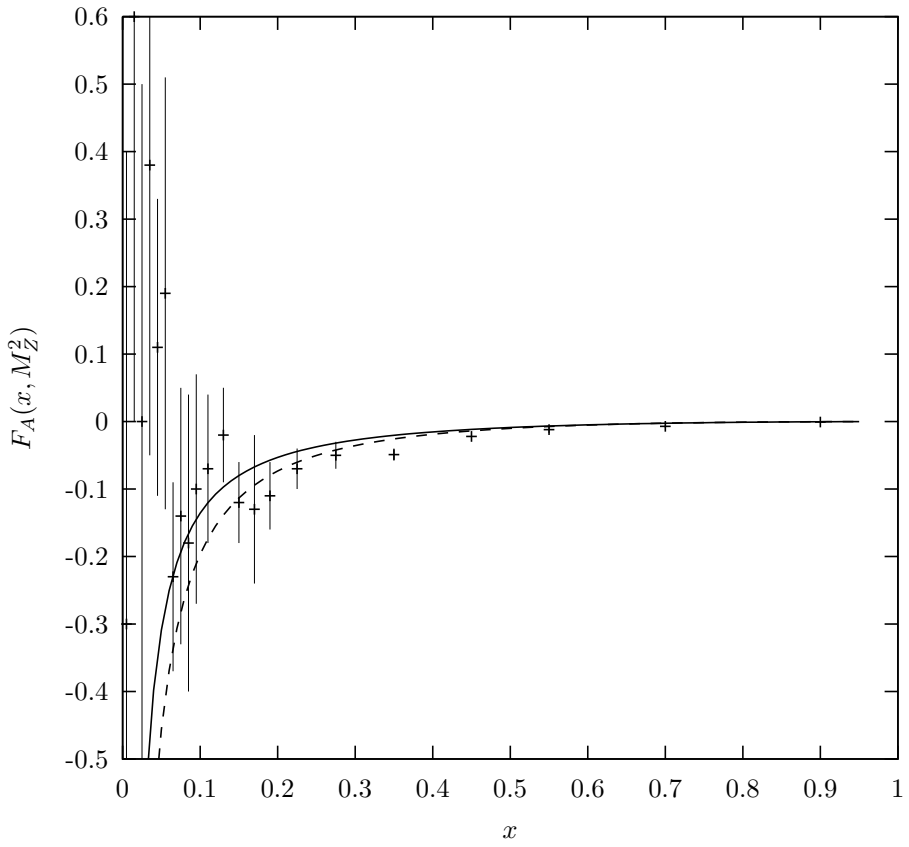

Figure 4.25: *Contributions to the asymmetry fragmentation function* $F_A(x, Q^2)$ *(4.6.7) at* $Q = M_Z$ *using the fragmentation density set of [43]. Dashed line: LO. Solid line: NLO and NNLO. The experimental data are taken from OPAL [18].*

of validity we have imposed a lower bound on the integration which is given by $x = 0.1$. The same bound has been imposed by us on the experimental values which are obtained from table 1 in [18]. Between the brackets in (4.6.13), (4.6.14) we have quoted the LO results. It turns out that the latter are in better agreement with experiment than the NLO and NNLO numbers. Further the values of the integrals, quoted in (4.6.13) and (4.6.14) for NNLO, also hold in NLO since the order α_s^2 corrections are extremely small.
The OPAL-data indicate that at low x, $F_A(x, M_Z^2)$ might become positive. If this is the case one has to assume that in this region $D^H_{V,U}(x, \mu^2) > D^H_{V,D}(x, \mu^2)$ provided the zeroth order contribution to $\mathbb{C}^{\rm NS}_{A,q}$ which is given by $\delta(1-z)$ dominates the integral.

4.6.1 Conclusions

Summarizing the above we conclude that the order α_s^2 corrections to F_A are negligible and we do not expect that this will change when the effect of the three-loop DGLAP splitting functions are taken into account. By making some assumptions on the fragmentation densities in (4.6.11) we get a reasonable estimate of the asymmetric

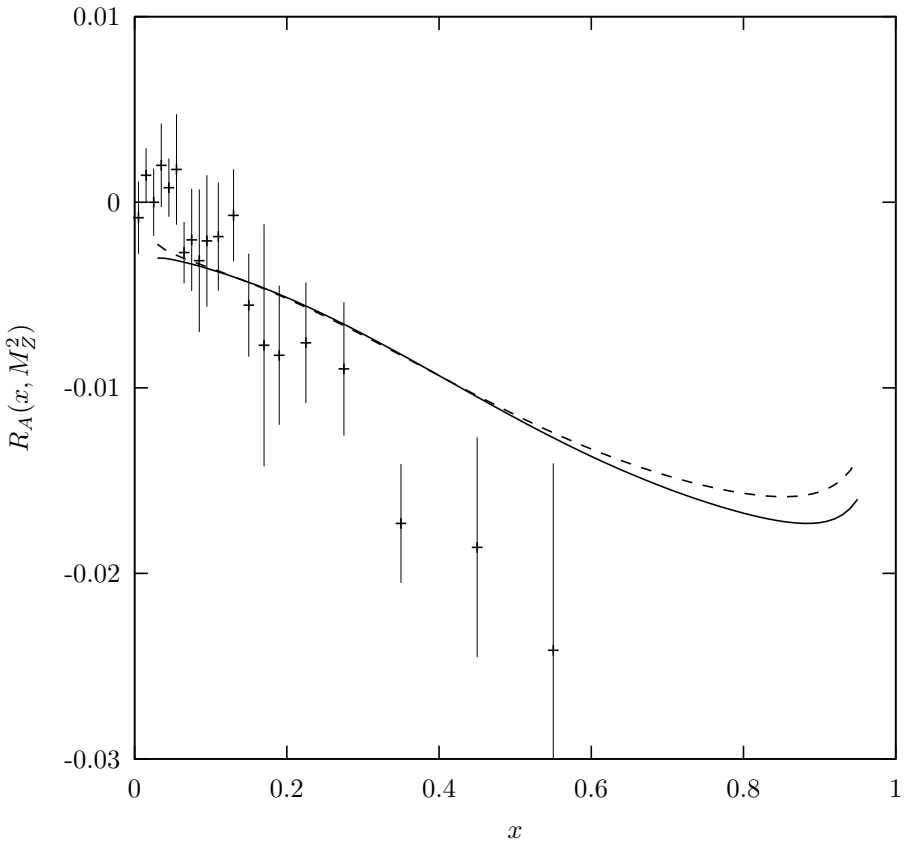

Figure 4.26: *The ratio $R_A(x, Q^2)$ (4.6.12) at $Q = M_Z$ using the fragmentation density set of [43]. Dashed line: LO. Solid line: NLO and NNLO. The exprimental data are taken from OPAL [18].*

fragmentation function F_A. The above results reveal that the measurement of F_A puts a constraint on the valence fragmentation densities $D_{V,f}^H$ for each charged (anti) hadron H and (anti) quark species f.

Appendix A

In this appendix we will present the explicit expressions for the coefficient functions of the fragmentation process in (4.2.1) which are calculated in section 4.4 in the $\overline{\text{MS}}$and A-scheme. In order to make the presentation self contained we also give the order α_s contributions $\bar{c}_{k,p}^{(1)}$ (4.4.42)-(4.4.49) ($\overline{\text{MS}}$-scheme) and $c_{k,p}^{(1)}$ (4.4.59)-(4.4.65) (A-scheme) which have already been presented in the $\overline{\text{MS}}$-scheme in the literature [19, 25, 26]. The coefficient functions $\mathbb{C}_{k,p}$ $(p = q, g)$ will be expanded in the renormalized coupling constant $\alpha_s \equiv \alpha_s(M^2)$ where we have chosen the renormalization scale R to be equal to the factorization scale M. If one wants to chose R different from M, $\alpha_s(M^2)$ has to be expressed into $\alpha_s(R^2)$ following the prescription in (4.4.51). The non-singlet coefficient functions $\mathbb{C}_{k,q}^{\text{NS}}$ $(k = T, A, L)$ we shall split into

a part due to identical quark contributions (AB and CD in fig. 4.8) represented by $\mathbb{C}_{k,q}^{\mathrm{NS,id}}$ and a remaining part given by $\mathbb{C}_{k,q}^{\mathrm{NS,nid}}$. The expression for the non-singlet coefficient is very long and we will split it up into various contributions. First we have the soft plus virtual gluon contributions which are represented by the distributions $\delta(1-z)$ and $\mathcal{D}_i(z)$ (4.3.42). They are indicated by $\mathbb{C}_{k,q}^{\mathrm{NS}}\big|_{S+V}$ $(k = T, A)$. The remaining part which is integrable at $z = 1$ will be called $\mathbb{C}_{k,q}^{\mathrm{NS}}\big|_{H}$ where H refers to hard gluon contributions although $\mathbb{C}_{k,q}^{\mathrm{NS}}\big|_{H}$ also originates from subprocesses with (anti) quarks in the final state (see fig. 4.8 except for C^2 and D^2). Following this prescription the non-singlet coefficient function is constituted by the following parts

$$\mathbb{C}_{k,q}^{\mathrm{NS}} = \mathbb{C}_{k,q}^{\mathrm{NS,nid}} + \mathbb{C}_{k,q}^{\mathrm{NS,id}}, \quad k = T, L, \tag{A.1}$$

$$\mathbb{C}_{A,q}^{\mathrm{NS}} = \mathbb{C}_{A,q}^{\mathrm{NS,nid}} - \mathbb{C}_{A,q}^{\mathrm{NS,id}}, \tag{A.2}$$

$$\mathbb{C}_{k,q}^{\mathrm{NS,nid}} = \mathbb{C}_{k,q}^{\mathrm{NS,nid}}\Big|_{S+V} + \mathbb{C}_{k,q}^{\mathrm{NS,nid}}\Big|_{H}, \quad k = T, A. \tag{A.3}$$

A.1 The coefficient functions in the $\overline{\mathrm{MS}}$-scheme

The soft plus virtual gluon contributions (A.3) to $\overline{\mathbb{C}}_{T,q}^{\mathrm{NS}}$ (4.4.46) read as follows

$$\begin{aligned}
\overline{\mathbb{C}}_{T,q}^{\mathrm{NS}}\Big|_{S+V} = \overline{\mathbb{C}}_{T,q}^{\mathrm{NS,nid}}\Big|_{S+V} &= \delta(1-z) + C_F \frac{\alpha_s}{4\pi}\Bigg[\Big(4\mathcal{D}_0(z) + 3\delta(1-z) \Big) L_M \\
&+ 4\mathcal{D}_1(z) - 3\mathcal{D}_0(z) + \delta(1-z)\Big(-9 + 8\zeta(2) \Big) \Bigg] \\
&+ \left(\frac{\alpha_s}{4\pi}\right)^2 \Bigg[C_F^2 \Bigg\{ \Big(16\mathcal{D}_1(z) + 12\mathcal{D}_0(z) \Big) L_M^2 + \Big(24\mathcal{D}_2(z) - 12\mathcal{D}_1(z) \\
&+ \Big(16\zeta(2) - 45 \Big)\mathcal{D}_0(z) \Big) L_M + \delta(1-z)\Bigg[\left(\frac{9}{2} - 8\zeta(2)\right) L_M^2 + \Big(40\zeta(3) \\
&+ 24\zeta(2) - \frac{51}{2} \Big) L_M \Bigg] \Bigg\} \\
&+ C_A C_F \Bigg\{ -\frac{22}{3}\mathcal{D}_0(z) L_M^2 + \left(-\frac{44}{3}\mathcal{D}_1(z) + \left(\frac{367}{9} - 8\zeta(2)\right)\mathcal{D}_0(z) \right) L_M \\
&+ \delta(1-z)\Bigg[-\frac{11}{2} L_M^2 + \left(-12\zeta(3) - \frac{44}{3}\zeta(2) + \frac{215}{6} \right) L_M \Bigg] \Bigg\} \\
&+ n_f C_F T_f \Bigg\{ \frac{8}{3}\mathcal{D}_0(z) L_M^2 + \left(\frac{16}{3}\mathcal{D}_1(z) - \frac{116}{9}\mathcal{D}_0(z) \right) L_M + \delta(1-z)\Bigg[2L_M^2
\end{aligned}$$

$$+\left(\frac{16}{3}\zeta(2)-\frac{38}{3}\right)L_M\Bigg]\Bigg\}+\bar{c}_{T,q}^{\mathrm{NS},(2),\mathrm{nid}}\Big|_{S+V}\Bigg], \tag{A.4}$$

with

$$\begin{aligned}\bar{c}_{T,q}^{\mathrm{NS},(2),\mathrm{nid}}\Big|_{S+V} &= C_F^2\Bigg[8\mathcal{D}_3(z)-18\mathcal{D}_2(z)+\Big(16\zeta(2)-27\Big)\mathcal{D}_1(z)+\Big(-8\zeta(3)\\ &+\frac{51}{2}\Big)\mathcal{D}_0(z)+\delta(1-z)\left(30\zeta(2)^2-78\zeta(3)-39\zeta(2)+\frac{331}{8}\right)\Bigg]\\ &+C_AC_F\Bigg[-\frac{22}{3}\mathcal{D}_2(z)+\left(\frac{367}{9}-8\zeta(2)\right)\mathcal{D}_1(z)+\Big(40\zeta(3)+\frac{44}{3}\zeta(2)\\ &-\frac{3155}{54}\Big)\mathcal{D}_0(z)+\delta(1-z)\left(-\frac{49}{5}\zeta(2)^2+\frac{140}{3}\zeta(3)+\frac{215}{3}\zeta(2)-\frac{5465}{72}\right)\Bigg]\\ &+n_fC_FT_f\Bigg[\frac{8}{3}\mathcal{D}_2(z)-\frac{116}{9}\mathcal{D}_1(z)+\left(\frac{494}{27}-\frac{16}{3}\zeta(2)\right)\mathcal{D}_0(z)\\ &+\delta(1-z)\left(\frac{8}{3}\zeta(3)-\frac{76}{3}\zeta(2)+\frac{457}{18}\right)\Bigg].\end{aligned} \tag{A.5}$$

The hard gluon contribution to $\overline{\mathbb{C}}_{T,q}^{\mathrm{NS,nid}}$ (A.3) is given by

$$\begin{aligned}\overline{\mathbb{C}}_{T,q}^{\mathrm{NS,nid}}\Big|_H &= C_F\frac{\alpha_s}{4\pi}\Bigg[-2(1+z)L_M-2(1+z)\ln(1-z)+4\frac{1+z^2}{1-z}\ln z\\ &+3(1-z)\Bigg]+\left(\frac{\alpha_s}{4\pi}\right)^2\Bigg[C_F^2\Bigg\{\Bigg[-8(1+z)\left(\ln(1-z)-\frac{3}{4}\ln z\right)\\ &-\frac{8}{1-z}\ln z-10-2z\Bigg]L_M^2+\Bigg[4(1+z)\Big(\mathrm{Li}_2(1-z)-3\ln z\ln(1-z)\\ &-3\ln^2(1-z)+\frac{11}{2}\ln^2 z-2\zeta(2)\Big)+\frac{32}{1-z}\Big(\ln z\ln(1-z)-\ln^2 z\\ &+\frac{3}{2}\ln z\Big)+4(1-z)\ln(1-z)-(52+20z)\ln z+5+31z\Bigg]L_M\Bigg\}\\ &+C_AC_F\Bigg\{\Bigg[\frac{11}{3}(1+z)L_M^2+\Bigg[(1+z)\Big(-2\ln^2 z+4\zeta(2)+\frac{22}{3}\ln(1-z)\\ &+\frac{34}{3}\ln z\Big)+\frac{1}{1-z}\left(4\ln^2 z-\frac{44}{3}\ln z\right)+\frac{7}{9}-\frac{275}{9}z\Bigg]L_M\Bigg\}\\ &+n_fC_FT_f\Bigg\{-\frac{4}{3}(1+z)L_M^2+\Bigg[-\frac{8}{3}(1+z)\Big(\ln(1-z)+\ln z\Big)\end{aligned}$$

$$+\frac{16}{3}\frac{1}{1-z}\ln z+\frac{28}{9}+\frac{52}{9}z\Bigg]L_M\Bigg\}+\bar{c}_{T,q}^{\mathrm{NS},(2),\mathrm{nid}}\Big|_H\Bigg], \tag{A.6}$$

with

$$\begin{aligned}
\bar{c}_{T,q}^{\mathrm{NS},(2),\mathrm{nid}}\Big|_H = C_F^2\Bigg[\,&16(1+2z)\Big(-2\mathrm{Li}_3(-z)+\ln z\mathrm{Li}_2(-z)\Big)+\frac{1}{1-z}\Big(\\
&96\mathrm{Li}_3(-z)+72\zeta(3)-48\ln z\mathrm{Li}_2(-z)-192S_{1,2}(1-z)-24\mathrm{Li}_3(1-z)\\
&+8\ln(1-z)\mathrm{Li}_2(1-z)-80\ln z\mathrm{Li}_2(1-z)+20\ln z\ln^2(1-z)\\
&-4\ln^2 z\ln(1-z)-\frac{80}{3}\ln^3 z+120\zeta(2)\ln z+12\mathrm{Li}_2(1-z)-12\ln z\cdot\\
&\cdot\ln(1-z)+33\ln^2 z-106\ln z\Big)+(1+z)\Big(8\mathrm{Li}_3(1-z)+52\ln z\cdot\\
&\cdot\mathrm{Li}_2(1-z)-8\ln z\ln^2(1-z)+8\ln^2 z\ln(1-z)-64\zeta(2)\ln z-32\zeta(3)\\
&+17\ln^3 z-4\ln^3(1-z)\Big)+(100+116z)S_{1,2}(1-z)-16z\zeta(2)\ln(1-z)\\
&+(-48+24z)\mathrm{Li}_2(1-z)-(20+4z)\ln z\ln(1-z)+(8+4z)\ln^2(1-z)\\
&+\Big(-45-23z+8z^2+\frac{12}{5}z^3\Big)\ln^2 z+\Big(20-36z-16z^2-\frac{24}{5}z^3\Big)\zeta(2)\\
&+\Big(-\frac{24}{5z^2}-\frac{16}{z}+8+8z-16z^2-\frac{24}{5}z^3\Big)\Big(\mathrm{Li}_2(-z)+\ln z\ln(1+z)\Big)\\
&+(-29+67z)\ln(1-z)+\Big(\frac{24}{5z}+\frac{218}{5}+\frac{248}{5}z+\frac{24}{5}z^2\Big)\ln z-\frac{24}{5z}+\frac{187}{10}\\
&-\frac{187}{10}z+\frac{24}{5}z^2\Bigg]\\
&+C_AC_F\Bigg[8(1+2z)\Big(2\mathrm{Li}_3(-z)-\ln z\mathrm{Li}_2(-z)\Big)+\frac{1}{1-z}\Big(-48\mathrm{Li}_3(-z)\\
&-36\zeta(3)+24\ln z\mathrm{Li}_2(-z)+24\mathrm{Li}_3(1-z)-8\ln(1-z)\mathrm{Li}_2(1-z)\\
&-8\ln z\mathrm{Li}_2(1-z)+6\ln^3 z-24\zeta(2)\ln z-\frac{44}{3}\mathrm{Li}_2(1-z)\\
&-\frac{44}{3}\ln z\ln(1-z)-\frac{11}{3}\ln^2 z+\frac{206}{3}\ln z\Big)+(1+z)\Big(-12\mathrm{Li}_3(1-z)\\
&+4\ln(1-z)\mathrm{Li}_2(1-z)+4\ln z\mathrm{Li}_2(1-z)+12\zeta(2)\ln z-2\zeta(3)-3\ln^3 z
\end{aligned}$$

$$+\frac{34}{3}\mathrm{Li}_2(1-z)+\frac{34}{3}\ln z\ln(1-z)+\frac{11}{3}\ln^2(1-z)\Big)+4(1-z)S_{1,2}(1-z)$$
$$+8z\zeta(2)\ln(1-z)+\left(\frac{47}{6}+\frac{47}{6}z-4z^2-\frac{6}{5}z^3\right)\ln^2 z+\Big(-\frac{28}{3}-\frac{28}{3}z$$
$$+8z^2+\frac{12}{5}z^3\Big)\zeta(2)+\left(\frac{12}{5z^2}+\frac{8}{z}-4-4z+8z^2+\frac{12}{5}z^3\right)\Big(\mathrm{Li}_2(-z)$$
$$+\ln z\ln(1+z)\Big)+\left(\frac{97}{9}-\frac{383}{9}z\right)\ln(1-z)-\Big(\frac{12}{5z}+\frac{122}{15}+\frac{184}{5}z$$
$$+\frac{12}{5}z^2\Big)\ln z+\frac{12}{5z}+\frac{2513}{270}+\frac{3587}{270}z-\frac{12}{5}z^2\Big]$$
$$+n_f C_F T_f\Big[\frac{8}{3}\frac{1+z^2}{1-z}\left(\mathrm{Li}_2(1-z)+\ln z\ln(1-z)+\frac{1}{4}\ln^2 z\right)+\frac{4}{3}(1+z)\cdot$$
$$\cdot\Big(2\zeta(2)-\ln^2(1-z)\Big)+\left(\frac{28}{9}+\frac{52}{9}z\right)\ln(1-z)+\Big(\frac{20}{3}+12z$$
$$-\frac{64}{3}\frac{1}{1-z}\Big)\ln z-\frac{118}{27}-\frac{34}{27}z\Big], \tag{A.7}$$

where the definition of the polylogarithms $\mathrm{Li}_n(z)$ and $S_{n,p}(z)$ can be found in [41]. The quantity $\overline{\mathbb{C}}_{T,q}^{(2),\mathrm{NS,nid}}$ representing the second moment of the sum of the expressions (A.4) and (A.6) (see also (4.4.71)) is equal to

$$\overline{\mathbb{C}}_{T,q}^{(2),\mathrm{NS,nid}}=1+C_F\frac{\alpha_s}{4\pi}\Big[-\frac{8}{3}L_M+\frac{32}{3}\Big]+\left(\frac{\alpha_s}{4\pi}\right)^2\Big[C_F^2\Big\{\frac{32}{9}L_M^2+\Big(-\frac{593}{27}$$
$$-\frac{4}{3}\zeta(2)+8\zeta(3)\Big)L_M+\frac{25057}{1620}-\frac{8}{3}\zeta(2)+\frac{186}{5}\zeta(3)-\frac{64}{5}\zeta(2)^2\Big\}$$
$$+C_A C_F\Big\{\frac{44}{9}L_M^2+\left(-\frac{3607}{54}+\frac{34}{3}\zeta(2)-4\zeta(3)\right)L_M+\frac{775373}{3240}-\frac{320}{9}\zeta(2)$$
$$-\frac{1579}{15}\zeta(3)+\frac{32}{5}\zeta(2)^2\Big\}$$
$$+n_f C_F T_f\Big\{-\frac{16}{9}L_M^2+\frac{512}{27}L_M-\frac{4708}{81}+\frac{32}{9}\zeta(2)+16\zeta(3)\Big\}\Big]. \tag{A.8}$$

The identical quark contributions stemming from the combinations AB and CD in fig. 4.8 is given by

$$\overline{\mathbb{C}}_{T,q}^{\mathrm{NS},(2),\mathrm{id}}=\left(\frac{\alpha_s}{4\pi}\right)^2\Big[(C_F^2-\frac{1}{2}C_A C_F)\Big\{\Big[4\frac{1+z^2}{1+z}\Big(-4\mathrm{Li}_2(-z)$$

$$- 4\ln z\ln(1+z) + \ln^2 z - 2\zeta(2)\Big) + 8(1+z)\ln z + 16(1-z)\Big] L_M \Big\}$$

$$+ \bar{c}_{T,q}^{\mathrm{NS},(2),\mathrm{id}}\Big], \tag{A.9}$$

$$\bar{c}_{T,q}^{\mathrm{NS},(2),\mathrm{id}} = (C_F^2 - \frac{1}{2}C_A C_F)\Big[16\frac{1+z^2}{1+z}\Big(\mathrm{Li}_3\Big(\frac{1-z}{1+z}\Big) - \mathrm{Li}_3\Big(-\frac{1-z}{1+z}\Big)$$

$$+ \frac{1}{2}S_{1,2}(1-z) - \mathrm{Li}_3(1-z) - S_{1,2}(-z) + \frac{1}{2}\mathrm{Li}_3(-z) + \frac{1}{2}\ln z\mathrm{Li}_2(1-z)$$

$$- \ln(1-z)\mathrm{Li}_2(-z) - \ln(1+z)\mathrm{Li}_2(-z) - \ln z\mathrm{Li}_2(-z) - \frac{1}{2}\zeta(2)\ln(1-z)$$

$$- \frac{1}{2}\zeta(2)\ln(1+z) - \zeta(2)\ln z - \ln z\ln(1-z)\ln(1+z) + \frac{1}{4}\ln^2 z\ln(1-z)$$

$$- \frac{1}{2}\ln z\ln^2(1+z) - \frac{3}{4}\ln^2 z\ln(1+z) + \frac{3}{8}\ln^3 z + \frac{1}{2}\zeta(3) - \frac{1}{2}\ln z\Big)$$

$$+ 16(1+z)\Big(-S_{1,2}(-z) + \frac{1}{2}\mathrm{Li}_3(-z) - \ln(1+z)\mathrm{Li}_2(-z)$$

$$- \frac{1}{2}\ln z\ln^2(1+z) + \frac{1}{4}\ln^2 z\ln(1+z) - \frac{1}{2}\zeta(2)\ln(1+z) + \frac{1}{2}\zeta(3)$$

$$+ \frac{1}{2}\mathrm{Li}_2(1-z) + \frac{1}{2}\ln z\ln(1-z)\Big) + \Big(-\frac{24}{5z^2} + \frac{16}{z} + 16z^2 - \frac{24}{5}z^3\Big)\cdot$$

$$\cdot\Big(\mathrm{Li}_2(-z) + \ln z\ln(1+z)\Big) + \Big(-4 + 4z + 16z^2 - \frac{24}{5}z^3\Big)\zeta(2) + \Big(12 + 8z$$

$$- 8z^2 + \frac{12}{5}z^3\Big)\ln^2 z + 16(1-z)\ln(1-z) + \Big(\frac{24}{5z^2} + \frac{118}{5} - \frac{42}{5}z$$

$$+ \frac{24}{5}z^2\Big)\ln z - \frac{24}{5z} + \frac{46}{5} - \frac{46}{5}z + \frac{24}{5}z^2\Big]. \tag{A.10}$$

Notice that the identical quark contribution in (A.9) and (A.10) carries the colour factor $C_F^2 - \frac{1}{2}C_A C_F$. The second moment of (A.9) becomes

$$\overline{\mathbb{C}}_{T,q}^{(2),\mathrm{NS},\mathrm{id}} = \Big(\frac{\alpha_s}{4\pi}\Big)^2 (C_F^2 - \frac{1}{2}C_A C_F)\Big[\Big(-\frac{743}{27} + \frac{68}{3}\zeta(2) - 8\zeta(3)\Big)L_M + \frac{9851}{60}$$

$$- \frac{536}{9}\zeta(2) - \frac{1262}{15}\zeta(3) + \frac{64}{5}\zeta(2)^2\Big]. \tag{A.11}$$

The purely singlet coefficient function becomes

$$\overline{\mathbb{C}}_{T,q}^{\rm PS} = n_f \left(\frac{\alpha_s}{4\pi}\right)^2 \Bigg[C_F T_f \Bigg\{ \left(8(1+z)\ln z + \frac{16}{3z} + 4 - 4z - \frac{16}{3}z^2 \right) L_M^2$$
$$+ \left(16(1+z)\left(\mathrm{Li}_2(1-z) + \ln z \ln(1-z) + \frac{3}{2}\ln^2 z\right) + \left(\frac{32}{3z} + 8 \right.\right.$$
$$\left.\left. - 8z - \frac{32}{3}z^2 \right) \ln(1-z) + \left(\frac{64}{3z} - 8 - 40z - \frac{32}{3}z^2\right) \ln z - \frac{16}{3z} - \frac{184}{3} \right.$$
$$\left. + \frac{136}{3}z + \frac{64}{3}z^2 \right) L_M \Bigg\} + \bar{c}_{T,q}^{\rm PS,(2)} \Bigg] , \tag{A.12}$$

$$\bar{c}_{T,q}^{\rm PS,(2)} = C_F T_f \Bigg[8(1+z) \left(6S_{1,2}(1-z) - 2\mathrm{Li}_3(1-z) + 2\ln(1-z)\mathrm{Li}_2(1-z) \right.$$
$$+ 6\ln z \mathrm{Li}_2(1-z) - 2\zeta(2)\ln z + \ln z \ln^2(1-z) + 3\ln^2 z \ln(1-z)$$
$$\left. + \frac{11}{6}\ln^3 z \right) + \left(\frac{64}{3z} - 8 - 40z - \frac{32}{3}z^2\right) \left(\mathrm{Li}_2(1-z) + \ln z \ln(1-z) \right)$$
$$+ \left(\frac{16}{3z} + 4 - 4z - \frac{16}{3}z^2\right) \ln^2(1-z) + \left(\frac{64}{3z} - 14 - 14z + \frac{16}{3}z^2\right) \ln^2 z$$
$$- \left(\frac{32}{3z} + 32 + 32z + \frac{32}{3}z^2\right) \left(\mathrm{Li}_2(-z) + \ln z \ln(1+z) \right) + \left(-\frac{64}{3z} - 8 \right.$$
$$\left. - 24z + \frac{32}{3}z^2 \right) \zeta(2) + \left(-\frac{16}{3z} - \frac{184}{3} + \frac{136}{3}z + \frac{64}{3}z^2\right) \ln(1-z) - \left(\frac{32}{3z} \right.$$
$$\left. + \frac{400}{3} + \frac{208}{3}z + \frac{256}{9}z^2 \right) \ln z - \frac{160}{27z} - \frac{236}{3} + \frac{140}{3}z + \frac{1024}{27}z^2 \Bigg] . \tag{A.13}$$

Taking the second moment of (A.12) gives the result

$$\overline{\mathbb{C}}_{T,q}^{(2),\rm PS} = n_f \left(\frac{\alpha_s}{4\pi}\right)^2 C_F T_f \left[\frac{16}{9}L_M^2 - \frac{512}{27}L_M + \frac{4924}{81} - \frac{32}{9}\zeta(2) \right] . \tag{A.14}$$

The gluonic coefficient function is equal to

$$\overline{\mathbb{C}}_{T,g} = C_F \frac{\alpha_s}{4\pi} \left[\left(\frac{8}{z} - 8 + 4z \right) L_M + \left(\frac{8}{z} - 8 + 4z\right) \left(\ln(1-z) + 2\ln z \right) - \frac{8}{z} \right.$$
$$\left. + 8 \right] + \left(\frac{\alpha_s}{4\pi}\right)^2 \Bigg[C_F^2 \Bigg\{ \left[\left(\frac{16}{z} - 16 + 8z\right) \ln(1-z) + (8-4z)\ln z + 8 \right.$$

$$
\begin{aligned}
&- 2z \Big] L_M^2 + \Big[\Big(\frac{64}{z} - 48 + 24z\Big) \Big(\mathrm{Li}_2(1-z) + \ln z \ln(1-z) \Big) + \Big(\frac{32}{z} \\
&- 32 + 16z \Big) \Big(\ln^2(1-z) - 2\zeta(2) \Big) + (24 - 12z) \ln^2 z + \Big(-\frac{48}{z} + 64 \\
&- 12z \Big) \ln(1-z) + (-16 + 20z) \ln z + \frac{8}{z} - 20 + 8z \Big] L_M \\
&+ C_A C_F \Big\{ \Big[\Big(\frac{16}{z} - 16 + 8z\Big) \ln(1-z) - \Big(\frac{16}{z} + 16 + 16z\Big) \ln z - \frac{124}{3z} \\
&+ 32 + 4z + \frac{16}{3} z^2 \Big] L_M^2 + \Big[-\Big(\frac{64}{z} + 48z\Big) \mathrm{Li}_2(1-z) - (64 + 16z) \cdot \\
&\cdot \ln z \ln(1-z) + \Big(\frac{32}{z} + 32 + 16z\Big) \Big(\mathrm{Li}_2(-z) + \ln z \ln(1+z) \Big) + \Big(\frac{96}{z} \\
&- 64 + 48z \Big) \zeta(2) + \Big(\frac{16}{z} - 16 + 8z\Big) \ln^2(1-z) - \Big(\frac{64}{z} + 48 + 56z\Big) \ln^2 z \\
&+ \Big(-\frac{344}{3z} + 96 - 8z + \frac{32}{3} z^2\Big) \ln(1-z) + \Big(-\frac{400}{3z} + 64 + 40z + \frac{32}{3} z^2\Big) \ln z \\
&+ \frac{188}{3z} - \frac{32}{3} - \frac{100}{3} z - \frac{32}{3} z^2 \Big] L_M + \bar{c}_{T,g}^{(2)} \Big], \qquad \text{(A.15)}
\end{aligned}
$$

$$
\begin{aligned}
\bar{c}_{T,g}^{(2)} = C_F^2 \Big[&\Big(\frac{16}{z} + 32 + 16z\Big) \Big(4 S_{1,2}(-z) + 4 \ln(1+z) \mathrm{Li}_2(-z) + 2 \ln z \cdot \\
&\cdot \ln^2(1+z) - \ln^2 z \ln(1+z) + 2\zeta(2) \ln(1+z) \Big) + \Big(\frac{32}{z} - 192 + 32z\Big) \cdot \\
&\cdot \mathrm{Li}_3(-z) + \Big(-\frac{160}{z} + 240 - 120z \Big) S_{1,2}(1-z) - \frac{16}{z} \mathrm{Li}_3(1-z) + \Big(\frac{48}{z} \\
&- 32 + 16z \Big) \ln(1-z) \mathrm{Li}_2(1-z) + (48 - 24z) \ln z \mathrm{Li}_2(1-z) + \Big(-\frac{32}{z} \\
&+ 64 - 32z \Big) \ln z \mathrm{Li}_2(-z) + \Big(\frac{40}{3z} - \frac{40}{3} + \frac{20}{3} z\Big) \ln^3(1-z) + \Big(\frac{44}{3} - \frac{22}{3} z\Big) \cdot \\
&\cdot \ln^3 z + \Big(\frac{48}{z} - 40 + 20z\Big) \ln z \ln^2(1-z) + \Big(\frac{32}{z} - 8 + 4z\Big) \ln^2 z \ln(1-z)
\end{aligned}
$$

$$+\left(\frac{16}{z}-48+24z\right)\zeta(2)\ln(1-z)+(-16+8z)\zeta(2)\ln z+\Big(\frac{112}{z}-208$$

$$+40z\Big)\zeta(3)+\Big(-\frac{96}{z}+80-28z\Big)\mathrm{Li}_2(1-z)+\left(-\frac{96}{z}+80-12z\right)\cdot$$

$$\cdot\ln z\ln(1-z)+\Big(-\frac{64}{5z^2}-64-96z+\frac{16}{5}z^3\Big)\Big(\mathrm{Li}_2(-z)$$

$$+\ln z\ln(1+z)\Big)+\left(-\frac{48}{z}+56-14z\right)\ln^2(1-z)+\Big(-32+83z$$

$$-\frac{8}{5}z^3\Big)\ln^2 z+\Big(\frac{96}{z}-112-44z+\frac{16}{5}z^3\Big)\zeta(2)+\left(\frac{8}{z}-24z\right)\ln(1-z)$$

$$+\Big(\frac{144}{5z}+\frac{418}{5}-\frac{262}{5}z-\frac{16}{5}z^2\Big)\ln z+\frac{316}{5z}-\frac{604}{5}+\frac{154}{5}z-\frac{16}{5}z^2\Big]$$

$$+C_AC_F\Big[\left(\frac{16}{z}+32+16z\right)\Big(-2S_{1,2}(-z)-2\ln(1+z)\mathrm{Li}_2(-z)$$

$$+\ln z\mathrm{Li}_2(-z)-\ln z\ln^2(1+z)-\zeta(2)\ln(1+z)\Big)+\left(\frac{32}{z}+32+16z\right)\cdot$$

$$\cdot\Big(\mathrm{Li}_3\left(-\frac{1-z}{1+z}\right)-\mathrm{Li}_3\left(\frac{1-z}{1+z}\right)+\ln z\ln(1-z)\ln(1+z)+\ln(1-z)\cdot$$

$$\cdot\mathrm{Li}_2(-z)\Big)+\left(\frac{48}{z}+32+16z\right)\mathrm{Li}_3(-z)+\left(-\frac{240}{z}-160z\right)S_{1,2}(1-z)$$

$$+\left(\frac{48}{z}+80+40z\right)\mathrm{Li}_3(1-z)-\left(\frac{48}{z}+16+40z\right)\ln(1-z)\mathrm{Li}_2(1-z)$$

$$-\left(\frac{192}{z}+32+144z\right)\ln z\mathrm{Li}_2(1-z)+\left(\frac{8}{3z}-\frac{8}{3}+\frac{4}{3}z\right)\ln^3(1-z)$$

$$-\left(\frac{160}{3z}+\frac{88}{3}+\frac{124}{3}z\right)\ln^3 z-\left(\frac{8}{z}+24+12z\right)\ln z\ln^2(1-z)-\Big(\frac{48}{z}$$

$$+64+48z\Big)\ln^2 z\ln(1-z)+\left(\frac{16}{z}+32\right)\zeta(2)\ln(1-z)+\Big(\frac{224}{z}-96$$

$$+128z\Big)\zeta(2)\ln z+\left(\frac{40}{z}+48+24z\right)\ln^2 z\ln(1+z)+\left(\frac{8}{z}+40+12z\right)\cdot$$

$$\cdot\zeta(3) + \Big(-\frac{304}{3z} + 32 + 24z + \frac{32}{3}z^2 \Big) \mathrm{Li}_2(1-z) + \Big(-\frac{496}{3z} + 96 + 16z + \frac{32}{3}z^2 \Big) \ln z \ln(1-z) + \Big(\frac{80}{3z} + 80 + 56z + \frac{32}{3}z^2\Big) \Big(\mathrm{Li}_2(-z) + \ln z \ln(1+z) \Big) + \Big(-\frac{172}{3z} + 48 - 8z + \frac{16}{3}z^2\Big) \ln^2(1-z) + \Big(-\frac{232}{3z} - 16 + 2z - \frac{16}{3}z^2 \Big) \ln^2 z + \Big(\frac{136}{3z} + 40z - \frac{32}{3}z^2\Big) \zeta(2) + \Big(\frac{356}{3z} - \frac{236}{3} - \frac{4}{3}z - \frac{32}{3}z^2 \Big) \ln(1-z) + \Big(\frac{496}{3z} + \frac{772}{3} + \frac{172}{3}z + \frac{256}{9}z^2\Big) \ln z + \frac{4438}{27z} - 36 - 106z - \frac{928}{27}z^2 \Big] . \tag{A.16}$$

The second moment of (A.15) reads as follows

$$\overline{\mathbb{C}}^{(2)}_{T,g} = C_F \frac{\alpha_s}{4\pi} \Big[\frac{16}{3} L_M - \frac{64}{3} \Big] + \Big(\frac{\alpha_s}{4\pi}\Big)^2 \Big[C_F^2 \Big\{ -\frac{64}{9} L_M^2 + \Big(\frac{2672}{27} - \frac{128}{3}\zeta(2) \Big) L_M - \frac{140657}{405} + \frac{1120}{9}\zeta(2) + \frac{1408}{15}\zeta(3) \Big\} + C_A C_F \Big\{ -\frac{88}{9} L_M^2 + \frac{2864}{27} L_M - \frac{26431}{81} + \frac{104}{9}\zeta(2) + 48\zeta(3) \Big\} \Big] . \tag{A.17}$$

Adding the second moments in (A.8), (A.11), (A.14) and (A.17) one obtains (4.5.3). Finally we have the coefficient function belonging to the special non-singlet contribution $\mathcal{F}'^{\mathrm{NS}}_{T,q}$ (4.4.3). It only contributes to Z-production provided one does not sum over all flavours belonging to one family. Furthermore no collinear singularities show up so that no mass factorization is needed. Hence one can equate the coefficient function to

$$\overline{\mathbb{C}}'^{\mathrm{NS}}_{T,q} = \mathcal{F}'^{\mathrm{NS}}_{T,q} , \tag{A.18}$$

where

$$\overline{\mathbb{C}}'^{\mathrm{NS}}_{T,q} = \Big(\frac{\alpha_s}{4\pi}\Big)^2 C_F T_f \Big[\Big(-\frac{128}{z^2} + \frac{128}{z} - 64\Big) \mathrm{Li}_2(1-z) + \Big(\frac{128}{5z^2} + \frac{128}{5}z^3\Big) \cdot \Big(\mathrm{Li}_2(-z) + \ln z \ln(1+z) \Big) - \frac{64}{5} z^3 \ln^2 z + \Big(\frac{128}{z^2} - \frac{128}{z} + 64 + \frac{128}{5}z^3\Big) \cdot \zeta(2) + \Big(\frac{64}{1-z} + \frac{64}{1+z} + \frac{512}{5z} - \frac{896}{5} + \frac{64}{5}z - \frac{128}{5}z^2 \Big) \ln z - \frac{512}{5z} + \frac{448}{5}$$

$$+\frac{32}{5}z-\frac{128}{5}z^2\Bigg]. \tag{A.19}$$

The second moment of (A.19) gives

$$\overline{\mathbb{C}}_{T,q}^{\prime\,\mathrm{NS}}=\left(\frac{\alpha_s}{4\pi}\right)^2 C_F T_f\left[-\frac{1016}{5}-32\zeta(2)+\frac{1088}{5}\zeta(3)\right]. \tag{A.20}$$

Next, we present the non-singlet longitudinal coefficient function

$$\begin{aligned}\overline{\mathbb{C}}_{L,q}^{\mathrm{NS}}=&\frac{\alpha_s}{4\pi}C_F\Big[\,2\,\Big]+\left(\frac{\alpha_s}{4\pi}\right)^2\Bigg[C_F^2\Big\{\,(8\ln(1-z)-4\ln z+2+4z)\,L_M\,\Big\}\\&+C_AC_F\Big\{-\frac{22}{3}L_M\Big\}+n_fC_FT_f\Big\{\frac{8}{3}L_M\Big\}+\bar{c}_{L,q}^{\mathrm{NS},(2),\mathrm{nid}}+\bar{c}_{L,q}^{\mathrm{NS},(2),\mathrm{id}}\Bigg],\end{aligned} \tag{A.21}$$

$$\begin{aligned}\bar{c}_{L,q}^{\mathrm{NS},(2),\mathrm{nid}}=&C_F^2\Big\{16S_{1,2}(1-z)-32\mathrm{Li}_3(-z)+16\ln z\mathrm{Li}_2(-z)-16\zeta(2)\cdot\\&\cdot\ln(1-z)-12\mathrm{Li}_2(1-z)+4\ln z\ln(1-z)+4\ln^2(1-z)-\Big(\,10-8z\\&-4z^2-\frac{8}{5}z^3\,\Big)\ln^2 z+\left(24-16z-8z^2-\frac{16}{5}z^3\right)\zeta(2)+\Big(\,\frac{24}{5z^2}+\frac{16}{z}\\&-16z-8z^2-\frac{16}{5}z^3\,\Big)\Big(\,\mathrm{Li}_2(-z)+\ln z\ln(1+z)\,\Big)+(14+4z)\ln(1-z)\\&+\Big(-\frac{24}{5z}-\frac{78}{5}+\frac{32}{5}z+\frac{16}{5}z^2\,\Big)\ln z+\frac{24}{5z}-\frac{211}{5}+\frac{86}{5}z+\frac{16}{5}z^2\Big\}\\&+C_AC_F\Big\{-8S_{1,2}(1-z)+16\mathrm{Li}_3(-z)-8\ln z\mathrm{Li}_2(-z)+8\zeta(2)\cdot\\&\cdot\ln(1-z)+\left(-\frac{12}{5z^2}-\frac{8}{z}+8z+4z^2+\frac{8}{5}z^3\right)\Big(\,\mathrm{Li}_2(-z)+\ln z\ln(1+z)\,\Big)\\&+\left(2-4z-2z^2-\frac{4}{5}z^3\right)\Big(\,\ln^2 z-2\zeta(2)\,\Big)-\frac{46}{3}\ln(1-z)+\Big(\,\frac{12}{5z}\\&+\frac{22}{15}+\frac{4}{5}z-\frac{8}{5}z^2\,\Big)\ln z-\frac{12}{5z}+\frac{2017}{45}-\frac{254}{15}z-\frac{8}{5}z^2\Big\}\\&+n_fC_FT_f\Big\{\frac{8}{3}\Big(\,\ln(1-z)+\ln z\,\Big)-\frac{100}{9}+\frac{8}{3}z\Big\},\end{aligned} \tag{A.22}$$

$$\bar{c}_{L,q}^{\mathrm{NS},(2),\mathrm{id}} = (C_F^2 - \frac{1}{2}C_A C_F)\Bigg[32S_{1,2}(1-z) - 16\mathrm{Li}_3(-z) + 32\ln(1+z)\mathrm{Li}_2(-z)$$
$$+ 16\zeta(2)\ln(1+z) + 16\ln z\ln^2(1+z) - 8\ln^2 z\ln(1+z) - 16\zeta(3)$$
$$+ \left(\frac{24}{5z^2} - \frac{16}{z} - 16 - 16z + 8z^2 - \frac{16}{5}z^3\right)\Big(\mathrm{Li}_2(-z) + \ln z\ln(1+z)\Big)$$
$$+ \left(4 + 8z - 4z^2 + \frac{8}{5}z^3\right)\Big(\ln^2 z - 2\zeta(2)\Big) + \Big(-\frac{24}{5z} + \frac{112}{5} - \frac{8}{5}z$$
$$+ \frac{16}{5}z^2\Big)\ln z + \frac{24}{5z} + \frac{64}{5} - \frac{104}{5}z + \frac{16}{5}z^2\Bigg]. \tag{A.23}$$

Taking the second moment of (A.21) gives

$$\overline{\mathbb{C}}_{L,q}^{(2),\mathrm{NS}} = C_F\frac{\alpha_s}{4\pi}\Big[1\Big] + \left(\frac{\alpha_s}{4\pi}\right)^2\Bigg[C_F^2\Big\{-\frac{8}{3}L_M + \frac{33}{10} + \frac{48}{5}\zeta(3)\Big\}$$
$$+ C_A C_F\Big\{-\frac{11}{3}L_M + \frac{221}{10} - \frac{24}{5}\zeta(3)\Big\} + n_f C_F T_f\Big\{\frac{4}{3}L_M - \frac{22}{3}\Big\}\Bigg]. \tag{A.24}$$

The purely singlet contribution (4.4.49) is equal to

$$\overline{\mathbb{C}}_{L,q}^{\mathrm{PS}} = \left(\frac{\alpha_s}{4\pi}\right)^2 n_f C_F T_f\Bigg[\Big\{16\ln z + \frac{32}{3z} - 16z + \frac{16}{3}z^2\Big\}L_M$$
$$+ 16\mathrm{Li}_2(1-z) + 16\ln z\,\ln(1-z) + 24\ln^2 z + \left(\frac{32}{3z} - 16z + \frac{16}{3}z^2\right)\cdot$$
$$\cdot\ln(1-z) + \left(\frac{64}{3z} - 32 - 32z + \frac{16}{3}z^2\right)\ln z - \frac{16}{z} - \frac{112}{3} + \frac{208}{3}z - 16z^2\Bigg], \tag{A.25}$$

and the second moment is given by

$$\overline{\mathbb{C}}_{L,q}^{(2),\mathrm{PS}} = \left(\frac{\alpha_s}{4\pi}\right)^2 n_f C_F T_f\Big[\frac{8}{3}L_M - \frac{52}{3}\Big]. \tag{A.26}$$

The gluonic contribution to the longtidunal coeffcient function presented in (4.4.48) is given by

$$\overline{\mathbb{C}}_{L,g} = \frac{\alpha_s}{4\pi}C_F\Big[\frac{8}{z} - 8\Big] + \left(\frac{\alpha_s}{4\pi}\right)^2\Bigg[C_F^2\Big\{\Big[16\ln z - 8 + \frac{16}{z} - 8z\Big]L_M$$

$$
\begin{aligned}
&+\left(-\frac{32}{3}+\frac{64}{5z^2}+\frac{32}{15}z^3\right)\Big(\,\mathrm{Li}_2(-z)+\ln z\ln(1+z)\,\Big)+16\mathrm{Li}_2(1-z)\\
&+16\ln z\,\ln(1-z)+\frac{32}{15}\zeta(2)z^3+\left(24-\frac{16}{15}z^3\right)\ln^2 z+\left(\frac{32}{z}-24-8z\right)\cdot\\
&\cdot\ln(1-z)+\left(-\frac{8}{5}+\frac{96}{5z}-\frac{224}{15}z-\frac{32}{15}z^2\right)\ln z+\frac{24}{5}-\frac{96}{5z}+\frac{248}{15}z\\
&-\frac{32}{15}z^2\Bigg\}\\
&+C_AC_F\Bigg\{\Bigg[\left(-32+\frac{32}{z}\right)\ln(1-z)-\left(32+\frac{32}{z}\right)\ln z-\frac{272}{3z}+80\\
&+16z-\frac{16}{3}z^2\Bigg]L_M+\left(32+\frac{32}{z}\right)\Big(\,\mathrm{Li}_2(-z)+\ln z\ln(1+z)\,\Big)\\
&-\frac{64}{z}\mathrm{Li}_2(1-z)-64\ln z\ln(1-z)+\left(-64+\frac{96}{z}\right)\zeta(2)+\left(-16+\frac{16}{z}\right)\cdot\\
&\cdot\ln^2(1-z)-\left(48+\frac{64}{z}\right)\ln^2 z+\left(144-\frac{464}{3z}+16z-\frac{16}{3}z^2\right)\ln(1-z)\\
&+\left(112-\frac{352}{3z}+32z-\frac{16}{3}z^2\right)\ln z+\frac{448}{3z}-\frac{320}{3}-\frac{160}{3}z+\frac{32}{3}z^2\Bigg\}\Bigg].
\end{aligned}
\tag{A.27}
$$

Taking the second moment of (A.27) one obtains

$$
\begin{aligned}
\overline{\mathbb{C}}_{L,g}^{(2)}=C_F\,\frac{\alpha_s}{4\pi}\left[\,4\,\right]+\left(\frac{\alpha_s}{4\pi}\right)^2\Bigg[C_F^2\left\{\,\frac{16}{3}L_M-\frac{108}{5}-\frac{96}{5}\zeta(3)\,\right\}\\
+C_AC_F\left\{\,-\frac{44}{3}L_M+\frac{272}{3}\,\right\}\Bigg].
\end{aligned}
\tag{A.28}
$$

Adding (A.24), (A.26) and (A.28) one ontains the result presented in (4.5.2). Finally we have the coefficient function belonging to the special non-singlet contribution $\mathcal{F}_{L,q}^{\prime\mathrm{NS}}$ (4.4.3). It only contributes to Z-production for the reasons as mentioned above (A.18). Since $\mathcal{F}_{L,q}^{\prime\mathrm{NS}}$ is collinearly finite the coefficient function $\overline{\mathbb{C}}_{L,q}^{\prime\mathrm{NS}}$ is given by

$$
\overline{\mathbb{C}}_{L,q}^{\prime\mathrm{NS}}=\mathcal{F}_{L,q}^{\prime\mathrm{NS}},
\tag{A.29}
$$

where

$$
\overline{\mathbb{C}}_{L,q}^{\prime\mathrm{NS}}=\left(\frac{\alpha_s}{4\pi}\right)^2C_FT_f\Bigg[\left(\frac{128}{z^2}-\frac{128}{z}+32\right)\mathrm{Li}_2(1-z)+\Big(-\frac{128}{5z^2}-\frac{64}{3}
$$

$$+\frac{256}{15}z^3\Big)\Big(\mathrm{Li}_2(-z)+\ln z\ln(1+z)\Big)-\frac{128}{15}z^3\ln^2 z+\Big(-\frac{128}{z^2}+\frac{128}{z}$$
$$-32+\frac{256}{15}z^3\Big)\zeta(2)+\left(-\frac{512}{5z}+\frac{256}{5}+\frac{128}{15}z-\frac{256}{15}z^2\right)\ln z+\frac{512}{5z}-\frac{448}{5}$$
$$+\frac{64}{15}z-\frac{256}{15}z^2\Big]. \tag{A.30}$$

The second moment of this special contribution is given by

$$\overline{\mathbb{C}}_{L,q}^{\prime(2),\mathrm{NS}}=\left(\frac{\alpha_s}{4\pi}\right)^2 C_F T_f\left[\frac{1316}{5}-\frac{1088}{5}\zeta(3)\right]. \tag{A.31}$$

Finally we present the asymmetric coefficient functions. In this case the soft and virtual gluon contributions are the same as for the coefficient function $\mathbb{C}_{T,q}^{\mathrm{NS}}$

$$\overline{\mathbb{C}}_{A,q}^{\mathrm{NS}}\Big|_{S+V}=\overline{\mathbb{C}}_{T,q}^{\mathrm{NS}}\Big|_{S+V}. \tag{A.32}$$

The hard gluon contribution to the asymmetric coefficient function is given by

$$\overline{\mathbb{C}}_{A,q}^{\mathrm{NS,nid}}\Big|_{H}=C_F\frac{\alpha_s}{4\pi}\Big[-2(1+z)L_M+4\frac{1+z^2}{1-z}\ln z-2(1+z)\ln(1-z)+1$$
$$-z\Big]+\left(\frac{\alpha_s}{4\pi}\right)^2\Big[C_F^2\Big\{\Big(\Big(-\frac{8}{1-z}+6+6z\Big)\ln z-8(1+z)\ln(1-z)$$
$$-10-2z\Big)L_M^2+\Big(4(1+z)\mathrm{Li}_2(1-z)+\Big(-\frac{32}{1-z}+22+22z\Big)\ln^2 z$$
$$+\Big(\frac{32}{1-z}-12-12z\Big)\ln z\ln(1-z)-12(1+z)\ln^2(1-z)-8(1+z)\cdot$$
$$\cdot\zeta(2)+\Big(\frac{48}{1-z}-48-24z\Big)\ln z-4(1-z)\ln(1-z)+7+29z\Big)L_M\Big\}$$
$$+C_AC_F\Big\{\frac{11}{3}(1+z)L_M^2+\Big(2\frac{1+z^2}{1-z}\ln^2 z+4(1+z)\zeta(2)+\Big(-\frac{44}{3}\frac{1}{1-z}$$
$$+\frac{34}{3}+\frac{34}{3}z\Big)\ln z+\frac{22}{3}(1+z)\ln(1-z)+\frac{73}{9}-\frac{341}{9}z\Big)L_M\Big\}$$
$$+n_fC_FT_f\Big\{-\frac{4}{3}(1+z)L_M^2+\Big(\frac{8}{3}\frac{1+z^2}{1-z}\ln z-\frac{8}{3}(1+z)\ln(1-z)$$
$$+\frac{4}{9}+\frac{76}{9}z\Big)L_M\Big\}+\bar{c}_{A,q}^{\mathrm{NS},(2),\mathrm{nid}}\Big|_{H}\Big], \tag{A.33}$$

$$\bar{c}_{A,q}^{\mathrm{NS},(2),\mathrm{nid}}\Big|_H = C_F^2 \Bigg[\left(-\frac{192}{1-z} + 116 + 100z\right) S_{1,2}(1-z) + \Big(\frac{96}{1-z} - 64 - 32z \Big) \mathrm{Li}_3(-z) + \left(-\frac{24}{1-z} + 8 + 8z\right) \mathrm{Li}_3(1-z) + \Big(-\frac{80}{1-z} + 52 + 52z \Big) \ln z \mathrm{Li}_2(1-z) + \left(-\frac{48}{1-z} + 32 + 16z\right) \ln z \mathrm{Li}_2(-z) + \frac{8}{1-z} \cdot \cdot \ln(1-z) \mathrm{Li}_2(1-z) + \left(-\frac{80}{3}\frac{1}{1-z} + 17 + 17z\right) \ln^3 z + \Big(-\frac{4}{1-z} + 8 + 8z \Big) \ln^2 z \ln(1-z) + \left(\frac{20}{1-z} - 8 - 8z\right) \ln z \ln^2(1-z) - 4(1+z) \cdot \cdot \ln^3(1-z) + \left(\frac{120}{1-z} - 64 - 64z\right) \zeta(2) \ln z - 16\zeta(2) \ln(1-z) + \Big(\frac{72}{1-z} - 32 - 32z \Big) \zeta(3) + \Big(\frac{12}{1-z} - 36 + 12z \Big) \mathrm{Li}_2(1-z) + \Big(-\frac{8}{z} - 8 - 8z - 8z^2 \Big) \Big(\mathrm{Li}_2(-z) + \ln z \ln(1+z) \Big) + \left(\frac{33}{1-z} - 35 - 25z + 4z^2\right) \ln^2 z - \left(\frac{12}{1-z} + 24\right) \ln z \ln(1-z) + (4 + 8z) \ln^2(1-z) + (-4 - 28z - 8z^2) \cdot \cdot \zeta(2) + \left(-\frac{106}{1-z} + 44 + 90z\right) \ln z + (21 + 17z) \ln(1-z) + \frac{41}{2}(1-z) \Bigg]$$

$$+ C_A C_F \Bigg[-4(1-z) S_{1,2}(1-z) + 12\frac{1+z^2}{1-z} \mathrm{Li}_3(1-z) + \Big(-\frac{48}{1-z} + 32 + 16z \Big) \mathrm{Li}_3(-z) - 4\frac{1+z^2}{1-z} \ln z \mathrm{Li}_2(1-z) + \Big(\frac{24}{1-z} - 16 - 8z \Big) \ln z \mathrm{Li}_2(-z) - 4\frac{1+z^2}{1-z} \ln(1-z) \mathrm{Li}_2(1-z) + 3\frac{1+z^2}{1-z} \ln^3 z - 12\frac{1+z^2}{1-z} \zeta(2) \ln z + 8\zeta(2) \ln(1-z) + \left(-\frac{36}{1-z} - 2 - 2z\right) \zeta(3) + \left(-\frac{44}{3}\frac{1}{1-z} + \frac{34}{3} + \frac{34}{3}z\right) \Big(\mathrm{Li}_2(1-z) + \ln z \ln(1-z) \Big) + \Big(\frac{4}{z} + 4$$

$$+ 4z + 4z^2 \Big) \Big(\mathrm{Li}_2(-z) + \ln z \ln(1+z) \Big) + \Big(-\frac{11}{3}\frac{1}{1-z} + \frac{35}{6} + \frac{35}{6}z$$

$$- 2z^2 \Big) \ln^2 z + \frac{11}{3}(1+z)\ln^2(1-z) + \left(-\frac{16}{3} - \frac{16}{3}z + 4z^2\right)\zeta(2)$$

$$+ \left(\frac{206}{3}\frac{1}{1-z} + 4 - \frac{190}{3}z\right)\ln z + \left(-\frac{53}{9} - \frac{233}{9}z\right)\ln(1-z) - \frac{485}{54}$$

$$+ \frac{1705}{54}z \Bigg]$$

$$+ n_f C_F T_f \Bigg[\frac{2}{3}\frac{1+z^2}{1-z} \Big(4\mathrm{Li}_2(1-z) + \ln^2 z + 4\ln z \ln(1-z) \Big) - \frac{4}{3}(1+z)\cdot$$

$$\cdot \ln^2(1-z) + \frac{8}{3}(1+z)\zeta(2) + \left(-\frac{64}{3}\frac{1}{1-z} + 4 + \frac{44}{3}z\right)\ln z + \left(\frac{4}{9} + \frac{76}{9}z\right)\cdot$$

$$\cdot \ln(1-z) + \frac{110}{27} - \frac{262}{27}z \Bigg]. \tag{A.34}$$

The first moment of the coefficient function $\overline{\mathbb{C}}_{A,q}^{\mathrm{NS,nid}}$ reads as follows

$$\overline{\mathbb{C}}_{A,q}^{(1),\mathrm{NS,nid}} = 1 + \left(\frac{\alpha_s}{4\pi}\right)^2 \Bigg[C_F^2 \Bigg\{ \Big(13 - 12\zeta(2) + 8\zeta(3) \Big) L_M - \frac{301}{4} + 28\zeta(2)$$

$$+ 34\zeta(3) - \frac{64}{5}\zeta(2)^2 \Bigg\} + C_A C_F \Bigg\{ \left(-\frac{13}{2} + 6\zeta(2) - 4\zeta(3)\right) L_M + \frac{301}{8}$$

$$- 14\zeta(2) - 61\zeta(3) + \frac{32}{5}\zeta(2)^2 \Bigg\} + n_f C_F T_f \Bigg\{ 16\zeta(3) \Bigg\} \Bigg]. \tag{A.35}$$

The contributions to $\overline{\mathbb{C}}_{A,q}^{\mathrm{NS}}$ due to identical quarks in the final state is equal to

$$\overline{\mathbb{C}}_{A,q}^{\mathrm{NS,id}} = \left(\frac{\alpha_s}{4\pi}\right)^2 (C_F^2 - \frac{1}{2}C_A C_F) \Bigg[\Bigg(4\frac{1+z^2}{1+z} \Big(-4\mathrm{Li}_2(-z) - 4\ln z \ln(1+z)$$

$$+ \ln^2 z - 2\zeta(2) \Big) + 8(1+z)\ln z + 16 - 16z \Bigg) L_M + \bar{c}_{A,q}^{\mathrm{NS},(2),\mathrm{id}} \Bigg], \tag{A.36}$$

$$\bar{c}_{A,q}^{\mathrm{NS},(2),\mathrm{id}} = 16\frac{1+z^2}{1+z} \Bigg(\mathrm{Li}_3\left(\frac{1-z}{1+z}\right) - \mathrm{Li}_3\left(-\frac{1-z}{1+z}\right) + \frac{1}{2}S_{1,2}(1-z)$$

$$- \mathrm{Li}_3(1-z) + \frac{1}{2}\ln z \mathrm{Li}_2(1-z) - \ln z \mathrm{Li}_2(-z) - \ln(1-z)\mathrm{Li}_2(-z)$$

$$+\frac{3}{8}\ln^3 z+\frac{1}{4}\ln^2 z\ln(1-z)-\ln z\ln(1-z)\ln(1+z)-\zeta(2)\ln z-\frac{1}{2}\zeta(2)\cdot$$

$$\cdot\ln(1-z)\Big)+16\frac{z}{1+z}\Big(2S_{1,2}(-z)-\mathrm{Li}_3(-z)+2\ln(1+z)\mathrm{Li}_2(-z)$$

$$+\ln z\ln^2(1+z)-\zeta(3)+\zeta(2)\ln(1+z)\Big)+\left(-\frac{24}{1+z}+8-16z\right)\ln^2 z\cdot$$

$$\cdot\ln(1+z)+8(1+z)\mathrm{Li}_2(1-z)+8\left(\frac{1}{z}+z^2\right)\Big(\mathrm{Li}_2(-z)+\ln z\ln(1+z)\Big)$$

$$+(8+12z-4z^2)\ln^2 z+8(1+z)\ln z\ln(1-z)+4(1-z+2z^2)\zeta(2)$$

$$+\left(-\frac{16}{1+z}+46-2z\right)\ln z+16(1-z)\ln(1-z)+30-30z. \tag{A.37}$$

The first moment of (A.36) is given by

$$\overline{\mathbb{C}}_{A,q}^{(1),\mathrm{NS,id}}=\left(\frac{\alpha_s}{4\pi}\right)^2(C_F^2-\frac{1}{2}C_AC_F)\left[\Big(13-12\zeta(2)+8\zeta(3)\Big)L_M-\frac{301}{4}\right.$$

$$\left.+28\zeta(2)+34\zeta(3)-\frac{64}{5}\zeta(2)^2\right]. \tag{A.38}$$

Subtracting (A.38) from (A.35) gives the result presented in (4.6.2).
Finally we have the coefficient function belonging to the special non-singlet contribution $\mathcal{F}_{A,q}^{\prime\mathrm{NS}}$ (4.4.4). It only contributes to the interference of γ and Z-production and it vanishes for reasons mentioned above (A.18). The coefficient function $\overline{\mathbb{C}}_{A,q}^{\prime\mathrm{NS}}$ is given by

$$\overline{\mathbb{C}}_{A,q}^{\prime\mathrm{NS}}=\mathcal{F}_{A,q}^{\prime\mathrm{NS}}, \tag{A.39}$$

where

$$\overline{\mathbb{C}}_{A,q}^{\prime\mathrm{NS}}=\left(\frac{\alpha_s}{4\pi}\right)^2C_FT_f\left[-\frac{64}{3}\left(\frac{1}{z}+z^2\right)\Big(\mathrm{Li}_2(-z)+\ln z\ln(1+z)\Big)\right.$$

$$+\left(\frac{64}{z}-32\right)\mathrm{Li}_2(1-z)+\frac{32}{3}z^2\ln^2 z+\left(-\frac{64}{z}+32-\frac{64}{3}z^2\right)\zeta(2)$$

$$\left.+\left(-\frac{32}{1-z}+\frac{32}{1+z}-\frac{128}{3}+\frac{160}{3}z\right)\ln z+\frac{128}{3}-\frac{80}{3}z\right]. \tag{A.40}$$

The first moment of (A.40) is given by

$$\overline{\mathbb{C}}_{A,q}^{\prime(1),\mathrm{NS}}=\left(\frac{\alpha_s}{4\pi}\right)^2C_FT_f\left[\frac{256}{3}+16\zeta(2)-96\zeta(3)\right], \tag{A.41}$$

A.2 The coefficient functions in the annihilation scheme

In this section we shall present the expressions for the coefficient functions in the A-scheme (see (4.4.60) - (4.4.67)). When going from the $\overline{\rm MS}$-scheme to the A-scheme neither $\bar{c}^{(1)}_{L,i}$ $(i = q, g)$ nor $\overline{\mathbb{C}}^{\rm PS}_{L,q}$ change

$$\bar{c}^{(1)}_{L,i} = c^{(1)}_{L,i}, \quad k = q, g, \tag{A.42}$$

$$\overline{\mathbb{C}}^{\rm PS}_{L,q} = \mathbb{C}^{\rm PS}_{L,q}. \tag{A.43}$$

Since the special non-singlet contributions (A.18), (A.29) and (A.39) are finite they do not depend upon the chosen mass factorization scheme

$$\overline{\mathbb{C}}^{\prime \rm NS}_{k,q} = \mathbb{C}^{\prime \rm NS}_{k,q}, \quad k = T, A, L. \tag{A.44}$$

Starting with the transverse coefficient functions we have

$$\begin{aligned}
\mathbb{C}^{\rm NS,nid}_{T,q}\Big|_{S+V} &= \delta(1-z) + C_F \frac{\alpha_s}{4\pi} \left[\left(4\mathcal{D}_0(z) + 3\delta(1-z) \right) L_M + 3\delta(1-z) \right] \\
&+ \left(\frac{\alpha_s}{4\pi}\right)^2 \left[C_F^2 \left\{ \left(16\mathcal{D}_1(z) + 12\mathcal{D}_0(z) \right) L_M^2 + 12\mathcal{D}_0(z) L_M \right.\right. \\
&\left. + \delta(1-z) \left(\left(-8\zeta(2) + \frac{9}{2} \right) L_M^2 + \left(24\zeta(3) - 12\zeta(2) + \frac{21}{2} \right) L_M \right) \right\} \\
&+ C_A C_F \left\{ -\frac{22}{3}\mathcal{D}_0(z)\, L_M^2 + \left(-\frac{44}{3}\mathcal{D}_1(z) + \left(\frac{367}{9} - 8\zeta(2) \right) \mathcal{D}_0(z) \right) L_M \right. \\
&\left. + \delta(1-z) \left(-\frac{11}{2} L_M^2 + \left(-12\zeta(3) - \frac{44}{3}\zeta(2) + \frac{215}{6} \right) L_M \right) \right\} \\
&+ n_f C_F T_f \left\{ \frac{8}{3}\mathcal{D}_0(z)\, L_M^2 + \left(\frac{16}{3}\mathcal{D}_1(z) - \frac{116}{9}\mathcal{D}_0(z) \right) L_M + \delta(1-z) \left(2\, L_M^2 \right.\right. \\
&\left.\left. + \left(\frac{16}{3}\zeta(2) - \frac{38}{3} \right) L_M \right\} \right) + c^{\rm NS,(2),nid}_{T,q}\Big|_{S+V} \Bigg],
\end{aligned}$$

$$\begin{aligned}
c^{\rm NS,(2),nid}_{T,q}\Big|_{S+V} &= C_F^2 \left[-\frac{3}{2}\delta(1-z) \right] + C_A C_F \left[\left(-44\zeta(3) + \frac{123}{2} \right) \delta(1-z) \right] \\
&+ n_f C_F T_f \left[(16\zeta(3) - 22)\delta(1-z) \right],
\end{aligned} \tag{A.45}$$

$$\mathbb{C}^{\rm NS,nid}_{T,q}\Big|_{H} = C_F \frac{\alpha_s}{4\pi} \left[-2(1+z) L_M - 2 \right] + \left(\frac{\alpha_s}{4\pi}\right)^2 \left[C_F^2 \left\{ \left(-4\frac{1+z^2}{1-z} \ln z \right.\right.\right.$$

$$
\begin{aligned}
&+ 2(1+z)(\ln z - 4\ln(1-z)) - 10 - 2z \Big) L_M^2 + \Big(2\frac{1+z^2}{1-z}(4\ln z \ln(1-z) \\
&- 4\ln^2(z) + 3\ln z) + 2(1+z)\ln^2 z - 8\ln(1-z) - (6z+10)\ln z - 28 \\
&+ 10z \Big) L_M \Big\} \\
&+ C_A C_F \Big\{ \frac{11}{3}(1+z) L_M^2 + \Big(2\frac{1+z^2}{1-z}\left(\ln^2 z - \frac{11}{3}\ln z\right) + 2(1+z)\Big(2\ln z \\
&+ \frac{11}{3}\ln(1-z) + 2\zeta(2) \Big) + \frac{7}{9} - \frac{275}{9}z \Big) L_M \Big\} \\
&+ n_f C_F T_f \Big\{ -\frac{4}{3}(1+z) L_M^2 + \Big(\frac{8}{3}\frac{1+z^2}{1-z}\ln z - \frac{8}{3}(1+z)\ln(1-z) + \frac{28}{9} \\
&+ \frac{52}{9}z \Big) L_M \Big\} + c_{T,q}^{\mathrm{NS},(2),\mathrm{nid}}\Big|_H \Big], \qquad \text{(A.46)}
\end{aligned}
$$

$$
\begin{aligned}
c_{T,q}^{\mathrm{NS},(2),\mathrm{nid}}\Big|_H &= C_F^2 \Big[-16 S_{1,2}(1-z) + 32\mathrm{Li}_3(-z) - 16\ln z \mathrm{Li}_2(-z) \\
&+ 16\zeta(2)\ln(1-z) - 8\mathrm{Li}_2(1-z) + \left(-\frac{24}{5z^2} - \frac{16}{z} + 16z + 8z^2 + \frac{16}{5}z^3\right) \cdot \\
&\cdot \Big(\mathrm{Li}_2(-z) + \ln z \ln(1+z) \Big) + \left(6 - 8z - 4z^2 - \frac{8}{5}z^3\right)\ln^2 z \\
&- 8\ln z \ln(1-z) + \left(-8 + 16z + 8z^2 + \frac{16}{5}z^3\right)\zeta(2) + \Big(\frac{24}{5z} + \frac{58}{5} + \frac{8}{5}z \\
&- \frac{16}{5}z^2 \Big)\ln z - 24\ln(1-z) - \frac{24}{5z} + \frac{121}{5} - \frac{116}{5}z - \frac{16}{5}z^2 \Big] \\
&+ C_A C_F \Big[8 S_{1,2}(1-z) - 16\mathrm{Li}_3(-z) + 8\ln z \mathrm{Li}_2(-z) - 8\zeta(2)\ln(1-z) \\
&+ \left(\frac{12}{5z^2} + \frac{8}{z} - 8z - 4z^2 - \frac{8}{5}z^3\right)\Big(\mathrm{Li}_2(-z) + \ln z \ln(1+z) \Big) + \Big(-2 \\
&+ 4z + 2z^2 + \frac{4}{5}z^3 \Big)\ln^2 z + \left(4 - 8z - 4z^2 - \frac{8}{5}z^3\right)\zeta(2) + \Big(-\frac{12}{5z} - \frac{22}{15}
\end{aligned}
$$

$$- \frac{4}{5}z + \frac{8}{5}z^2 \Big) \ln z + \frac{46}{3}\ln(1-z) + \frac{12}{5z} - \frac{2017}{45} + \frac{254}{15}z + \frac{8}{5}z^2 \Big]$$

$$+ n_f C_F T_f \Big[- \frac{8}{3}(\ln z + \ln(1-z)) + \frac{100}{9} - \frac{8}{3}z \Big]. \tag{A.47}$$

Taking the Mellin transform with $m = 2$ (4.4.71) gives

$$\mathbb{C}_{T,q}^{(2),\mathrm{NS,nid}} = 1 + C_F \frac{\alpha_s}{4\pi} \Big[- \frac{8}{3}L_M + 2 \Big] + \Big(\frac{\alpha_s}{4\pi}\Big)^2 \Big[C_F^2 \Big\{ \frac{32}{9}L_M^2 + \Big(\frac{31}{27} - \frac{4}{3}\zeta(2)$$

$$+ 8\zeta(3) \Big) L_M + \frac{439}{90} + 2\zeta(2) - \frac{64}{5}\zeta(3) \Big\}$$

$$+ C_A C_F \Big\{ \frac{44}{9}L_M^2 + \Big(-\frac{3607}{54} + \frac{34}{3}\zeta(2) - 4\zeta(3) \Big) L_M + \frac{7001}{180} - \zeta(2)$$

$$- \frac{188}{5}\zeta(3) \Big\} + n_f C_F T_f \Big\{ - \frac{16}{9}L_M^2 + \frac{512}{27}L_M - \frac{44}{3} + 16\zeta(3) \Big\} \Big]. \tag{A.48}$$

The contribution due to identical quarks in the final state (see the discussion below (4.4.14) and it is given by

$$\mathbb{C}_{T,q}^{\mathrm{NS},(2),\mathrm{id}} = \Big(\frac{\alpha_s}{4\pi}\Big)^2 \Big[(C_F^2 - \frac{1}{2}C_A C_F) \Big\{ \Big(4\frac{1+z^2}{1+z}(-4\mathrm{Li}_2(-z) + \ln^2 z$$

$$- 4\ln z \ln(1+z) - 2\zeta(2)) + 8(1+z)\ln z + 16 - 16z \Big) L_M \Big\}$$

$$+ c_{T,q}^{\mathrm{NS},(2),\mathrm{id}} \Big], \tag{A.49}$$

$$c_{T,q}^{\mathrm{NS},(2),\mathrm{id}} = (C_F^2 - \frac{1}{2}C_A C_F) \Big[- 32 S_{1,2}(-z) + 16\mathrm{Li}_3(-z) - 32\ln(1+z)\mathrm{Li}_2(-z)$$

$$+ 8\ln^2 z \ln(1+z) - 16\ln z \ln^2(1+z) - 16\zeta(2)\ln(1+z) + 16\zeta(3)$$

$$+ \Big(-\frac{24}{5z^2} + \frac{16}{z} + 16 + 16z - 8z^2 + \frac{16}{5}z^3 \Big) \Big(\mathrm{Li}_2(-z) + \ln z \ln(1+z) \Big)$$

$$+ \Big(-4 - 8z + 4z^2 - \frac{8}{5}z^3 \Big) \ln^2 z + \Big(8 + 16z - 8z^2 + \frac{16}{5}z^3 \Big) \zeta(2) + \Big(\frac{24}{5z}$$

$$- \frac{112}{5} + \frac{8}{5}z - \frac{16}{5}z^2 \Big) \ln z - \frac{24}{5z} - \frac{64}{5} + \frac{104}{5}z - \frac{16}{5}z^2 \Big], \tag{A.50}$$

with the second moment equal to

$$\mathbb{C}_{T,q}^{(2),\mathrm{NS,id}} = \left(\frac{\alpha_s}{4\pi}\right)^2 (C_F^2 - \frac{1}{2}C_A C_F) \left[\left(-\frac{743}{27} + \frac{68}{3}\zeta(2) - 8\zeta(3)\right) L_M - \frac{91}{90} \right.$$
$$\left. - 2\zeta(2) + \frac{16}{5}\zeta(3) \right]. \tag{A.51}$$

The purely singlet coefficient function (4.4.63) and its second moment are given by

$$\mathbb{C}_{T,q}^{\mathrm{PS}} = \left(\frac{\alpha_s}{4\pi}\right)^2 n_f C_F T_f \left[\left\{ 8(1+z)\ln z + \frac{16}{3z} + 4 - 4z - \frac{16}{3}z^2 \right\} L_M^2 + \left\{ \right.\right.$$
$$8(1+z)(2\mathrm{Li}_2(1-z) + 3\ln^2 z + 2\ln z \ln(1-z)) + \left(\frac{64}{3z} - 8 - 40z \right.$$
$$\left. - \frac{32}{3}z^2 \right) \ln z + \left(\frac{32}{3z} + 8 - 8z - \frac{32}{3}z^2\right) \ln(1-z)$$
$$\left. - \frac{16}{3z} - \frac{184}{3} + \frac{136}{3}z + \frac{64}{3}z^2 \right\} L_M + c_{T,q}^{\mathrm{PS},(2)} \left. \right], \tag{A.52}$$

$$c_{T,q}^{\mathrm{PS},(2)} = -16\mathrm{Li}_2(1-z) - 24\ln^2 z - 16\ln z \ln(1-z) + \left(-\frac{64}{3z} + 32 + 32z \right.$$
$$\left. - \frac{16}{3}z^2 \right) \ln z + \left(-\frac{32}{3z} + 16z - \frac{16}{3}z^2\right) \ln(1-z) + \frac{16}{z} + \frac{112}{3} - \frac{208}{3}z$$
$$+ 16z^2, \tag{A.53}$$

$$\mathbb{C}_{T,q}^{(2),\mathrm{PS}} = \left(\frac{\alpha_s}{4\pi}\right)^2 n_f C_F T_f \left[\frac{16}{9}L_M^2 - \frac{512}{27}L_M + \frac{52}{3} \right]. \tag{A.54}$$

Finally we have the gluonic contribution presented in (4.4.67) which reads as follows

$$\mathbb{C}_{T,g} = C_F \frac{\alpha_s}{4\pi} \left[\left(\frac{8}{z} - 8 + 4z\right) L_M - \frac{8}{z} + 8 \right] + \left(\frac{\alpha_s}{4\pi}\right)^2 \left[C_F^2 \left\{ \left((8-4z)\ln z \right.\right.\right.$$
$$\left. + \left(\frac{16}{z} - 16 + 8z\right) \ln(1-z) + 8 - 2z \right) L_M^2 + \left(\left(-\frac{32}{z} + 32 - 16z\right) \cdot \right.$$
$$\cdot \mathrm{Li}_2(1-z) + (8-4z)\ln^2 z + \left(-\frac{32}{z} + 32 - 16z\right) \zeta(2) + (16+4z)\ln z$$
$$\left. + \left(-\frac{48}{z} + 48 - 8z\right) \ln(1-z) + \frac{48}{z} - 68 + 16z \right) L_M \right\}$$

$$+ C_A C_F \Bigg\{ \Bigg(\Bigg(-\frac{16}{z} - 16 - 16z \Bigg) \ln z + \Bigg(\frac{16}{z} - 16 + 8z \Bigg) \ln(1-z) - \frac{124}{3z}$$
$$+ 32 + 4z + \frac{16}{3} z^2 \Bigg) L_M^2 + \Bigg(\Bigg(-\frac{64}{z} - 48z \Bigg) \mathrm{Li}_2(1-z) + \Bigg(-\frac{64}{z} - 48$$
$$- 56z \Bigg) \ln^2 z + (-64 - 16z) \ln z \ln(1-z) + \Bigg(\frac{16}{z} - 16 + 8z \Bigg) \ln^2(1-z)$$
$$+ \Bigg(\frac{96}{z} - 64 + 48z \Bigg) \zeta(2) + \Bigg(-\frac{400}{3z} + 64 + 40z + \frac{32}{3} z^2 \Bigg) \ln z + \Bigg(-\frac{344}{3z}$$
$$+ 96 - 8z + \frac{32}{3} z^2 \Bigg) \ln(1-z) + \frac{188}{3z} - \frac{32}{3} - \frac{100}{3} z - \frac{32}{3} z^2 + \Bigg(\frac{32}{z} + 32$$
$$+ 16z \Bigg) \Big(\mathrm{Li}_2(-z) + \ln z \ln(1+z) \Big) \Bigg) L_M \Bigg\} + c_{T,g}^{(2)} \Bigg] , \tag{A.55}$$

$$c_{T,g}^{(2)} = C_F^2 \Bigg[\Bigg(-\frac{64}{5z^2} + \frac{32}{3} - \frac{32}{15} z^3 \Bigg) \Big(\mathrm{Li}_2(-z) + \ln z \ln(1+z) \Big) + \Bigg(-8$$
$$+ \frac{16}{15} z^3 \Bigg) \ln^2 z - \frac{32}{15} z^3 \zeta(2) + \Bigg(\frac{64}{5z} + \frac{88}{5} - \frac{16}{15} z + \frac{32}{15} z^2 \Bigg) \ln z + \Bigg(-\frac{16}{z}$$
$$+ 16 \Bigg) \ln(1-z) + \frac{256}{5z} - \frac{304}{5} + \frac{112}{15} z + \frac{32}{15} z^2 \Bigg]$$
$$+ C_A C_F \Bigg[\Bigg(-\frac{32}{z} - 32 \Bigg) \Big(\mathrm{Li}_2(-z) + \ln z \ln(1+z) \Big) + \frac{64}{z} \mathrm{Li}_2(1-z)$$
$$+ \Bigg(\frac{64}{z} + 48 \Bigg) \ln^2 z + 64 \ln z \ln(1-z) + \Bigg(-\frac{16}{z} + 16 \Bigg) \ln^2(1-z) + \Bigg(-\frac{96}{z}$$
$$+ 64 \Bigg) \zeta(2) + \Bigg(\frac{352}{3z} - 112 - 32z + \frac{16}{3} z^2 \Bigg) \ln z + \Bigg(\frac{464}{3z} - 144 - 16z$$
$$+ \frac{16}{3} z^2 \Bigg) \ln(1-z) - \frac{448}{3z} + \frac{320}{3} + \frac{160}{3} z - \frac{32}{3} z^2 \Bigg] . \tag{A.56}$$

The second moment of (A.55) is given by

$$\mathbb{C}_{T,g}^{(2)} = C_F \frac{\alpha_s}{4\pi} \Bigg[\frac{16}{3} L_M - 4 \Bigg] + \Big(\frac{\alpha_s}{4\pi} \Big)^2 \Bigg[C_F^2 \Bigg\{ -\frac{64}{9} L_M^2 + \Bigg(\frac{1424}{27} - \frac{128}{3} \zeta(2) \Bigg) \cdot$$
$$\cdot L_M + \frac{64}{15} + \frac{96}{5} \zeta(3) \Bigg\} + C_A C_F \Bigg\{ -\frac{88}{9} L_M^2 + \frac{2864}{27} L_M - \frac{272}{3} \Bigg\} \Bigg] . \tag{A.57}$$

Adding equations (A.48), (A.51), (A.54) and (A.57) we obtain (4.5.3). Notice that the total second moment $\mathbb{C}_T^{(2)} = \mathbb{C}_{T,q}^{(2),\mathrm{NS,nid}} + \mathbb{C}_{T,q}^{(2),\mathrm{NS,id}} + \mathbb{C}_{T,q}^{(2),\mathrm{PS}} + \mathbb{C}_{T,g}^{(2)}$ is factorization scheme independent. Next we present the longitudinal coefficient functions presented in (4.4.60) and (4.4.66). They are given by

$$\mathbb{C}_{L,q}^{\mathrm{NS,nid}} = C_F \frac{\alpha_s}{4\pi} \left[2 \right] + \left(\frac{\alpha_s}{4\pi}\right)^2 \left[C_F^2 \left\{ (-4\ln z + 8\ln(1-z) + 2 + 4z) L_M \right\} \right.$$
$$\left. + C_A C_F \left\{ -\frac{22}{3} L_M \right\} + n_f C_F T_f \left\{ \frac{8}{3} L_M \right\} + c_{L,q}^{(2),\mathrm{NS,nid}} \right], \tag{A.58}$$

$$c_{L,q}^{(2),\mathrm{NS,nid}} = C_F^2 \left\{ 16 S_{1,2}(1-z) - 32\mathrm{Li}_3(-z) + 16\ln z \mathrm{Li}_2(-z) - 16\zeta(2) \cdot \right.$$
$$\cdot \ln(1-z) + 8\mathrm{Li}_2(1-z) + \left(\frac{24}{5z^2} + \frac{16}{z} - 16z - 8z^2 - \frac{16}{5}z^3\right) \left(\mathrm{Li}_2(-z) \right.$$
$$\left. + \ln z \ln(1+z) \right) + \left(-6 + 8z + 4z^2 + \frac{8}{5}z^3\right) \ln^2 z + 8\ln z \ln(1-z) + \left(8 \right.$$
$$\left. - 16z - 8z^2 - \frac{16}{5}z^3 \right) \zeta(2) + \left(-\frac{24}{5z} - \frac{58}{5} - \frac{8}{5}z + \frac{16}{5}z^2\right) \ln z$$
$$\left. + 24\ln(1-z) + \frac{24}{5z} - \frac{121}{5} + \frac{116}{5}z + \frac{16}{5}z^2 \right\}$$
$$+ C_A C_F \left\{ -8 S_{1,2}(1-z) + 16\mathrm{Li}_3(-z) - 8\ln z \mathrm{Li}_2(-z) + 8\zeta(2)\ln(1-z) \right.$$
$$+ \left(-\frac{12}{5z^2} - \frac{8}{z} + 8z + 4z^2 + \frac{8}{5}z^3\right) \left(\mathrm{Li}_2(-z) + \ln z \ln(1+z) \right) + \left(2 - 4z \right.$$
$$\left. - 2z^2 - \frac{4}{5}z^3 \right) \ln^2 z + \left(-4 + 8z + 4z^2 + \frac{8}{5}z^3\right) \zeta(2) + \left(\frac{12}{5z} + \frac{22}{15} + \frac{4}{5}z \right.$$
$$\left. - \frac{8}{5}z^2 \right) \ln z - \frac{46}{3}\ln(1-z) - \frac{12}{5z} + \frac{2017}{45} - \frac{254}{15}z - \frac{8}{5}z^2 \right\}$$
$$+ n_f C_F T_f \left\{ \frac{8}{3}(\ln z + \ln(1-z)) - \frac{100}{9} + \frac{8}{3}z \right\}. \tag{A.59}$$

The second moment of (A.58) reads

$$\mathbb{C}_{L,q}^{(2),\mathrm{NS,nid}} = C_F \frac{\alpha_s}{4\pi} \left[1 \right] + \left(\frac{\alpha_s}{4\pi}\right)^2 \left[C_F^2 \left\{ -\frac{8}{3} L_M - \frac{287}{45} - 2\zeta(2) + \frac{64}{5}\zeta(3) \right\} \right.$$

$$+ C_A C_F \left\{ -\frac{11}{3} L_M + \frac{4069}{180} + \zeta(2) - \frac{32}{5}\zeta(3) \right\}$$

$$+ n_f C_F T_f \left\{ \frac{4}{3} L_M - \frac{22}{3} \right\} \Bigg] . \tag{A.60}$$

The identical quark contribution (A.1) and its second moment are given by

$$\mathbb{C}_{L,q}^{\mathrm{NS,id}} = \left(\frac{\alpha_s}{4\pi}\right)^2 (C_F^2 - \frac{1}{2} C_A C_F) \Bigg[32 S_{1,2}(-z) - 16 \mathrm{Li}_3(-z)$$

$$+ 32 \ln(1+z) \mathrm{Li}_2(-z) - 8 \ln^2 z \ln(1+z) + 16 \ln z \ln^2(1+z)$$

$$+ 16 \zeta(2) \ln(1+z) - 16 \zeta(3) + \left(\frac{24}{5z^2} - \frac{16}{z} - 16 - 16z + 8z^2 - \frac{16}{5} z^3 \right) \cdot$$

$$\cdot \Big(\mathrm{Li}_2(-z) + \ln z \ln(1+z) \Big) + \left(4 + 8z - 4z^2 + \frac{8}{5} z^3 \right) \ln^2 z + \Big(-8 - 16z$$

$$+ 8z^2 - \frac{16}{5} z^3 \Big) \zeta(2) + \left(-\frac{24}{5z} + \frac{112}{5} - \frac{8}{5} z + \frac{16}{5} z^2 \right) \ln z + \frac{24}{5z} + \frac{64}{5}$$

$$- \frac{104}{5} z + \frac{16}{5} z^2 \Bigg] . \tag{A.61}$$

The second moment of (A.61) reads

$$\mathbb{C}_{L,q}^{(2),\mathrm{NS,id}} = \left(\frac{\alpha_s}{4\pi}\right)^2 (C_F^2 - \frac{1}{2} C_A C_F) \left[\frac{91}{90} + 2\zeta(2) - \frac{16}{5}\zeta(3) \right] . \tag{A.62}$$

The gluonic contribution to the longitudinal coefficient function presented in (4.4.66) and its second moment read as follows

$$\mathbb{C}_{L,g} = C_F \frac{\alpha_s}{4\pi} \left[\frac{8}{z} - 8 \right] + \left(\frac{\alpha_s}{4\pi}\right)^2 \Bigg[C_F^2 \left\{ \left(16 \ln z + \frac{16}{z} - 8 - 8z \right) L_M + \Big(\frac{64}{5z^2}$$

$$- \frac{32}{3} + \frac{32}{15} z^3 \Big) \Big(\mathrm{Li}_2(-z) + \ln z \ln(1+z) \Big) + \left(8 - \frac{16}{15} z^3 \right) \ln^2 z$$

$$+ \frac{32}{15} z^3 \zeta(2) + \left(-\frac{64}{5z} - \frac{88}{5} + \frac{16}{15} z - \frac{32}{15} z^2 \right) \ln z + \left(\frac{16}{z} - 16 \right) \ln(1-z)$$

$$- \frac{256}{5z} + \frac{304}{5} - \frac{112}{15} z - \frac{32}{15} z^2 \Bigg\}$$

$$+ C_A C_F \Bigg\{ \Bigg(\left(-\frac{32}{z} - 32 \right) \ln z + \left(\frac{32}{z} - 32 \right) \ln(1-z) - \frac{272}{3z} + 80 + 16z$$

$$
\begin{aligned}
&- \frac{16}{3}z^2 \Big) L_M - \frac{64}{z}\mathrm{Li}_2(1-z) + \left(\frac{32}{z} + 32\right)\Big(\mathrm{Li}_2(-z) + \ln z \ln(1+z) \Big) \\
&+ \Big(- \frac{64}{z} - 48 \Big) \ln^2 z - 64 \ln z \ln(1-z) + \left(\frac{16}{z} - 16\right) \ln^2(1-z) + \Big(\frac{96}{z} \\
&- 64 \Big) \zeta(2) + \left(-\frac{352}{3z} + 112 + 32z - \frac{16}{3}z^2\right) \ln z + \Big(- \frac{464}{3z} + 144 + 16z \\
&- \frac{16}{3}z^2 \Big) \ln(1-z) + \frac{448}{3z} - \frac{320}{3} - \frac{160}{3}z + \frac{32}{3}z^2 \Big\} \Big] . \qquad \text{(A.63)}
\end{aligned}
$$

The second moment of (A.63) reads

$$
\begin{aligned}
\mathbb{C}_{L,g}^{(2)} &= C_F \frac{\alpha_s}{4\pi} \Big[4 \Big] + \left(\frac{\alpha_s}{4\pi}\right)^2 \Big[C_F^2 \Big\{ \frac{16}{3} L_M - \frac{64}{15} - \frac{96}{5}\zeta(3) \Big\} \\
&+ C_A C_F \Big\{ - \frac{44}{3} L_M + \frac{272}{3} \Big\} \Big] . \qquad \text{(A.64)}
\end{aligned}
$$

Adding (A.60), (A.62), (A.26) and (A.64) one obtains (4.5.2) which is the same as the one found in the $\overline{\mathrm{MS}}$-scheme (see below (A.28)). Finally we give the expression for the asymmetric coefficient function presented in (4.4.63)

$$
\begin{aligned}
\mathbb{C}_{A,q}^{\mathrm{NS,nid}}\Big|_H &= C_F \frac{\alpha_s}{4\pi} \Big[- 2(1+z) L_M - 4 + 2z \Big] + \left(\frac{\alpha_s}{4\pi}\right)^2 \Big[C_F^2 \Big\{ \Big(\Big(- \frac{8}{1-z} \\
&+ 6 + 6z \Big) \ln z - 8(1+z) \ln(1-z) - 10 - 2z \Big) L_M^2 + \Big(- \frac{16}{1-z} + 10 \\
&+ 10z \Big) \ln^2 z + 8 \frac{1+z^2}{1-z} \ln z \ln(1-z) + \left(\frac{12}{1-z} - 12 - 16z\right) \ln z + (-16 \\
&+ 8z) \ln(1-z) - 26 + 8z \Big) L_M \Big\} \\
&+ C_A C_F \Big\{ \frac{11}{3}(1+z) L_M^2 + \Big(2 \frac{1+z^2}{1-z} \ln^2 z + 4(1+z)\zeta(2) + \Big(- \frac{44}{3} \frac{1}{1-z} \\
&+ \frac{34}{3} + \frac{34}{3}z \Big) \ln z + \frac{22}{3}(1+z) \ln(1-z) + \frac{73}{9} - \frac{341}{9}z \Big) L_M \Big\} \\
&+ n_f C_F T_f \Big\{ - \frac{4}{3}(1+z) L_M^2 + \Big(\frac{8}{3} \frac{1+z^2}{1-z} \ln z - \frac{8}{3}(1+z) \ln(1-z) + \frac{4}{9} \\
&+ \frac{76}{9}z \Big) L_M \Big\} + c_{A,q}^{\mathrm{NS},(2),\mathrm{nid}} \Big] , \qquad \text{(A.65)}
\end{aligned}
$$

$$c_{A,q}^{\mathrm{NS},(2),\mathrm{nid}} = C_F^2 \Bigg[-16zS_{1,2}(1-z) + 32z\mathrm{Li}_3(-z) - 16z\ln z\mathrm{Li}_2(-z)$$
$$+ 16z\zeta(2)\ln(1-z) + (-16+8z)\mathrm{Li}_2(1-z) + \left(-\frac{8}{z} - 16 + 16z^2 + 8z^3\right) \cdot$$
$$\cdot \Big(\mathrm{Li}_2(-z) + \ln z \ln(1+z) \Big) + (12 - 6z - 8z^2 - 4z^3)\ln^2 z$$
$$+ (-16+8z)\ln z\ln(1-z) + (-16+8z+16z^2+8z^3)\zeta(2)$$
$$+ (34z - 8z^2)\ln z + (12-36z)\ln(1-z) - 4 + 5z - 8z^2 \Bigg]$$
$$+ C_A C_F \Bigg[8zS_{1,2}(1-z) - 16z\mathrm{Li}_3(-z) + 8z\ln z\mathrm{Li}_2(-z) - 8z\zeta(2)\ln(1-z)$$
$$+ \left(\frac{4}{z} + 8 - 8z^2 - 4z^3\right) \Big(\mathrm{Li}_2(-z) + \ln z\ln(1+z) \Big) + (-4 + 2z + 4z^2$$
$$+ 2z^3)\ln^2 z + (8 - 4z - 8z^2 - 4z^3)\zeta(2) + \left(\frac{32}{3} - \frac{82}{3}z + 4z^2\right)\ln z + \Big(-\frac{4}{3}$$
$$+ \frac{50}{3}z \Big)\ln(1-z) - \frac{568}{9} + \frac{317}{9}z + 4z^2 \Bigg]$$
$$+ n_f C_F T_f \left[\left(-\frac{16}{3} + \frac{8}{3}z\right)(\ln z + \ln(1-z)) + \frac{176}{9} - \frac{100}{9}z \right], \qquad \text{(A.66)}$$

$$\mathbb{C}_{A,q}^{\mathrm{NS,id}}\Big|_H = \left(\frac{\alpha_s}{4\pi}\right)^2 (C_F^2 - \frac{1}{2}C_A C_F) \Bigg[\Bigg(-4\frac{1+z^2}{1+z} \Bigg(4\mathrm{Li}_2(-z) + 4\ln z\ln(1+z)$$
$$- \ln^2 z + 2\zeta(2) \Bigg) + 8(1+z)\ln z + 16 - 16z \Bigg) L_M + c_{A,q}^{\mathrm{NS},(2),\mathrm{id}} \Bigg], \qquad \text{(A.67)}$$

$$c_{A,q}^{\mathrm{NS},(2),\mathrm{id}} = 32zS_{1,2}(-z) - 16z\mathrm{Li}_3(-z) + 32z\ln(1+z)\mathrm{Li}_2(-z)$$
$$- 8z\ln^2 z\ln(1+z) + 16z\ln z\ln^2(1+z) + 16z\zeta(2)\ln(1+z) - 16z\zeta(3)$$
$$+ \left(\frac{8}{z} + 16 + 16z - 16z^2 + 8z^3\right) \Big(\mathrm{Li}_2(-z) + \ln z\ln(1+z) \Big) + (-8 - 4z$$
$$+ 8z^2 - 4z^3)\ln^2 z + (16 + 8z - 16z^2 + 8z^3)\zeta(2) + (-8 + 16z - 8z^2)\ln z$$

$$+ 8 - 8z^2. \tag{A.68}$$

The first moments of (A.65) and (A.67) are given by

$$\mathbb{C}_{A,q}^{(1),\mathrm{NS,nid}} = 1 + \left(\frac{\alpha_s}{4\pi}\right)^2 \left[C_F^2 \left\{ (13 - 12\zeta(2) + 8\zeta(3))L_M + \frac{19}{2} - 6\zeta(2) \right.\right.$$
$$\left. - 8\zeta(3) \right\} + C_A C_F \left\{ \left(\frac{13}{2} + 6\zeta(2) - 4\zeta(3) \right) L_M - \frac{19}{4} + 3\zeta(2) - 40\zeta(3) \right\}$$
$$\left. + n_f C_F T_f \left\{ 16\zeta(3) \right\} \right], \tag{A.69}$$

$$\mathbb{C}_{A,q}^{(1),\mathrm{NS,id}} = \left(\frac{\alpha_s}{4\pi}\right)^2 (C_F^2 - \frac{1}{2} C_A C_F) \left[(13 - 12\zeta(2) + 8\zeta(3))L_M + \frac{19}{2} - 6\zeta(2) \right.$$
$$\left. - 8\zeta(3) \right]. \tag{A.70}$$

Subtracting (A.70) from (A.69) yields (4.6.2) which is the same as found in the $\overline{\mathrm{MS}}$-scheme (see below (A.38)).

References

[1] "QCD 20 years later", vol. 1, Editors: P.M. Zerwas and H.A. Kastrup, World Scientific, Singapore 1992. 75

[2] J. Mnich, Phys. Rep. **271** (1996) 181. 75, 76, 81, 85

[3] T. Matsuura, R. Hamberg, and W.L. van Neerven, Nucl. Phys. **B345** (1990) 331, *ibid.* Nucl. Phys. **B359** (1991) 343;
W.L. van Neerven, and E.B. Zijlstra, Nucl. Phys. **B382** (1992) 11. 75, 76, 81, 93

[4] E.B. Zijlstra, and W.L. van Neerven, Nucl. Phys. **B383** (1992) 525, *ibid.* Phys. Lett. **297B** (1992) 377. 75

[5] S.A. Larin and J.A.M. Vermaseren, Phys. Lett. **256B** (1991) 345;
S.A. Larin, F.V. Tkachov and J.A.M. Vermaseren, Phys. Rev. Lett. **66** (1991) 862;
S.A. Larin, T. van Ritbergen, and J.A.M. Vermaseren, Nucl. Phys. **B427** (1994) 41. 75, 80, 110, 122

[6] S.G. Gorishni, A.L. Kataev, and S.A. Larin, Phys. Lett. **159B** (1991) 144;
L.R. Surguladze, and M.A. Samuel, Phys. Rev. Lett. **66** (1991) 560, Erratum Phys. Rev. Lett. **66** (1991) 2416;
K.G. Chetyrkin and O.V. Tarasov, Phys. Lett. **B327** (1994) 114;

S.A. Larin, T. van Ritbergen, and J.A.M. Vermaseren, Phys. Lett. **B320** (1994) 159, *ibid.* Nucl. Phys. **B438** (1995) 278. 76

[7] K.G. Chetyrkin and F.V. Tkachov, Nucl. Phys. **B192** (1981) 159;
D.I. Kazakov and A.B. Kotikov, Nucl. Phys. **B307** (1988) 721. 76

[8] Brandelik *et al.* (DASP Collaboration), Nucl. Phys. **B148** (1979) 189. 76

[9] H. Albrecht *et al.* (ARGUS Collaboration), Z. Phys. **C44** (1989) 547. 76

[10] W. Braunschweig *et al.* (TASSO), Z. Phys. **C42** (1989) 189, *ibid.* Z. Phys. **C47** (1990) 187. 76

[11] A. Peterson *et al.* (Mark II), Phys. Rev. **D37** (1988) 1. 76, 113, 119, 124

[12] H. Aihara *et al.* (TPC/2γ Collaboration), Phys. Rev. Lett. **61** (1988) 1263. 76

[13] O. Podobrin (CELLO), Ph. D. thesis, Universität Hamburg. 76

[14] T. Kumita *et al.* (AMY), Phys. Rev. **D42** (1990) 1339;
Y.K. Li *et al.* (AMY Collaboration), Phys. Rev. **D41** (1990) 2675. 76

[15] P. Abreu *et al.* (DELPHI Collaboration), Phys. Lett. **B311** (1993) 408. 76, 113, 114, 115, 120

[16] D. Buskulic *et al.* (ALEPH Collaboration), Phys. Lett. **B357** (1995) 487, *ibid.* Z. Phys. **C66** (1995) 355. 76, 113

[17] R. Akers *et al.* (OPAL Collaboration), Z. Phys. **C58** (1993) 387, *ibid.* Z. Phys. **C63** (1994) 181. 8, 76, 111, 112, 113, 114, 115, 120, 123, 126, 127, 128

[18] R. Akers *et al.* (OPAL Collaboration), Z. Phys. **C68** (1995) 203. 8, 76, 77, 82, 84, 85, 107, 109, 112, 116, 118, 119, 120, 121, 128

[19] P. Nason, and B.R. Webber, Nucl. Phys. **B421** (1994) 473. 76, 85

[20] V.N. Gribov and L.N. Lipatov, Sov. J. Nucl. Phys. **15** (1972) 675;
G. Altarelli and G. Parisi, Nucl. Phys. **B126** (1977) 298;
Yu.L. Dokshitzer, Sov. Phys. JETP **46** (1977) 641. 76, 80, 110

[21] K.E. Chetyrkin, A.L. Kataev, and F.V. Tkachov, Phys. Lett. **85B** (1979) 277;
M. Dine, and J. Sapirstein, Phys. Rev. Lett. **43** (1979) 668;
W. Celmaster, and R.J. Gonsalves, Phys. Rev. Lett. **44** (1980) 560. 77, 112

[22] B.R. Webber, Cavendish Laboratory Report Nos. Cavendish-HEP-94/17, hep-ph/9411384, 1994 (unpublished). 82, 89, 92

[23] J.A.M. Vermaseren, FORM2, published by Computer Algebra Nederland (CAN), Kruislaan 413, 1089 SJ Amsterdam, The Netherlands. 83, 92, 93, 109

[24] S.A. Larin, Phys. Lett. **303B** (1993) 113, *ibid.* Phys. Lett. **334B** (1994) 192. 84, 85, 109, 128

[25] R. Baier, and K. Fey, Z. Phys. **C2** (1979) 339. 8, 84, 85, 128

[26] G. Altarelli, R.K. Ellis, G. Martinelli, and S.-Y. Pi, Nucl. Phys. **B160** (1979) 301. 7, 14, 17, 19, 43, 51, 86

[27] T. Matsuura, and W.L. van Neerven, Z. Phys. **C38** (1988) 623. 86, 89

[28] T. Matsuura, S.C. van der Marck, and W.L. van Neerven, Nucl. Phys. **B319** (1989) 570. 86, 89

[29] G. Kramer and B. Lampe, Z. Phys. **C34** (1987); Erratum **C42** (1989) 504. 89

[30] G. Pasarino and M. Veltman, Nucl. Phys. **B160** (1979) 151;
W. Beenakker, Ph. D. thesis University of Leiden, The Netherlands (1989). 59, 92

[31] W. Beenakker, H. Kuijf, W.L. van Neerven, and J. Smith, Phys. Rev. **D40** (1989) 54. 92

[32] Erdélyí, Magnus, Oberhettinger, Tricomi, "Higher Transcendental functions", Bateman Manuscript Project. Vol 1, McGraw-Hill 1953. 92

[33] W.L. Neerven, Nucl. Phys. **B286** (1986) 453. 92

[34] G. 't Hooft and M. Veltman, Nucl. Phys. **B44** (1972) 189. 92

[35] P. Breitenlohner and B. Maison, Common. Math. Phys. **53** (1977) 11, 39, 55. 92

[36] D. Akyeampong and F. Delbourgo, Nuovo Cim. **17A** (1973) 578, *ibid.* Nuovo Cim. **18A** (1973) 94, *ibid.* Nuovo Cim. **19A** (1974) 219. 17, 19, 20, 30, 38, 94

[37] G. Altarelli, R.K. Ellis, and G. Martinelli, Nucl. Phys. **B157** (1979) 461. 14, 17, 95

[38] B. Humpert, and W.L. van Neerven, Nucl. Phys. **B184** (1981) 225. 100, 101, 102, 104

[39] G. Curci, W. Furmanski, and R. Petronzio, Nucl. Phys. **B175** (1980) 27;
W. Furmanski, and R. Petronzio, Phys. Lett. **97B** (1980) 437, *ibid.* Z. Phys. **C11** (1982) 293. 100, 101, 102, 104

[40] E.G. Floratos, C. Kounnas, and R. Lacaze, Nucl. Phys. **B192** (1981) 417. 100, 132

[41] R. Barbieri, J.A. Mignaco, and E. Remiddi, Nuovo Cim. **11A** (1972) 824;
L. Lewin, "Polylogarithms and Associated Functions" (North Holland, Amsterdam 1983);
A. Devoto, and D.W. Duke, Riv. Nuovo Cim. **7-6** (1984) 1. 109

[42] R. Mertig and W.L. van Neerven, Z. Phys. **C70** (1996) 637. 8, 112, 113, 114, 115, 118, 119, 120, 121, 124, 125, 126, 127, 128

[43] J. Binnewies, B.A. Kniehl, and G. Kramer, Z. Phys. **C65** (1995) 471. 112, 113, 116, 118, 119, 124, 125

[44] J. Binnewies, B.A. Kniehl, and G. Kramer, Phys. Rev. **D52** (1995) 4947. 116

[45] P.J. Rijken and W.L. van Neerven, INLO-PUB-4/96, hep-ph/9604436, to be published in Phys. Lett. B. 122

[46] D.J. Broadhurst and A.L. Kataev, Phys. Lett. **315B** (1993) 179;
G.T. Gabadadze and A.L. Kataev, JETP Lett. **61** (1995) 448.

Samenvatting

Hogere orde QCD correcties op tijdachtige processen

In de twintig jaar volgend op de Tweede Wereldoorlog werd er een grote verscheidenhied aan nieuwe deeltjes, waaronder de hadronen, ontdekt. De hadronen zijn opgebouwd uit twee (de mesonen) of drie (de baryonen) quarks, waarvan er nu zes "smaken" bekend zijn: "up", "down", "strange", "charm", "bottom" en "top". De laatste werd in 1994 gevonden. Vele pogingen om tot een theoretisch model te komen dat de eigenschappen van de hadronen verklaart, die een gevolg zijn van de sterke wisselwerking tussen de quarks, hebben aangetoond dat de enige kandidaat hiervoor Quantum Chromo Dynamica (QCD) is. Technisch gezien kan QCD beschreven worden als een $SU(3)_C$ lokaal ijkinvariante Yang-Mills veldentheorie. De krachten tussen de quarks worden beschreven door de uitwisseling van massaloze vectorbosonen: de gluonen. Deze beschrijving is analoog aan die in het standaard model van de elektrozwakke wisselwerkingen waarin de elektromagnetische en de zwakke krachten worden beschreven door de uitwisseling van het massaloze foton en de massieve Z en $W^{\pm}$ bosonen. In QCD worden de quarks in de fundamentele representatie geplaatst. Dit betekent dat elk type quark voorkomt in drie "kleuren" en dat er acht kleurcombinaties voor de gluonen zijn. Het feit dat de symmetriegroep $SU(3)_C$ niet-abels is, brengt met zich mee dat in QCD de gluonen onderling wisselwerken. Hetzelfde geldt voor de vectorbosonen Z en $W^{\pm}$ die voorkomen in het bovengenoemde standaard model van de elektrozwakke wisselwerkingen. Dit in tegenstelling tot de fotonen waarvan de onderliggende symmetrie abels is, namelijk $U(1)$.

Door gebruik te maken van stroomalgebra voorspelde Bjorken het schaalgedrag van de zeer inelastische structuurfuncties die voorkomen in de werkzame doorsnede van elektron–protonverstrooiing. Dit verschijnsel werd voor de eerste keer ontdekt in de experimenten gedaan op SLAC tussen 1967 en 1969. Deze structuurfuncties zijn relativistisch invariante dimensieloze grootheden die all informatie bevatten over de structuur van het proton. Helaas verschaft stroomalgebra geen informatie over deze functies zelf, maar alleen over de geïntegreerde structuurfuncties. Een andere beperking van stroomalgebra is dat het hiermee onmogelijk is voorspellingen te doen voor andere zeer inelastische processen, zoals massieve leptonpaarproductie

in hadron–hadronbotsingen. Deze restricties verdwenen met de introductie van het parton model door Feynman.

Het partonmodel kan op de volgende wijze samengevat worden. In zeer inelastische botsingsprocessen, gepaard gaande met de uitwisseling van een ruimteachtig foton, verstrooit een elektron op inelastische wijze aan een proton. Bovengenoemde experimenten op SLAC lieten zien dat de structuurfuncties niet afhangen van de twee variabelen ν (energieverlies van het elektron) en q^2 (vierimpuls in het kwadraat van het virtuele foton), maar dat ze slechts afhankelijk zijn van de schaalvariabele $x = -q^2/(2M\nu)$, die wordt begrensd door 0 en 1, met M de massa van het proton. Bjorken en Paschos, die Feynmans partonmodel toepasten op zeer inelastische elektron–protonverstrooiing, namen aan dat bij vaste x en zeer grote $-q^2$ het elektron de "partonen", waaruit het proton opgebouwd is, ziet als stilstaande, vrije puntachtige deeltjes. Met deze interpretatie kan de verstrooiing van het elektron aan het proton beschreven worden door een incoherente som van elektron–protonbotsingen gewogen door een kansdichtheidfunctie, genaamd partondichtheid. De variabele x wordt geïnterpreteerd als de fractie van de impuls van het proton dat overgedragen wordt aan het parton dat verstrooit aan het elektron. De partondichtheid $f_i^p(x)$ geeft de kans om een parton van het type "i" met een fractie "x" van de impuls aan te treffen in het proton. Een belangrijk resultaat van het partonmodel is dat de zeer inelastische structuurfuncties geschreven kunnen worden als de som van alle partondichtheden gewogen door de lading in het kwadraat van elk parton. De verklaring van het schaalgedrag van de zeer inelastische structuurfuncties volgt dan uit het feit dat de partondichtheden alleen afhangen van de schaalvariabele x, wat tevens inhoudt dat zij onafhankelijk zijn van q^2. Een tweede belangrijke voorspelling van het partonmodel is dat andere zeer inelastische verstrooiingsprocessen beschreven worden door dezelfde partondichtheden als die gevonden worden in zeer inelastische elektron–protonverstrooiing, waardoor relaties gelegd worden tussen verschillende processen.

De experimenten die volgden na die op SLAC in 1969, konden vanwege een hogere statistiek de zeer inelastische structuurfuncties nauwkeuriger bepalen. Dit liet een kleine afwijking van het schaalgedrag van de zeer inelastische structuurfuncties, gevonden bij eerdere experimenten, zien. Dit gebroken schaalgedrag kan in QCD verklaard worden, daar in deze theorie de partonen, die dan geassocieerd worden met de quarks en de gluonen, zich niet langer gedragen als vrije deeltjes maar met elkaar wisselwerken. Deze verklaring berust op het feit dat QCD een asymptotisch vrije theorie is, d.w.z. de sterkte van de wisselwerking wordt kleiner naarmate de energieschaal groter wordt, waardoor bij grote impulsoverdracht de partonen bijna vrije deeltjes zijn en dus slechts een kleine afwijking van het schaalgedrag wordt gezien. Doordat de koppelingsconstante α_s afneemt bij grotere energieschalen, is het mogelijk een reeksontwikkeling van de structuurfuncties in α_s te maken. In deze expansie worden de resultaten van het partonmodel gerepresenteerd door de laagste orde term. Er is sprake van het verbeterde partonmodel als ook de hogere orde QCD correcties worden meegenomen.

In het voorafgaande is slechts beargumenteerd wat de oorzaak is van de breking

van het schaalgedrag van de structuurfuncties, maar om deze breking kwantitatief te begrijpen, is het nodig om op zijn minst de eerste orde term in de storingsreeks uit te rekenen. Nu, om de convergentie van deze reeks te verzekeren, moet de sterke koppelingsconstante α_s voldoende klein zijn, of de energieschaal waarop de wisselwerking plaatsvindt, voldoende groot. Vergeleken met deze schaal kunnen de massa's van de lichte quarks u, d en s verwaarloosd worden, dit in tegenstelling tot de zware quarks c, b en t die hun experimentele waarde ongelijk aan nul houden. Vanwege de nu massaloze lichte quarks treden er in een eerste orde berekening zogenaamde collineaire divergenties, soms ook wel massasingulariteiten genoemd, op. Deze divergenties (oneindigheden) vinden hun oorsprong in het parallel zijn van de impulsen van twee massaloze partonen die afgestraald worden van een derde massaloos parton. Deze divergenties worden via een renormalisatieprocedure (massafactorisatie) geabsorbeerd door de partondichtheden. Om er zeker van te zijn dat de zo verkregen partondichtheden eenduidig gedefinieerd zijn, is het noodzakelijk dat de massasingulariteiten hetzelfde zijn als voor elk ander proces. Deze renormalisatie van de partondichtheden introduceert een willekeurige schaal μ^2 (factorisatieschaal) waarvan de partondichtheden afhankelijk worden. Een andere consequentie van massafactorisatie is dat de structuurfuncties geschreven kunnen worden als een convolutie tussen de partondichtheden en zogenaamde coëfficiëntfuncties, waarvan de laatsten afhangen van zowel μ^2 als q^2. Op deze wijze worden de structuurfuncties afhankelijk van q^2 dat verklaart waarom er geen perfect schaalgedrag gevonden wordt. Omdat deze functies fysische en dus meetbare grootheden zijn, moeten zij onafhankelijk zijn van de factorisatieschaal μ^2. Dit zal slechts dan gebeuren als alle termen in de eerder genoemde reeksontwikkeling bepaald kunnen worden. Omdat dit in de praktijk uitgesloten is, zullen de resultaten voor de structuurfuncties altijd afhangen van de geïntroduceerde willekeurig schaal μ^2. Deze afhankelijk is één van de problemen in QCD om tot nauwkeurige voorspellingen met betrekking tot fysische grootheden te komen.

Afgezien van zeer inelastische lepton–hadronverstrooiingen, zijn er meer processen waar het verbeterde parton model toegepast kan worden. Hiervan zijn twee voorbeelden massieve leptonpaarproductie in hadron–hadronverstrooiing en hadronproductie in elektron–positronannihilatie. In tegenstelling tot eerstgenoemde, dat een ruimteachtig proces is, zijn de andere twee processen tijdachtig van aard. De begrippen ruimte- en tijdachtig hebben betrekking op de vierimpuls van het virtuele vectorboson, γ, Z en $W^{\pm}$, van het standaard model van de elektrozwakke wisselwerkingen, dat in bovengenoemde reacties uitgewisseld wordt.

Begin jaren zeventig zagen Drell en Yan in dat het partonmodel toegepast kon worden op leptonpaarproductie in hadron–hadronverstrooiing. Hiervoor maakten zij twee aannames. In de eerste plaats veronderstelden zij dat het leptonpaar geproduceerd wordt door parton–antipartonannihilatie waar het parton en antiparton elk afkomstig zijn van één van de inkomende hadronen. Ten tweede namen zij aan dat de kansdichtheid om een (anti)parton in het hadron aan te treffen gelijk is aan die in het geval van zeer inelastische elektron–protonverstrooiing. Door deze partondicht-

heden te gebruiken, kan men een voorspelling doen ten aanzien van de werkzame doorsnede in het Drell-Yan proces. Bovendien stelt deze laatste reactie ons in staat de partondichtheden van onstabiele deeltjes als pionen en kaonen te bepalen, hetgeen onmogelijk is in zeer inelastische lepton–hadronverstrooiingen.
Experimenten in de zeventiger jaren onthulden dat wanneer de werkzame doorsnede voor het Drell-Yan proces in laagste orde storingstheorie wordt uitgerekend, deze ongeveer twee maal groter is dan gemeten. Deze factor wordt wel de "Drell-Yan K-factor" genoemd, en wordt verklaard door het meenemen van hogere orde QCD correcties, wat een mooie kwantitatieve test van QCD oplevert.

Berekeningen van de eerste orde correcties in 1979 en 1980 konden de grote K-factor slechts voor een deel verklaren. Hieruit bleek bovendien dat de correcties bij zowel lage als hoge energieën erg groot zijn, waardoor de convergentie van de storingsreeks twijfelachtig wordt. Ook waren deze resultaten erg afhankelijk van de willekeurige factorisatieschaal μ^2. Om meer inzicht te krijgen in de convergentieeigenschappen van de reeksontwikkeling en de afhankelijkheid van berekende grootheden van de factorisatieschaal is het nodig de tweede orde correcties op verscheidene observabelen te bepalen. Deze correcties zijn kompleet in het geval van de differentiële werkzame doorsnede $d\sigma/dQ$ waarin Q de invariante massa van het leptonpaar voorstelt. Echter voor de dubbel differentiële werkzame doorsnede $d^2\sigma/dQdp_T$, waarbij p_T de transversale impuls van het elektrozwakke vectorboson voorstelt, is er slechts een gedeelte van de tweede orde correcties bekend, namelijk die het gevolg zijn van de virtuele en zachte gluonische bijdragen. Deze treden op als de frequenties van de gluonen, die in de virtuele correcties en de remstralingsprocessen optreden, naar nul gaan. Het meenemen van alleen dit type gluonen is bekend als de virtuele-plus zachte-gluonenbenadering. Een analyse van deze benadering bij hoge energieën (630 GeV bij $Sp\bar{p}S$ in Genève en 1.8 TeV bij de Tevatron (Fermilab)) is reeds gedaan. In dit proefschrift wordt in hoofdstuk 2 de analyse uitgevoerd bij energieën (15 GeV tot 40 GeV) die typisch zijn voor experimenten met vaste trefschijf. Om een idee te krijgen hoe goed de virtuele- en zachte-gluonenbenadering zal werken, is er allereerst onderzocht in welke situaties deze benadering redelijke resultaten geeft voor de werkzame doorsnede $d\sigma/dQ$ omdat in dit geval de volledige tweede orde correcties bekend zijn. Deze benadering is in twee verschillende factorisatieschema's onderzocht: het DIS-schema en het $\overline{\text{MS}}$-schema. In het eerste schema wordt bij de massafactorisatie de gehele coëfficiëntfunctie geabsorbeerd door de partondichtheden, terwijl in het andere schema slechts de divergenties worden geabsorbeerd. In beide schema's blijkt de benadering beter te werken voor grotere waarden van Q. In het DIS-schema blijkt de benadering te grote resultaten te geven met een afwijking die niet groter is dan 10%, terwijl in het $\overline{\text{MS}}$-schema de benadering te kleine waarden geeft met een afwijking kleiner dan 20%. Bij een beschouwing van de virtuele- plus zachte-gluonenbenadering voor de werkzame doorsnede $d^2\sigma/dQdp_T$ is er precies het omgekeerde te zien als voor $d\sigma/dQ$: de benadering werkt beter in het $\overline{\text{MS}}$-schema dan in het DIS-schema en de afwijkingen zijn maximaal respectievelijk 14% en 25%. Als algemene leidraad hebben we daarom aangehouden dat voor energieën die karakteristiek zijn voor experimenten met een vaste trefschijf en voor een verhouding

($\sqrt{\tau}$) tussen de invariante massa van het leptonpaar en de massamiddelpuntsenergie groter dan 0.3 de benadering redelijk zal zijn. Eerst passen we de virtuele- plus zachte-gluonenbenadering toe op het experiment E537, dat verstrooiing van $\bar{p}$ en π^- aan wolfraam bestudeert bij een energie $\sqrt{s} = 15.4$ GeV. In dit geval ligt $\sqrt{\tau}$ tussen 0.26 en 0.59 zodat in het grootste deel van dit interval bovengenoemde benadering toegepast kan worden. Het blijkt dat de metingen in overeenstemming zijn met de theoretische voorspellingen in zowel het DIS als het $\overline{\text{MS}}$-schema. In het geval van het experiment E615, waar metingen zijn verricht aan π^--wolfraam verstrooiing bij een hogere energie van $\sqrt{s} = 21.8$ GeV en voor $\sqrt{\tau}$-waarden tussen de 0.18 en 0.60, blijkt dat de benadering in het DIS-schema goede resultaten geeft voor $d\sigma/dQ$. Dit geldt zelfs voor $\sqrt{\tau} < 0.3$ waar de benadering twijfelachtig is. Voor de werkzame doorsnede $d^2\sigma/dQdx_F$ is er alleen overeenstemming met experiment indien $0.18 < \sqrt{\tau} < 0.28$, ofschoon in dit gebied deze benadering niet geldig is. Bovendien blijken voor $d\sigma/dQ$ de tweede orde correcties de K-factor niet te verklaren. Bij dit experiment is het niet goed werken van de benadering voor $d^2\sigma/dQdx_F$ vooral te wijten aan het feit dat men in dit experiment de Υ-resonantie bij $\sqrt{\tau} = 0.43$ niet heeft afgetrokken van de metingen, waardoor het lastig is de benadering te testen. Het laatste experiment waar de virtuele- plus zachte-gluonenbenadering onderzocht is, is E772 dat de verstrooiing van een proton aan deuterium bestudeert bij een massamiddelpuntsenergie $\sqrt{s} = 38.8$ GeV. Ondanks dat in dit experiment $\sqrt{\tau} = 0.21$ is, blijkt de benadering toch te werken in het DIS-schema met medeneming van de tweede orde correcties en is er geen tegenspraak met de data.

Bij het berekenen van hogere orde QCD correcties op de werkzame doorsnede in het Drell-Yan proces heeft men tot nog toe alle quarkmassa's gelijk aan nul genomen. Deze approximatie is een goede voor de lichte quarks u, d en s, maar is in het algemeen onwaar voor de zwaardere quarks c, b en t. Voor, bijvoorbeeld, vectorboson (γ, Z en $W^\pm$) productie in het Drell-Yan proces kan men de massa's van de bottom- en topquark niet verwaarlozen, behalve de charm die wel als massaloos behandeld kan worden. Om deze reden is in hoofdstuk 3 het effect van de zware quarks op de werkzame doorsnede $d\sigma/dQ$, met Q de invariante massa van het leptonpaar, bestudeerd en vergeleken met het geval waarin deze massa's wel verwaarloosd worden. Voor een deel zijn er reeds resultaten bekend in de literatuur, die echter alleen betrekking hebben op Z-productie waar de zware quarks in één- en tweeluscorrecties voorkomen en die bovendien niet volledig zijn. In dit proefschrift worden alle tweeluscorrecties, waaronder ook de bijdragen tot $W^\pm$ en γ-productie, gecompleteerd met de berekening van de vele parton subprocessen die in de literatuur nog niet gedaan zijn. Het gaat hierbij om vele twee naar drie deeltjes processen voor γ, Z en $W^\pm$-productie waarbij twee zware quarks in de eindtoestand voorkomen. De bijdrage van de zware quarks tot $d\sigma/dQ$ blijkt erg klein te zijn, namelijk circa 1% van eerste orde gecorrigeerde werkzame doorsnede, en dan nog alleen voor Z-productie bij energieën die met de komst van de Large Hadron Collider (LHC) gehaald zullen worden. In de limiet dat $m << Q$ waarbij m de massa van het zware quark is, kan men een analytische uitdrukking voor de werkzame doorsnede afleiden. Deze uitdrukking blijkt de exacte waarde voor $d\sigma/dQ$ goed te benaderen voor bot-

tomquarkproductie bij energieën groter dan 1.8 TeV en voor charmquarkproductie zelfs voor energieën vanaf 630 GeV. Dat deze benadering goed is, houdt in dat bij hoge energieën de bottomquark als een lichte quark beschouwd kan worden en wordt verklaard doordat de werkzame doorsnede gedomineerd wordt door logaritmen van het type $\ln(Q^2/m^2)$ hetgeen aanleiding geeft tot grote correcties. Deze logaritmen moeten door middel van de massafactorisatie geabsorbeerd worden door de charm en bottom partondichtheden, waarna beide quarks als massaloos genomen kunnen worden.

Een ander belangrijk tijdachtig proces waar QCD correcties kunnen worden toegepast, is hadronproductie in elektron–positronannihilatie. Dit proces wordt ééndeeltje-inclusief genoemd als slechts één hadron in de eindtoestand wordt waargenomen. Analoog aan zeer inelastische elektron–protonverstrooiing kan men de werkzame doorsnede in relativistisch invariante functies uitdrukken die in dit geval fragmentatiefuncties worden genoemd. De laatsten beschrijven hoe het virtuele foton of het virtuele Z-boson, die in elektron–positronannihilatie worden geproduceerd, koppelen aan het waargenomen hadron. De hoekverdeling van de differentiële werkzame doorsnede kan in drie stukken verdeeld worden. De eerste twee zijn de longitudinale en transversale werkzame doorsneden corresponderend met de polarisatietoestanden van het virtuele foton en Z-boson met betrekking tot de bundelrichting. De derde wordt gegeven door de asymmetrische werkzame doorsnede die ontstaat door de pariteit brekende termen in de koppeling van het Z-boson aan het inkomende elektron en positron. Deze laatste werkzame doorsnede is afwezig in puur elektromagnetische wisselwerkingen. Van deze werkzame doorsneden kunnen de longitudinale, transversale en asymmetrische fragmentatiefuncties afgeleid worden.
In het partonmodel vervalt het foton of het Z-boson in een quark–antiquarkpaar. Eén van deze beide fragmenteert dan in het hadron dat in de eindtoestand wordt waargenomen. Uit dit model volgt dat er slechts twee fragmentatiefunties zijn, namelijk de transversale en de asymmetrische, die weer het bekende schaalgedrag vertonen. Het blijkt dat deze functies slechts afhangen van een schaalvariabele z die gelijk is aan de fractie van de bundelenergie meegenomen door het gedetecteerde hadron. Om de fragmentatie van een parton (quark, antiquark) in hadronen te kunnen beschrijven, voert men de partonfragmentatiedichtheid in. Deze dichtheid $D_i^H(z)$ is gedefinieerd als zijnde de kans dat een parton van het soort "i" fragmenteert in een hadron "H" met een fractie "z" van de impuls van het parton. Uit het partonmodel volgt dan dat de fragmentatiefuncties geschreven kunnen worden als een som over de fragmentatiedichtheden gewogen door de lading in het kwadraat van elk parton. Net als voor zeer inelastische elektron–protonverstrooiing wordt de afwijking van het schaalgedrag van de fragmentatiefuncties verklaard door hogere orde QCD correcties in rekening te brengen. Hierbij worden deze functies behalve van z ook afhankelijk van de bundelenergie ($\frac{1}{2}Q$). Verder voorspelt QCD het bestaan van de longitudinale fragmentatiefunctie, die evenredig is aan de sterke koppelingsconstante α_s, en van de gluonische fragmentatiedichtheid, die beiden afwezig zijn in het partonmodel.
Sinds 1979 zijn de eerste orde correcties op de longitudinale en transversale fragmen-

tatiefuncties bekend. In 1994 zijn de correcties ook op de asymmetrische fragmentatiefunctie uitgerekend. Een analyse van deze correcties laat zien dat de berekende waarden voor de longitudinale fragmentatiefunctie ver beneden de data zijn. Verwacht wordt dat een groot deel van deze discrepantie te wijten is aan het weglaten van hogere orde QCD correcties, en daarom zijn in hoofdstuk 4 de tweede orde QCD correcties op deze fragmentatiefuncties gepresenteerd. De tweede orde bijdragen tot de longitudinale fragmentatiefunctie $F_L(z, Q^2)$, die in feite een eerste orde correctie zijn, zijn erg groot, namelijk 44% tot 67% van de laagste orde bijdrage voor z-waarden tussen 0.001 en 1. Deze correcties brengen F_L nog niet geheel in overeenstemming met de data, maar er is een duidelijke verbetering te zien in vergelijking tot de laagste orde bijdrage. Gesteld mag worden dat de correcties tot $F_L(z, Q^2)$ groot zijn, en daarom belangrijk zijn voor een nauwkeurige bepaling van α_s en de gluonfragmentatiedichtheid $D_g(z)$. De orde α_s^2 bijdrage tot de asymmetrische fragmentatiefunctie $F_A(z, Q^2)$ zijn verwaarloosbaar, terwijl die tot de transversale fragmentatiefunctie $F_T(z, Q^2)$ klein zijn maar zeker wel belangrijk. Doordat de QCD correcties op de fragmentatiefuncties slechts tot op eindige orde worden meegenomen, hangen zij ook nog af van een onfysische factorisatieschal. De laatste afhankelijkheid verdwijnt als de berekeningen tot op alle orden in storingsrekening zouden kunnen worden uitgevoerd wat helaas onmogelijk is. Vandaar dat in de praktijk de storingsreeks in zo hoog mogelijke orde moet worden uitgerekend dat de afhankelijkheid van deze schaal niet meer kan worden waargenomen. Bij de tweede orde bijdragen tot deze en in iets mindere mate ook bij $F_L(z, Q^2)$, is een duidelijke reductie van de afhankelijkheid van deze functies van de factorisatieschaal te zien. Bij een verandering van deze schaal is in laagste orde bij $F_L(z, Q^2)$ een variatie te zien van maximaal 55%, terwijl met medeneming van de orde α_s^2 bijdrage dit maximum daalt tot 25%. In het geval van $F_T(z, Q^2)$ toont deze tot en met de orde α_s bijdrage een variatie van 15%, en tot en met de orde α_s^2 bijdrage een variatie van nog geen 5%. Deze percentages zijn geldig voor $Q = M_Z$. Bij een lagere waarde van Q, bijvoorbeeld 30 GeV, wordt de maximale afwijking van $F_T(z, Q^2)$ ten gevolge van een schaalverandering 10%.

Curriculum vitae

Op 23 oktober 1969 ben ik geboren te Nijmegen. Na aldaar in 1988 aan het Dominicus College het eindexamen Atheneum B te hebben afgelegd, ben ik begonnen aan de studie Natuurkunde aan de Katholieke Universiteit Nijmegen. Het propaedeutisch examen volgde in augustus 1989. Tijdens de studie heb ik drie studentassistentschappen vervuld bij de vakken Wiskunde IV en Wiskundige Methoden der Fysica I. Verder ben ik medeorganisator geweest van een studieuitwisseling tussen studievereniging "Marie Curie" en het MPTI te Moskou. Mijn afstudeerscriptie betrof de Slavnov-Taylor identiteiten in het standaard model van de elektrozwakke wisselwerkingen. Dit onderzoek vond plaats onder leiding van dr. W.L.G.A.M. van Neerven. Ik heb in januari 1993 het doctoraalexamen Natuurkunde afgelegd.

Op 1 maart 1993 trad ik in dienst van de Rijksuniversiteit Leiden om bij prof. dr. F.A. Berends en dr. W.L.G.A.M. van Neerven op het Instituut-Lorentz aan een promotieonderzoek te beginnen op het gebied van storingstheoretische Quantum Chromo Dynamica. Ik heb gedurende vier semesters werkcolleges bij de vakken Quantumtheorie II en Veldentheorie verzorgd. Tijdens mijn promotieperiode werden de volgende hoge-energiefysica scholen bezocht: de zomerschool "42nd Scottish Universities Summer School in Physics", twee maal de AIO-winterschool in Dalfsen en de zomerschool "CTEQ-DESY 1995 Summer School" in Bad Lauterberg (Duitsland).

List of publications

- P.J. Rijken and W.L. van Neerven
  Order α_s^2 contributions to the Drell-Yan cross section at fixed target energies
  Phys. Rev. **D51** (1995) 44

- P.J. Rijken and W.L. van Neerven
  Heavy flavor contributions to the Drell-Yan cross section
  Phys. Rev. **D52** (1995) 149

- P.J. Rijken and W.L. van Neerven
  $\mathcal{O}(\alpha_s^2)$ Contributions to the longitudinal fragmentation function in e^+e^- annihilation
  Phys. Lett. **B386** (1996) 422

- P.J. Rijken and W.L. van Neerven
  Higher order QCD corrections to the transverse and longitudinal fragmentation functions in electron-positron annihilation
  INLO-PUB-09/96, hep-ph/9609377, accepted for publication in Nucl. Phys. **B**

- P.J. Rijken and W.L. van Neerven
  $\mathcal{O}(\alpha_s^2)$ Contributions to the asymmetric fragmentation function in e^+e^- annihilation
  INLO-PUB-10/96, hep-ph/9609379, accepted for publication in Phys. Lett. **B**